

UNIVERSITY OF SOUTHAMPTON

School of Civil Engineering and the Environment

**Integrity of the Adhesive Bonding in Steel Beams Strengthened
with a Carbon Fibre Composite Plate**

by

Jun Deng

Thesis for the Degree of Doctor of Philosophy

October 2005

UNIVERSITY OF SOUTHAMPTON

ABSTRACT

SCHOOL OF CIVIL ENGINEERING AND THE ENVIRONMENT

Doctor of Philosophy

INTEGRITY OF THE ADHESIVE BONDING IN STEEL BEAMS
STRENGTHENED WITH A CARBON FIBRE COMPOSITE PLATE

by Jun Deng

Since the 1990s, the use of carbon fibre reinforced polymer (CFRP) materials has made large advances in the civil engineering construction field, particularly in the bridge upgrade and rehabilitation. To date, there are many applications in metallic beams strengthened with a bonded CFRP plate. However, the design method and technique are not sophisticated, and some specific areas require further research. In this technique, the structural adhesive bonding is the most distinct element to be considered. The main aspects discussed in this thesis are interfacial stress analysis, the behaviour under static loading and the fatigue performance.

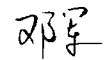
Firstly, an analytical solution and a numerical procedure are presented to calculate the stresses in beams reinforced by CFRP plates with a uniform thickness as well as with ends that are tapered. Finite element analysis was employed to validate the analytical results and a parametric study was carried. Secondly, ten retrofitted steel beams were tested under static loading to investigate the factors influencing the strength, such as different length and thickness of CFRP plates, the effects of the end taper and of the adhesive spew fillets beyond the plate ends. The test results were also used to validate the results of the analytical stress analysis. Thirdly, nine further retrofitted steel beams were tested under fatigue loading. Backface-strain technique was applied to monitor crack initiation and growth, and to assess the effect of the spew fillets. An S-N curve based on the peak interfacial stresses is proposed to predict the fatigue performance of the retrofitted beams. Finally, Finite element analysis was employed to investigate the geometric effect of the spew fillet and of the taper at the plate end of the retrofitted beam. The results confirm that the spew fillet size has a large effect on the strain in the plate ends. In the conclusion, a simple and integrated design method/technique for steel beams reinforced by bonded CFRP plates is proposed, based on the findings obtained from the studies presented.

Acknowledgments

I would like to sincerely thank my supervisor Prof. Marcus Lee for his dedicated guidance, enthusiastic encouragement and continuous support during this work. The door to Prof. Lee's office was always open whenever I ran into a trouble or had a question in my research.

I would also like to thank Prof. Stuart Moy for his help, encouragement and suggestions.

In addition, I would like to express my gratitude to Dr. Maria Lopez, my host supervisor during this work was carried out at Pennsylvania State University, for her supervision, advice and help.



Jun Deng

To my wife

Table of Contents

List of Tables	v
List of Figures	vi
Notation	xi
Chapter 1 Introduction.....	1
1.1 Advanced composite materials.....	1
1.1.1 Definition and characteristic	1
1.1.2 Historic development	2
1.1.3 The benefits of the composite materials.....	3
1.1.4 Applications of composite materials.....	3
1.2 Mechanics of composite materials	3
1.2.1 Fibres.....	4
1.2.2 Matrices.....	5
1.2.3 Composites.....	5
1.2.4 Failure modes and criteria.....	7
1.3 Use of composite materials in civil engineering	8
1.3.1 All composite structures.....	9
1.3.2 Upgrade of non-metallic structures	10
1.3.3 Upgrade of metallic structures	11
1.4 Outline of current study.....	13
1.4.1 Background	13
1.4.2 Contents of thesis	14
1.5 Summary	16
Chapter 2 Literature review	20
2.1 Strengthening of beams using externally-bonded plates.....	20
2.1.1 Conventional techniques	20
2.1.2 RC beams strengthened with CFRP plates.....	22
2.1.3 Metallic beams strengthened with CFRP plates.....	24
2.1.4 Metallic beams strengthened with UHM CFRP plates	25

2.1.5	Metallic beams strengthened by innovative methods	26
2.2	Stress analysis of bonded structures	27
2.2.1	Lap joints.....	27
2.2.2	End effect of lap joints	28
2.2.3	Retrofitted beam.....	30
2.3	Fatigue behaviour of bonded structures	31
2.3.1	Fatigue performance of lap joints	32
2.3.2	Fatigue performance of RC beam strengthened with Steel/CFRP.....	34
2.3.3	Fatigue performance of metallic beams strengthened with CFRP.....	36
2.4	Design guidance for strengthening metallic structures	37
2.5	Conclusion.....	38
Chapter 3	Materials	40
3.1	Metals.....	40
3.1.1	Overview	40
3.2.2	Mechanical properties of metallic materials	41
3.2.3	Metal used in this study.....	41
3.2	CFRP	41
3.2.1	Overview	41
3.2.2	Manufacture characteristics of CFRP	42
3.2.3	Static behaviours of CFRP.....	43
3.2.4	Fatigue behaviours of CFRP	44
3.2.5	CFRP used in this study	45
3.3	Adhesives	46
3.3.1	Overview	47
3.3.2	Elastic parameters of adhesive	48
3.3.3	Strength of adhesive bonding.....	50
3.3.4	Fatigue behaviour of adhesive bonding	51
3.3.5	Adhesive used in this study	52
3.4	Conclusion.....	53
Chapter 4	Stress analysis of metallic beams reinforced with a bonded CFRP plate	57
4.1	Introduction and objectives	57

4.2 Basic assumptions	58
4.3 Stress analysis	58
4.3.1 Stress solution for the symmetric load case	58
4.3.2 Stress solution for the asymmetric load case	68
4.3.3 Maximum shear stress and normal stress without taper.....	69
4.3.4 Maximum principle stress	70
4.4 Longitudinal strain at the CFRP plate bottom.....	70
4.4.1 Calculation for longitudinal strain	70
4.4.2 Analysis of the longitudinal strain at the plate bottom close to the end of plate	71
4.5 Finite element analysis.....	72
4.6 Results and discussion.....	73
4.7 Parametric study	74
4.8 Conclusion.....	75
Chapter 5 Behaviour under static loading of steel beams reinforced with a bonded CFRP plate.....	86
5.1. Introduction and objectives	86
5.2 Experimental study.....	87
5.2.1 Specimen preparation.....	87
5.2.2 Experimental setup.....	89
5.3 Test results and discussion	89
5.3.1 Strength of specimens	90
5.3.2 Stiffness of specimens.....	91
5.3.3 Failure mode.....	92
5.3.4 Strain distributions in specimen S305	95
5.4 Conclusion.....	96
Chapter 6 Fatigue test of steel beams reinforced with a bonded CFRP plate....	111
6.1 Introduction and objectives	111
6.2 Experimental details.....	112
6.2.1 Specimen preparation.....	112
6.2.2 Experimental setup.....	113
6.2.3 Test procedure	114

6.3 Test results and analysis	115
6.3.1 Backface-strain technique	115
6.3.2 Stiffness change	118
6.3.3 Crack propagation and failure.....	118
6.3.4 S-N Curve.....	120
6.3.5 Strength of specimen F40-2 after fatigue testing	121
6.3.6 The effect of the load range	121
6.4 Conclusion.....	122
Chapter 7 Finite element analysis for the end effect.....	139
7.1 Introduction and objectives	139
7.2 Geometry and material properties	140
7.3 Finite element analysis	141
7.4 Results and discussion.....	142
7.4.1 Stresses for without fillet case.....	142
7.4.2 Effect of the spew fillet configuration on stress distribution	143
7.4.3 Effect of the taper on stress distribution	144
7.4.4 End effect on the maximum interfacial stresses.....	145
7.4.5 Effect of the spew fillet size on the strain distribution in the plate bottom	146
7.5 Conclusion.....	146
Chapter 8 Conclusions, design suggestions and future works	161
8.1 Conclusions	161
8.2 Design suggestions	162
8.3 Future works.....	165
References	166
Appendix A - Tensile tests on steel to obtain mechanical properties	A1
Appendix B - Manufacturing of CFRP plates.....	B1
Appendix C - Tensile tests on unidirectional CFRP to obtain mechanical properties	C1
Appendix D - Shear tests on thick adherend lap-shear joints	D1
Appendix E – List of publications	E1

List of Tables

Table 1.1 Properties of typical fibre, matrix and structural materials.....	17
Table 3.1 Mechanical properties of metallic materials	54
Table 3.2 Mechanical properties of CFRP prepreg.....	54
Table 3.3 Mechanical properties of adhesive.....	54
Table 4.1 Comparison of the maximum stresses	76
Table 4.2 Reduction of the maximum stresses by the taper.....	76
Table 5.1 Test specimen details	98
Table 5.2 Results of tests and calculation of the specimens	98
Table 6.1 Specimen details and test results.....	123
Table 6.2 Comparisons of the spew fillet size and the number of cycles in same retrofitted beams.....	123
Table 7.1 The maximum interfacial stresses and reduction ratio.....	148

List of Figures

Figure 1.1	Multiphase media.....	18
Figure 1.2	Variation of laminate stiffness with the direction of loading	18
Figure 1.3	Utilisation of advanced polymer composites in construction.....	19
Figure 1.4	Organization of the study.....	19
Figure 3.1	Normalized $S-N$ curves.	55
Figure 3.2	Butt joint.	55
Figure 3.3	Thick adherend lap shear joint.....	56
Figure 3.4	Idealised Wohler diagram.	56
Figure 4.1	Geometric parameters.....	77
Figure 4.2	An infinitesimal element of a retrofitted beam.....	77
Figure 4.3	Geometric parameters of taper.....	77
Figure 4.4	Convergence of the numerical procedure	78
Figure 4.5	FE mesh of a half beam model	78
Figure 4.6	Convergence of the finite element analyses	79
Figure 4.7	Comparisons of shear and normal stresses for plates without taper under thermal Load	79
Figure 4.8	Comparisons of shear and normal stresses for plates without taper under UDL.....	80
Figure 4.9	Comparisons of shear and normal stresses for plates without taper under concentrated load	80
Figure 4.10	Comparisons of shear and normal stresses for plates with taper under thermal load.....	81
Figure 4.11	Comparisons of shear and normal stresses for plates with taper under UDL.....	81
Figure 4.12	Comparisons of shear and normal stresses for plates with taper under concentrated load.....	82
Figure 4.13	Comparison of stresses for plates with and without taper under thermal load.....	82

Figure 4.14 Variation of the maximum stress with the thickness of adhesive.....	83
Figure 4.15 Variation of the maximum stress with the shear modulus of adhesive	83
Figure 4.16 Variation of the maximum stress with the thickness of CFRP plate	84
Figure 4.17 Variation of the maximum stress with the elastic modulus of CFRP plate	84
Figure 4.18 Comparison of shear stress ratio for different a and t_{end}	85
Figure 4.19 Comparison of normal stress ratio for different a and t_{end}	85
Figure 5.1 Curing specimens.....	99
Figure 5.2 Typical retrofitted specimens	99
Figure 5.3 Schematic three-point bending setup.....	100
Figure 5.4 Schematic four-point bending setup	100
Figure 5.5 The test setup	101
Figure 5.6 Dimensions of a typical specimen and the location of strain gauges and potentiometers	101
Figure 5.7 Comparisons of Load-deflection curves in specimens with different length CFRP plates under three-point bending	102
Figure 5.8 Comparisons of Load-deflection curves between specimens with different length CFRP plates under four-point bending.....	102
Figure 5.9 Comparisons of Load-deflection curves between specimens with different thick CFRP plates under three-point bending	103
Figure 5.10 Comparisons of Load-deflection curves in specimens without or with tapers or spew fillets under three-point bending	103
Figure 5.11 Comparisons of deflection measurement in different specimens at 70kN.....	104
Figure 5.12 The typical debonding failure specimen S304.....	104
Figure 5.13 The debonded CFRP plates of S304, S405 and S406.....	105
Figure 5.14 The debonded CFRP plate of S305, S304S and S304T.....	105
Figure 5.15 Maximum stresses versus crack length a in specimen S304	106
Figure 5.16 Energy release rate G varied with the crack length in specimen S304...	106
Figure 5.17 Debonding of the CFRP plate in specimen S305D	107
Figure 5.18 Strains at the end of plate of S305 during the test	107
Figure 5.19 Strains at the end of plate of S305D during the test	108
Figure 5.20 Strains at the end of plate of S304S during the test.....	108

Figure 5.21 Strain in the CFRP plate for specimen S305	109
Figure 5.22 Strain distributions in the CFRP plate at different load levels in Beam S305.....	109
Figure 5.23 Strain in the middle of specimen from G7-10 under different load level in S305	110
Figure 5.24 Comparison of experimental and analytical results of S305	110
Figure 6.1 Schematic of fatigue test setup	124
Figure 6.2 Test setup	124
Figure 6.3 Instrumentation on test specimens.....	125
Figure 6.4 Strain measured at the plate ends of specimen F125 from three static load cycles	125
Figure 6.5 Strain measured at the plate ends of specimen F90 from three static load cycles	126
Figure 6.6 Strain measured at the plate ends of specimen F70 from three static load cycles	126
Figure 6.7 Strain measured at the plate ends of specimen F55 from three static load cycles	127
Figure 6.8 Strain measured at the plate ends of specimen F50 from three static load cycles	127
Figure 6.9 Strain measured at the plate ends of specimen F40-1 from three static load cycles	128
Figure 6.10 Strain measured at the plate ends of specimen F40-2 from three static load cycles	128
Figure 6.11 Strain ranges measured in F90.....	129
Figure 6.12 Strain ranges measured in F70.....	129
Figure 6.13 Strain ranges measured in F55.....	130
Figure 6.14 Strain ranges measured in F50.....	130
Figure 6.15 Strain ranges measured in F40-1	131
Figure 6.16 Strain ranges measured in F40-2	131
Figure 6.17 Strain range measured in ends A	132
Figure 6.18 The strain ranges measured in specimen F55	132
Figure 6.19 Deflections of beam F70 measured during the fatigue test	133
Figure 6.20 Debonding in F125	133

Figure 6.21 The typical debonding	134
Figure 6.22 Crack growth in specimen F90	134
Figure 6.23 Crack growth in specimen F70	135
Figure 6.24 Crack growth in specimen F55	135
Figure 6.25 Crack growth in specimen F50	136
Figure 6.26 P-N curve in logarithmic representation.....	136
Figure 6.27 S-N curve in logarithmic representation.....	137
Figure 6.28 Comparisons of Load-deflection curves between specimens with fatigue test and without fatigue test.....	137
Figure 6.29 Comparisons of stain at the plate ends between beams F40-2 and S304s	138
Figure 6.30 Comparisons of the stain ranges obtained for specimens F70A, F70* A and F55A.....	138
Figure 7.1 Schematic representations of spew fillet configurations for all cases	149
Figure 7.2 Convergence of the finite element results in the longitudinal direction..	150
Figure 7.3 Convergence of the finite element results in the vertical direction	150
Figure 7.4 Finite element meshes and the principal stress patterns of the without taper cases	151
Figure 7.5 Finite element meshes and the principal stress patterns of the with taper cases	152
Figure 7.6 Comparisons of the shear and the normal stresses on the upper and the lower surfaces.....	153
Figure 7.7 Contour plots of the shear stress for the without taper cases.....	154
Figure 7.8 Contour plots of the shear stress for the with taper cases	155
Figure 7.9 Contour plots of the normal stress for the without taper cases.....	156
Figure 7.10 Contour plots of the normal stress for the with taper cases.....	157
Figure 7.11 Comparisons of the upper interfacial stresses for the without taper cases (a)-(d).....	158
Figure 7.12 Comparisons of the upper interfacial stresses for the with taper cases (e)-(h)	158
Figure 7.13 Schematic locations of crack initiation and paths of crack propagation.....	159

Figure 7.14 Comparisons of the upper interfacial stresses for the without taper case (a), the outside taper case (e) and the inside taper case (g)159

Figure 7.15 Comparisons of the lower interfacial stresses for without taper case (a), outside taper case (e) and inside taper case (g).....160

Figure 7.16 Comparisons of the effect of fillet size for the strain on the CFRP plate bottom surface160

Notation

Latin symbols

A	area
a	length of taper/length of crack
b	width
C, m	crack growth material constants
c	length of lap
E	Young's modulus
E'	Young's modulus for plane strain case
F	strength parameters
G	shear modulus /energy release rate
G_c	fracture toughness
h	step length
I	second moment of area
i	step number
K	slope parameter /stress intensity factor
k	slope of the taper
L	length
L'	effective length
M	bending moment
N	longitudinal force /number of cycles
N_s	longitudinal force applied to the end of plate by the spew fillet
P	applied load
R	crack growth resistance /correlation coefficient
S	compliance parameter /number of steps
T	temperature
T_g	glass transition temperature
t	thickness
t_{end}	thickness at the end of the taper
u	longitudinal displacement
V	volume fraction /shear force
ν	Poisson's ratio /transverse displacement

Greek symbols

α	thermal expansion coefficient
γ	shear strain
ε	normal strain
Δ	range
δ	longitudinal displacement of the adhesive in joints /small distance from the plate end
η	adhesive thickness in joints
θ	angle between the load direction and the fibre direction
σ, σ'	normal stress
$\sigma_{I_{max}}$	maximum principal interfacial stress
τ	shear stress

Subscripts

1	fibre or longitudinal direction /butt joints
2	transverse direction /shear-lap joints
6, 12	in-plane
I	Mode I
II	Mode II
a	adhesive
b	beam
c	composite
f	fibre/failure state
m	matrix
max	maximum
p	plate
pb	plate bottom
u	ultimate state

Abbreviations

FRP	Fibre Reinforced Polymer
CFRP	Carbon FRP
GFRP	Glass FRP
PFRP	Pultruded FRP
RC	Reinforced Concrete
FE	Finite Element

Chapter 1

Introduction

With over fifty years of excellent performance records in the aerospace industry, advanced composite materials have been introduced, followed by rapid growth, in the application in construction around the world. These high-performance materials have been familiarized by the civil engineer and have been utilized in construction, particularly in the upgrade and the rehabilitation of bridges and building structures. This chapter provides an overview about these new materials, of which the behaviour is quite different from that of the conventional materials such as concrete, steel and wood. After the applications of composites materials in civil engineering are reviewed, the outline of the current research study is presented, which focuses on the strengthening of steel beams.

1.1 Advanced composite materials

The field of composite materials is both old and new. It is old in the sense that most natural objects, including the human body, plants, and animals, are composites. It is new in the sense that only since the early 1960s have engineers and scientists exploited seriously the vast potential of fabricated fibrous composite materials. Development of new composites and new applications of composites is now accelerating.

1.1.1 Definition and characteristic

Simply, a composite is a material that is composed of two or more distinct phases, as shown in Figure 1.1. Thus a composite is heterogeneous. The fibrous composites studied here are materials in which one phase acts as a reinforcement of a second

phase called the matrix. The objective is to combine the fibres and the matrix to form an efficient material for the intended application.

A wide variety of fibres and matrix materials are now available for use in advanced composites. The selection of the specific fibre and matrix to be used in a composite is not arbitrary. The two or more phases of a composite must be carefully chosen if the composite material is to be structurally efficient. The behaviour and properties of composites are determined by the properties of the constituents composed, the form and the structural arrangement of the constituents and the interaction between the constituents.

1.1.2 Historic development

Clayman [1] indicated that one of the most efficient structures known is the muscles of the human body. Other obvious examples of naturally occurring fibrous composites include the wings of a bird, the fins of a fish, trees, and grass. All of these structures are typified by two or more phases, one of which is stronger and stiffer than the others and serves as the primary load-carrying component. Wainwright [2] also reported the mechanics of a wide variety of organisms that are fibrous composites.

The earliest applications of composites were conducted by the Egyptian as early as 4000 B.C. in making laminated writing materials from the papyrus plant [3]. However, it was not until 1939, roughly 6,000 years later, that continuous glass fibres were produced commercially. Without doubt, the progress in the use of fibrous composites in the latter half of the 20th century has been much greater than that during the preceding 6,000 years.

The applications over the past quarter-century have been primarily in speciality areas such as athletic equipment and aerospace structures. More recently the applications are seen in civil infrastructures, including the all-composite bridges. It is clear that as more engineers become familiar with the potential engineering and economic advantages, as well as the analysis and design procedures with these materials, the number and range of applications will grow even more rapidly. And as

the amount of material produced increases, the cost/weight ratio will continue to decrease, thereby making composites more affordable for even more applications.

1.1.3 The benefits of the composite materials

Indeed, the advantages of composite materials are many and varied due to the numbers of materials for either the fibres or the matrix. Generally, composites are often the preferred material for designers for a variety of reasons, including low weight, high stiffness, high strength, electrical conductivity or nonconductivity, low thermal expansion, corrosion resistance, longer fatigue life, optimal design, reduced maintenance, etc.

1.1.4 Applications of composite materials

Composite materials have been applied in a number of fields [4], which mainly include:

- Aerospace [5], including aircraft, rockets, space systems, areopropulsion etc.
- Transportation, including automobiles, trucks, railway carrier etc.
- Marine, including fishing boats, military ships, racing sailboats etc.
- Recreational and sporting equipment, including bicycles, boats, rackets etc.
- Infrastructure, including buildings, bridges, windmill etc.

1.2 Mechanics of composite materials

Composite materials can be classified into three categories depending on the type, geometry and orientation of the reinforcement phase [6]. The composite materials used in civil engineering are mostly fibre reinforced polymer (FRP). FRP are mainly formed through the physical combination of two materials: fibres and polymer.

1.2.1 Fibres

A wide variety of fibres are available for use in composites, and the number is ever-increasing [7]. In civil engineering, three types of fibres dominate: glass, aramid and carbon. Glass fibres have been in use since the 1930s; however, it was only in the 1960s that carbon and aramid fibres which exhibit significantly higher stiffness were developed for structural applications. These new high-specific stiffness (stiffness divided by density) and high-specific strength (strength divided by density) fibres are called advanced fibres. Table 1.1 shows the indicative properties of the different fibres [8]. Of the properties the most important that differ between the fibre types are tensile stiffness and strength.

Glass fibre is the most widely used reinforced material. Glass fibre accounts for almost 90% of the reinforcement in thermosetting resins. The strongest glass fibre type is E-glass; the other two are S-glass and D-glass. The strength of glass fibres is not advanced like aramid and carbon fibres. Moreover, it is sensitive to moisture and stress corrosion at high stress levels. Nevertheless, glass is an important engineering fibre because of its high specific strength and low cost.

Aramid fibre is produced by spinning long-chain polyamide polymers using standard textile techniques. It is better known under the trade name Kevlar. The low-density, high-tensile-strength, low-cost fibre produces tough, impact resistant structures with about half the stiffness of carbon structures. However, the poor compressive and shear strength and sensitivity to elevated temperatures, moisture and ultra violet radiation limit the use of Aramid fibres in civil engineering.

Carbon fibre is characterized by a combination of light weight, high strength and high stiffness. Their high modulus and strength depend on the degree of preferred orientation. Carbon fibres are available in a variety of different grades, according to the process by which they are manufactured: high strength (HS), high modulus (HM) and ultra-high modulus (UHM). For structural strengthening purposes, carbon fibres are the most suitable and were used in the study presented.

1.2.2 Matrices

The matrix protects the fibres from the environment and transfer forces between the fibres. Polymer matrices include thermoset (epoxy, polyester) and thermoplastic (poly-ether-ether-ketone (PEEK), polysulfone); of the two thermoset is mostly used in civil engineering. The polyesters were the first resins that found widespread applications in fibre-glass-cloth composite systems, which have been used in the 20⁰ - 75⁰C temperature range. Epoxy resins are capable of upper service temperatures in the range from 125 to 175⁰C, depending on the composition. Moreover, epoxy resins have good strength, bond, creep properties and chemical resistance. Therefore, epoxy resin is more favoured than polyester in civil engineering, in which the materials usually are exposed under sun shine, despite being more expensive than polyester. The properties of matrix materials are also shown in Table 1.1 [8].

1.2.3 Composites

Composite materials are often both heterogeneous and anisotropic. Because of the inherent heterogeneous nature of composite materials, they can be viewed and analyzed at different levels and on different scales, depending on the particular characteristic and behaviour under consideration. In engineering applications, the material usually is assumed homogeneous and the effects of the constituent materials are detected only as average apparent properties of the composite. The composite, mechanical properties are dependent on the fibres, the matrix, the fibre amount and the fibre direction. Figure 1.2 shows how the properties of a unidirectional or quadriaxial composite vary as the direction of loading is rotated with respect to the fibre direction [8].

For structural strengthening purposes, it is most common to use unidirectional composites, which was also used in this study. The unidirectional composites are composed by the continuous fibres in the same direction. It may be manufactured in a variety of ways, including from prepreg tapes, filament winding, pultrusion, or resin transfer molding (RTM). The stiffness and the strength in the fibre direction, especially the stiffness, are usually dominated by the fibre properties and are typically

much greater than in the transverse direction, depending on the matrix material and the quality of the fibre/matrix bond. The properties of a unidirectional composite are orthotropic, with different properties in the material principal directions (parallel and perpendicular to the fibre). For a sufficient size in the transverse plane (perpendicular to the fibres), the effective properties in the transverse plane may be isotropic. Such a material is called transversely isotropic.

The properties of a composite are controlled by the relative volume of fibre and matrix used. The fibre volume fraction V_f is defined as

$$V_f = \frac{\text{volume of fibres}}{\text{volumn of composite}} \quad (1.1)$$

V_f is normally 30-60%.

The longitudinal modulus E_1 , or modulus of elasticity in the fibre direction, can be predicted very well by Eq. (1.2) below, called the rule of mixtures (ROM) formula. The main assumption in this formulation is that the strains in the direction of the fibres are the same in the matrix and the fibre. This implies that the fibre-matrix bond is perfect.

$$E_1 = E_f V_f + E_m (1 - V_f) \quad (1.2)$$

where E_f and E_m are elastic modulus of fibre and matrix, respectively.

In the determination of the modulus in the direction transverse to the fibres, the main assumption is that the stress is the same in the fibre and the matrix and the fibre-matrix bond is perfect. The transverse modulus E_2 can be given as:

$$\frac{1}{E_2} = \frac{1 - V_f}{E_m} + \frac{V_f}{E_f} \quad (1.3)$$

The mechanics of materials approach leads to a ROM equation for the in-plane (longitudinal) Poisson's ratio ν_{12} :

$$\nu_{12} = \nu_f V_f + \nu_m (1 - V_f) \quad (1.4)$$

and in-plane shear modulus G_{12} :

$$\frac{1}{G_{12}} = \frac{1 - V_f}{G_m} + \frac{V_f}{G_f} \quad (1.5)$$

where ν_f and ν_m are the Poisson ratio of the fibre and of the matrix, respectively, and G_m and G_f are the shear modulus of the fibre and of the matrix, respectively.

A thin, unidirectional laminate is assumed to be under a state of plane stress. Therefore, the stress-strain relationship along the principal material axes can be determined by the above parameters in accordance with Hook's law of elastic mechanics:

$$\begin{bmatrix} \varepsilon_1 \\ \varepsilon_2 \\ \varepsilon_6 \end{bmatrix} = \begin{bmatrix} S_{11} & S_{12} & 0 \\ S_{21} & S_{22} & 0 \\ 0 & 0 & S_{66} \end{bmatrix} \begin{bmatrix} \sigma_1 \\ \sigma_2 \\ \sigma_6 \end{bmatrix} \quad (1.6)$$

where $[\varepsilon]$, $[\sigma]$ and $[S]$ are the principal strain, the principal stress and the compliance matrices, respectively. The element ε_6 in $[\varepsilon]$ is equal to half of shear strain γ_{12} . In $[S]$

$$S_{11} = \frac{1}{E_1}, S_{12} = S_{21} = -\frac{\nu_{12}}{E_1} = -\frac{\nu_{21}}{E_2}, S_{22} = \frac{1}{E_2}, \text{ and } S_{66} = \frac{1}{2G_{12}}$$

In the case when the laminate is loaded in some arbitrary direction, the principal matrices should be adjusted to:

$$[\sigma] = [T][\bar{\sigma}], [\varepsilon] = [T][\bar{\varepsilon}], \text{ and } [\bar{S}] = [T]^{-1}[S][T]$$

where

$$[T] = \begin{bmatrix} m^2 & n^2 & 2mn \\ n^2 & m^2 & -2mn \\ -mn & mn & m^2 - n^2 \end{bmatrix} \quad (1.7)$$

in which $m = \cos\theta$ and $n = \sin\theta$. θ is the angle between the load direction and the fibre direction.

1.2.4 Failure modes and criteria

Strength is more difficult to predict than the elastic properties because it depends on the mechanisms of damage accumulation and failure as well as on the properties of the constituents, and the failure behaviour of fibre composites is often complex. Damage and fracture of composite materials may occur in a variety of failure modes including the following:

- Axial tensile failure: tends to occur on fibre breaking and fail in a brittle manner.

- Transverse tensile failure: tends to occur on fibre-matrix debonding or matrix cracking.
- Axial compression failure: tends to occur on fibre buckling.
- Transverse compression failure: tends to compressive failure in the matrix and/or fibre crushing, or lead to an overall shear failure mode.
- In-plane shear failure: tends to occur on matrix cracking and/or fiber-matrix debonding.

Failures of composites subjected to arbitrary (in-plane) stress states are more complex. A number of failure criteria have been proposed, and the most popular ones among these criteria are: maximum stress criterion, maximum strain criterion, Tsai-Hill failure criterion [9], Tsai-Wu failure criterion [10], and truncated-maximum-strain criterion.

Tsai-Hill criterion, the most commonly applied to composite materials [11], is suitable for multiaxial in-plane loading when the applied stress are both tensile or both compressive:

$$\frac{(\sigma_1^f)^2}{(F_1)^2} - \frac{(\sigma_1^f \sigma_2^f)}{(F_1)^2} + \frac{(\sigma_2^f)^2}{(F_2)^2} + \frac{(\sigma_6^f)^2}{(F_6)^2} = 1 \quad (1.8)$$

where σ_1^f , σ_2^f and σ_6^f are the stresses in the composite, and F_1 , F_2 and F_6 , are the corresponding strength parameters, which usually are obtained by tests.

More information on composite mechanics and failure criteria can be found in references [12-14].

1.3 Use of composite materials in civil engineering

The earliest use of composites in the civil infrastructure commenced during World War II when progress was made with the manufacture of Radomes to house electronic radar equipment [15]. The main growth of interest and technology of FRP in construction were commenced in the 1960s with the development of higher strength, higher stiffness and lower density FRP materials. As the cost of FRP materials

continues to decrease and the need for aggressive infrastructure renewal becomes increasingly, FRP materials are now finding wider acceptance in the conservative infrastructure construction industry. Hollaway [15] presented a chart for the progressive development of FRP composites utilization from the 1970s to the present time, which is reproduced in Figure 1.3.

1.3.1 All composite structures

The production processes of composite structure are different from conventional structures. The FRP materials and their various manufacturing methods, especially the pultrusion technique, lend themselves to the development of building systems and building blocks.

In 1974 the first all composite building structure was erected in Lancashire, UK [15]. The system was constructed from a series of unit building block and consisted of an icosahedron shape in which the flat surfaces of the geometrical form were folded into four pyramidal shapes (the building blocks), which were all joined along their flanged edges. The blocks in this system were manufactured by hand lay-up, a manual production method.

From the mid-1980s, the development of an automated building block was undertaken by Maunsell Structural Plastics, London [15]. This Advanced Composite Construction System (ACCS) construction consisted of a number of interlocking fibre reinforced polymer composite Maunsell plank units that can be assembled into a number of different high performance structures for use in the construction industry. Three examples manufactured by this system are Aberfeldy Bridge [16], a two-storey building [17] and Bonds Mill Bridge [18].

In 2002, Europe's first plastic public highway bridge, made entirely from glass FRP (GFRP) and carbon FRP (CFRP) decks and main girders, was developed by Advanced Structural Systems for Tomorrow's Infrastructure (ASSET) [19], a European consortium led by Mouchel Parkman. The objectives of ASSET were to develop a competitively priced structure with distinct user benefits, such as durability,

lightweight, as well as a speedy system of construction. The focus was on the development of an optimised profile as a structural member capable of carrying various loads and made of glass/carbon fibres and thermosetting resin, manufactured by pultrusion.

Reviews of the all composite structures constructed in recent years were presented by Turvey [20] and Keller [21]. They indicate that two principal types of connection - bolted connections and adhesively bonded connections - were used for Pultruded FRP (PFRP) profiles. Although the latter allow for a much smoother and uniform load transfer and offer better durability [21], in practice, the former appear to be the preferred form of connection in PFRP materials [20]. Mottram and Zheng [22] and Mottram and Turvey [23] present reviews on the research to understand and develop practical bolted connections for PFRP structural systems. To improve the understanding and applications of PFRP structural systems, research has also been done for the material properties [24], and the structural performance of beams [25], columns [26] and frames [27].

1.3.2 Upgrade of non-metallic structures

It must be noted that applications of all composite structures up to date have been in the realm of demonstrators rather than in the commercial area. However, the applications in upgrade and retrofit, especially for non-metallic structures, are worldwide as reinforcement using FRP is cheaper and better than conventional materials and techniques.

Significant research has already been conducted on the use of FRP for strengthening of beams and slabs. Carolin [28] has made an experimental and theoretical study on strengthening for increased shear bearing capacity of RC beams. Saadatmanesh and Ehsani [29] and An et al. [30] indicated the flexural strength of RC beams can be significantly increased by gluing GFRP plate to the tensile face. Quantrill and Hollaway [31] introduced the prestressed method in this reinforcing technique. Meanwhile, a number of applications were conducted to strengthen

buildings in UK [32], Switzerland [33] and USA [34], and bridges in UK [35], Switzerland [36], Sweden [28] and USA [37].

Wrapping a column with fibre composite significantly increases the structural capacity of the column as well. Much work has been carried out in the USA [38,39] and Japan [40] with the aim of developing cost-effective retrofitting to increase the seismic resistance of columns. Teng and Lam [41] provided a critical review of existing studies on the behaviour of FRP-confined concrete and the modelling of this behaviour. Some applications have been reported by Nanni [42] and Hollaway and Head [43].

In addition to the strengthening of RC beams and columns, FRP can also be used in many other non-metallic structures. Recent research developments have focussed upon hybrid systems that combine advanced composites with concrete [43]. An extensive programme of work has been undertaken at Southampton on the use of concrete filled FRP tubes [44]. FRP materials in the form of externally bonded laminates and near surface mounted bars can be used for the strengthening of masonry structures [39,45,46]. A number of techniques have been proposed and some of them have actually been applied in practice to increase the shear capacity and the flexibility of wood members [33,46]. Ojha [47] reported applications for silos, chimneys, etc.

1.3.3 Upgrade of metallic structures

Using FRP materials to upgrade metallic (steel, cast and wrought irons) structures is, so far, not as widespread as the upgrading or retrofitting of RC structures, as it poses a different and a more difficult set of problems [48]. However, since the use of FRP provides a cost saving in the region of around 18% over steel, FRP strengthening is becoming an attractive technique for extending the life of metallic structures, especially in cases where there are severe access constraints, with associated high costs and installation time.

Research has now established the effectiveness of strengthening of metallic beams by bonding CFRP plates. Mertz and Gillespie [49], Sen et al. [50], Moy and Nikoukar

[51], Tavakkolizadeh and Saadatmanesh [52], and Nikoukar [53] confirmed the improvement of strength and stiffness of metallic beams with bonded CFRP plates. Furthermore, two innovative methods, prestressing the CFRP plate [54] and load-relief jacking [55], were introduced to transfer permanent stress from metallic beams to CFRP plates. Smith and Teng [56], Denton [57] and Mukhopadhyaya and Swamy [58] investigated the interfacial stresses in the retrofitted beam and indicated the bonding is the weakest link in metallic strengthening due to the high stress concentration. The fatigue performance of metallic beams with CFRP bonded plates was investigated by Miller et al. [59], El Tawil et al. [60] and Nikoukar [53].

A number of metallic beams in building or bridge have been strengthened with CFRP plates. Garden [61] has described carbon and glass fibre prepreg layers being applied around the flanges and web of a curve steel beam in a history building to restore the flexural and torsional capacity. Moy et al. [62] reported that CFRP plates were chosen to upgrade the cast iron beams by bonding onto the tensile flanges in London underground systems. Miller et al. [59], Hollaway and Cadei [48], Luke and Canning [35] and Dodds [63] reported that bridge metallic girders were reinforced by CFRP in some practical applications.

Moy et al. [62,64] and Leonard [65] reported using carbon fibre composite strengthening for cast iron struts, which brace the brick walls of ventilation shafts at Shadwell station of East London Railway. The struts are of cruciform section and ultra-high-modulus carbon fibre composites were placed on two opposite arms of the cruciform strut.

Polymer composites and high-strength epoxy adhesives used to repair damaged steel connections could help many structures withstand earthquakes. Mosallam et al. [66] reported the results of a pilot research project on the use of polymer composites and high-strength adhesives for the structural repair of damaged steel frame connections. The primary repair system developed consists of 3-D braided graphite/epoxy composite connectors attached to the flanges of both beams and columns by adhesives or bolts.

More introductions to FRP applications in Civil Engineering can be found in reviews from references [15,33,48,67-71].

1.4 Outline of current study

1.4.1 Background

Hollaway and Cadei [48] listed several reasons for the structural repair and upgrade. Firstly, the design strength of structures may not be achieved in practice due to design errors, the use of inferior materials, or poor construction. Secondly, in service, increased safety requirements and increase in the magnitude or intensity of applied loads, a change in use or modernization or an upgrading of design standards may render all or part of a structure inadequate. Finally, the load-carrying capacity of structures may be compromised by deterioration of the material as a result of corrosion.

In the UK, the overground railway system owned and maintained by Network Rail has 42,700 bridges, of which 39% are metallic. The Highways Agency and County Councils and Unitary Authorities are also responsible for a large number of metallic structures [53]. According to the National Bridge Inventory compiled by the Federal Highway Administration (FHWA), more than 43% of the total of 587,550 bridges in the US are made of steel [72]. In addition to corrosion, many of these are in need of strengthening due to increased vehicle loading and under-investment in the maintenance regime. In the US, for the seven year period between 1990 and 1996, 17% of the Federal-aid highway funds were spent for rehabilitation and replacement of existing bridges whereas only 4.5% was spent for construction of new bridges [43].

From the reviews in Section 1.3.3, using CFRP to upgrade metallic structures was focused on strengthening beams in building or bridges. But this application requires a number of considerations. Firstly, the lateral buckling in the compression flanges of the metallic beams should be considered. Secondly, the elastic modulus of the CFRP composites used in construction should be higher than that of the metal. Finally, the

stress concentrations at the end of the reinforcing composite plate need to be carefully considered to prevent debonding since one of the weakest links in the repaired metallic beam is the bonding.

In the above considerations, the structural adhesive bonding is a very important issue. Buyukozturk et al. [73] indicated that the potential of brittle debonding failures is an important concern regarding the effectiveness and safety of a bonded structure. To date, design method and technique are not sophisticated and FE analysis and high safe factors were adopted.

CIRIA report C595 [8] indicated that further research and testing are required in most aspects of externally bonded FRP strengthening of metallic structures. Specific areas requiring further research for design include:

1. The effect of differential thermal expansion on the adhesive joint
2. Delamination strength of wrought iron substrates
3. Laboratory tests on the application of FRP to riveted and bolted structures
4. Production of S-N curves for FRP strengthening systems.
5. Experimental validation of elastic and fracture mechanics approaches to adhesive joint analysis for FRP-metal joints (including tapered plates)
6. Experimental validation of curtailment length requirements
7. Calibration of factors of safety for adhesion strength

The study presented in this thesis has included items 1, 4, 5 and 6 of the above aspects. Based on the results obtained, a simple design method will be introduced for steel beams reinforced by bonded CFRP plates.

1.4.2 Contents of thesis

The layout of this thesis is as follows. Firstly, a literature review of the studies and application on beams reinforced with a bonded plate will be given in Chapter 2. It will concentrate on the performance of beams strengthened with externally-bonded plates, the interfacial stress analysis and the fatigue behaviour of the bonding structures.

Secondly, the materials used in this study will be introduced in Chapter 3, which includes the material properties, static and fatigue behaviour, and manufacture. Since the physical properties of metals, CFRP composites and adhesives, in particular, are significantly influenced by age, the manufacture process, the environment and the utilized position, the data provided by the manufactures cannot be directly used and mechanical tests have to be performed to confirm them. Therefore, the material test methods, processes, and conclusions will be included.

The stress analysis of bonding interface will be given in Chapter 4. An analytical solution and a numerical procedure will be presented to calculate the stresses in the beams reinforced by uniform thickness and tapered end CFRP plates, respectively. FE analysis will be employed to validate the analytical results and a parametric study will be reported to show how the maximum stresses have been influenced by the material dimensions and properties.

Next, the static behaviour of bonding in the reinforced beam will be introduced in Chapter 5. After the static tests are described, the following aspects will be discussed: the influencing factors on the strengthening and failure modes of the metallic beams reinforced by different types of CFRP plates, the effects of the taper at the plate ends and of the spew fillet beyond the plate ends, and the validation of the analytical method of calculating the interfacial stresses.

Chapter 6 will detail the fatigue behaviour of bonding in reinforced beams. This chapter will present the laboratory fatigue tests of nine small-scale steel beams bonded with CFRP plates. The results will be discussed to assess the fatigue behaviour of the adhesive joint in the metallic beams bonded with a CFRP plate. S-N curve based the peak stresses of the bonded joints at the end of the CFRP plate to predict the fatigue stress range for the retrofitted beams will be proposed.

The effects of tapers and spew fillets occurring at plate ends in steel beams reinforced with a CFRP plate will be investigated in Chapter 7. A total of eight cases will be compared and discussed. FE analysis will be employed to obtain the stress in the adhesive layer and the strain in the bottom of the CFRP plate.

Finally, conclusion, design suggestions and future work will be given in Chapter 8.

Summarily, the main aspects discussed in this study are stress analysis, static test and fatigue test of reinforced metallic beams, of which the organization is shown in Figure 1.4.

1.5 Summary

In this chapter, firstly, a brief background of advanced composite materials, including definition, characteristics, historical development and applications, was provided. Then, with the introduction of mechanics of composite materials, the complexity of elastic parameters and failure modes of composites due to the particular mechanical properties of fibres and matrices is shown. After that, the wide application and rapid growth of the use of composite materials in civil engineering was reviewed. Finally, background to the current research study, which is to provide a better understanding of the behaviour of steel beams reinforced by bonded CFRP plates, and the contents of this thesis were described.

Table 1.1 Properties of typical fibre, matrix and structural materials

	Tensile Strength (MPa)	Young's Modulus (GPa)	Poisson's ratio	Failure strain (%)	Density (kN/m⁻³)	Coefficient of thermal (1.0⁻⁶/°C)
Fibre materials						
HS Carbon fibre	4300-4900	230-240	0.2	1.9-2.1	18.0	-0.38
HM Carbon fibre	2740-5940	295-390	0.2	0.7-1.9	17.3-18.1	-0.83
UHM Carbon fibre	2600-4020	440-640	0.2	0.4-0.8	19.1-21.2	-1.1
Aramid fibre	3200-3600	125-130	/	2.4	13.9-14.7	2.1
Glass fibre	2400-3500	70-85	0.22	3.5-4.7	26.0	4.9
Matrix materials						
Epoxy	60-85	2.6-3.8	0.3-0.4	1.5-8.0	11.1-12.0	30-70
Polyester	50-75	3.1-4.6	0.35-0.38	1.0-2.5	11.1-12.5	30-70
PEEK	170	3.6	0.3	50	12.6-13.2	47
Conventional structural materials						
Steel (AISI 1025)	394	207	0.3	/	78.0	11
Aluminim (2024 T3)	414	73	0.33	/	28.0	23
Concrete	20	40	/	0.05	24.0	12

Note: HS=high strength, HM=high modulus, UHM=ultra-high modulus, PEEK=poly-ether-ether-ketone

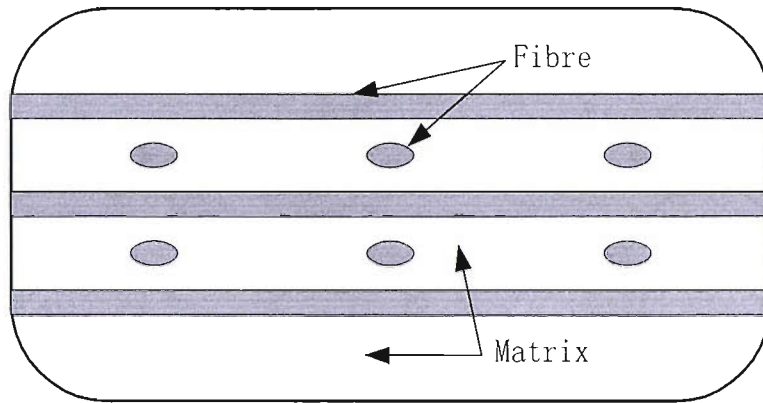


Figure 1.1 Multiphase media

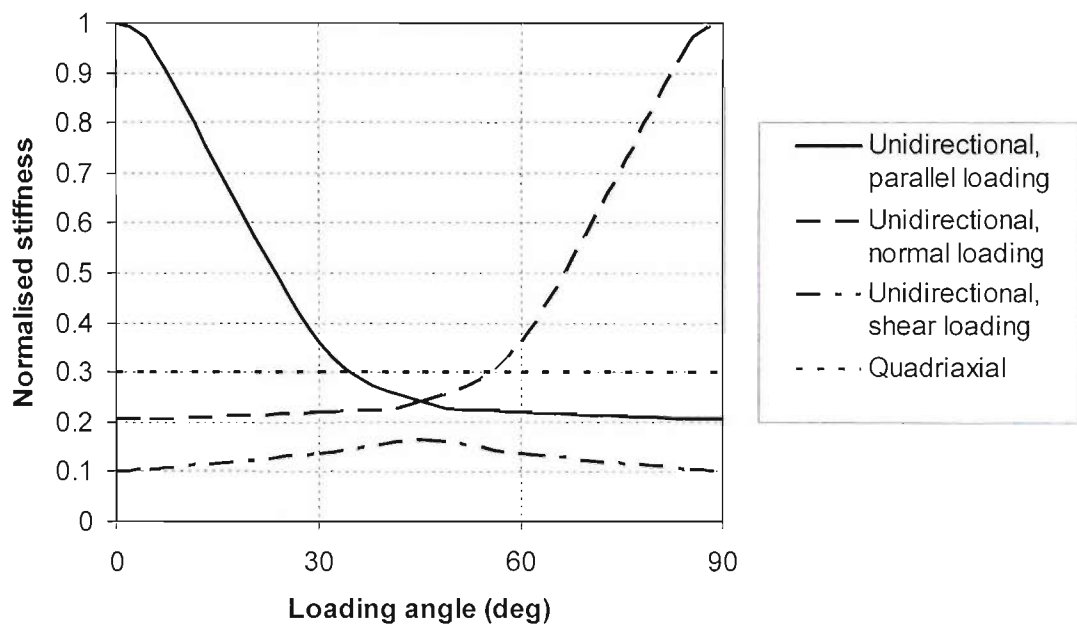


Figure 1.2 Variation of laminate stiffness with the direction of loading [8]

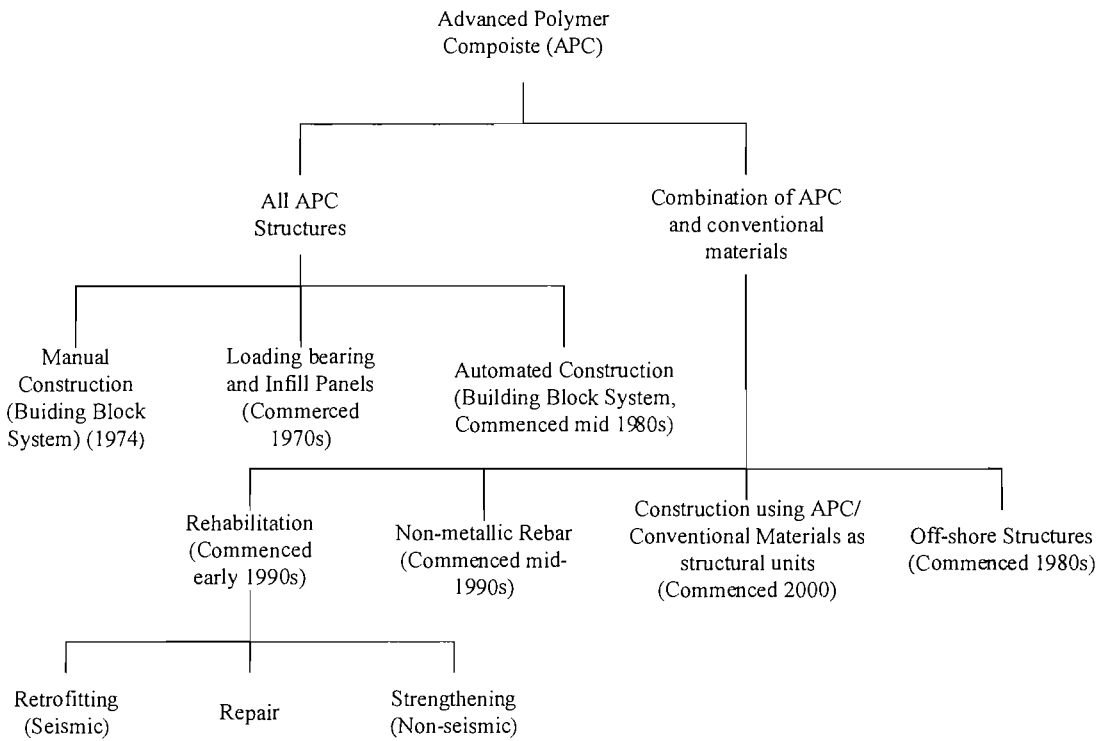


Figure 1.3 Utilisation of advanced polymer composites in construction [15]

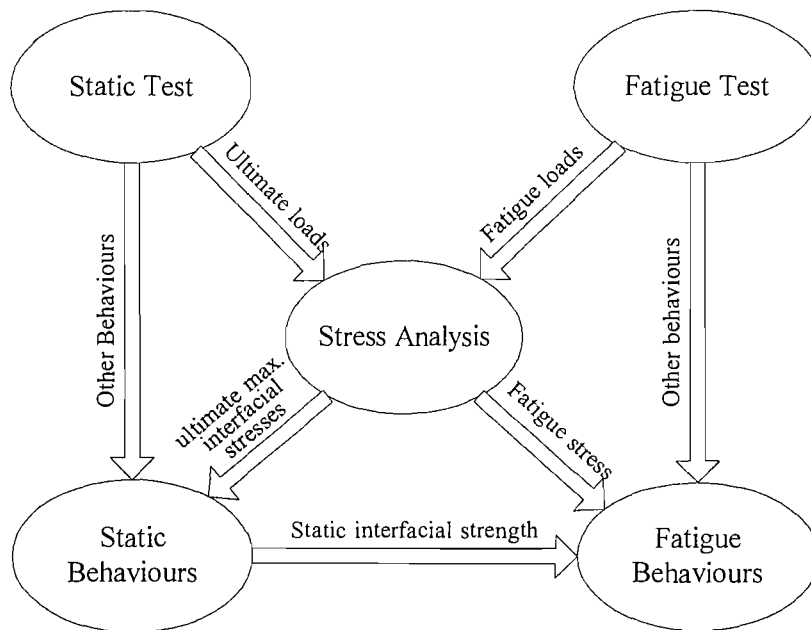


Figure 1.4 Organization of the study

Chapter 2

Literature review

Advanced composite materials have been employed in the aerospace and other industries for many years, but their use in civil engineering is relatively recent. The most popular use of composites in construction has been in repairs and upgrading of beams in bridges and buildings. This chapter gives a review of the studies and applications on beams reinforced with a bonded plate. The review concentrates on the performance of beams strengthened with externally-bonded plates, the interfacial stress analysis and the fatigue behaviour of the bonding structures. Research on the stress analysis and the fatigue performance of lap shear joints is also included, since the bonding behaviour of a composite-reinforced beam loaded in flexure is similar to that of a plated joint loaded in tension.

2.1 Strengthening of beams using externally-bonded plates

Many studies and applications have been made for repair and upgrade of beams. To date, conventional techniques have been gradually replaced by adhesive bonding techniques, where appropriate. With the development of composite materials, such techniques have become popular to reinforce structures. In recent years, composite materials, particularly CFRP, have been widely applied to the strengthening and upgrade of reinforced concrete (RC) and metallic structures.

2.1.1 Conventional techniques

Conventionally, repair and upgrade of concrete or metallic structures involve the use of steel cover plates fixed by bolting, riveting, welding, or clamping. When bolts, rivets and clamps are used, it is very labour intensive. Moreover, the use of bolts,

rivets, and welds may create fatigue sensitive details. Therefore, the adhesive bonding technique, which does not scathe the original structure and hence avoid undesirable crack and stress concentration, was introduced as an alternative.

The first recorded use of bonded steel plates as additional external reinforcement occurred in 1964 in Durban, South Africa, where a concrete beam in a real estate building needed to be strengthened due to a mistake in the construction stage [74]. Since then, this technique has been carried out throughout the world: in Belgium reported by Lerchental [75], in South Africa reported by Fleming and King [76], in Switzerland reported by Hugenschmidt [77], in UK reported by Swamy and Jones [78], in Japan reported by Raithby [79], and in USA reported by Klaiber et al. [80].

In 1975, the first application of bonded steel plates on a bridge in the UK occurred at the Quinton interchange on the M5. Raithby [79] reported that loading tests carried out before and after strengthening demonstrated the effectiveness of the technique in providing increased flexural stiffness and in reducing crack opening under load. Hutchinson [81] reported that the tests of the cores, which were taken through the plates in 1995, showed that the adhesive layer was performing satisfactorily and there was only some slight corrosion at the steel surface.

Although this technique had been applied successfully in practice, there are, however, many disadvantages with the use of steel plates. Firstly, the transport and the mounting of steel plates are difficult due to their heavy weight, and falsework usually is needed to maintain steelwork in position and to apply the pressure for the upside down bonding. Secondly, the possibility of corrosion exists since the steel plates are not protected. Thirdly, steel plates are limited in thickness, of which the minimum is typically 6 mm to prevent distortion during the grit-blasting operation and to provide flatness, and in length, of which the maximum is 6-8 m and joints might be needed to lengthen the plates. Finally, steel plates are difficult to shape and to fit complex surfaces.

2.1.2 RC beams strengthened with CFRP plates

For plate bonding, composites overcome the many disadvantages of steel. Firstly, the composites are lighter, and hence transportation and handling are easier and less falsework is required [82]. Secondly, compared with steel, composites exhibit excellent fatigue and long term endurance. Thirdly, the thickness and the length of composite plates are not restricted. Finally, composites can be produced to fit any complex surfaces. One of the major drawbacks in using composites is, of course, the high material cost compared to steel.

Alexander and Cheng [83], in their study using CFRP sheets to strengthen concrete bridge girders, concluded that bonding of composites was becoming more common and competitive from the practical and economical viewpoint. Moreover, Hollaway [48] indicated that despite fibre composites being between 4 and 20 times more expensive than steel in term of unit volume, the use of composites provides a total cost saving in the region of around 18% over steel when the effects of materials, the cost of installation and traffic management are included. Therefore, composites have in most cases driven out the use of steel.

In 1982, the use of carbon fibre reinforced epoxy resin composites for the post-strengthening of reinforced concrete beams was successfully demonstrated at the EMPA laboratories [33]. Loading tests were performed on more than 100 flexural and 30 shear beams with spans from 2 m to 7 m. Rostasy et al. [84] tested the interface shear strength of bonded carbon fibre plates and applied the results for the retrofitting of a box girder bridge in Germany.

In addition to the above pioneering works, the ROBUST project [32], which was initiated by the UK Government's LINK Structure Composites programme in May 1994, investigated the technical and commercial viability of the use of carbon and glass fibre-reinforced polymer composites as an alternative to steel plates in bridge strengthening applications. It has provided detailed information on the use of FRP for concrete bridge strengthening and showed that FRP is more economical than steel in building repair and upgrade.

Shahawy et al. [85] indicated that the flexural strength of strengthened concrete beams is significantly increased with the number of CFRP laminate layers. Furthermore, Quantrill and Hollaway [31] reported that prestressed CFRP plates have the potential to provide a more efficient solution to the strengthening of concrete beams. While such experiments in laboratories are successful, the practical application on site remains a problem due to the difficulty in maintaining the prestress for a long time. Smith and Teng [86] concluded that the most commonly reported debonding failure occurs at or near the plate end in CFRP strengthened beams. They also showed that additional plate end anchorage can improve the bonding between the CFRP plate and the beam.

The first public structure to be strengthened with bonded CFRP strips was the Ibach Bridge, Lucerne in 1991 [33]. Since then, there have been many more applications [28,43] of CFRP strengthening of RC beams, and the technology is clearly reaching commercial maturity.

Design guidelines have been proposed by Saadatmanesh and Malek [87] in 1998. In September 1999, the Japan Building Disaster Prevention Association (JBDPA) published the Seismic Retrofitting ‘Design and Construction Guidelines for Existing Reinforced Concrete Bridges with fibre reinforced polymer materials’ [15]. A synthesis of the provisions of the Canadian Highway Bridge Design Code for fibre reinforced structures has been published in 2000 [88]. The Concrete Society in UK also published a design guidance for strengthening concrete structures using fibre composite materials in 2000 [89]. ACI Committee 440 published another similar guidance in 2002 as well [90].

In summary, after nearly 20 years of development, the technique of strengthening RC beams with CFRP plates is mature not only in its theoretical advance, but also in practical applications. However, issues on durability and fatigue behaviours still require further study, and long term observations are needed in practical applications.

2.1.3 Metallic beams strengthened with CFRP plates

Whilst relatively few metallic structures have been strengthened and stiffened by CFRP plates to date, some laboratory research has already established the potential of this technique.

Sen et al. [50] reported the results of an experimental investigation to determine the feasibility of using CFRP epoxy laminates to repair steel composite bridge members. Six steel beams acting compositely with a wide reinforced concrete slab, were repaired by 2 or 5 mm thick CFRP laminates, with a Young's modulus of 114 GPa, bonded to the tension flange and tested to failure. In their tests, two sets of clamps were attached over the end of CFRP laminates to prevent peel failure. The results indicated significant ultimate strength gains but increases in the elastic stiffness were relatively modest.

The advantages of using advanced composite materials in the rehabilitation of deteriorating bridges were investigated by Mertz and Gillespie [49]. As part of their small-scale tests, they retrofitted eight 1.52-m-long W203x4.5 steel beams using five different retrofitting schemes. They reported an average of 60% strength increase in CFRP retrofitted systems. They also tested and repaired two 6.4-m-long corroded steel girders. Their results showed an average of a 25% increase in stiffness and a 100% increase in the ultimate load-carrying capacity.

In another study conducted by Tavakkolizadeh and Saadatmanesh [52], a total of three large scale composite girders made of steel beams and a concrete slab were bonded with one, three and five layers of 1.27 mm thick CFRP sheet, with a Young's modulus of 144 GPa. The overall lengths of the sheets were identical but the cut-off points for each layer were staggered to prevent premature failure at termination point due to stress concentration. They reported that the epoxy-bonded CFRP sheet increased the ultimate load-carrying capacity of the steel-concrete composite by 44%, 51% and 76% for one-, three-, and five-layer retrofitted systems, respectively.

The first application of advanced composites for steel bridge girder rehabilitation was cited by Miller et al. [59]. Bridge I-704 carries high average daily truck traffic (approximately 6,000) over Christina Creek just outside of Newark, Delaware. The rehabilitation consisted of bonding one layer of CFRP plates to the outer face of the tension flange of a girder. The 5.25 mm thick FRP plates with a Young's modulus 112 GPa were installed over the entire 230 mm wide flange and full length by using four 1.5 m length sections that had a 300 mm staggered joint and were bevelled at a 45° angle at the ends. The performance of the bonded CFRP cover plates was evaluated using pre- and post- diagnostic field load tests. The results indicated an over 10% increase in global flexural stiffness due to the retrofit.

2.1.4 Metallic beams strengthened with UHM CFRP plates

No reports have been found where ultra-high-modulus (UHM) fibres were applied in laboratory tests, but this section does provide examples where UHM fibres have been used in practice.

The first commercial project to adopt the non-prestressed method of strengthening cast iron beams on a highway bridge by means of tapered CFRP plates is the Bid Bridge in Kent [48]. Twelve 6-m-long CFRP pre-preg plates, 0.5 mm in thickness were bonded together to form the required thickness, were glued to seven of the nine cast iron beams. It was pointed out that the inclusion of tapers reduces stress concentrations in the adhesive at the end of the plates and improves durability.

In the case studies reported by Luke and Canning [35], Nunnery Bridge is a cast iron beam/brick jack-arch bridge over a river at Castle Hedingham, Essex, with a span of 4.9 m. 16 mm thick tapered UHM CFRP laminates bonded to the soffit of the cast iron beams was proposed. Two options were proposed for the bonding of the UHM CFRP plates: factory vacuum-bonded multiple 4 mm thick pultruded CFRP plates with staggered curtailment of the plates to create a taper, or factory vacuum cured pre-preg CFRP laminates with a more gradual taper to a nominal end thickness of 1 mm. The first option was chosen in this particular case, with the plates having minimum tensile modulus of 450 GPa. In another case, the UHM CFRP plates with a maximum

thickness of 24 mm were used to strengthen another cast iron bridge - New Moss Road Bridge, Irlam, Greater Manchester.

Bridge MR46A is the Amersham branch of London Underground's Metropolitan line and carries twin rail trucks over Station Road, Harrow, adjacent to North Harrow Station. Dodds [63] reported that the cross beams, about 9 m in length, and the edge beams, about 26 m in length, were strengthened by pre-preg UHM CFRP plates with a Young's modulus of 360 GPa. 5 m long CFRP plates were attached centrally to the cross beams. These plates have a 1.5 m long taper at each end. 13 m long CFRP plates were attached centrally to the edge beams. These plates have a 3.5 m long taper at each end.

2.1.5 Metallic beams strengthened by innovative methods

In the case where the dead load is too large and the permanent stress needs to be transfer from the metallic beam to the CFRP plates, two methods can be used: prestressing the CFRP plates and load-relief jacking. Both of them are more complex to install and will result in higher stresses in the adhesive joint than the unstressed method.

Luke [54] reported the first known application of the prestressed CFRP technique for flexural upgrading of cast iron bridges on Hythe Bridge, Oxford. Four HM prestressed CFRP plates, 4.5 mm thick, were applied to the bottom flange of each beam, and were stressed to a total of 18 tonnes. Tapers were included at the ends of plates and a means of attaching jacking equipment was provided to the anchorage. It was concluded that the stressed composite technique offered the most satisfactory solution.

Smith [55] reported that Maunders Road Bridge was the first Network Rail cast iron bridge to be strengthened by CFRP laminates. The required strength gain could only be achieved by utilising the combined cast-iron/CFRP composite section to withstand the dead load effects in addition to the imposed vehicle loads. Therefore, an innovative scheme was adapted where the structure was jacked at the midspan

position prior to the application of laminates, and the jacks being released once the bonding adhesive had cured. The results obtained during installation validated the assumptions made during the design process.

2.2 Stress analysis of bonded structures

In bonded structures, joints are often points of weakness where failure occurs. In order to ensure their integrity, a knowledge of the stress distribution in the bonded area is important. In adhesive joints, significant stress concentration in the adhesive occurs at the cut-off ends of adherends, where there is a discontinuity caused by the abrupt termination of the components.

2.2.1 Lap joints

Goland and Reisner [91] presented the classical analysis of the stress distribution in a single-lap shear joint. This analysis simulates the joints as consisting of two elastic beams bonded with an adhesive layer. The effects of the bending moment on the end of the overlap of the adherends due to the load eccentricity are considered first. Hart-Smith [92] proposed analysis procedures and failure criterion which improved upon Goland and Reisner's classical formula. Hart-Smith [93] also extended the classical elastic solution for double-lap shear joints by Volkerson [94] to include both the adhesive plasticity and the thermal mismatch. The closed-form solution for single-lap joints by Goland and Reisner [91] and that for double-lap joints by Hart-Smith [93] are the most widely used and are suggested by the guidance document CIRIA C595 [8]. This is because the explicit analytical expressions for the stresses provided by them are convenient to use by designers.

Wu et al. [95] pointed out the errors in the classical theory by Goland and Reinssner and proposed a correct expression for the adhesive stresses in Goland and Reinssner's solution. An improvement on the inconsistent plane stress and plane strain relations used in Goland and Reissner's paper was achieved. Tsai et al. [96] improved the classical theoretical solutions for both single-lap and double-lap joints.

The adherend's shear deformations are included in the theoretical analyses. The improved theoretical solutions are validated to provide a better prediction than the classical solution by comparing with the experimental and numerical solutions. Her [97] presented a simplified model for both single-lap and double-lap joints. This study also shows good agreement between the analytical and the finite element results.

2.2.2 End effect of lap joints

All of the literatures reviewed in the above sections confirm that high stress concentrations occur at the cut-off ends of adherends. To reduce these stress concentrations, tapers and spew fillets are introduced at the ends of the overlap.

The use of a taper at the ends of the adherends has been shown to effectively limit peel stresses by Hart-Smith [98], Vinson & Sierakowski [99] and Adam et al. [100]. The experimental and FEA results of Sancaktar and Nirantar [101] indicate that tapering the ends of the adherends had a substantial influence on the stress distribution and the failure load for single lap joints.

Hart-Smith [98] proposed the use of scarf joints and step lap joints to minimise stress concentrations. But the geometric complexity of the tapered joint has posed a mathematically intractable problem for any closed-form solutions. Amijima et al. [102] reported a modified computer program, which was applied to analyse the bond stresses in tapered single and double lap joints. The modification was based on the use of the offset beam element for the portion of the tapered adherend(s). Lee [103] developed a non-linear numerical analysis technique for the tapered joints. The numerical results obtained were very accurate and stable, showing the major advantages of the integral equation technique over other numerical methods. Albat and Romilly [104] presented an analytical method to calculate adhesive stresses for tapered double sided reinforcedments and tapered double-doubler joints. In their analysis, stepped-lap joints were treated as tapered double-doubler joints with changing thickness of the substrate.

It is unlikely that closed-form solutions can be derived to predict the effects of spew fillets as well as tapers. Finite element analysis has to be used to calculate the adhesive stresses in lap joints with spew fillets. Adam et al. [100] examine the effect of triangular spew fillets and tapers occurring at the ends of the overlap. They indicated that the most highly stressed region in an adhesive joint occurs at or near one corner and, in theory, the singularity at the sharp corner implies infinite stresses. But the maximum shear stress in the adhesive reduces with the size of the spew fillet and an improvement in the strength of the joints of over five times when an inside taper combined with a spew fillet was introduced. Tsai and Morton [105] also indicated that the adhesive shear and peel stress concentrations in the adhesive can be reduced greatly by introducing a fillet at the end of the overlap through experimental and numerical results. Moreover, the agreement between the results was good if the geometrically nonlinear deformation was considered in the numerical analysis.

Lang and Mallick [106] developed a comparative analysis of the effect of the adhesive spew geometry on the stress state in single lap joints. Several different spew configurations were considered, which included full and half triangular, full and half rounded, full rounded with fillet, oval, square and arc. The analysis shows that shaping the spew to have a smoother transition in joint geometry can significantly reduce the peak stresses. Lang and Mallick [107] also investigate the effect of a recess (i.e. removing portions of the adhesive from the interior of the overlap) on the spew.

Belingardi et al. [108] showed the magnitudes of the stress peaks for both the shear and the peeling components in single lap joints decrease with the reduction of the spew fillet angle and the maximum advantage is obtained with a 45° angle, since smaller angles are more difficult to achieve in practice. In accordance with their FE and experimental results, Kadioglu et al. [109] also recommended that high strength adhesive in lap joints which have a limited strain to failure should be tested with a 45° fillet. Rispler et al. [110] developed a method to optimise the shape of adhesive fillets in lap joints, which can reduce the peak peel stresses by up to 66%.

2.2.3 Retrofitted beam

The distribution of the interface stress in a composite beam loaded in flexure is similar to that in a plated joint loaded in tension. Roberts and Hajikazemi [111] presented an analytical solution for predicting the displacements, strains and stresses in reinforced concrete beams, strengthened on the tension faces with externally bonded steel plates. But this solution is restricted to a uniform distributed load and is complex. Malek et al. [112] presented a method to predict the distribution of interfacial stresses in RC beams reinforced with a FRP plate. The maximum interfacial stresses are given by two simple equations. Smith and Teng [56], having carried out a review of the approximate closed-form solutions for interfacial stresses in literature, presented a new solution which was intended for application to beams with a bonded thin plate. The beams could be made of any materials. However, the bending moment in the adhesive layer was ignored in Smith et al.'s model, which violates the equilibrium condition in the differential segments of the adhesive layer. Rabinovich & Frostig [113] and Yang et al. [114] presented closed-form high-order analyses of reinforced concrete beams strengthened with FRP plates, which satisfy the free surface condition at the ends of the adhesive layer. The solution methodology is general in nature and can be applied to the analysis of other types of composite structures.

Ascione and Feo [115] developed a finite element model to predict the shear and the normal stresses in the adhesive layer of plated reinforced concrete beams and the numerical results agreed with the experimental results obtained by Jones et al. [116] and the theoretical results presented by Roberts [117]. Miller et al. [59] performed experimental and analytical studies to quantify the force transfer between the CFRP plate and the steel substrate. The analytical solution predicted the longitudinal strain distribution along the CFRP plates and showed that approximately 98% of the total force transfer occurs within the first 100 mm length from the end of the cover plate.

Another important problem in steel beams reinforced with CFRP plates is the large difference between the coefficients of thermal expansion. Typical coefficient of thermal expansion for steel is $10.2 \times 10^{-6}/^{\circ}\text{C}$ and that for CFRP is close to zero. Denton

[57] indicated that substantial longitudinal shear stresses and normal tensile stresses can be developed in the adhesive layer near to the ends of the FRP plate as a result of the difference between the coefficients. For a 50°C temperature increase, the stresses in the adhesive at the ends of the plate could be close to the failure stress.

Hollaway [48] indicated that the CFRP composite plate must be adequately anchored to prevent peeling failure at the end of the members. However, the anchors to the members usually complicate the technique and are not reliable during the long service life. Barnes and Mays [118] indicate that the strengthening technique becomes more practical if the need for end anchorages can be avoided. Therefore, the technique without anchors is preferred. As an alternative to anchors, the taper is used at the ends of the plates to reduce the stress concentrations in the retrofitted beams. All the CFRP plates used by Miller et al. [59] had been bevelled to a 45° angle at all terminations in the experiments. A numerical solution was adopted by Denton [57]. Unfortunately, the shear stress distribution for the tapered plate case obtained by Denton [57] is erroneous.

2.3 Fatigue behaviour of bonded structures

Highway bridges in the UK are designed for lives of 120 years. Depending on the type of highway, components in decks can experience up to 7×10^8 stress cycles [119]. In the US, major highway bridges generally experience more than 1.5×10^6 truck passages per year, which can be translated to between 1×10^8 and 3×10^8 stress cycles during their 100 year service life [120]. Consequently, fatigue damage is one of the main problems that occur in old metallic bridges. It is therefore necessary to predict the fatigue behaviour of the updated bridge structures [121,122]. Hollaway and Cadei [48] pointed out that the adhesive bonding between the CFRP plate and the metallic substrate is the weakest link and its fatigue performance, in particular, is a major consideration. Many studies have been carried out to investigate the fatigue behaviour of the adhesive bonding, but mainly in lap joints. In addition, tests on retrofitted concrete beams and metallic beams have shown that the use of CFRP improves fatigue behaviour.

2.3.1 Fatigue performance of lap joints

Kinloch [123] mentioned three approaches for obtaining the adhesive fatigue properties of a joint. Firstly, thick adherent shear-test specimens are used to obtain information on the bulk adhesive dynamic fatigue properties. The second approach is the testing of model-scale or full-scale bonded structures to establish the fatigue life. This gives more information on the actual joint, but is expensive and cannot be used for other applications. The third one is the use of continuum fracture mechanics to describe crack growth in a joint subjected to cyclic loading. For this, the presence of a crack must be assumed, because the crack initiation period is difficult to model. Since all three approaches have shortcomings, lap joints are employed to test the structural fatigue performance in practice.

Mays and Tilly [119] investigate the fatigue performance of steel-to-steel lap joints for endurance of up to 10^8 cycles. All specimens were of the double-lap type and two grades of two-part cold cure epoxy resin adhesive were used in their tests. A sinusoidal load was applied between a peak load, selected to give failure at endurance up to 100 million cycles, and 10% of that peak at 25 Hz frequency. The fatigue performance of the joints was found to be temperature dependent. The resin used in their study changed little in performance over the temperature range -25°C to 45°C but was considerably weaker at 55°C .

Krenk et al. [124] investigated the crack growth and fatigue life of one-side adhesive lap-joints under cyclic loading. A finite element model was made of the test specimen using 2D isoparametric elements. The adhesive was represented by plane strain elements, while the adherends were represented by plane stress elements, due to the adhesive thicknesses (0.1 mm and 0.3 mm) were much smaller than that of the adherends. The cracked specimen was modelled by ignoring the stiffness of the adhesive elements in the cracked zone, which was used to estimate the crack length from the bending stiffness, measured across the original opening. While static tests indicate higher failure load from joints with relatively thick adhesive, the fatigue tests with cyclic load did not show any significant influence from the adhesive thickness. An S-N curve was developed from the test results.

Cheuk et al. [125] showed the two important features of fatigue crack growth in bonded joints as compared to fatigue crack growth in homogeneous materials are: crack growth rates exhibit a much stronger dependence on the strain-energy release rate; and the crack growth rates are very sensitive to the ratio of mode I to mode II cracking. They tested two specimens of adhesively bonded metal-to-composite double lap joints. Sinusoidal tensile load ranging from 0 to 22 kN at a frequency of 3 Hz was applied to 50,000 cycles. The experiments revealed that fatigue cracks grew within the ply of the composite adherend adjacent to the adhesive. Two different crack paths were observed for crack initiated from the spew fillet. The scanning electronic microscope (SEM) analysis also indicated that the tensile mode seems to be the dominant mode of crack growth when the crack is short and the shear mode becomes dominant as the crack grows longer.

Keller and Tirelli [126] reported research in the fatigue behaviour of adhesive connections has been done mainly in areas outside of civil engineering load-carrying structures (aircraft and vehicle construction). In these areas, traditional laminated FRP materials are mainly used and the adhesive thicknesses are very thin: far below 1 mm. Much larger tolerances in the connections of civil engineering structures require adhesive thicknesses of up to 20 mm. Therefore, it is difficult to compare and transfer research results between these very different area and modes of application.

Keller and Tirelli [126] investigated the fatigue behaviour of a symmetric full-scale double-lap connection of which the geometry was chosen in order to eliminate the scale effect and to minimize peeling stresses. Ten fatigue experiments were conducted. The specimens were sinusoidally loaded in tension at an amplitude ratio of $R=0.1$ and at different upper boundary values from 20% up to 90% of the average static failure load of the reference specimens. The fatigue experiments were performed load-control at frequencies up to 10 Hz. The failures of specimens were very brittle, without announcement by visible cracks on the specimen surfaces or deformations. The crack initiated and propagated within the last cycle and started in the adhesive fillet, at the location of maximum peeling stresses and then entered directly into the 10 mm thick profiles at a 45° angle. The experiments showed a fatigue limit at approximately 25% of the static failure load at 10 million cycles.

de Goeij et al. [127] give an overview of studies performed on adhesive composite joints under cyclic loading from experimental and analytical methods, and indicated that characterising or predicting the fatigue properties of a complex joint in an actual structure will be difficult with data obtain from simple test specimens. Obtaining S-N curves from prototypes is effective but can be very expensive. Until now, modelling is restricted to the adhesive region itself, while in many experiments, failure is at the interface. This boundary zone at the interface is not taken into account in the modelling programs.

2.3.2 Fatigue performance of RC beam strengthened with Steel/CFRP

Oh et al. [128] investigated the fatigue behaviour of reinforced concrete beams strengthened with steel plates. Six strengthened beams were tested under cyclic load, of which the maximum levels were 60% (76 kN), 70% (88 kN) and 80% (100 kN) of the static failure load (126 kN) and the minimum level was set to 10 kN. The frequency of the fatigue load was 3 Hz and the repetition of load continued up to 4,000,000 cycles, if not failed. The results show that the fatigue resistance of strengthened beams is much higher than that of unstrengthened beams; the failure of the strengthened beams was primarily caused by the sudden separation of steel plates without causing large deformation; a fatigue load below 70% of the static failure load does not decrease the ultimate strength of the strengthened beams.

In the area of fatigue behaviour of RC beams strengthened with CFRP, the earliest research has been conducted by Meier et al. [129], as reported 1992. In their study, the beam had a span of 2 m, was 300 mm wide and 250 mm deep. The CFRP sheet was 0.3 mm by 200 mm in cross section and was bonded to the tensile face. Beams strengthened with CFRP sheets were cycled at moderate load levels from 1 to 19 kN at a frequency of 4 Hz, and observed for damage to the sheet and the sheet-to-concrete bond. Failure of the beams was initiated in each instance by fatigue failure of the reinforcing steel bars. The test results showed that the use of CFRP improved fatigue behaviour.

Furthermore, Shahawy and Beitelman [130], El-Tawil et al. [60] and Hefferman and Erki [131] investigated the fatigue behaviour of reinforced concrete beams externally strengthened with thin CFRP laminates, which are generally preferred to the more rigid, thicker, CFRP plates because they are easier to handle and they do not peel off easily, especially if they are wrapped around the stem of the girder. In the study of Hefferman and Erki [131], ten RC beams attached with CFRP sheets were loaded with a sinusoidal load at 3 Hz. The tensile stress ranges, which would meet the short, medium and long life requirements, are approximately from 60%, 50% and 40% of the nominal yield stress of the steel bars, respectively, combined with a lower stress limit of 20%. All fatigue failures were initiated by fatigue fracture of one or more of the reinforcing steel bars. The fatigue life of a CFRP strengthened reinforced concrete beam appeared to be at least as long as a conventionally reinforced concrete beam with an equivalent strength subjected to the same loads. No significant degradation in the CFRP sheets or the CFRP to concrete interface occurred due to cyclic loading. Similar results were obtained from testing six 5 m long beams.

Barnes and Mays [118] investigated concrete beams strengthened with CFRP plates. To prevent peel failure at the ends of the CFRP plates, steel plates were bonded to the CFRP plates and secured to the beam using two mild steel bolts. Each beam was subjected to a cyclic load in four-point bending at a frequency of 1 Hz. To achieve a meaningful comparison, the loading options were selected to apply the same loads to give the same stress range in the bar or apply the same percentage of the ultimate load to both plated and unplated beams. All six beams failed in a primary tension flexural mode with no significant shear cracks present. Therefore, it is recommended that the criterion for the fatigue design of CFRP plated beam should be to limit the stress range in the rebars to that permitted in an unplated beam.

In most cases of strengthened concrete beams, it has been observed that failure was initiated by the yielding of the reinforcing steel in tension. However, debonding of the FRP lamination as a secondary failure must be considered as well. Bizindavyi et al. [132] investigated the fatigue failure by the debonding of FRP reinforcement. Various experimental and analytical investigations of the behaviour of bonded FRP-to-concrete joints were carried out by them to gain an insight into the debonding phenomena. As observed from the cyclic bond stress-slip relationships, all cyclic

shear tests showed a quasi-linear hysteretic behaviour with very narrow hysteresis loops, but with decreasing slope as the number of cycles increased. From the S-N curves thus obtained, it can be observed that the shorter the bonded joint is and the higher the stress level on the joint, the shorter the fatigue life of the specimen.

2.3.3 Fatigue performance of metallic beams strengthened with CFRP

To assess the bond fatigue resistance of the steel bridge girder strengthened with CFRP plates, two test programmes were conducted by Miller et al. [59]. First, seven small-scale specimens with double reinforcing plates were subjected to cyclic loads at a stress range of 82.7 MPa for 2.55 million cycles. Upon testing, all seven specimens reached 2.55 million cycles without failing. Moreover, all CFRP plates remained fully bonded to the steel substrate without deterioration based on the strain data taken before and after the cycling. Next, the remaining two full-scale bridge girders strengthened with CFRP plate were fatigued for 10 million cycles at a stress range of 34 MPa. Throughout the 10 million cycles, the CFRP plates were monitored and inspected for debonding. The retrofit was viewed as having good fatigue resistance.

Tavakkolizadeh et al. [133] reported the only fatigue tests on notched steel beams strengthened with CFRP. Several retrofitting of notched steel beams with CFRP patches, with a Young's modulus of 144 GPa, for medium cycle fatigue loading ($R=0.1$) were employed in the tests. A total of 21 specimens were tested, with plain beams used as control specimens. The steel beams were tested under four point bending with a loading rate of between 5 and 10 Hz. Different constant stress ranges between 69 and 379 MPa were considered. The results showed that the CFRP patch not only tends to extend the fatigue life of a detail by more than three times, but also decreases the crack growth rate significantly.

If a bridge is strengthened with CFRP plates, it is not usually economic to close the bridge during the curing period, usually about 24 hours. It was found that trains cross a London Underground bridge at Acton in West London every two to three minutes during the curing period. The Concrete Society [89] suggested that the change in the adhesive properties caused by the cyclic load during the curing period

are likely to be small, perhaps a 10% reduction in the strength of the fully cured materials. Nikoukar [53] and Moy [134] investigated the development of stiffness and strength in CFRP reinforced steel beams subjected to cyclic loading during the early age cure of the adhesive. Five pairs of steel beams were reinforced with a single carbon fibre composite plate attached to the tension flange. A sinusoidal load was applied to five specimens at a frequency of 0.25 Hz and this was continued for up to 160 hours. The tests confirmed cyclic load during adhesive cure will have an effect on the final stiffness and failure load of the reinforced beam if the maximum cyclic load was larger than 42 kN, and the bond will fail to develop if the deformation for the adhesive during cure is excessive. They also suggested that it was prudent to limit the shear stress in the adhesive layer to a maximum of 1 MPa.

2.4 Design guidance for strengthening metallic structures

The 'LINK' (Inland Surface Transport Project) investigated the use of carbon fibre materials for the strengthening of metallic structures. The results from this work were drawn together to form the design guidance "FRP composites life extension and strengthening of metallic structures" [135]. This guidance demonstrates that FRP composites can be used with confidence in the strengthening or repair of metallic structures. The guidance applies to both serviceability and ultimate limit state requirements. Suggestions for design details are given as well.

The current best-practice for the strengthen metallic structures with FRPs is described in the CIRIA report "Strengthening Metallic Structure using Externally-Bonded FRPs" [8], which covers all aspects of a strengthening scheme, including procurement, design, installation and inspection. The design process and detailed design are given in this report. Two approaches to adhesive stress analysis are presented: a stress based approach, and a fracture mechanics based approach. The effects of fatigue loads in the retrofitted metallic structure were presented as well. Moreover, further research was proposed in this document, which has already been detailed in Chapter 1.

2.5 Conclusion

In this chapter, the technique of strengthening beams using externally-bonded plates was reviewed firstly. It is found that the adhesive bonding technique has been successfully used for strengthening beams, and that CFRP plates are more beneficial as the externally-bonded plates than steel plates. Theoretical and laboratorial studies have confirmed that externally-bonded plates improve the load carry capacity, the ductility, and the stiffness of a beam. However, the review on stress analysis of the bonded structures indicates that the stress concentrations at the cut-off ends of the substrate are the major weakness of a bonded structure. Solutions for the interfacial stress distribution and the peak interfacial stresses have been reviewed for both lap joints and retrofitted beams. Tapers and spew fillets in lap joints have been found to reduce the stress concentration, but research on this effect for retrofitted beams is scarce. Finally, the fatigue behaviour of the bonding structures was reviewed. It is found that the externally-bonded CFRP plate improves the fatigue performance of both RC and metallic beams. But the investigations on the fatigue performance of lap joints show that crack initiates and develops in the adhesive layer or the interface under fatigue load in most of the experiments. Therefore, plate debonding may significantly reduce the fatigue life of a retrofitted beam.

The following specific areas for study are lacking in the current literature and are included in this study:

- 1) Further research on interfacial stress analysis of retrofitted beams, including the correct and simplified expression for the interfacial stresses, the closed-form solution under the combination of mechanical and thermal loads, the solution for asymmetric load cases, the numerical procedure for the beams reinforced with a tapered plate, and the effects of tapers and spew fillets.
- 2) Further experimental work on retrofitted metallic beams, including validation of the analytical method for calculating the interfacial stresses, the effect of the taper and the spew fillet, and the failure criterion based on the calculated stresses to predict debonding.

- 3) Study on fatigue performance of the adhesive bonding between the CFRP plate and the metallic beam, leading to the development of an S-N curve to predict fatigue lives.

Chapter 3

Materials

Before embarking on the study of strengthening of structures, the nature of the materials involved must be determined, since each material has its own characteristics that would govern how the external-bonding should be used. Of particular importance are the mechanical properties of the materials, which have direct influence on the strength and endurance of the strengthened structures. This chapter will give an overview of the materials and review the literature related to the static and the fatigue properties. In addition, the materials used in this study will be introduced.

3.1 Metals

3.1.1 Overview

A wide range of metallic materials has been used in construction, and the most commonly used are cast iron, wrought iron and steel. As the oldest form of structural metallic materials, cast iron was developed for construction at the end of the 18th century. Following the collapse of the cast-iron Dee Bridge in 1847, wrought iron, as a higher performance structural material, replaced cast iron for rail bridge construction. Now steel is widely used in building structures, industrial structures and bridges. Although steel has replaced historic cast iron and wrought iron from the early 20th century, a significant number of wrought iron or cast iron structures are still in service and need be strengthened following increases in design loading and possibly deterioration. A more detailed description of structural metallic materials can be found in reference [136].

3.2.2 Mechanical properties of metallic materials

CIRIA C595 [8] gives a table of the static mechanical properties of metallic materials, which is reproduced in Table 3.1.

Fatigue performance of metallic structures is a well researched area and very detailed guidance on design is available. Both American and British codes [121,122] give S-N curves for steel that show the relationship between the stress range and the number of cycles to failure according to different structural details. Fatigue failures in welded or bonded strengthened construction rarely occur in a region of plain material since the fatigue strength of the welded or bonding joints are usually much lower.

3.2.3 Metal used in this study

Mild steel universal beams were used in the research reported in this thesis. Specimens cut from the web of a steel beam were tested according to the recommendations in BS EN 10002-1 [137]. Details of the test are described in Appendix A. The results show the mean Young's modulus and the mean tensile yield strength of the steel used is 206 GPa and 357 MPa, respectively.

3.2 CFRP

3.2.1 Overview

High performance carbon fibre reinforced polymers are used worldwide because of its outstanding mechanical properties and light weight. In addition, with reducing costs, this material has also become cost efficient for applications in civil engineering. With new standards and technology for the construction and repairing projects established for CFRP, it has been used efficiently for repair, rehabilitation, replacement and new construction [33,138].

CFRP composites are directional, in that the maximum mechanical properties and strength is offered in the fibre direction. These materials weigh less than one fifth of steel, are corrosion and weather resistance, have low maintenance and long term durability, and are highly formable as they can be shaped to any desired form and surface texture.

3.2.2 Manufacture characteristics of CFRP

Carbon fibre is created using polyacrylonitrile (PAN), pitch or rayon fibre precursors [4]. PAN based fibres offer good strength and modulus values up to 620 GPa. They also offer excellent compressive strength for structural applications up to 7GPa. Pitch fibres are made from petroleum or coal tar pitch. Their extremely high modulus values (up to 950GPa) and favourable coefficient of thermal expansion make them the material used in space/satellite applications. The tensile strength of carbon fibres is not much stronger than that of glass while their modulus is about three to four times higher. Carbon fibres supplied as reinforcement include roving, milled fibre, chopped strands, continuous, chopped or thermoformable mat, in which the highest strength and modulus are obtained by using unidirectional continuous reinforcement.

CFRP composites can be divided in a variety of ways in accordance with different manufacture processes, which mainly include filament wound, pultruded, pre-impregnated (prepreg) or laid-up in the final shape. Filament winding entails the wrapping of resin-impregnated (wet or dry) fibres around a mandrel. Pultrusion entails the continuous production of a composite shape by pulling resin impregnated fibres through a hot die. Prepregs are made by passing reinforcing fibres or forms such as fabrics through a resin, which is saturated (impregnated) into the fibre and then heated to advance the curing reaction to different curing stages. Prepreg sheets have the advantage of assuring a better wetting of the individual fibres, but have disadvantages in terms of shelf life and curing. Lay-up fabrication consists of the placement of multiple layers of resin-impregnated fibres or fabrics onto a desired shape. This can be done by prepreg tapes or dry fabrics that are impregnated with resin at the time of lay-up.

CFRPs for externally bonded strengthening can be applied in two ways: tape/sheet bonding or laminate/plate bonding. Tapes/sheets of prepreg or dry-fibre are thin, flexible fabric-like materials, which may be laid-up on the strengthening surface. Laminates/plates either are pultruded or are formed from prepreg sheets by stacking some layers of the sheet and curing under pressure and elevated temperature to consolidate them into the desired thickness. Strengthening metallic structures mainly choose unidirectional CFRP laminate/plate bonding, which was also used in this study.

3.2.3 Static behaviours of CFRP

Because the tensile strength of the composite depends on the weakest fibres and on the redistribution of load when they fail, the matrix and the interface properties are particularly important. This is especially so for high failure strain fibres because at higher strains the interfacial stresses are higher. With the current moves to improve carbon fibres with higher failure strains, composite manufacturers are paying greater attention to optimising fibre-resin interactions. Under compression loading, composites tend to fail by buckling failure of the fibre [139]. Compressive strengths of 78% of the tensile strength have been reported for CFRP [43]. Under flexural loading, a composite can fail in tension, in compression or by interlaminar shear depending on the local stresses and local strengths.

As mentioned in Chapter 1, there are three types of CFRP composites: high strength (HS), high modulus (HM) and ultra-high modulus (UHM). Unlike metals, CFRP has a near linear elastic response to failure, with no or very limited plastic deformation. In the properties shown in Table 1.1, tensile strength decreases with increasing modulus, the strain at rupture will then also be much lower. Because of the material brittleness at high modulus, it becomes critical in joint and connection details, which can have high stress concentrations. As a result of this phenomenon, CFRP materials are more effective with adhesive bonding.

Mechanical properties of CFRP mainly depend on the fibres, the matrix and the forms. However, some other aspects also can significantly influence the static strength and stiffness of CFRP. Firstly, the manufacture method can influence the mechanical

properties of the CFRP material. Therefore, different partial factors were given in accordance with the manufacturing process in CIRIA C595 [8] and Concrete Society Technical Report No. 55 [89]. Secondly, thermal exposure up to a certain temperature may be an advantage as it can result in a post cure for the CFRPs. However, the polymer hardens and becomes increasingly brittle at low temperatures [140], and the polymer begins to soften as the elevated temperature approaches, or even below, its glass transition temperature (T_g) [141]. Thirdly, the environmental effects, such as water, salt solution and UV radiation, produce unnoticeable damages to the unidirectional CFRPs [142]. However, the carbon fibre is electrically conductive and, therefore, might give galvanic corrosion in direct contact with metals [143].

3.2.4 Fatigue behaviours of CFRP

The fatigue behaviour of composite materials has been extensively researched in the past 40 years. Research by Talreja [144] has indicated that CFRPs are insensitive to fatigue even at stresses close to the static fracture strength. The S-N curves presented by Curtis [145] show the CFRPs have better fatigue behaviour than GFRPs and Kevlar FRPs (KFRPs). Walton and Yeung [146] have found that composite tendon members can easily surpass the performance available from steel. Barnes [118] indicated the unidirectional composites have better fatigue performance. Based on experimental research, some models have also been proposed to predict fatigue damage and the life of composites [147].

In isotropic materials, ‘fatigue’ means that repeated stresses, below the general elastic limit of the materials, produced local plastic strains at stress concentrations that result in crack initiation and propagation perpendicular to the local tensile stress [5]. In composite materials, fatigue can still occur, in the sense that degradation can occur with repeated stresses below those needed for static failure. However, the fatigue behaviour of fibrous composite materials is more complex than that of metals, due to the multiplicity of damage modes that can be grown by fatigue cycles, and their possible interaction. The carbon fibres themselves are not usually fatigue sensitive. Cracks tend to form in the matrix or at the fibre-matrix interface, in response to local tensile stresses, and to propagate along low energy paths parallel to the fibres. These

fatigue processes tend to occur throughout the highly stressed regions of the composite and lead to a general degradation of the materials, rather than producing a discrete crack, of which propagation is usually perpendicular to the cyclic load axis, like isotropic materials. Furthermore, the reduction in stiffness and residual strength begins very early in the fatigue life and reaches significant magnitudes long before the component breaks in the CFRPs than other homogeneous monolithic materials, such as metals.

Fatigue in CFRP materials is influenced by a number of parameters [8]: the fibre and matrix materials, interface effects, frequency effect and manufacturing process. Curtis [145] indicated that the resin epoxy has more effect on fatigue behaviour of unidirectional CFRP under parallel tensile load than the fibre. The toughened epoxies gave better static strengths and low cycle fatigue strength than the standard epoxy, but for large number of cycles the fatigue strengths were considerably lower. Moreover, creep, thermal cycle, environment also might influence the fatigue performance of CFRP.

Concrete Society [89] reported the stress range in the CFRP should be limited to the appropriate 80% of design ultimate strength in bridge reinforced beams. Jones et al. [148] characterised the fatigue life of a composite component by an S-N curve, of the form:

$$\frac{\sigma_{max}}{\sigma_f} = 1 - K \log_{10}(N_f) \quad (3.1)$$

where σ_{max} is the maximum stress in a fatigue cycle and N_f is the number of fatigue cycles to failure. σ_f is the static failure stress corresponding to σ_{max} . The slope parameter K depends on the type of matrix and fibre and on the R ratio, which is the ratio of minimum to maximum stress in a cycle. K is usually 0.1 or less for FRP. Typical values of K are shown in the S-N curves in Figure 3.1.

3.2.5 CFRP used in this study

The material selected for this study is SE84LV/HMC/300/400/35%±3%pop, which is manufactured by Structural Polymer System Ltd (SP). SE 84 is a series of

exceptionally versatile hot-melt, epoxy prepregs. It can be cured at temperatures as low as 80⁰C, or it can be used for faster moulding of components at 120⁰C. This is achieved with an extremely good outlife of up to 8 weeks at 21⁰C. It is a toughened system, and offers excellent mechanical properties on a wide variety of reinforcing fabrics and fibres. The SE 84 series is commonly used in vacuum bagging, press-moulding, autoclave and other pressure moulding processes. It has excellent, controllable flow and tack characteristics. SE 84 can be varied by selection of the appropriate resin variant, of which SE 84LV is a low viscosity system used with heavy fibre weights where low-flow processing conditions (vacuum bag pressure and minimum cure temperature) are likely to be used. High modulus carbon (HMC) fibre prepreg was chosen from SE 84LV serials for this study. The details of manufacture are introduced in Appendix B.

The mechanical properties of SE84LV/HMC provided by manufacturer are shown in Table 3.2. Since the data in manufacturer's data and information sheets are intended to show typical values for a product and not to be taken as guaranteed minima, laboratorial tests have to be done. The test procedure used is from ISO 527-5 [149]. The results are given in Table 3.2 and details of the test are described in Appendix C.

3.3 Adhesives

The development of stronger and more reliable adhesives is currently a popular endeavour as evidenced by their ever-expanding usage. With the development of adhesives, adhesive bonding has shown itself capable of replacing or supplementing conventional methods such as riveting, welding, and mechanical fastening in a variety of application. The strength and durability of bonded structures in aircraft construction and timber assemblies has been demonstrated over many years, but the extension of this experience to infrastructure is comparatively restricted, particularly for what are required to sustain large externally applied forces. However, recent advance in the science and technology of adhesions, such as composites, and adhesives suggests that structural adhesives have enormous potential in future construction applications.

3.3.1 Overview

An adhesive may be defined as a material which, when applied to surfaces, can join them together and resist their separation [150]. Some fifty years ago the only adhesives of major importance were animal glues and other natural products which had been used for centuries. The rapid increase in the use of adhesives in industry has been due to the development of synthetic resins from the early 1940s, which do not have the limitations of natural products and which can bond both metals and other non-porous materials [151].

Over the past fifty years, there has been an intense development of synthetic adhesives to meet more technically demanding applications. These synthetic polymers and ancillary products, which include thermosetting and thermoplastic types, have been developed to possess a balance of properties that enables them to adhere readily to other materials, to have an adequate cohesive strength and appropriate mechanical characteristics when cured, to possess good durability, and to meet various application and manufacturing requirements. Thermoplastic adhesives may be softened by heating and rehardened on cooling. Contrarily, thermosetting adhesives do not melt or flow when heated, but become more rubbery and lose strength with increasing temperature. Therefore, thermosetting materials may be regarded as structural resins and are found widespread use in civil engineering applications, of which the most widely accepted and used are epoxies [150].

Epoxy adhesives have this name because their most important components, the resin, contain epoxide rings; this is a three-member ring with two carbon atoms singly bonded to an oxygen atom [100]. Epoxy resins can be regarded as compounds which normally contain more than one epoxy group per molecule. To the base resin is added a variety of materials, such as hardeners, flexibilisers, tougheners and fillers. Hardener or curing agent hardens epoxides by chemical reaction which produces a crosslinked polymer. In epoxies, therefore, the resins are hooks and the hardener are eyes. In practice most epoxy resin systems have fillers incorporated, often simply to reduce cost although they may assist in gap filling, reduction of creep, reduction of exotherm, corrosion inhibition and fire retardation.

The reduction in strength and modulus and the enhancement of creep during service at high temperatures place a technological limit on the efficiency and life of the adhesive. A most important characteristic temperature is the glass transition temperature (T_g). When a crystalline solid melts, there is a discontinuity in any plot of a fundamental quantity such as volume or enthalpy against temperature. For the civil engineer, quasi-static mechanical methods utilising a flexural test on a hardened adhesive prism are more convenient for determining the heat distortion temperature (HDT), which is nearly the same as the glass transition temperature of polymers [150]. It will be noted that these HDT or T_g values of adhesives used in civil engineering application, which are about 60⁰C [8,89], may not be much in excess of anticipated maximum service temperatures. In the UK, on the soffits of concrete bridge temperature extremes may lie between -20⁰C and +38⁰C [152], and in steel bridges maximum temperature extremes of 60 to 65⁰C may occur [150]. Furthermore, HDT or T_g will be lowered by water absorption into the polymer. Indeed, the T_g should be one of the first criteria in assessing the likely suitability of candidate adhesives [150].

In addition to mechanical properties, some other behaviours of adhesive in the unmixed, mixing, curing, application phases are required to consider when choosing the adhesive, which include shelf life, viscosity, usable life, wetting ability, rate of strength development, moisture resistance, etc.

3.3.2 Elastic parameters of adhesive

Usually, stress-strain curves of polymeric adhesives depart considerably from linearity, and Poisson's ratio varies between the extremes of 0.5 and 0.33 [100]. Accurate stress and strain data for adhesives under well-defined stress states are required to perform analytical/numerical analyses on adhesive joints. One initial experimental problem is the ability to fabricate reliable flaw-free bulk adhesive specimens with viscous cold-curing compounds. Work at Oxford Brookes University [153] has demonstrated that the centrifuging of mixed adhesive can largely overcome such problems.

Tensile behaviour is relatively straightforward to measure using the standard test method and test specimen developed for plastics [154]. However, it is well known that unlike metals, polymeric adhesives have different behaviour depending on the type of loading they are subjected to [109] and the material thicknesses used in the situation [155]. In 1963, Kuenzi and Stevens [156] performed in situ determinations on a number of adhesives by analysing axially loaded butt joints with a small bond line thickness to diameter ratio. Bredemo and Gradin [155] presented analytical expressions for the stiffness of an adhesive butt joint with rigid adherends, which were compared with a solution obtained by means of the FE methods. They indicated the apparent Young's modulus in situ increases with joint width to adhesive thickness ratio and the increase appears to have saturated when the ratio is round 60.

To evaluate shear property of adhesive, Lilleheden [157] indicated that published results claiming variability between thin-film in situ and bulk properties and a thickness dependency in situ are erroneous. However, Jangblad et al. [158] confirmed the in-situ method is preferred since it exhibits greater stability than the bulk method and actually involves adhesive layers manufactured in the same circumstances as the final object of all adhesive research, the bonded structural joint. For many years, the napkin-ring methods, suggested in ASTM E229 [159], was used to evaluate the shear strain curve of adhesives. The Arcan specimen [160], which is a butterfly shape with an adhesive between two wings, is also available. However, a more practical method for stress-strain curve determination is the use of the thick adherend lap-shear specimen due to its simplicity and cost-effectiveness, which is also suggested in ASTM D3983 [161] and ISO 11003-2 [162].

Jangblad et al. [158] presented a method for determining the elastic parameters for adhesives based on the two specimens mentioned above: the butt joint, shown in Figure 3.2 and the thick adherend lap-shear joint, shown in Figure 3.3. By assuming $\varepsilon_y = \varepsilon_z = 0$ everywhere in the adhesive in butt joint, equilibrium and Hooke's law imply that

$$\frac{P_l \eta_l}{t_l b_l \delta_l} = \frac{E(1-\nu)}{(1-2\nu)(1+\nu)} \quad (3.2)$$

where P_l is the longitudinal force applied on the butt joint, t_l and b_l the thickness and the width of the butt joint, respectively, η_l , and δ_l the adhesive thickness and

longitudinal displacement of the adhesive layer in butt joint, respectively. E is the Young's modulus and ν the Poisson's ratio of the adhesive. In thick adherend lap-shear joint, the adhesive layer is regarded as thin and the state of stress is assumed to be one of uniform shear in x - y plane. Imposing Hook's law and equilibrium lead to

$$\frac{P_2 \eta_2}{c b_2 \delta_2} = G = \frac{E}{2(1 + \nu)} \quad (3.3)$$

where P_2 is the longitudinal force applied on the thick adherend lap-shear joint, t_2 the thickness of the adherend, b_2 the width of the thick adherend lap-shear joint and c the length of lap. η_2 is the adhesive thickness, δ_2 longitudinal displacement of the adhesive in the thick adherend lap-shear joint, and G the shear modulus of the adhesive. From the equations (3.2) and (3.3), the values of E , ν and G can be determined for the adhesive.

To measure the displacement δ_1 in butt joint, Bredemo and Gradin [155] suggested a strain gauge arrangement. To measure the displacement δ_2 in thick adherend lap-shear joint, lasers and moiré interferometry were found to be accurate and reproducible by Lilleheden [157]; Weissberg and Arcan [160] suggested a 2670-114 crack opening displacement (COD) gauge (5 mm base), which measures movements with an accuracy of .0015 mm in the Instron machine; Kadioglu et al. [109] and ISO 11003-2 [162] suggested a extensometry designed by Althof; ASTM D3983 [161] suggested the extensometer called KGR-1; Tsai et al. [163] presented a convenient and cost-effective method using strain gauges.

3.3.3 Strength of adhesive bonding

Similar to testing the elastic properties, the strength of adhesives can be obtained by bulk specimens using the standard test method and test specimen developed for plastics. In addition to the different in-situ behaviour, however, the strength of adhesive in bonded joints is mainly dependent upon the adhesion between constituents.

The strength of bonded assemblies depends not only on cohesive strength of the adhesive, but also on the degree of adhesion to the bonding surfaces [150]. The use of

cold-cure epoxies generally necessitates the careful preparation of metallic adherends in particular, to ensure satisfactory long-term performance. The purpose of surface preparation is to remove contamination and weak surface layers, to change the substrate surface geometry, and/or introduce new chemical groups to provide, in the case of metals, an oxide layer more ‘receptive’ to the adhesive [150].

Kinloch [164] suggests that the measured bonded joint strength almost always reflects the value of two parameters: (1) the intrinsic adhesion; (2) the energy dissipated visco-elastically and plastically in the high strained volume around the tip of the propagating crack and in the bulk of the joint. The latter term generally dominates the measured bonded strength. ASTM D2094 [165] and ISO 6922 [166] suggested to test bond strength in axial-loading using butt joints. Moreover, ASTM D1002 [167] and BS 5350 C5 [168] recommend to test bond strength in longitudinal shear using single or double lap shear joints. Before the strength measured by the above standards is applied to bonded structures, however, the non-uniform stress distribution in the adhesion interface must be considered. This will be discussed in Chapter 4.

3.3.4 Fatigue behaviour of adhesive bonding

Adhesive properties that are based on the results of experiments on bulk adhesives cannot be used to predict the fatigue performance, as the fracture behaviour depends strongly on the adhesive bond line thickness [169,170]. Therefore, Althof [171] suggested the thick adherend shear joint specimen as a suitable configuration for evaluating the fatigue properties of adhesive. The fatigue results of Wohler’s tests [172] are customarily presented as S - N curves, in which the stress as a percentage (S) of the ultimate strength determined in a ‘static’ test is plotted against the number of cycle (N) at that stress to failure, on a logarithmic scale, as shown on Figure 3.4.

Whilst test methods for adhesive fatigue properties have been suggested by ISO 9644 [173] and ASTM D3166 [174], Geoiij et al. [127] indicated that predicting the fatigue properties of a complex joint in an actual structure will be difficult with data from simple test specimens.

The fatigue life is strongly influenced by the profile of the edges of the joint. Harris and Fay [175] indicated that the initiation of small cracks at the edges of the joint represents the major part of the fatigue life. Therefore, if the strain in the adhesive layer under full live loading at the serviceability limit state is kept below that at first cracking (corresponding to the first ‘knee’ in the loading-deflection curve), then fatigue failure without forewarning is relatively unlikely [8]. Experimental and numerical investigations to predict the fatigue life of bonding joints based on the fatigue crack initiation and growth mechanism have been conducted by Curley et al [176], Cheuk et al. [125]. Furthermore, Abdel Wahab et al. [177,178] presented a generalised numerical procedure using finite element analysis for prediction of the fatigue lifetime of adhesively bonded structures.

For adhesives used in civil engineering, the Concrete Society Committee [89] recommend that the sustained stress in the adhesive should be kept below 25% of the short-term strength, which equates to the recommended minimum materials partial factor of 4.0. CIRIA C595 [8] reported that tests carried out by the National Physical Laboratory on bonded joints suggest that the S-N curve formulation for FRP, Equation (3.1) and Figure 3.1, is also applicable to adhesive joints. This S-N curve suggests that the peak shear stress in a fatigue cycle should not exceed 20-30% of the ultimate static failure strength.

3.3.5 Adhesive used in this study

Sikadur 31, supplied by Sika Ltd., was used in this study. This adhesive is a two component solvent free, cold cure, thixotropic epoxy adhesive suitable for damp and dry substrates. The main component in part A of Sikadur 31 is epoxy resin, and that in part B, the hardener, is Trimethylhexamethylene diamine. The advantages of this adhesive, which is widely used in civil engineering, include: excellent adhesion even in damp conditions, application in vertical and overhead situations, excellent water resistance, rapid working time for low temperature, resistant to chemical, solvents, oils and good resistance to creep. The Young’s modulus, shear modulus and Poison’s ratio of this adhesive are 8.0 GPa, 2.6 GPa and about 0.4, respectively. These values

were provided by the manufacturer. To confirm the data provided by manufacturer, the Young's modulus and shear modulus were tested by dogbone specimens and thick adherend lap joint specimens, respectively. The tensile tests for dogbone specimens [179] show the Young's modulus is about 9.3 GPa, a slightly elevated value compared to the manufacture's data. The shear tests for thick adherend lap joint specimens were conducted according to the recommendations in the standard BS ISO 11003-2 [162]. The results are given in Table 3.3 and details of the test are described in Appendix D.

3.4 Conclusion

In this chapter, three types of materials used in this study were introduced. Firstly, metals, as the materials of plain structure, have good static and fatigue performances, which have been well researched. Secondly, after the overview of the manufacture process and of the form of CFRPs, which may influence the mechanical properties significantly, these brittle ultra-strong materials were investigated with regard to their static and fatigue behaviour, as well as the influence of environment. A prepreg CFRP material was chosen for this study due to its outstanding behaviour, simple manufacture process and cost-effectiveness. Finally, the classification and properties of the adhesives were investigated, which showed epoxy resin was suitable for this study. The test and measure methods were presented and dogbone specimens and shear joints were used to test the properties of the adhesive used in this study.

Table 3.1 Mechanical properties of metallic materials [8]

		Cast Iron		Wrought	Steel	
		Historic	Modern	Iron	Historic	Modern
			(BSI 1997a)		(=pre 1950)	(=post 1950)
Modulus (GPa)	Tensile	66-94	100-145	154-220	200-205	200-210
	Compressive	84-91	150-400			
Strength (MPa)	Tensile	65-280	600-1200	278-593	286-494	275-355
	Compressive	587-772		247-309		
Elastic Limit (MPa)				154-408	278-309	275-355
Ultimate strain (%)			0.5-0.75	7-21	18-20	18-25
Poisson's ratio		0.25	0.26	0.25	0.26-0.34	0.30
Density (kg/m ³)		7050-7300		7700	7840	
Coefficient of thermal expansion (10 ⁻⁶ /°C)		10-11		12	12	

Table 3.2 Mechanical properties of CFRP prepreg

	Data from Manufacturer	Data from tests
Tensile modulus E_1 (GPa)	208.3	228.6
Tensile modulus E_2 (GPa)	/	7.44
Shear modulus G_{12} (GPa)	4.31	/
Poisson's ratio ν_{12}	0.337	0.30
Tensile strength F_1 (MPa)	1562	2206
Tensile strength F_2 (MPa)	/	22.5

Note: 1 is the direction parallel to fibre, and 2 is the direction perpendicular to fibre.

Table 3.3 Mechanical properties of adhesive

	Data from Manufacturer	Data from tests
Tensile modulus E (GPa)	8.0	9.3
Shear modulus G (GPa)	2.6	2.06

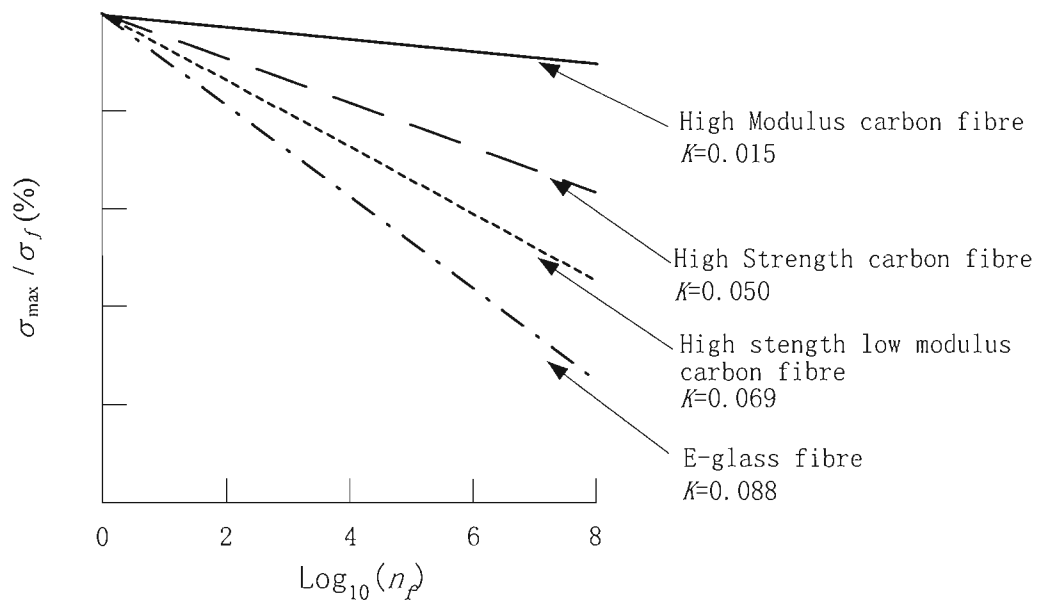


Figure 3.1 Normalized *S-N* curves [148].

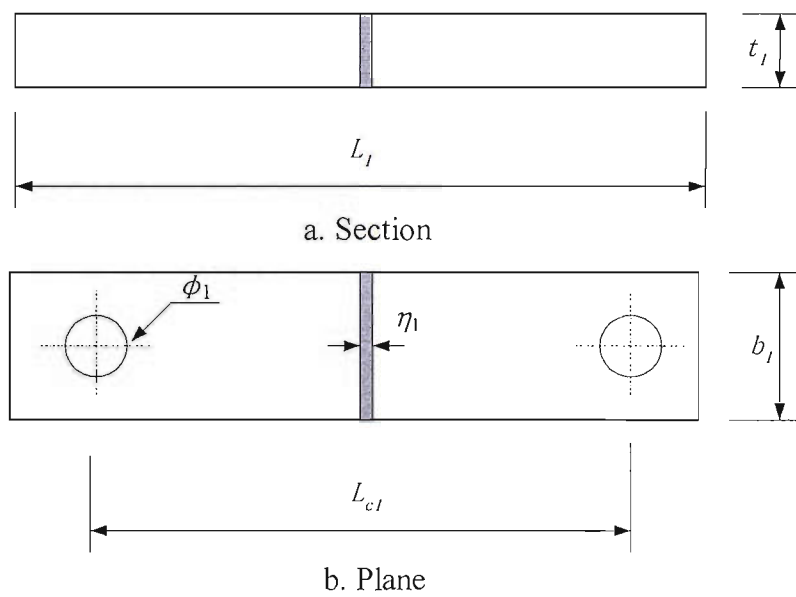


Figure 3.2 Butt joint.

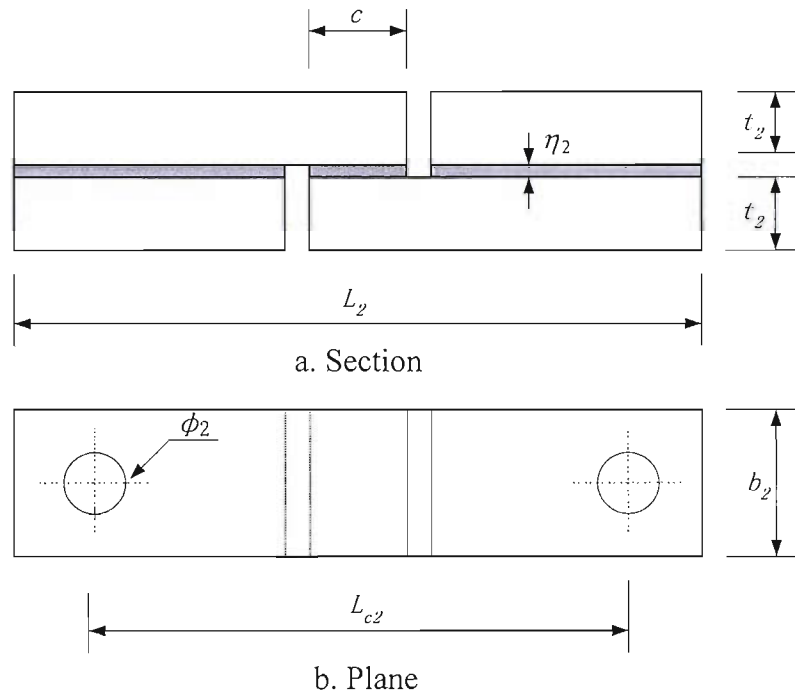


Figure 3.3 Thick adherend lap shear joint.

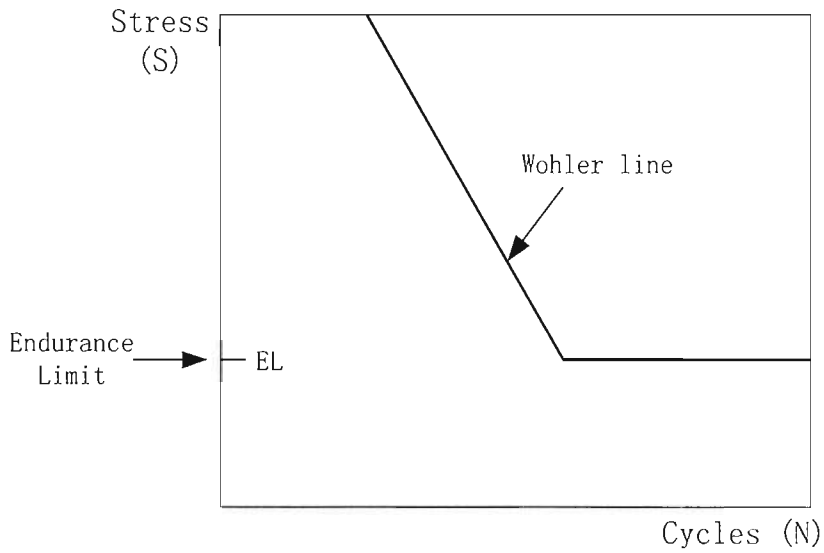


Figure 3.4 Idealised Wohler diagram [172].

Chapter 4

Stress analysis of metallic beams reinforced with a bonded CFRP plate

4.1 Introduction and objectives

Hollaway and Cadei [48] indicated that the adhesive bond has been found to be generally the weakest link, and is likely to control the mode of failure in the composite strengthening scheme for a metallic structure. In adhesive joints, significant stress concentration in the adhesive occurs at the ends of adherends, where there is a discontinuity caused by the abrupt termination of the components. In order to ensure its integrity, a knowledge of the stress distribution in the joints is therefore important.

Solutions for the interfacial stress distribution have been reviewed for both lap joints and retrofitted beams in Chapter 2. Goland and Reisner [91] made a classical analysis of the stress distribution in a single lap shear joint. Smith and Teng [56] gave a comprehensive review and presented a new solution which was intended for application to beams with a bonded thin plate. Moreover, Denton [57] indicated the shear and normal stresses can be developed in the adhesive layer at the ends of the FRP plate as a result of the difference between the thermal coefficients. The use of a taper at the ends of the adherends in lap joints has been shown to effectively limit peel stresses, but the geometric complexity of the tapered joint has posed a mathematically intractable problem for any closed-form solutions.

As a further development of the solutions by Smith and Teng [56] and Denton [57], this chapter presents a simple closed-form solution for obtaining the shear and the normal stresses in the adhesive layer of a retrofitted metallic beam (Figure 4.1) under mechanical and thermal loads. Since a taper at the ends of a CFRP plate

significantly reduces the stress concentration, a numerical procedure has also been developed to predict the interfacial stresses in metallic beams reinforced with a tapered plate. The results from the close-form solution and the numerical procedure are then compared with those obtained from finite elements. Finally, a parametric study was conducted to investigate the influence of different geometries and material properties.

4.2 Basic assumptions

The following assumptions were made in the analytical and the numerical studies:

1. All materials considered are linear elastic.
2. The beam is simply supported and slender, hence St. Venant theory, i.e. plane sections remaining plane, can be used.
3. The shear and the normal stresses in the adhesive layer do not vary through the thickness of the adhesive.
4. Shear deformations in the CFRP plate and the metallic beam are neglected.
5. Bending deformations of the adhesive are neglected.
6. In calculating the interfacial shear stress, bending of the CFRP plate is ignored. However, this bending effect is included when calculating the interfacial normal stress.

4.3 Stress analysis

4.3.1 Stress solution for the symmetric load case

4.3.1.1 Shear stresses without taper

Figure 4.2 shows an infinitesimal element of a beam with a reinforcing CFRP plate. In the figure, V , M and N are the shear force, the bending moment and the longitudinal tension, respectively, τ and σ the shear stress and the normal stress at the

interface, respectively, and t the component thickness. The subscripts b , a and p denote metallic beam, adhesive and CFRP plate, respectively. This notation will be used throughout this chapter. From Assumption 3, the shear force and the longitudinal tension in the adhesive can be ignored.

For the CFRP plate, the longitudinal equilibrium of the element, of length dx and width b , is given by

$$(N_p + dN_p) - N_p - \tau b dx = 0 \quad (4.1)$$

from which,

$$\frac{dN_p}{dx} = b \tau \quad (4.2)$$

where b is the width of the CFRP plate. The transverse equilibrium of the element is given by

$$V_p + dV_p + \sigma b dx - V_p = 0 \quad (4.3)$$

giving

$$\frac{dV_p}{dx} = -b \sigma \quad (4.4)$$

Similarly, the equilibrium of the metallic beam in the x and y directions can be expressed, respectively, as:

$$\frac{1}{b} \frac{dN_b}{dx} = -\tau \quad (4.5)$$

and

$$\frac{dV_b}{dx} = b \sigma - q \quad (4.6)$$

For the combined cross section, the force equilibrium in the longitudinal direction and the moment equilibrium can be described, respectively, as:

$$N_b = -N_p \quad (4.7)$$

and

$$M_b + M_p + M_a - N_b \left(\frac{t_b}{2} + t_a + \frac{t_p}{2} \right) = M(x) \quad (4.8)$$

where

$$M_a = - \int_0^x \tau(t) t_a dt = t_a N_b \quad (4.9)$$

According to Assumption 6, $M_p = 0$, and eq. (4.8) gives:

$$M_b = N_b(t_b / 2 + t_p / 2) + M(x) \quad (4.10)$$

where $M(x)$ is the applied moment.

Since the adhesive is elastic, the shear strain γ can be written as

$$\gamma = \frac{du(x, y)}{dy} + \frac{dv(x, y)}{dx} \quad (4.11)$$

where $u(x, y)$ and $v(x, y)$ are, respectively, the longitudinal and the transverse displacement at any point in the adhesive layer. The corresponding shear stress is given as

$$\tau = -G\left(\frac{du(x, y)}{dy} + \frac{dv(x, y)}{dx}\right) \quad (4.12)$$

where G is the shear modulus of the adhesive. Differentiating eq. (4.12) gives

$$\frac{d\tau}{dx} = -G\left(\frac{d^2u(x, y)}{dydx} + \frac{d^2v(x, y)}{dx^2}\right) \quad (4.13)$$

According to Assumption 3, the shear stress does not vary through the thickness of the adhesive, therefore $u(x, y)$ in the adhesive should vary linearly, giving

$$\frac{du}{dy} = \frac{1}{t_a}(u_b - u_p) \quad (4.14)$$

then

$$\frac{d^2u}{dydx} = \frac{1}{t_a}\left(\frac{du_b}{dx} - \frac{du_p}{dx}\right) \quad (4.15)$$

where u_b and u_p are the longitudinal horizontal displacements at the bottom of the metallic beam and the top of CFRP plate, respectively, and they are given as:

$$\frac{du_b}{dx} = \varepsilon_b(x) = \alpha_b \Delta T + \frac{M_b t_b / 2}{E_b I_b} + \frac{N_b}{E_b A_b} \quad (4.16)$$

and

$$\frac{du_p}{dx} = \varepsilon_p(x) = \alpha_p \Delta T - \frac{M_p t_p / 2}{E_p I_p} + \frac{N_p}{E_p A_p} \quad (4.17)$$

where ε is the strain, α the thermal expansion coefficient, ΔT the temperature change, and E , I and A the elastic modulus, the second moment of area and the cross-sectional area, respectively. Substituting (4.16) and (4.17) into (4.15) gives

$$\frac{d^2u}{dydx} = \frac{1}{t_a} ((\alpha_b - \alpha_p)\Delta T + \frac{M_b t_b / 2}{E_b I_b} + N_b \frac{1}{E_b A_b} - N_p \frac{1}{E_p A_p}) \quad (4.18)$$

Also substituting the longitudinal force from (4.7) and the bending moment from (4.10) into (4.18) gives

$$\frac{d^2u}{dydx} = \frac{1}{t_a} ((\alpha_b - \alpha_p)\Delta T + \frac{(M(x) + N_b(t_b/2 + t_p/2))t_b/2}{E_b I_b} + N_b(\frac{1}{E_b A_b} + \frac{1}{E_p A_p})) \quad (4.19)$$

From Assumption 5, $\frac{d^2v(x, y)}{dx^2} = 0$, and (4.13) becomes

$$\frac{d\tau}{dx} = -\frac{G}{t_a} ((\alpha_b - \alpha_p)\Delta T + \frac{(M(x) + N_b(t_b/2 + t_p/2))t_b/2}{E_b I_b} + N_b(\frac{1}{E_b A_b} + \frac{1}{E_p A_p})) \quad (4.20)$$

Differentiating eq. (4.20) with respect to x and substituting eq. (4.5) gives the following governing equation:

$$\frac{d^2\tau}{dx^2} = \lambda^2 \tau - g \lambda^2 M'(x) \quad (4.21)$$

The general solution for this equation has the form

$$\tau(x) = c_1 e^{\lambda x} + c_2 e^{-\lambda x} + g M'(x) \quad (4.22)$$

where

$$\lambda = \sqrt{\frac{Gb}{t_a} \left(\frac{(t_b/2 + t_p/2)t_b/2}{E_b I_b} + \frac{1}{E_b A_b} + \frac{1}{E_p A_p} \right)} \quad (4.23)$$

and

$$g = \frac{G t_b / 2}{\lambda^2 t_a} \frac{1}{E_b I_b}$$

Now let us consider the boundary conditions. Due to symmetry, the shear stress at mid-span is zero, i.e

$$\tau(L_p / 2) = c_1 e^{\lambda L_p / 2} + c_2 e^{-\lambda L_p / 2} + g M'(L_p / 2) = 0 \quad (4.24)$$

where L_p is the length of the CFRP plate (see Figure 4.1).

At the end of the CFRP plate, the longitudinal force N_b is zero, and eq. (4.20) can be written as

$$\frac{d\tau(0)}{dx} = c_1 \lambda - c_2 \lambda + g M''(0) = -\frac{G}{t_a} ((\alpha_b - \alpha_p)\Delta T + \frac{M(0)t_b/2}{E_b I_b}) \quad (4.25)$$

From the above two equations,

$$c_1 = \frac{-\frac{1}{\lambda} e^{-\lambda L_p / 2} \left(\frac{G}{t_a} (\alpha_b - \alpha_p) \Delta T + \frac{G}{t_a} \frac{M(0)t_b / 2}{E_b I_b} + gM''(0) \right) - gM'(L_p / 2)}{e^{\lambda L_p / 2} + e^{-\lambda L_p / 2}} \quad (4.26)$$

$$c_2 = \frac{\frac{1}{\lambda} e^{\lambda L_p / 2} \left(\frac{G}{t_a} (\alpha_b - \alpha_p) \Delta T + \frac{G}{t_a} \frac{M(0)t_b / 2}{E_b I_b} + gM''(0) \right) - gM'(L_p / 2)}{e^{\lambda L_p / 2} + e^{-\lambda L_p / 2}} \quad (4.27)$$

4.3.1.2 Normal stresses without taper

Since the normal stress is uniform through the thickness of the adhesive layer, the interfacial normal stress is given as

$$\sigma(x) = \frac{E_a}{t_a} (v_p(x) - v_b(x)) \quad (4.28)$$

where E_a is the elastic modulus of the adhesive, v_b and v_p the transverse displacements at the bottom of the metallic beam and the top of the CFRP plate, respectively, which are given by:

$$\frac{d^2 v_b(x)}{dx^2} = \frac{1}{E_b I_b} M_b(x) \quad (4.29)$$

and

$$\frac{d^2 v_p(x)}{dx^2} = \frac{1}{E_p I_p} M_p(x) \quad (4.30)$$

Considering the moment equilibrium of the infinitesimal element in Figure 4.2 gives

$$(M_b + dM_b) - M_b - (V_b + dV_b)dx + \frac{1}{2}(\sigma b - q)(dx)^2 + \tau b(t_b / 2)dx = 0 \quad (4.31)$$

Substituting eq. (4.6) into eq. (4.31) gives

$$\frac{dM_b}{dx} = V_b - \tau b t_b / 2 \quad (4.32)$$

Similarly,

$$\frac{dM_p}{dx} = V_p - \tau b t_p / 2 \quad (4.33)$$

Differentiating eq. (4.28) three times with respect to x and substituting eqs. (4.29), (4.30), (4.32) and (4.33) gives

$$\frac{d^3\sigma(x)}{dx^3} = \frac{E_a}{t_a} \left(\frac{1}{E_p I_p} (V_p - \tau b t_p / 2) - \frac{1}{E_b I_b} (V_b - \tau b t_b / 2) \right) \quad (4.34)$$

Differentiating (4.34) gives the following governing equation:

$$\frac{d^4\sigma(x)}{dx^4} + \frac{E_a b}{t_a} \left(\frac{1}{E_b I_b} + \frac{1}{E_p I_p} \right) \sigma(x) - \frac{E_a q}{t_a E_b I_b} - \frac{E_a b}{t_a} \left(\frac{t_b / 2}{E_b I_b} - \frac{t_p / 2}{E_p I_p} \right) \frac{d\tau(x)}{dx} = 0 \quad (4.35)$$

Assuming that $d^5\tau/dx^5 = 0$ and that the normal stress approaches zero for large values of x , the general solution to eq. (4.35) is

$$\sigma(x) = e^{-\beta x} (s_1 \cos(\beta x) + s_2 \sin(\beta x)) + m_1 \frac{d\tau}{dx} + m_3 q \quad (4.36)$$

where

$$\beta = \sqrt[4]{\frac{E_a b}{4t_a} \left(\frac{1}{E_b I_b} + \frac{1}{E_p I_p} \right)}, \quad m_1 = \frac{E_p I_p t_b / 2 - E_b I_b t_p / 2}{E_b I_b + E_p I_p}, \quad m_3 = \frac{E_p I_p}{b(E_b I_b + E_p I_p)}$$

At the end of the CFRP plate, the bending moment and the shear forces are zero. Hence, the boundary conditions can be written as:

$$\frac{d^2\sigma(0)}{dx^2} = \frac{E_a}{t_a} \left(\frac{1}{E_p I_p} M_p(0) - \frac{1}{E_b I_b} M_b(0) \right) = -\frac{E_a}{t_a} \frac{1}{E_b I_b} M(0) \quad (4.37)$$

and

$$\frac{d^3\sigma(0)}{dx^3} = m_2 \tau(0) - \frac{E_a}{t_a} \frac{1}{E_b I_b} V(0) \quad (4.38)$$

where $m_2 = \frac{E_a b}{t_a} \left(\frac{t_b / 2}{E_b I_b} - \frac{t_p / 2}{E_p I_p} \right)$. And from eq. (4.36) for $x=0$,

$$\frac{d^2\sigma(0)}{dx^2} = -2s_2\beta^2 + m_1 \frac{d^3\tau(0)}{dx^3} \quad (4.39)$$

and

$$\frac{d^3\sigma(0)}{dx^3} = 2\beta^3(s_1 + s_2) + m_2 \frac{d^4\tau(0)}{dx^4} \quad (4.40)$$

Combining (4.37) with (4.39), and (4.38) with (4.40) give, respectively,

$$s_1 = \frac{1}{2\beta^3} (m_2 \tau(0) - m_1 \frac{d^4\tau(0)}{dx^4}) - \frac{m_1}{2\beta^2} \frac{d^3\tau(0)}{dx^3} - \frac{E_a}{2\beta^3 t_a} \frac{1}{E_b I_b} (V(0) + \beta M(0)) \quad (4.41)$$

and

$$s_2 = \frac{m_1}{2\beta^2} \frac{d^3\tau(0)}{dx^3} + \frac{1}{2\beta^2} \frac{E_a}{t_a} \frac{1}{E_b I_b} M(0) \quad (4.42)$$

4.3.1.3 Shear stresses with taper

Because of the geometric complexity of the taper at the end of a CFRP plate, a general solution is difficult to obtain for the differential equation. A numerical solution is therefore attempted. The dimensions of the taper are shown in Figure 4.3. At the taper, the thickness of plate, t_p , is not constant, and is given as:

$$t_p = t_{end} + kx \quad \text{for } 0 \leq x \leq a \quad (4.43)$$

and

$$t_p = t_p \quad \text{for } a < x \leq L_p / 2 \quad (4.44)$$

where a is the length of taper, t_{end} the thickness at the end of the taper, and k the slope of the taper. Substituting eqs. (4.5), (4.43) and (4.44) into eq. (4.20) gives

$$\frac{d^2 N_b}{dx^2} - \omega N_b - B = 0 \quad (4.45)$$

where:

$$\omega = n_1 + \frac{n_2}{t_{end} + kx} \quad 0 \leq x \leq a$$

$$\omega = n_1 + \frac{n_2}{t_p} \quad a < x \leq L_p / 2$$

$$n_1 = \frac{Gb}{t_a} \left(\frac{(t_b / 2 + t_p / 2)t_b / 2}{E_b I_b} + \frac{1}{E_b A_b} \right)$$

$$n_2 = \frac{Gb}{t_a E_p b}$$

$$B = \frac{Gb}{t_a} \left((\alpha_b - \alpha_p) \Delta T + \frac{M(x)t_b / 2}{E_b I_b} \right)$$

To obtain a solution, the differential equation (4.45) is written in a finite-difference format as

$$\frac{N_{i-1} - 2N_i + N_{i+1}}{h^2} - \omega N_i = B \quad \text{for } 0 \leq i \leq S \quad (4.46)$$

where i , h , S are step number, step length and number of steps, respectively, with $h = L_p / 2S$. Eq. (4.46) can be rewritten as

$$N_{i-1} - (2 + \omega h^2)N_i + N_{i+1} = Bh^2 \quad \text{for } 0 \leq i \leq S \quad (4.47)$$

The boundary condition at the end of the CFRP plate is

$$N_0 = N(0) = 0 \quad (4.48)$$

Substituting (4.48) into (4.47) gives

$$-(2 + \omega h^2)N_1 + N_2 = Bh^2 \quad (4.49)$$

At the middle of span, the shear stress is zero, so

$$\frac{dN_b(L_p/2)}{dx} = \frac{N_{S+1} - N_{S-1}}{2h} = 0 \quad (4.50)$$

Substituting (4.50) into (4.47) gives

$$N_{S-1} - (1 + \omega h^2/2)N_S = Bh^2/2 \quad (4.51)$$

Combining (4.47), (4.49) and (4.51) gives

$$\begin{bmatrix} -2 - \omega h^2 & 1 & & & & \\ 1 & -2 - \omega h^2 & 1 & & & \\ & & \ddots & \ddots & \ddots & \\ & & & 1 & -2 - \omega h^2 & 1 \\ & & & & 1 & -1 - \omega h^2/2 \end{bmatrix} \begin{bmatrix} N_1 \\ N_2 \\ \vdots \\ N_{S-1} \\ N_S \end{bmatrix} = \begin{bmatrix} Bh^2 \\ Bh^2 \\ \vdots \\ Bh^2 \\ Bh^2/2 \end{bmatrix} \quad (4.52)$$

and N_i can be found by the solution of these linear equations.

According to (4.5),

$$\tau_i = -\frac{-N_{i+2} + 4N_{i+1} - 3N_i}{2hb} \quad \text{for } 0 \leq i \leq S-1 \quad (4.53)$$

and

$$\tau_i = 0 \quad \text{for } i = S \quad (4.54)$$

4.3.1.4 Normal stresses with taper

Differentiating (4.28) twice with respect to x and substituting eqs. (4.29), (4.30) and (4.6) gives

$$\frac{1}{b} \frac{d^3 V_b(x)}{dx^3} = \frac{E_a}{t_a} \left(\frac{1}{E_p I_p} M_p(x) - \frac{1}{E_b I_b} M_b(x) \right) \quad (4.55)$$

Substituting (4.32) and (4.8) into (4.55) gives

$$M_b^{(4)}(x) + f_4 M_b(x) = f_5 \quad (4.56)$$

where

$$f_4 = \frac{E_a b}{t_a} \left(\frac{1}{E_b I_b} + \frac{1}{E_p \times \frac{1}{12} b (kx + t_{end})^3} \right) \quad \text{for } 0 \leq x \leq a \quad (4.57)$$

$$f_4 = \frac{E_a b}{t_a} \left(\frac{1}{E_b I_b} + \frac{1}{E_p \times \frac{1}{12} b t_p^3} \right) \quad \text{for } a < x \leq L_p / 2 \quad (4.58)$$

$$f_5 = \frac{E_a b}{t_a} \times \frac{M(x) + N_b(x)(t_b / 2 + (kx + t_{end}) / 2)}{E_p \times \frac{1}{12} b (kx + t_{end})^3} - \frac{d^3 \tau(x)}{dx^3} b t_b / 2 \quad \text{for } 0 \leq x \leq a \quad (4.59)$$

$$f_5 = \frac{E_a b}{t_a} \times \frac{M(x) + N_b(x)(t_b / 2 + t_p / 2)}{E_p \times \frac{1}{12} b t_p^3} - \frac{d^3 \tau(x)}{dx^3} b t_b / 2 \quad \text{for } a < x \leq L_p / 2 \quad (4.60)$$

$$f_1 = f_2 = f_3 = 0$$

Substituting these into the fourth order finite-difference equation (4.56) gives

$$(M_b)_{i+2} - 4(M_b)_{i+1} + (6 + h^4 f_4)(M_b)_i - 4(M_b)_{i-1} + (M_b)_{i-2} = f_5 h^4 \quad (4.61)$$

Now let us considering the boundary conditions.

1. At the ends, where $x=0$

$$M_b(0) = M(0), \text{ or } (M_b)_0 = M(0) \quad (4.62)$$

and

$$M'_b(0) = V_b(0) - \tau(0) b t_b / 2 \quad (4.63)$$

so,

$$-\frac{1}{12}(M_b)_2 + \frac{2}{3}(M_b)_1 - \frac{2}{3}(M_b)_{-1} + \frac{1}{12}(M_b)_{-2} = (V_b(0) - \tau(0) b t_b / 2) h \quad (4.64)$$

When $i=0$, substituting (4.62) and (4.64) into (4.61) gives:

$$(M_b)_2 - 6(M_b)_1 + 2(M_b)_{-1} = 6h_2 \tau(0) b t_b / 2 + \frac{1}{2} h^4 f_5 - 6V_b(0) h - \frac{1}{2} (6 + h^4 f_4) M(0) \quad (4.65)$$

When $i=1$, substituting (4.62) into (4.61) gives:

$$(M_b)_3 - 4(M_b)_2 + (6 + f_4 h^4)(M_b)_1 + (M_b)_{-1} = h^4 f_5 + 4M(0) \quad (4.66)$$

2. At mid-span, when $x=L_p/2$

$$B = \begin{bmatrix} 6h\tau(0)t_b/2 + f_5h^4/2 - 6V_b(0)h - \frac{1}{2}(6 + h^4 f_4)M(0) \\ f_5h^4 + 4M(0) \\ f_5h^4 - M(0) \\ \vdots \\ f_5h^4 \\ f_5h^4 - q/3 - 2V(L_p/2)h \\ 0.5f_5h^4 - 2q/3 + 2V(L_p/2)h \end{bmatrix}_{(S+1) \times 1} \quad Y = \begin{bmatrix} (M_b)_{-1} \\ (M_b)_1 \\ (M_b)_2 \\ \vdots \\ (M_b)_{S-1} \\ (M_b)_S \end{bmatrix}_{(S+1) \times 1}$$

and $(M_b)_i$ can be obtained from the solution of these linear equations.

Differentiating (4.32) and expressing M''_b in finite difference format gives

$$\sigma_i = \frac{-(M_b)_{i+2} + 16(M_b)_{i+1} - 30(M_b)_i + 16(M_b)_{i-1} - (M_b)_{i-2}}{12h^2b} + \tau'_i t_b / 2 + \frac{q}{b} \quad (4.74)$$

To examine the convergence of the numerical procedure, the maximum stresses for plates with taper under thermal load obtained using different number of steps are shown in Figure 4.4. It indicates that the shear stresses converge at 500 steps and the normal stresses converge at 4000 steps.

4.3.2 Stress solution for the asymmetric load case

4.3.2.1 Shear stresses without taper

Assuming that the shear stress approaches $gM'(x)$ for large values of x , the general solution for shear stresses has the form:

$$\tau(x) = c_3 e^{-\lambda x} + gM'(x) \quad (4.75)$$

The boundary condition at the end of the plate gives zero longitudinal force, and c_3 can be given as

$$c_3 = \frac{1}{\lambda} \left(\frac{G}{t_a} (\alpha_b - \alpha_p) \Delta T + \frac{G}{t_a} \frac{M(0)t_b/2}{E_b I_b} + gM''(0) \right) \quad (4.76)$$

4.3.2.2 Normal stresses without taper

Eq. (4.36), the solution for normal stresses for the symmetric load case, can also be used for the asymmetric load case.

4.3.2.3 Shear stresses with taper

Assuming that the shear stress approaches $gM'(x_s)$ for large values of x_s (at least $a+50$ mm), the boundary condition for the symmetric load case at mid-span, where the shear stress is zero, can be substituted by the boundary condition at large value of x_s , where the shear stress is $gM'(x_s)$, so

$$\frac{dN_b(x_s)}{dx} = \frac{N_{S+1} - N_{S-1}}{2h} = -bgM'(x_s) \quad (4.77)$$

Therefore, the boundary equation (4.51) can be substituted by the following equation:

$$N_{S-1} - (1 + \omega h^2 / 2)N_S = Bh^2 / 2 + hbgM'(x_S) \quad (4.78)$$

where hx_S (equal x_s) is the calculated length of the retrofitted beam and no point load should be applied to the beam over this length.

4.3.2.4 Normal stresses with taper

Assuming that the boundary condition at mid-span does not affect the normal stress, the boundary condition equations in the asymmetric load case can be the same as (4.71) and (4.72), but the calculated length $L_p/2$ is substituted by $h \times S$.

4.3.3 Maximum shear stress and normal stress without taper

At the end of the CFRP plate, $x=0$, the maximum shear stress τ_{max} and normal stress σ_{max} can be written as:

$$\tau_{max} = \sqrt{\frac{G}{t_a b \bar{\lambda}}} (\alpha_b - \alpha_p) \Delta T + \bar{g} \sqrt{\frac{G}{t_a b \bar{\lambda}}} M(0) + \frac{\bar{g}}{b \bar{\lambda}} V(0) \quad (4.79)$$

and

$$\sigma_{max} = -\beta t_p \tau_{max} - \frac{E_a}{2\beta^3 t_a} \frac{1}{E_b I_b} (V(0) + \beta M(0)) + \frac{t_p G}{2t_a} ((\alpha_b - \alpha_p) \Delta T + \bar{g} M(0)) \quad (4.80)$$

where

$$\bar{g} = \frac{t_b / 2}{E_b I_b}, \quad \bar{\lambda} = \frac{(t_b / 2 + t_p / 2)t_b / 2}{E_b I_b} + \frac{1}{E_b A_b} + \frac{1}{E_p A_p}, \quad \beta = \sqrt[4]{\frac{E_a b}{4t_a E_p I_p}}$$

Eqs. (4.79) and (4.80) provide a simple means of calculating the maximum shear and normal stresses, respectively.

4.3.4 Maximum principal stress

Combining the maximum shear and normal stresses, the maximum principal stress σ_{1max} can be written as

$$\sigma_{1max} = \frac{\sigma_{max}}{2} + \sqrt{\left(\frac{\sigma_{max}}{2}\right)^2 + \tau_{max}^2} \quad (4.81)$$

4.4 Longitudinal strain at the CFRP plate bottom

4.4.1 Calculation for longitudinal strain

Integrating (4.5) and substituting with (4.7), the longitudinal force in the CFRP plate, N_p , is given as

$$N_p(x) = b \int_0^x \tau(t) dt \quad (4.82)$$

Substituting (4.22), the solution of shear stresses, into (4.82) gives

$$N_p(x) = -\frac{bc_3}{\lambda} e^{-\lambda x} + bgM(x) + \frac{bc_3}{\lambda} - bgM(0) \quad (4.83)$$

Integrating (4.4), the shear force in the CFRP plate, $V_p(x)$, is given as

$$V_p(x) = \int_0^x -b\sigma(t) dt \quad (4.84)$$

Substituting (4.84) into (4.33), and integrating (4.33), the bending moment in the CFRP plate, $M_p(x)$, is given as

$$M_p(x) = \int_0^x -b(x-t)\sigma(t) dt - \int_0^x \tau(x)bt_p / 2 dt \quad (4.85)$$

Substituting (4.22) and (4.36), the solutions for stresses, into (4.85) gives

$$M_p(x) = \frac{b}{2\beta^2} e^{-\beta x} (s_1 \sin(\beta x) - s_2 \cos(\beta x)) - \frac{b}{2\beta} (s_1 + s_2)x + bm_1\tau(0)x - (m_1 + \frac{t_p}{2})N_p(x) - \frac{1}{2}bm_3qx^2 + \frac{bs_2}{2\beta^2} \quad (4.86)$$

The longitudinal strain at plate bottom ε_{pb} is hence

$$\varepsilon_{pb} = \frac{N_p}{E_p A_p} + \frac{M_p t_p / 2}{E_p I_p} \quad (4.87)$$

4.4.2 Analysis of the longitudinal strain at the plate bottom close to the end of plate

When $x=\delta$, and δ is very small in comparison to the thickness of the CFRP plate, i.e. $\delta \ll t_p$, N_p and M_p are given as:

$$N_p(\delta) = b\delta\tau(0) \quad (4.88)$$

and

$$M_p(\delta) = -\frac{1}{2}b\delta^2\sigma(0) - \frac{t_p}{2}b\delta\tau(0) \quad (4.89)$$

Substituting (4.88) and (4.89) into (4.87) gives the longitudinal strain at the end of the plate as

$$\varepsilon_{pb} = -\frac{1}{E_p} \left(\frac{3\delta^2}{t_p^2} \sigma(0) + \frac{2\delta}{t_p} \tau(0) \right) \quad (4.90)$$

Since $\delta \ll t_p$, the second term on the right hand side of eq. (4.90) is much larger than the first item. Also $\tau(0)$ is positive, so ε_{pb} is negative (compressive).

If the plate end is not free, i.e. when there is a spew fillet covering the end, the longitudinal force in the CFRP plate can be gives as:

$$N_p(\delta) = b\delta\tau(0) + N_s \quad (4.91)$$

where N_s is longitudinal force applied to the end of plate by the spew fillet. N_s increases with the size of spew fillet. Substituting (4.91) into (4.87) gives:

$$\varepsilon_{pb} = \frac{N_s}{E_p A_p} + \frac{1}{E_p} \frac{3\delta^2}{t_p^2} (-\sigma(0)) - \frac{1}{E_p} \frac{2\delta}{t_p} \tau(0) \quad (4.92)$$

This equation shows ε_{pb} increases with N_s , and for large N_s , ε_{pb} may even become positive i.e. tensile. Contrarily, ε_{pb} reduces as the effect of the spew fillet lessens. In

additional, ε_{pb} reduces as the peel stress ' $-\sigma(0)$ ' reduces, but increased as the shear stress ' $\tau(0)$ ' increases.

4.5 Finite element analysis

Finite element (FE) analysis has been employed to validate the stress results obtained from the analytical procedure. The general purpose software package ABAQUS [180] was used. A linear 3-D FE Model was established, in which only one half of the beam was considered because of symmetry. All nodes at mid-span were restrained to produce the required symmetry, and nodes at the end of the beam were restrained to represent simply roll-supported conditions.

A FE mesh of a half model is shown in Figure 4.5. The steel beam was modelled with 4-node doubly curved shell elements (element S4R), which had reduced integration with hourglass control and finite membrane strains. The adhesive and the carbon plate were modelled with 8-node linear brick elements (element C3D8R), which also had reduced integration with hourglass control to prevent shear locking. In order to obtain accurate stress results at the ends of the plate, a fine mesh was deployed in these areas, as shown in the figure.

The geometric model used in the finite element analysis was the same as that used in the mathematical analysis, shown in Figure 4.1. The dimensions used were as follows: $L_p=5$ m, $L_0=0.5$ m, $b=211.9$ mm, $t_a=2$ mm, $t_p=12$ mm. The steel beam was a 533 x 210 UB122. The dimensions of the taper were $a=0.2$ m and $t_{end}=2$ mm (see Figure 4.3).

The material behaviour of the metallic beam was isotropic, with the elastic modulus $E_b=210$ GPa and the Poisson's ratio $\nu_b=0.3$. The material behaviour of the adhesive was also isotropic, with the elastic modulus $E_a=10$ GPa, the Poisson's ratio $\nu_a=0.3$, and the shear modulus $G=3.7$ GPa. The material behaviour of the CFRP plate was orthotropic with elastic moduli $E_{p1}=E_{p2}=10$ GPa, and $E_{p3}=310$ GPa. The Poisson's ratios $\nu_{p12}=0.3$, the shear moduli $G_{12}=4.7$ GPa.

In this work, the stresses were obtained from the average values of the stress in the bottom elements of the adhesive layer. To examine the convergence of the FE procedure, the maximum stresses in models with plates having no taper under thermal load were examined. The results with increasing number of elements in the longitudinal direction in the area near the ends of the plate are shown in Figure 4.6. It indicates that the shear stresses converge at the point of 50 elements and the normal stresses converge at the point of around 200 elements. Hence 200 elements in the longitudinal direction in the area near the ends of the plate were used.

4.6 Results and discussion

The FE results are compared with the analytical and the numerical results for the six cases shown in Figures 4.7-12, with the thermal load $\Delta T=50^{\circ}\text{C}$, the uniformly distributed load (UDL) $q=500\text{ kN/m}^2$, and the concentrated load $P=500\text{ kN}$. As shown in the figures, agreement is good for the distributions. The maximum values, given in Table 4.1, also agree well overall. These results demonstrate that the present procedure is accurate. From these results, it can be observed that:

1. High stress concentrations occur at the ends of adhesively bonded plates, and the normal, or peeling, stress disappears at around 20 mm from the end of the plates, which agrees with results from previous research [56].
2. The maximum stresses in the FE solution occur at a short distance from the ends. For the analytical solution, Assumption 2, i.e. St. Venant theory, means that the solution is not applicable at the plate end due to the free end and the high stress concentration.

The shear and the normal stresses for ‘the with’ and ‘the without’ taper cases under thermal load are compared in Figure 4.13, which clearly shows the significantly different stress distribution when a taper is included. Table 4.2 shows the differences in maximum stresses between the two cases. From these values, one can observe that the taper reduces the shear stresses by about 30% and the maximum normal stresses

by about 50%; hence including a taper is a very beneficial detail for avoiding debonding of the CFRP plate.

4.7 Parametric study

Various parameters influence the maximum values of the shear and the normal stresses in the adhesive layer. The most important ones are the thickness and the shear modulus of the adhesive, and the thickness and the elastic modulus of the CFRP plate. These parameters were studied using the analytical solutions, with the thermally-loaded model detailed in Section 4.5.

Figures 4.14-17 plot the maximum stresses versus the various adhesive and CFRP plate parameters. Figures 4.14 and 4.15 show that the maximum stresses reduce with the thickness of the adhesive but increase with the shear modulus; these are in agreement with the results from Her [97]. Figure 4.16 shows that the maximum stresses increase with the thickness of the CFRP plate. Figure 4.17 shows that the maximum shear stress increases with the elastic modulus of CFRP plate, but the maximum normal stress hardly changes.

Since a taper reduces the maximum stress, the taper parameters - the length of the taper a and the thickness at the end of the taper t_{end} - are also considered important. Figures 4.18 and 4.19 plot the normalised stresses at the tapered end of the plate versus the length of the taper for different tapered end thicknesses. The stresses shown have been normalised by the stresses at the end of the untapered plate. They indicate the beneficial effect of having a thin tapered end and a long taper. For the latter, the benefit appears to have saturated when the length of the taper is beyond 500 mm.

The results for mechanical loading, although not included here, show the same trend as those for thermal loading.

4.8 Conclusion

A simple closed-form solution to calculate the interfacial stresses of retrofitted metallic beams strengthened with CFRP plates under thermal and mechanical loads has been presented in this paper. A simple numerical solution, obtained using finite difference, has also been given for the case when the CFRP plates have tapered ends. FE analysis has been employed to validate the results from the analytical and the numerical solutions, and the agreement between the results obtained from the different solutions is good, which demonstrates that present procedure is simple yet accurate.

High stress concentrations have been shown to occur at the free ends of adhesively bonded plates. Including a taper of a certain geometry had been found to reduce about the maximum shear stresses by about 30% and the maximum normal stresses by about 50%. Hence a taper is very beneficial for avoiding debonding of the CFRP plates from the metallic beams.

The parametric study showed that the maximum shear and normal stresses decrease as the thickness of the adhesive increases, the shear modulus of adhesive decreases or the thickness of CFRP plate decreases. The decrease in the elastic modulus of the CFRP plate reduces the maximum shear stress, but has little influence on the normal stress. The dimensions of the taper also have an influence on the interfacial stresses. The maximum shear and normal stresses decrease as the thickness of the end of the taper decreases and the length of the taper increases. However, there is no further change in stress if the length of the taper is increased beyond 500mm.

Table 4.1 Comparison of the maximum stresses

End Condition	Load cases	Shear stress		Normal stress	
		Analytical (MPa)	FE (MPa)	Analytical (MPa)	FE (MPa)
Without Taper	Thermal	34.5	28.3	-25.6	-26.2
	UDL	17.4	14.9	-14.3	-14.3
	Concentrated	15.0	12.8	-11.2	-12.2
With Taper	Thermal	21.8	20.6	-14.2	-12.4
	UDL	10.8	10.7	-7.0	-6.4
	Concentrated	9.3	9.1	-6.1	-5.5

Table 4.2 Reduction of the maximum stresses by the taper

Load cases	Shear stress		Normal stress	
	Analytical	FE	Analytical	FE
Thermal	36.8%	27.2%	48.4%	51.1%
UDL	37.9%	28.2%	47.4%	55.2%
Concentrated	38.0%	28.9%	45.5%	54.9%

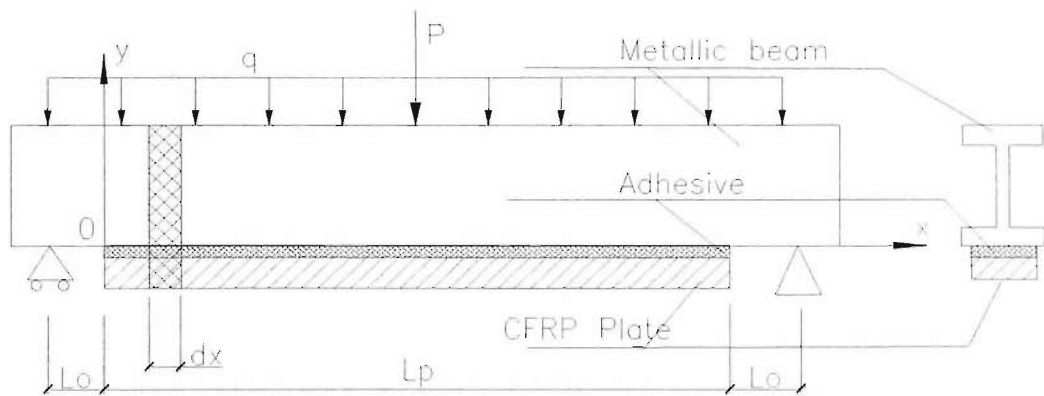


Figure 4.1 Geometric parameters

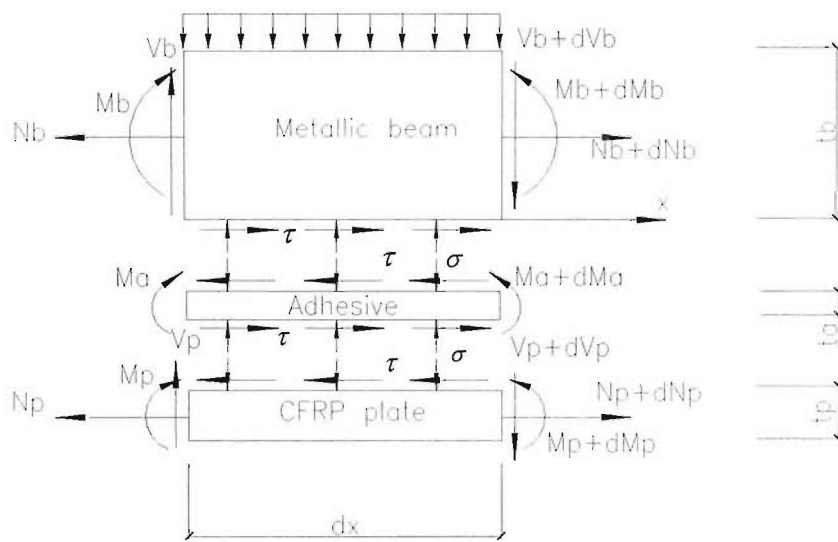


Figure 4.2 An infinitesimal element of a retrofitted beam

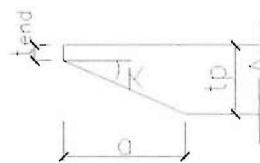


Figure 4.3 Geometric parameters of taper

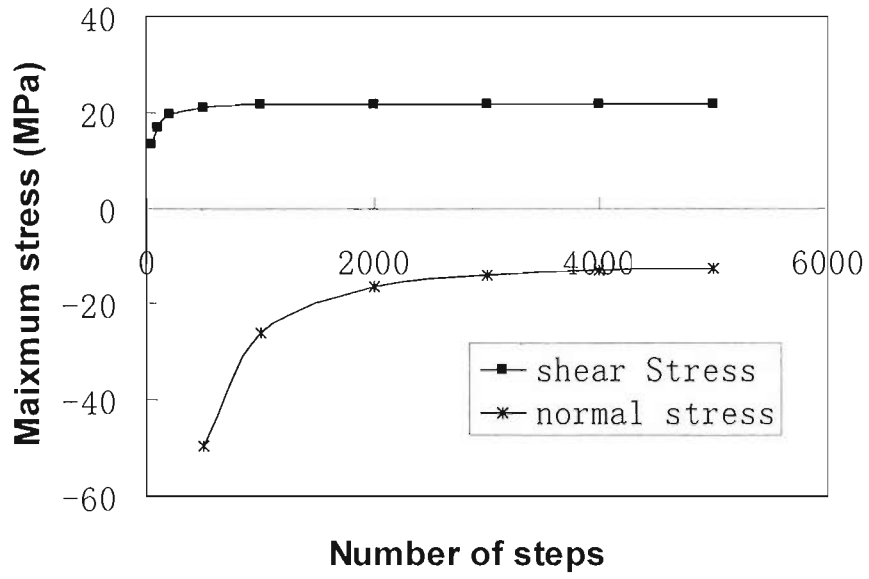


Figure 4.4 Convergence of the numerical procedure

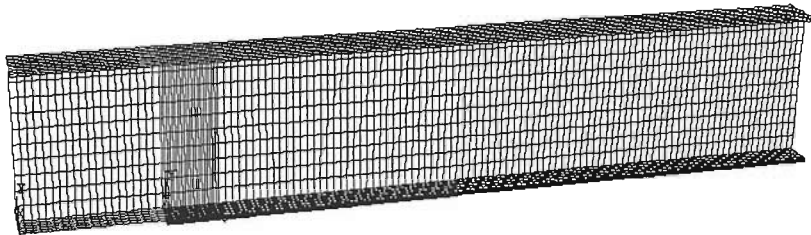


Figure 4.5 FE mesh of a half beam model

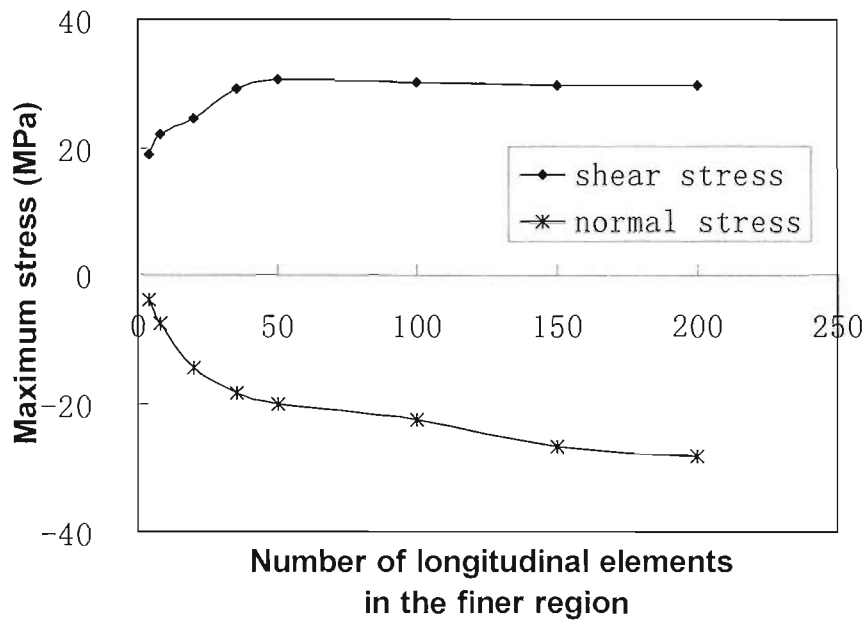


Figure 4.6 Convergence of the finite element analyses

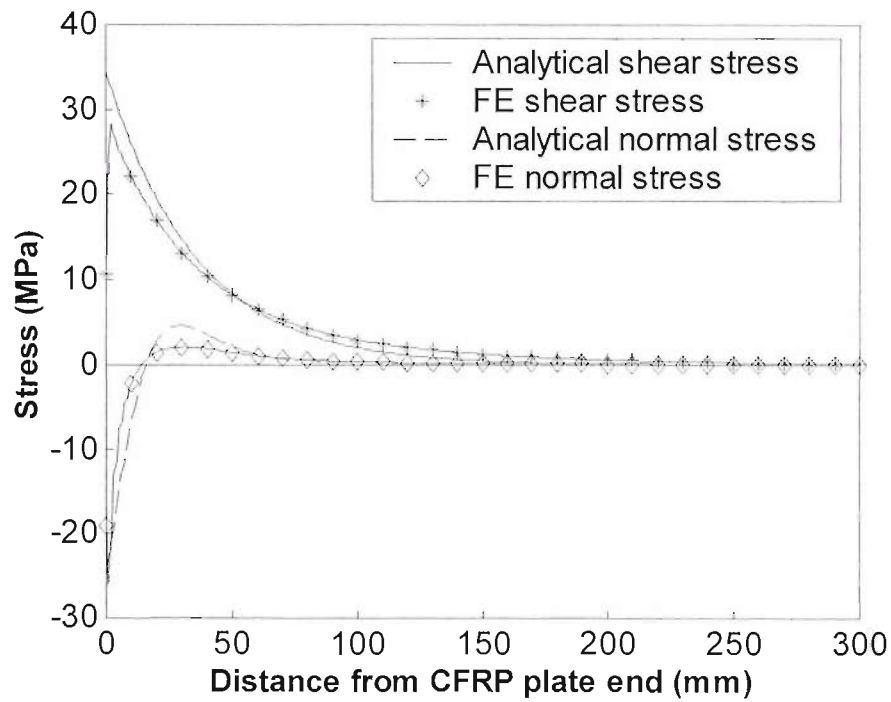


Figure 4.7 Comparisons of shear and normal stresses for plates without taper under thermal Load

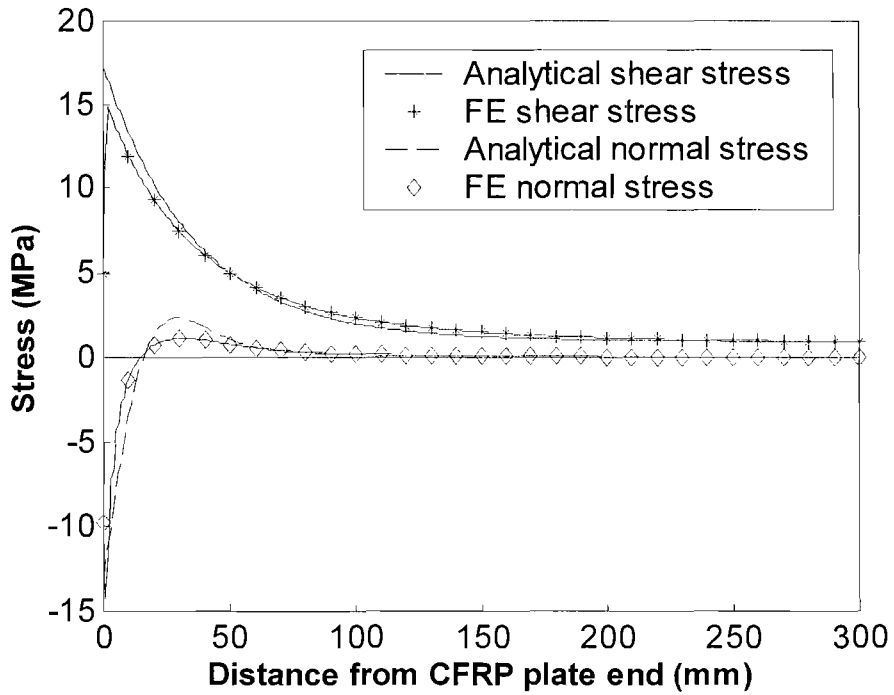


Figure 4.8 Comparisons of shear and normal stresses for plates without taper under UDL

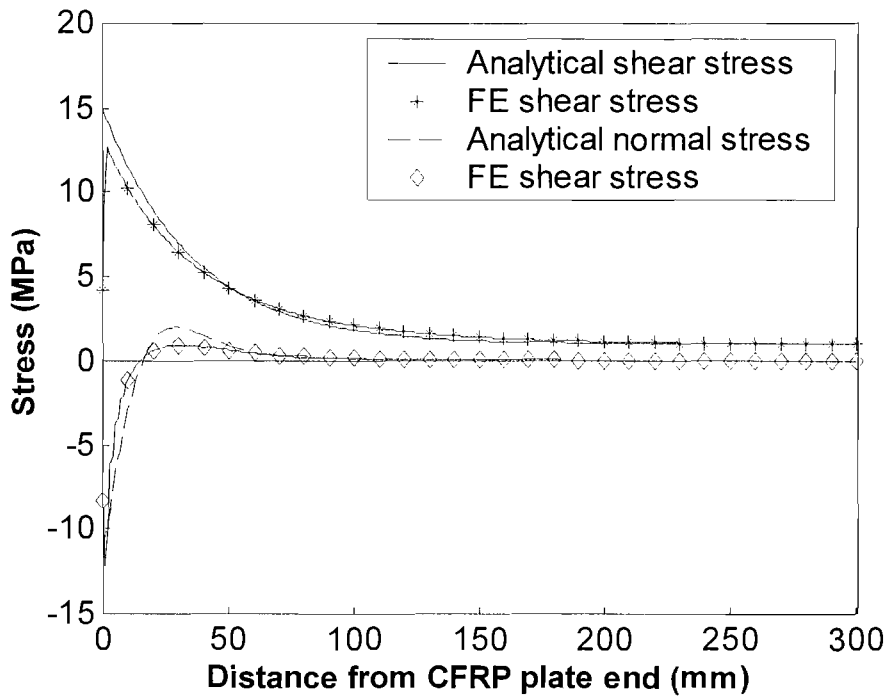


Figure 4.9 Comparisons of shear and normal stresses for plates without taper under concentrated load

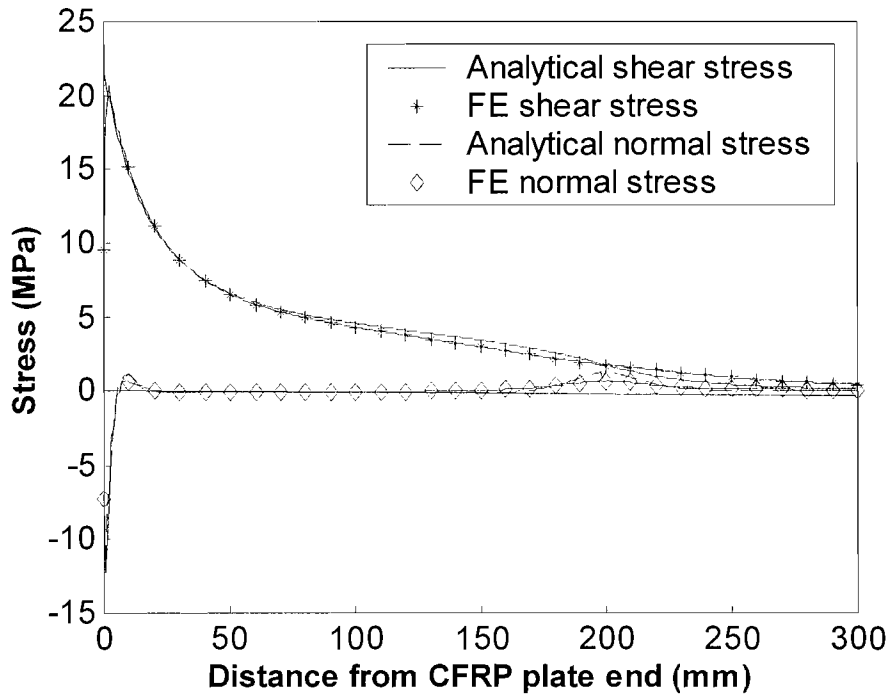


Figure 4.10 Comparisons of shear and normal stresses for plates with taper under thermal load

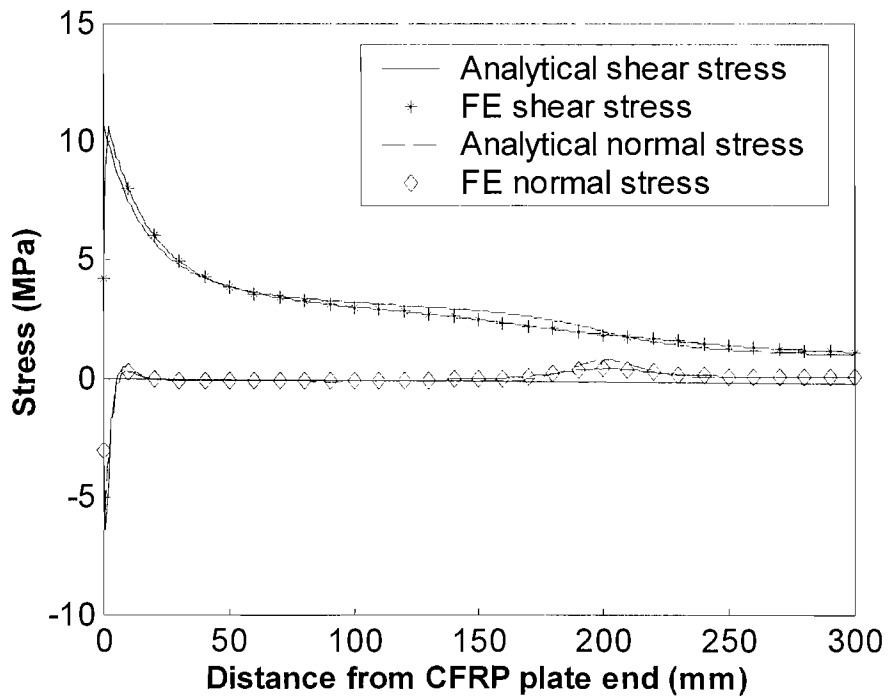


Figure 4.11 Comparisons of shear and normal stresses for plates with taper under UDL

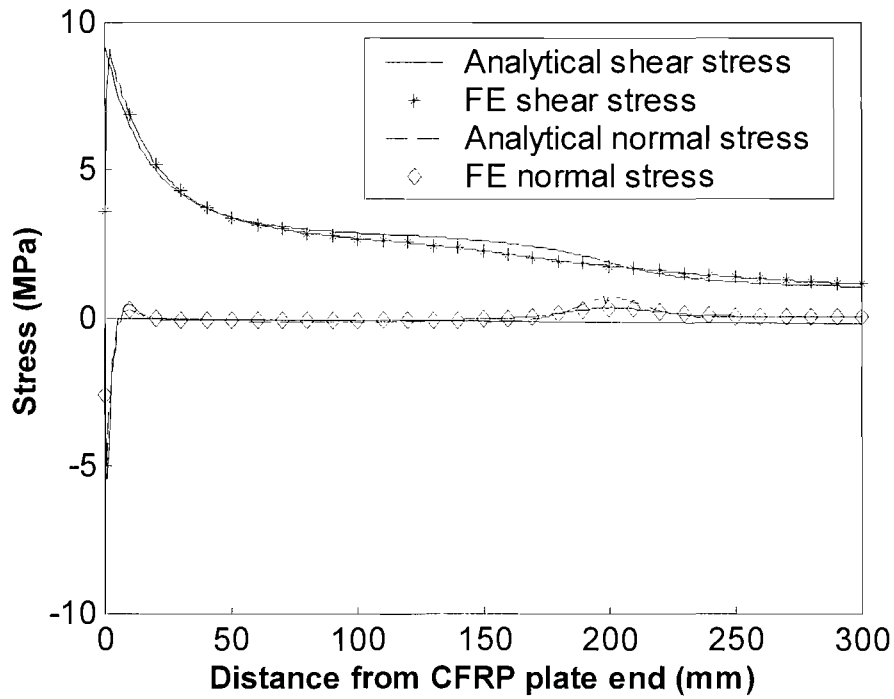


Figure 4.12 Comparisons of shear and normal stresses for plates with taper under concentrated load

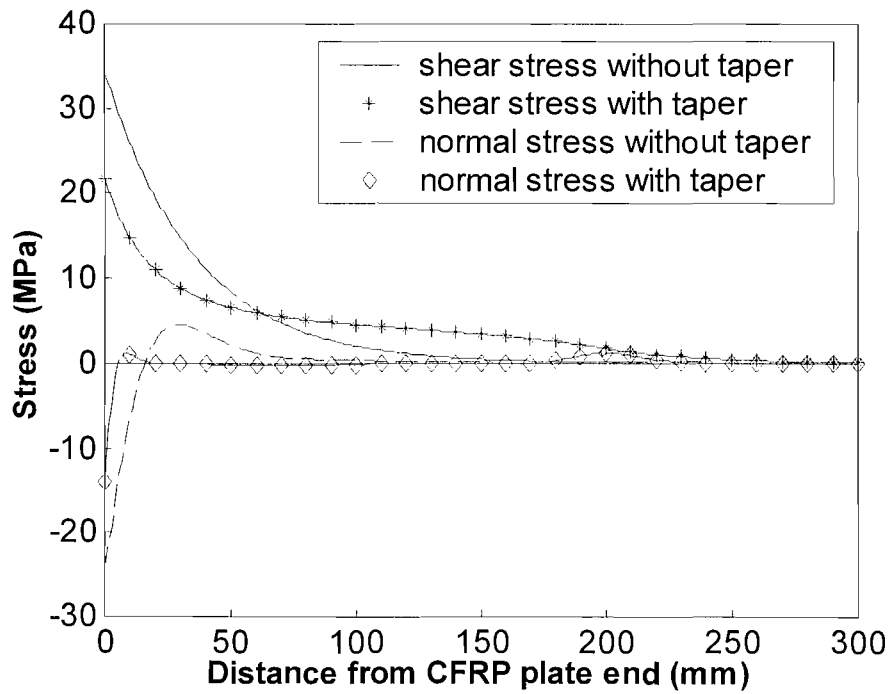


Figure 4.13 Comparison of stresses for plates with and without taper under thermal load

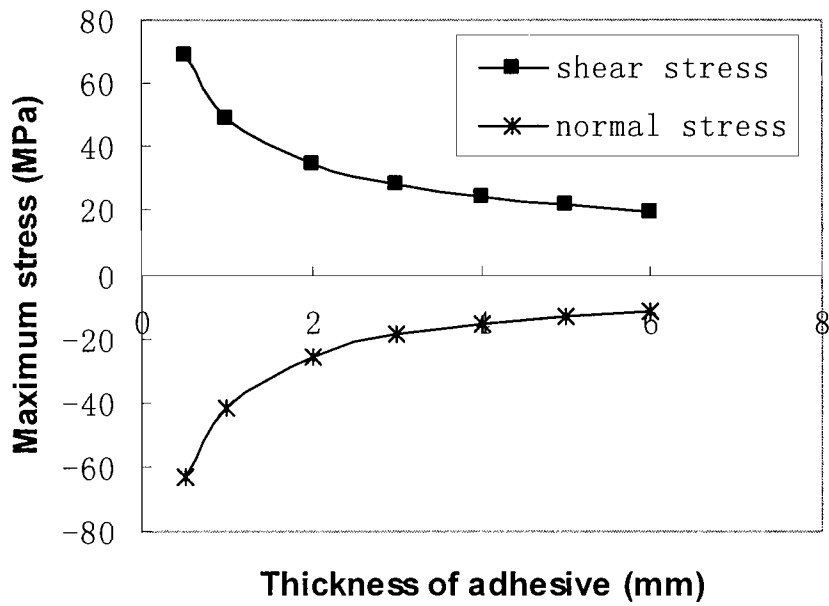


Figure 4.14 Variation of the maximum stress with the thickness of adhesive

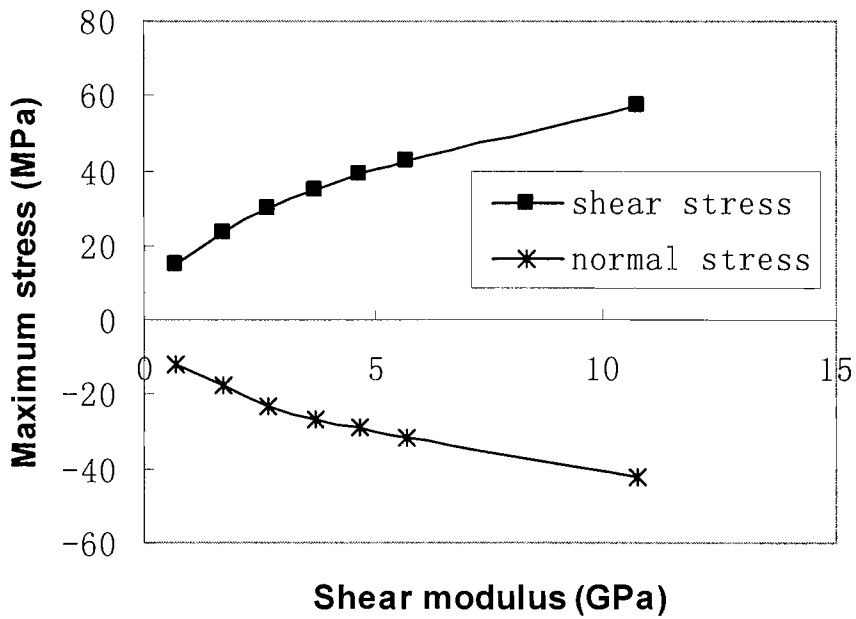


Figure 4.15 Variation of the maximum stress with the shear modulus of adhesive

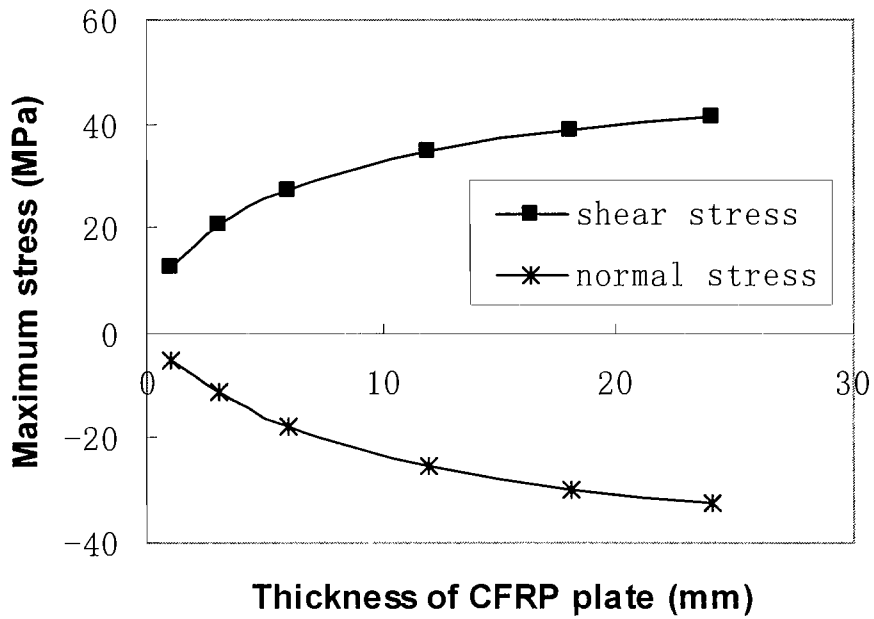


Figure 4.16 Variation of the maximum stress with the thickness of CFRP plate

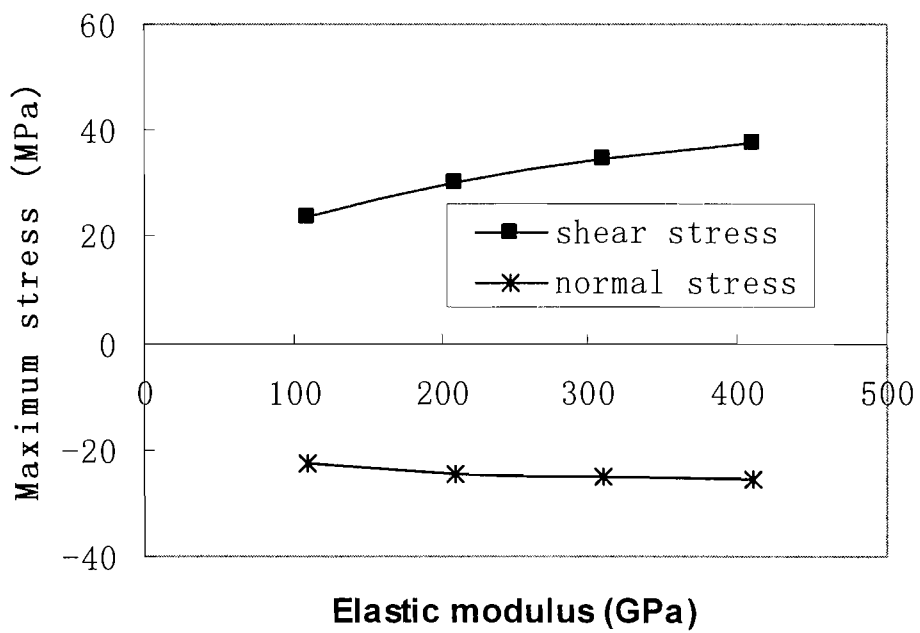


Figure 4.17 Variation of the maximum stress with the elastic modulus of CFRP plate

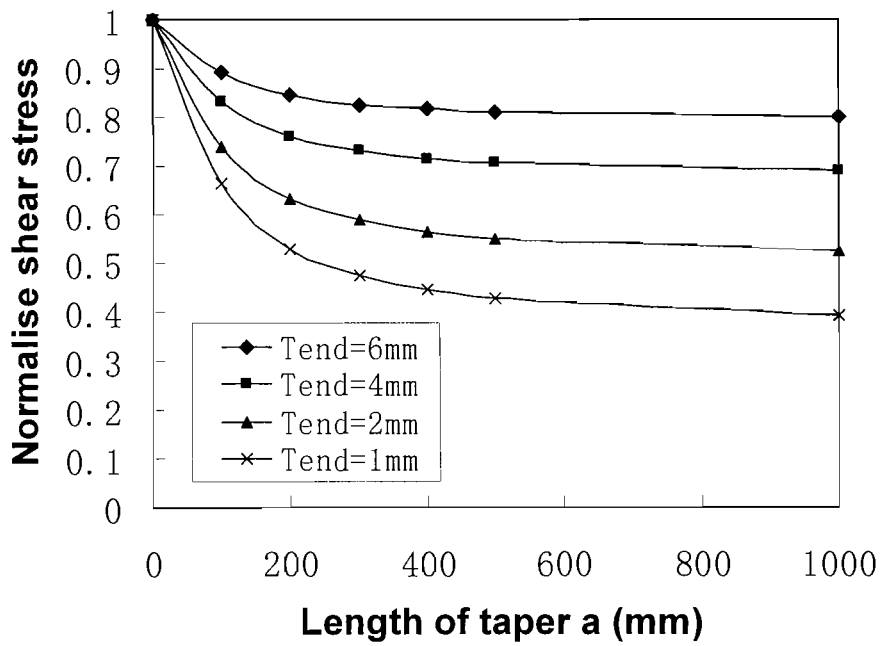


Figure 4.18 Comparison of shear stress ratio for different a and t_{end}

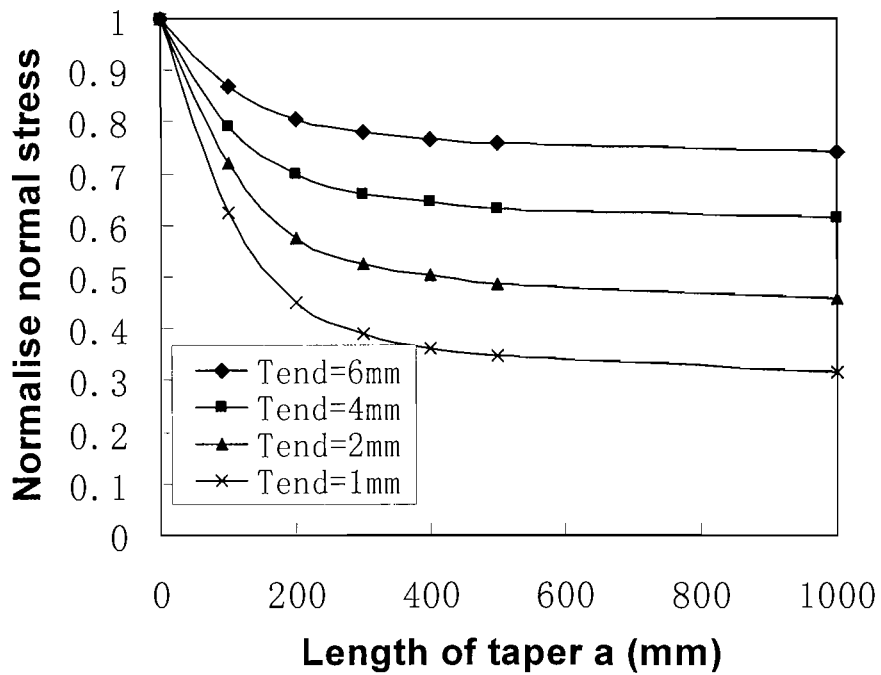


Figure 4.19 Comparison of normal stress ratio for different a and t_{end}

Chapter 5

Behaviour under static loading of steel beams reinforced with a bonded CFRP plate

5.1. Introduction and objectives

The literature review in Chapter 2 shows that the effectiveness of strengthening metallic beams by bonding CFRP plates has been established in theory, and that a number of metallic beams in buildings or bridges have been strengthened with CFRP in practice. It also shows that anchorage was used by Sen et al. [50] to prevent debonding failure, and tapers were employed to reduce the interfacial stress concentration in almost all of other research and applications. In addition to tapers, the use of spew fillets of adhesive beyond the end of the plate will help to reduce the stress and also provide some protection against the environmental attack on the adhesive layer [8].

For lap joints, theoretical analysis of interfacial stresses has been validated by tests [100,181]. For retrofitted metallic beams, however, all experimental studies have been focused on strength and stiffness improvements to date. Tests on debonding failure, investigations on the effects of tapered ends and of spew fillets, and the validation of the theoretically calculated maximum interfacial stresses are all absent. Buyukozturk et al. [73] reviewed recent research progress on issues relating to debonding problems, and indicate that specific research is needed to develop better failure criteria based on the calculated stresses, material properties and strengthening configuration for better prediction of debonding failure.

In this chapter, an experimental study of model-scale CFRP bonded steel beams is reported. The study investigated the different parameters that influence static strength, which include different lengths or thicknesses of CFRP plates, different load cases,

with or without tapers and adhesive spew fillets at the plate ends. Based on experimental observation, the effects of these influencing factors on the strength of the steel beams reinforced by different types of CFRP plates are evaluated. The test results are also used to validate the theoretical work on interfacial stresses in Chapter 4, and to establish the relationship between the theoretical maximum stresses in different specimens.

5.2 Experimental study

The strength of the adhesive bonding in steel beams reinforced with a CFRP plate was investigated by testing a number of small-scale specimens. In order to obtain an understanding of the various factors influencing strength, different plate lengths and thicknesses, three and four point bendings, with and without tapers, and presence of adhesive spew fillets at the ends of plate were considered. The matrix of the test specimens is shown in Table 5.1. Each specimen is identified with a serial number. The prefix 'S' symbolises static loading. The first digit 3 (or 4), indicates 3 (or 4) point bending. The second and third digits, multiplied by 100, denote the length, in mm, of the CFRP plate used in that specimen. The suffixes D, T and S in the last three specimens indicate double plate thickness, tapered plate and without spew fillets, respectively. It should be noted that the first beam, specimen S300, was unreinforced and used as a control specimen.

5.2.1 Specimen preparation

All the steel beams were 1.2m long mild steel 127x76UB13, with a measured mean yield strength of 357 MPa, and a mean modulus of elasticity of 206 GPa. To prevent premature flange buckling and web crushing, two 4 mm thick steel stiffeners were welded to each beam at mid span, one either side of the web. The flange surface of each specimen to which the CFRP plate was attached was first sand blasted to the SA2½ industry standard thoroughly. The CFRP plate was then attached within four hours.

The CFRP plates used were fabricated with 0.3 mm thick unidirectional epoxy prepreg SE84LV/HMC/300/400/35%+/-3%pop supplied by Structural Polymer Systems Ltd. Tensile tests, carried out in accordance with EN ISO 527, indicated that the modulus of elasticity was 208.3 GPa (manufacturer's data). 3 mm and 6 mm thickness CFRP plates were cut to a width of 76 mm and the appropriate length with a band saw. The ends of the plates were finished smoothly using sand papers. Before attaching the plate to the steel beam, both adhering surfaces were cleaned with 3M VHB surface cleaner. The tapered plates were manufactured using different lengths of prepreg laminates. The thickness of the tapered end was 0.9 mm and the length of the taper was 28 mm.

The adhesive used was Sikadur-31 Normal, a two-part thixotropic epoxy resin (see Chapter 3). It had a modulus of elasticity of 8 GPa, a shear modulus of 2.6 GPa (manufacturer's data). Two parts (resin and hardener, in 3:1 proportions) were mixed with 1% in weight of ballotini (1 mm diameter), which ensured a uniform thickness of the bond line.

After mixing, the adhesive was applied on to the beam and the plate. The method of applying the adhesive was to lay more adhesive along the centre than the outer edges, which allowed the air trapped between the adherends to escape when they were pushed together. After pressing the adherends together and scraping off the spewed adhesive, heavy steel blocks were placed on the top of the plate during curing to ensure the correct positioning of the plate on the steel beam, and a uniform thickness for the adhesive layer, as shown in Figure 5.1. After that, the excess adhesive along the longitudinal sides of the plate was scraped off, but not at the ends of the plate, so that a spew fillet would be present after curing. For specimen S304S (see Table 5.1), however, the excess adhesive was scraped off around all four edges. This specimen was used for comparison purposes with the other specimens. Each specimen was cured for at least 72 hours before testing. The ambient conditions during curing did not vary significantly from specimen to specimen. Some typical retrofitted specimens are shown in Figure 5.2.

5.2.2 Experimental setup

The specimens were tested in a servo-hydraulic Dennison 8032 test machine with a maximum capacity of 200 kN, subjected to either a three-point or a four-point bending set up. The clear span was 1.1 m and the loading points were 300 mm apart for the four-point bending tests. The schematic test setups for the three-point and four-point bending cases are shown in Figures 5.3 and 5.4, respectively. The specimens were supported on two saddle supports, which allowed the specimens to behave in a simply supported manner, and also limited the amount of longitudinal and transverse movement that could develop during testing. The test setup is shown in Figure 5.5.

For specimen S305, the strain distribution in the bottom of the CFRP plate was measured using seven 2 mm long strain gauges mounted along the longitudinal centre line of the CFRP plate (G1-G7 shown in Figure 5.6). In addition, three 5 mm long strain gauges were mounted on the steel beam – two on the flanges and one on the web in the middle of the specimens (G8-G10 shown in Figure 5.6). Strain gauges were also mounted at the ends of the plates in specimens S304S and S305D at locations G1 and G2. Deflections were measured at three locations using potentiometers, as shown in Figure 5.6. All data, including the load values measured by the sensor in the hydraulic, were automatically recorded by a data logging system. During loading, the strains, displacements and load were recorded every 0.1 second.

All specimens were tested under displacement control, with a stroke rate of 0.05 mm/sec. Loading of the specimen continued even after the debonding of the CFRP plate, which occurred in all but one cases. Loading was stopped when local post-yield buckling appeared in the beam.

5.3 Test results and discussion

A summary of the test results including the ultimate strengths with their associated deflections, and the failure modes are given in Table 5.2. Also included in the table are the maximum interfacial principal stresses at the plate end, calculated in accordance with the method detailed in Chapter 4.

5.3.1 Strength of specimens

The load versus displacement plots for specimens S303, S304, S305 and S310 are compared with that for the control beam, all under three-point bending, in Figure 5.7. The responses for the two retrofitted beams under four-point bending, S405 and S406, are given in Figure 5.8. Two aspects are noted from Figure 5.7. Firstly, all the retrofitted beams showed a strength enhancement over the plain control beam, and the strength enhancement increases with the length of the plate. Secondly, except for specimen S310, all the retrofitted beams failed by plate debonding, and after attaining a peak the load dropped suddenly and the load-displacement plot then after followed closely the response of the plain beam. Debonding failure occurred because the interfacial principal stress at the plate end has reached a critical value. This interfacial stress is dependent on the applied bending moment, as already shown in Chapter 4. The failure mode of debonding will be further discussed in Section 5.3.3.

The results for specimen S305, retrofitted with a 3 mm CFRP plate, and specimen S305D, retrofitted with a 6mm CFRP plate, are compared in Figure 5.9. It is clearly seen that the strength of specimen S305 is significantly higher than that of specimen S305D, since debonding occurred much earlier in specimen S305D, with the thicker plate. In other words, a thicker plate actually reduces the strength enhancement because it causes a higher stress concentration at the plate end. This finding concurs with the results of the theoretical stress analyses in Chapter 4.

The results for specimen S304, retrofitted with a constant thickness plate, and specimen S304T, retrofitted with a tapered plate, and specimen S304S, retrofitted with a plate without spew fillets (cleaned ends) are compared in Figure 5.10. The strength of specimen S304 is about 5% higher than that of S304S, which shows the spew fillet can increase the strength but only slightly in this case. This effect of spew fillet is far less than that found in lap joints, where a spew fillet can increase the strength by more than 100% [100]. The strength of S304T is a little lower than that of S304. This is an anomaly because a tapered end is expected to give better strength enhancement. Further investigation has found that at the plate end, specimen S304T had an average bond line thickness of 0.7 mm, rather than 1.0 mm, due to the

clamping used during curing. The reduction in the bond line thickness increased stress concentration and this more than cancelling the beneficial effect of the taper.

5.3.2 Stiffness of specimens

The load-deflection plots provide a measure of the stiffening effect as well. Figures 5.7-5.10 show that there was very little enhancement in stiffness prior to beam yielding, even for specimen S305D, which had a 6 mm thick CFRP plate. The lack of increase in stiffness in the elastic range is due to the relatively low Young's modulus (only slightly higher than that of steel) and the thin thickness of the CFRP plates. A significant increase in the thickness can increase the stiffness of the retrofitted beam, but then debonding would occur earlier since the maximum stresses increase with the thickness of CFRP plate.

The deflections measured at locations T1, T2 and T3 (see Figure 5.6) for the specimens under the three-point bending case at 70kN load level are compared in Figure 5.11. It can be observed that the deflections at mid-span (the extreme right set of data) of all the beams strengthened with different lengths of 3 mm thick CFRP plates are almost same, whereas that of S305D, with a 6 mm plate, is noticeably lower, indicating increasing the length of plate does not necessarily increase the stiffness in the middle, although it does delay debonding. The deflections in position T2 (middle set of data), which is at the end of plate in specimen S304, are reduced with the length of plate.

From these observations, it can be concluded that the length of plate has no significant influence on the deflections if the deflection position is far enough from the end of plate. It is the thickness, not the length, of the plate that is more effective in improving the stiffness.

5.3.3 Failure modes

There are three types of failure mode, as indicated in Table 5.2. The first, M1, applies to the plain control beam and specimen S310, which had the longest plate (1000 mm long). In the second mode, M2, the plate debonded but part of it remained attached to the beam. Total plate detachment is the third mode, M3.

The load-deflection plots in Figures 5.7-5.10 indicate that the loads suddenly dropped when the CFRP plates were debonded from the steel beams. A video recorder was used to record the progress of the debonding in specimen S304. The record shows debonding first occurred on one side of the CFRP plate, then quickly developed at the other side followed by the rapid detachment of the plate from the beam. From the strains recorded during the test, the measurement in all of the strain gauges dropped to zero in 0.1 second, which means the debonding process was instantaneous.

Figure 5.12 shows the failed specimen S304, indicating the typical total debonding between the steel beam and the adhesive. From the video record for the debonding process of this specimen, it was observed that debonding was initiated from one end (the right end in Figure 5.12) and progressed toward the other end. Figures 5.13 and 5.14 show all the debonded CFRP plates. These figures show that debonding developed from the right end mainly along the interface between the steel beam and the adhesive, but also at times irregularly along the interface between the CFRP plate and the adhesive. Both are indicative of adhesive failure. However, mixture failure (combination of adhesive failure on both interfaces, cohesive failure and delaminate failure in CFRP plate) occurred when debonding progressed toward the left end. Kadioglu et al. [109] show the stress concentration at the adhesive end in Thick Adherend Shear Test (TAST) causes the crack progressing along the interface between adherend and adhesive (adhesive failure) for all adhesives tested, if the cohesive failure at the end of the adherends was ignored.

As debonding progresses, the effective reinforcing length of the CFRP plate is reduced. Ignoring the debonded part of the plate and assuming the properties of the adhesive remain elastic, the interfacial stresses can be calculated by the analytical

method detailed in Chapter 4, with the effective plate length L'_p given by $L'_p = L_p - a$, where L_p is the actual plate length and a is the debonding length. This effective length influences the value of the bending moment at the location of the advancing debonded front. Moreover, in accordance with the observation given in Section 5.3.2, the stiffness would not be affected until debonding approaches the middle of the specimen. Also the stiffness would decrease rapidly to the level of that of a plain beam when debonding has reached the middle of the plate. Since the specimens were tested under the displacement mode, the deflections at the middle of the beams had remained almost constant but the load was reduced after debonding had crossed the middle of the beams. The calculated maximum interfacial stresses are plotted versus the debonding length in Figure 5.15 for specimen S304, in which the maximum interfacial stresses are shown to increase as debonding was advancing towards the middle of the plate but decrease as the applied load dropped, which led to a drop in the bending moment.

If debonding is analogous to the development of a crack, it is the result of the maximum principal stress occurring at the plate end. The maximum principal stresses for all specimens under the maximum applied loads in the tests are calculated analytically in accordance with Chapter 4. These analytical results are given in Table 5.2. For all the specimens except S310, which failed by buckling of compressive flange, the coefficient of variation is only 3%. This small variation indicates that the stresses obtained for all the specimens excluding S310 (which did not fail by debonding) are very close, confirming that the analytical predictions are reasonable.

Assuming the maximum interfacial stresses are the concentrated stresses at the crack front, the stress intensity factors are directly proportional to the maximum interfacial stresses. The energy release rate (G) is given by:

$$G = \frac{K_I^2}{E'} + \frac{K_{II}^2}{E'} \quad (5.1)$$

where K_I and K_{II} are the Mode I and Mode II stress intensity factors, respectively, and E' is the Young's modulus for the plane strain case. Guidance CIRIA C595 [8] also provides an equation to calculate the energy release rate G :

$$G = \frac{M^2}{2b_a} \left[\frac{1}{(EI)_I} - \frac{1}{(EI)_S} \right] \quad (5.2)$$

where M is the applied bending moment, b_a the width of adhesive layer, $(EI)_I$ and $(EI)_S$ the section bending stiffness of beam strengthened with the FRP plate and the plain beam, respectively. In term of Equation (4.79) and (4.80), M is directly proportional to the maximum interfacial stresses as well. Therefore, the schematic variation of the energy release rate with crack growth is similar to the square of the variation of the maximum interfacial stresses, shown in Figure 5.15. This variation for specimen S304 is shown in Figure 5.16. In this figure R is the crack growth resistance and G_c the fracture toughness. The area of the G curve above the $R=G_c$ line is the kinetic energy. When the energy release rate G becomes smaller than G_c , crack propagation was not caused by the stress concentration on the upper interface but caused by the kinetic energy. Since the CFRP plate was detached from the beam in the vertical direction, the crack growth caused by the kinetic energy was similar to that in double cantilever beam (DCB). This explains that mixture failure dominated at the end of the plate debonding. This also indicates that the fracture mechanics analysis suggested by guidance CIRIA 595 is reasonable.

The reason for total debonding not occurring in specimen S303 is that the CFRP plate is too short to create sufficient kinetic energy for total debonding. Similarly for specimen S305D, the load and the deflection when the plate is debonded is too low (see Figure 5.9) to release enough strain energy. The failure specimen S305D is shown in Figure 5.17. In Figure 5.13, the debonded face in specimen S406 is not as smooth as the others. This was because the adhesive spew fillet on the two sides of the CFRP plate was not cleaned up properly when the specimen was glued up.

The strains at the ends of the plates in specimens S305, S305D and S304S recorded are shown in Figure 5.18, 5.19 and 5.20, respectively. Due to the presence of the spew fillets, the initial absolute strains in specimen S305 are very low, and are even positive (i.e. tensile). In contrast, the strain curves for specimen S304S, which had no spew fillet, are linear initially. The strain curves for specimen S305D, Figure 5.19, in spite of including the spew fillets, also behave linearly. This is because the effect of the spew fillets, of which the size was small compared to the thickness of the

plate (6 mm), is low. Furthermore, debonding always starts at the end where the strain was initially lower in the same specimens.

5.3.4 Strain distributions in specimen S305

The CFRP plate in specimen S305 debonded at a load of 149 kN (see Table 5.2 and Figure 5.9). Within a very short time (less than 0.1 second) the strains in all the strain gauges on the plate dropped to zero, indicating that the debonding was instantaneous. Simultaneously, the load sustained by the specimen decreased to 108 kN. The strains in the plate recorded are shown in Figure 5.21, from which the following observation can be made:

- The specimen had a linear behaviour up to the yielding of the steel beam (at approximately 45 kN in accordance with the strain recorded in G7, and in G8, which is not included in Figure 5.21 because of the scale).
- After the steel beam has yielded (see also Figure 5.23), large deformation occurred and the strains increased rapidly in strain gauge G7, at mid-span. As load continued to increase, plasticity in the steel beam spread from the middle to the sides and the strain in G6 started to quickly increase.
- When the load was greater than about 130 kN, the strains in gauges G1, G2 and G3, close to the ends of CFRP plate, started to decrease with the load. When the load approached 149 kN, the failure load, The strain in G4, further away from the plate end, also dropped rapidly.

Therefore, the strain in the middle of CFRP plate increased rapidly, as described above, with the spread of plasticity in the steel beam. On the other hand, the reduction of the strain at the end of plate may indicate the plastication of the adhesive or the onset of debonding.

The longitudinal strain distributions in the CFRP plate recorded at different load levels in S305 are shown in Figure 5.22, which also gives an indication of the strain variations in different parts of the plate. It can be seen that there was a zone close to the plate end where the strain increased rapidly under lower load, and this zone spread toward the middle of the plate with increasing load.

The strains measured in gauges G7-G10, in the middle of specimen, at different load levels are compared in Figure 5.23. It should be noted that:

- Strain gauge G8 was not recording beyond 100 kN due to the excessive high strains at that location.
- The strains in the bottom of the specimen were much smaller than those in the top of the specimen due to the CFRP plate strengthening.
- Yielding of the steel beam started from the top, indicated by gauge G8, and spread to the bottom, indicated by gauge G9. The bottom of the beam had remained elastic up to failure, shown by G10.
- After the CFRP plate had debonded, the strain in the bottom of the steel beam increased suddenly (G10), and simultaneously the strain in the middle of the beam was reduced (G9).

Therefore, the strengthening effect was more pronounced after the steel beam had yielded. This is because the CFRP plate had about the same Young's modulus as that of steel. Since the thickness of the CFRP plate was less than half of that of the beam flange, except for specimen S305D, this means that prior to beam yielding, the longitudinal force in the CFRP plate was lower than that in the bottom steel flange. After beam yielding has occurred, the CFRP plate started to carry more of the applied loads.

The experimental data obtained from the test of specimen S305 are compared to the corresponding analytical results, calculated from the theory detailed in Chapter 4 at the load level of 40 kN, in Figure 5.24, which shows that the agreement is good.

5.4 Conclusion

In this chapter, an experimental study on steel beams bonded with a CFRP plate under static loading has been reported. The aim of the study was to investigate the various influencing factors that would cause the failure of the bonded beam. These factors include the effects of length and thickness of the CFRP plate, loading mode, taper and spew fillet plate.

The test results show that debonding, either complete or partial, was the main failure mode. Debonding occurs as a result of the maximum interfacial stress, which occurs at the end of the CFRP plate, reaching a critical value. This maximum interfacial stress can be predicted using the analytical method proposed in Chapter 4. The strength of the retrofitted beams increases with the length of the CFRP plate because a longer plate reduces the bending moment at the plate end and hence the magnitude of the stress level. On the other hand, a thicker plate tends to reduce strength, and this concurs with the theoretical work detailed in Chapter 4. The stiffness of a retrofitted beam was only marginally enhanced by the bonded CFRP plate, due to the relatively low Young's modulus and thickness of the plates used in the current study. The enhanced stiffness in the middle of the strengthened beams was found not to be influenced by the length of plate.

A spew fillet of adhesive was found to be able to reduce the maximum interfacial stresses, thereby increasing the strength of the retrofitted beam. However, the effect of spew fillet was found to be weaker than that of taper, which is different from the conclusion drawn on lap joints [100].

The coefficient of variation of the calculated maximum interfacial stresses at the plate ends of the test specimen, shown in Table 5.2, is small, illustrating that the formulation proposed in Chapter 4 has been validated by the test results.

The test results from S305 indicated the strain distribution in the CFRP plate under bending load and the variety of the strain distributions at different load levels. The strain distribution in the middle of the specimen indicated the strengthening effect is largely confined to the post-yield beams. The good agreement between the experimental data and the analytical results confirms the validity of the theory.

Table 5.1 Test specimen details

Specimen reference	Loading mode	Length of CFRP plate (mm)	Thickness of CFRP plate (mm)	Tapered plate	Spew fillets
S300	3 point bending	N/A(unreinforced)	N/A	N/A	N/A
S303	3 point bending	300	3	No	With
S304	3 point bending	400	3	No	With
S305	3 point bending	500	3	No	With
S310	3 point bending	1000	3	No	With
S405	4 point bending	500	3	No	With
S406	4 point bending	600	3	No	With
S305D	3 point bending	500	6	No	With
S304T	3 point bending	400	3	Yes	With
S304S	3 point bending	400	3	No	Without

Table 5.2 Results of tests and calculation of the specimens

Specimen	Max. Load (kN)	Ultimate mid-span deflection (mm) *	Failure mode **	Calculated Max. interfacial shear stress by Eq. (4.79) (MPa)	Calculated Max. interfacial normal stress by Eq. (4.80) (MPa)	Calculated Max. interfacial principal stress by Eq. (4.81) (MPa)
S300	122.6	20.07	M1	/	/	/
S303	120.0	5.12	M2	58.2	39.8	81.3
S304	135.0	7.00	M3	57.5	39.4	80.4
S305	149.1	12.43	M3	54.8	37.6	76.6
S310	159.5	20.10	M1	11.9	8.3	16.7
S405	157.5	7.45	M3	57.9	39.7	81.0
S406	185.5	18.32	M3	57.3	39.3	80.2
S305D	112.1	3.98	M2	51.3	42.0	77.2
S304T	130.1	6.71	M3	56.3	35.2	76.6
S304S	127.4	6.07	M3	54.1	37.2	75.9

Note:

*: ultimate mid-span deflection is the deflection when the CFRP plate debonded or when the steel beam failed.

** : Failure mode M1=beam flange buckling, failure mode M2=CFRP plate debonded but not detached totally from the steel beam, and failure mode M3=CFRP plate totally detached from the steel beam.

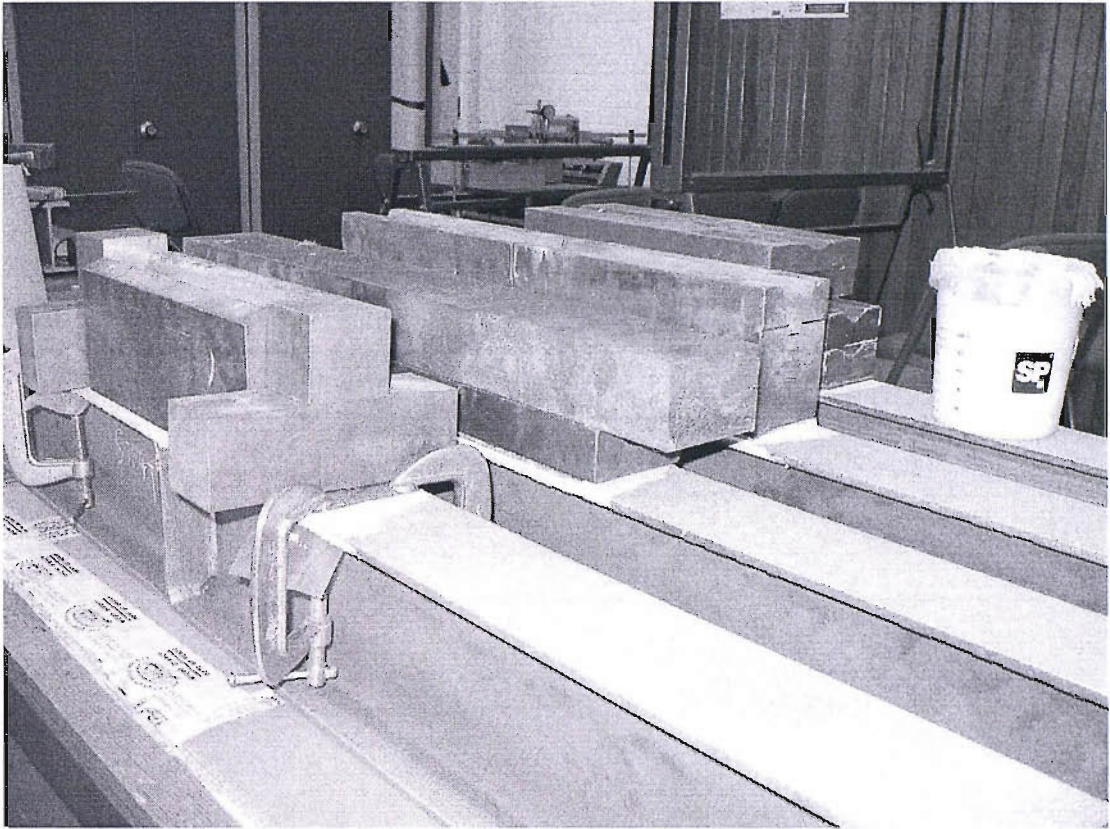


Figure 5.1 Curing specimens

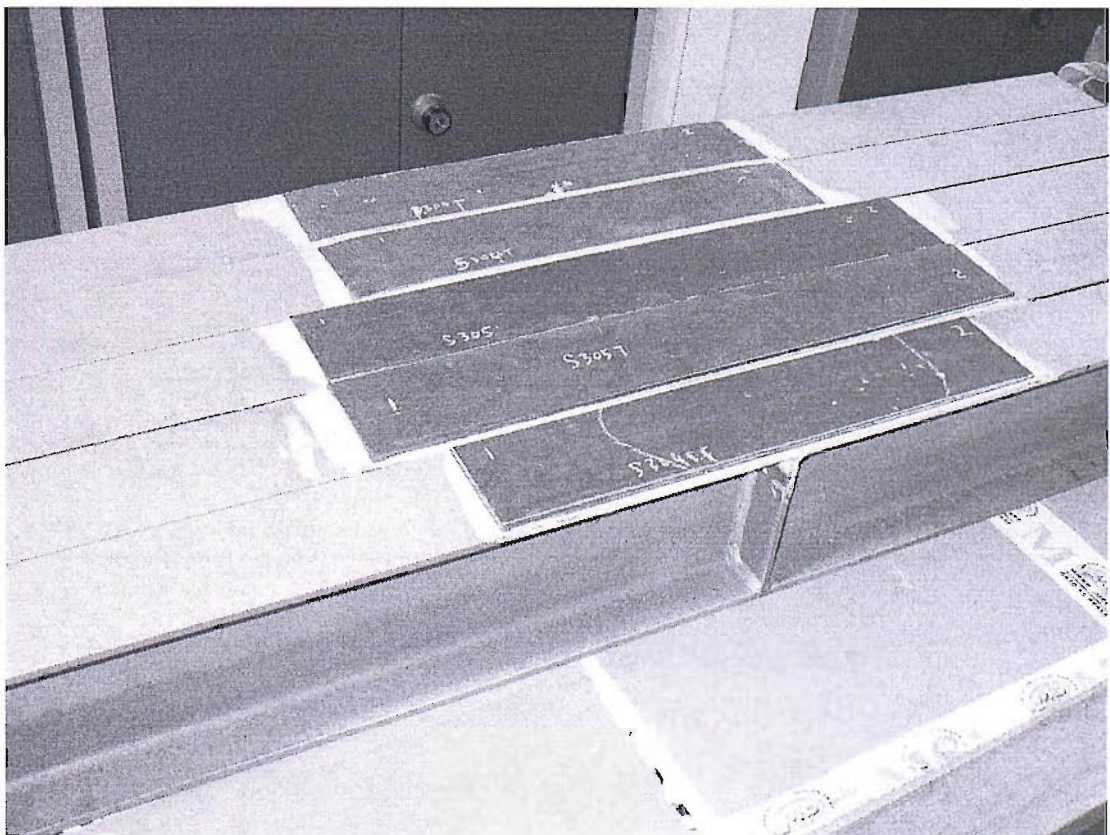


Figure 5.2 Typical retrofitted specimens

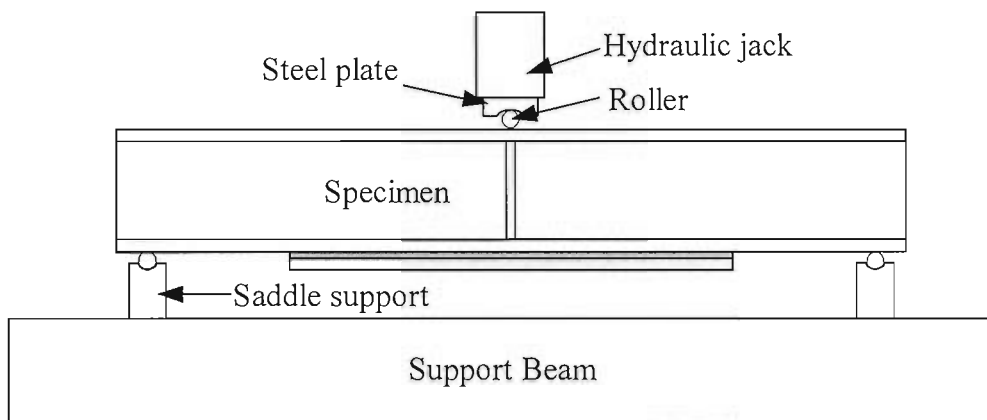


Figure 5.3 Schematic three-point bending setup

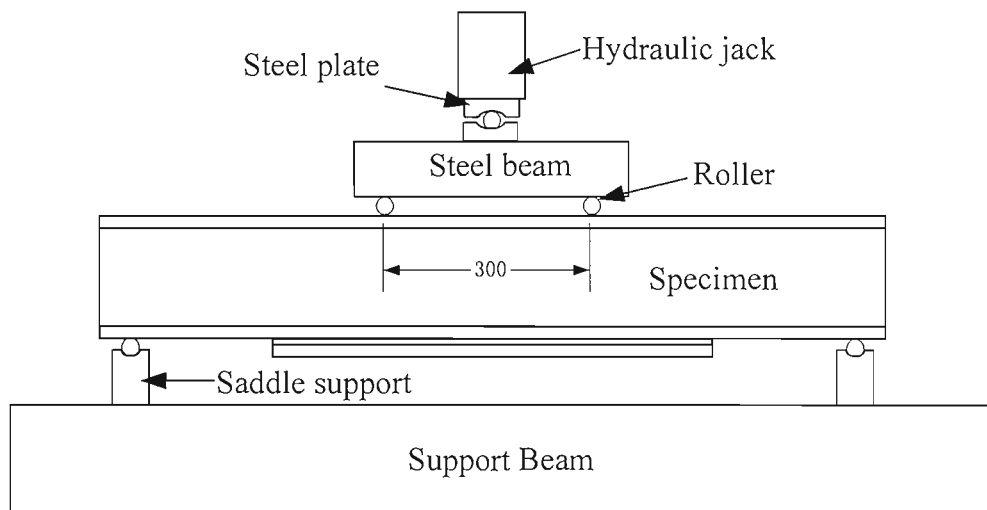


Figure 5.4 Schematic four-point bending setup

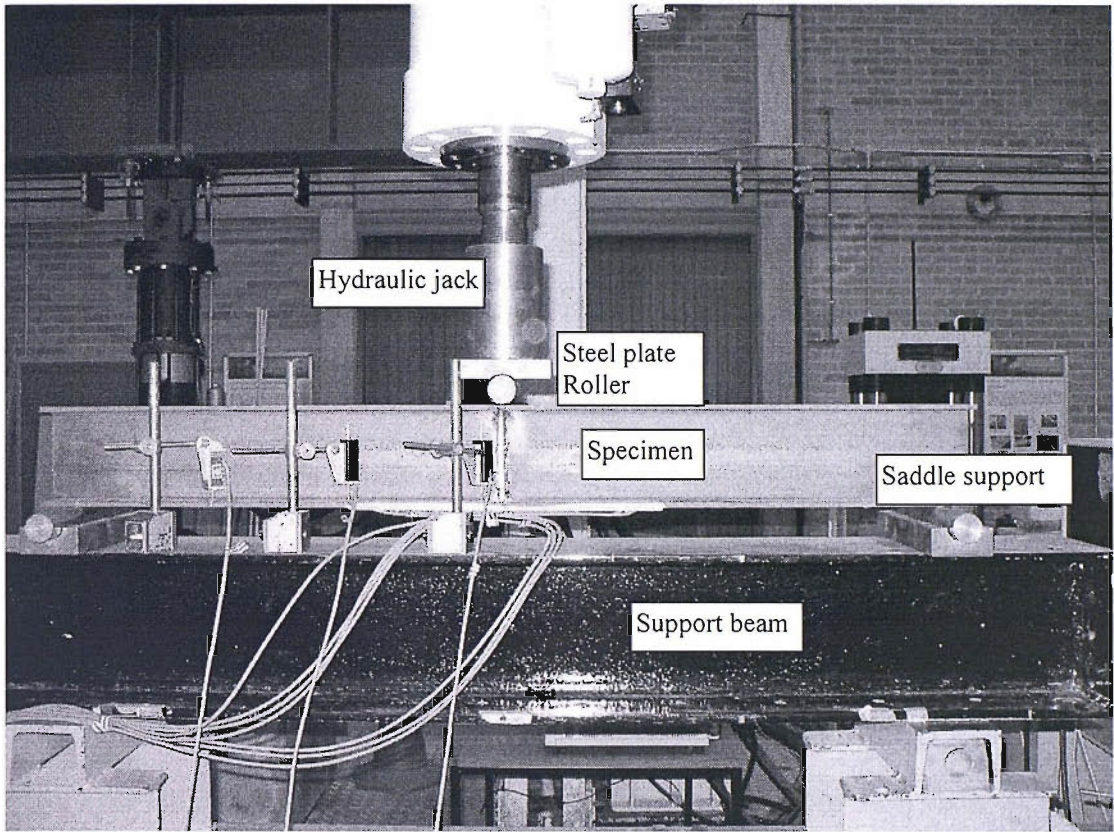


Figure 5.5 The test setup

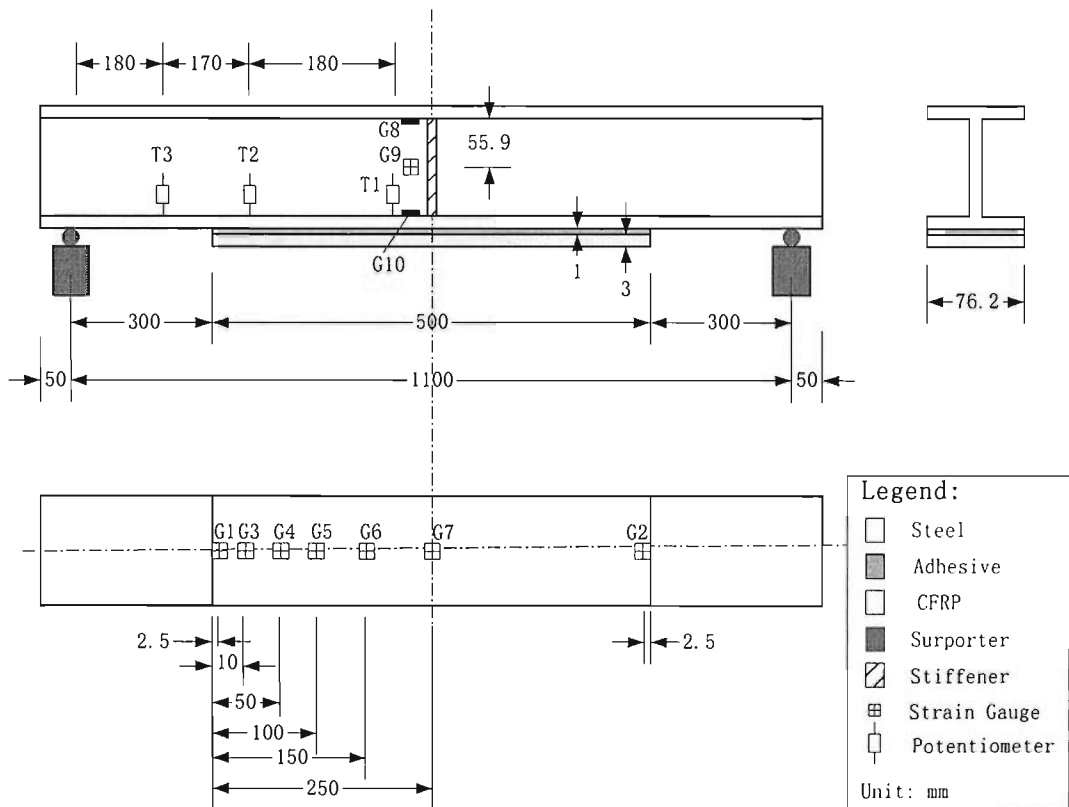


Figure 5.6 Dimensions of a typical specimen and the location of strain gauges and potentiometers

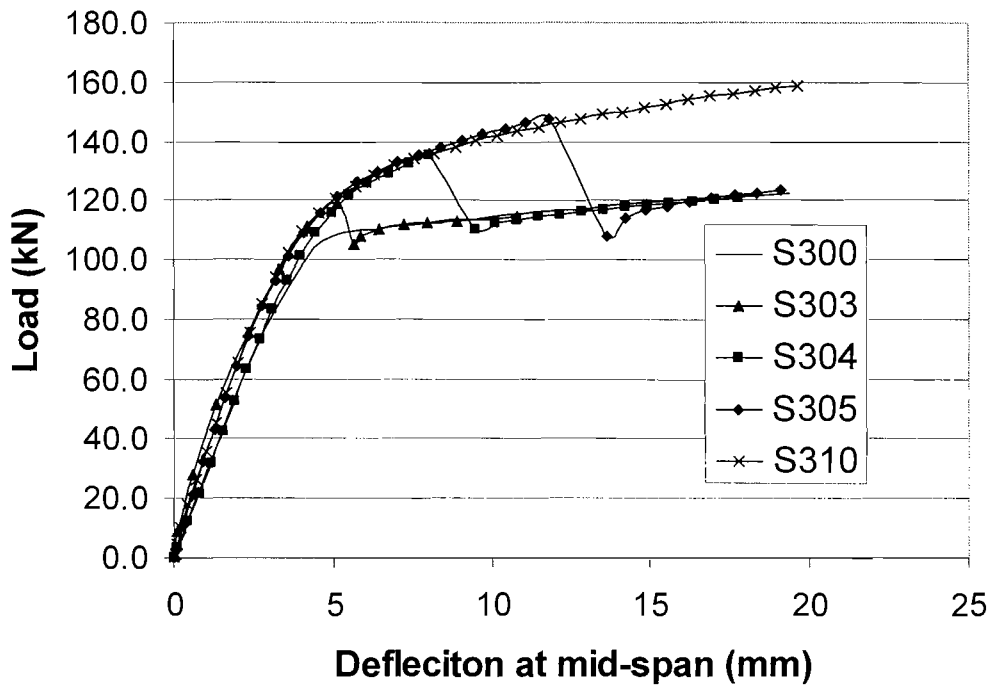


Figure 5.7 Comparisons of Load-deflection curves in specimens with different length CFRP plates under three-point bending

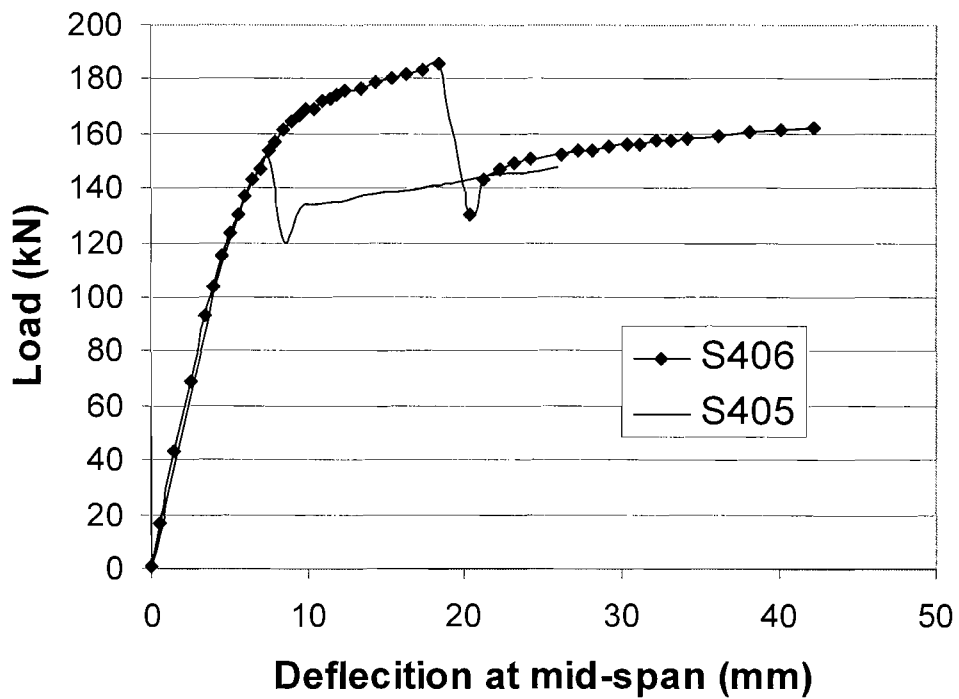


Figure 5.8 Comparisons of Load-deflection curves between specimens with different length CFRP plates under four-point bending

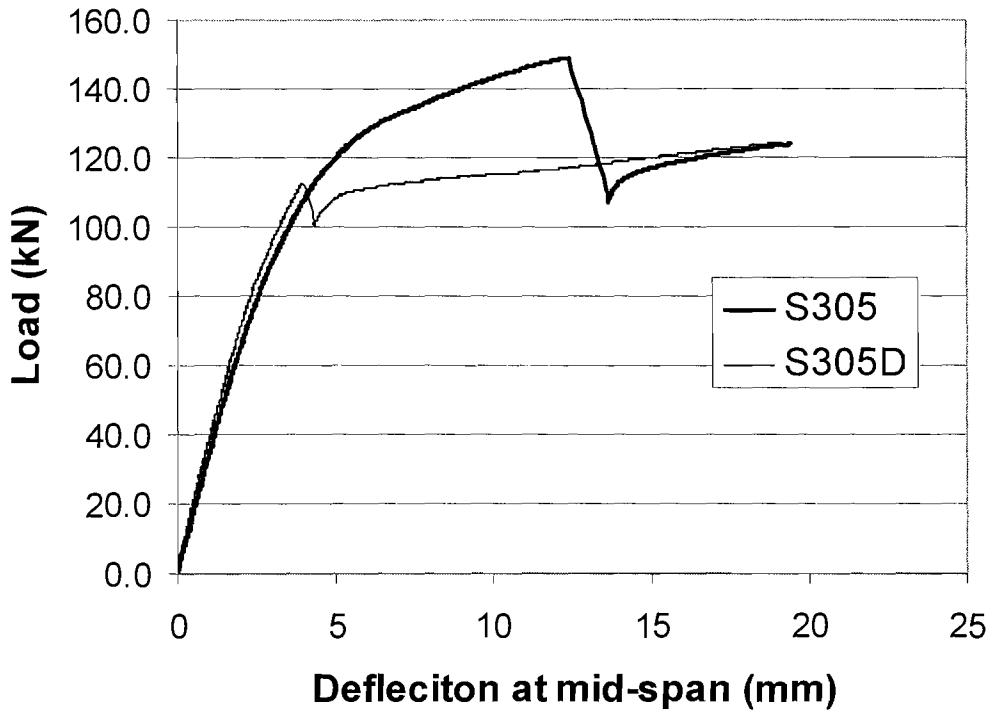


Figure 5.9 Comparisons of Load-deflection curves between specimens with different thick CFRP plates under three-point bending

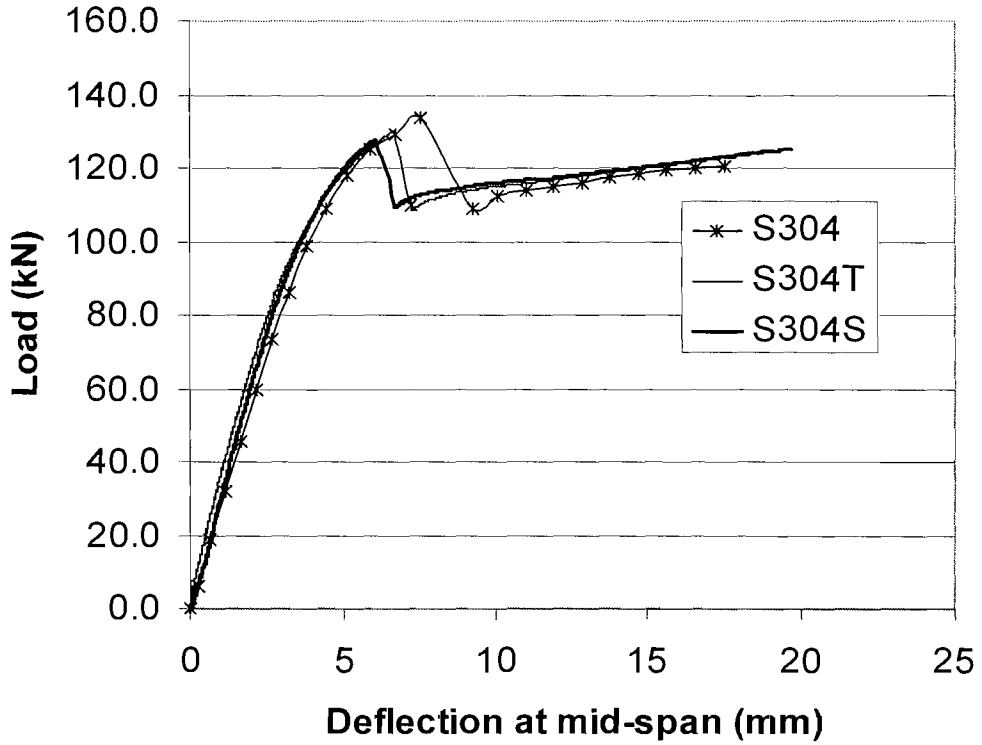


Figure 5.10 Comparisons of Load-deflection curves in specimens without or with tapers or spew fillets under three-point bending

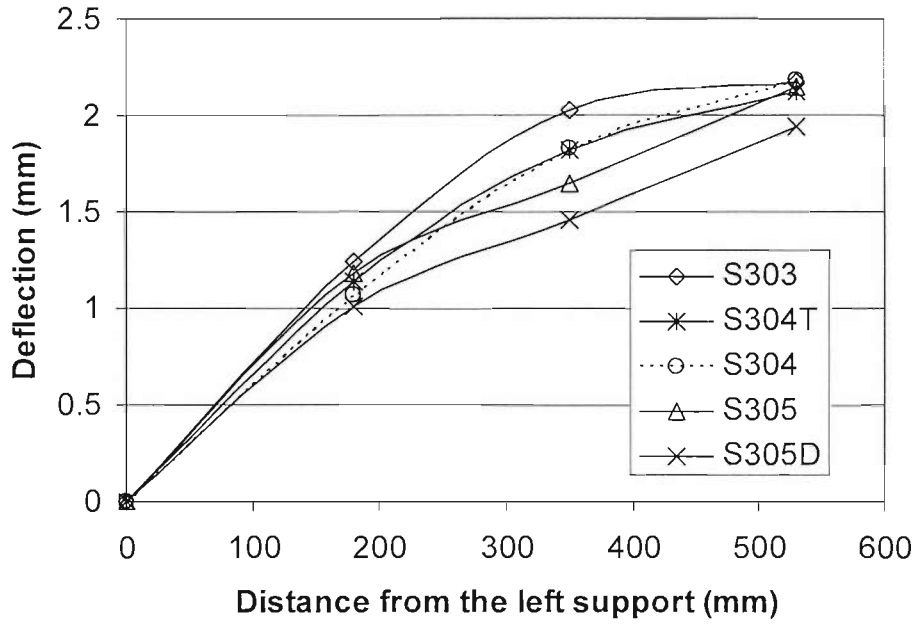


Figure 5.11 Comparisons of deflection measurement in different specimens at 70kN

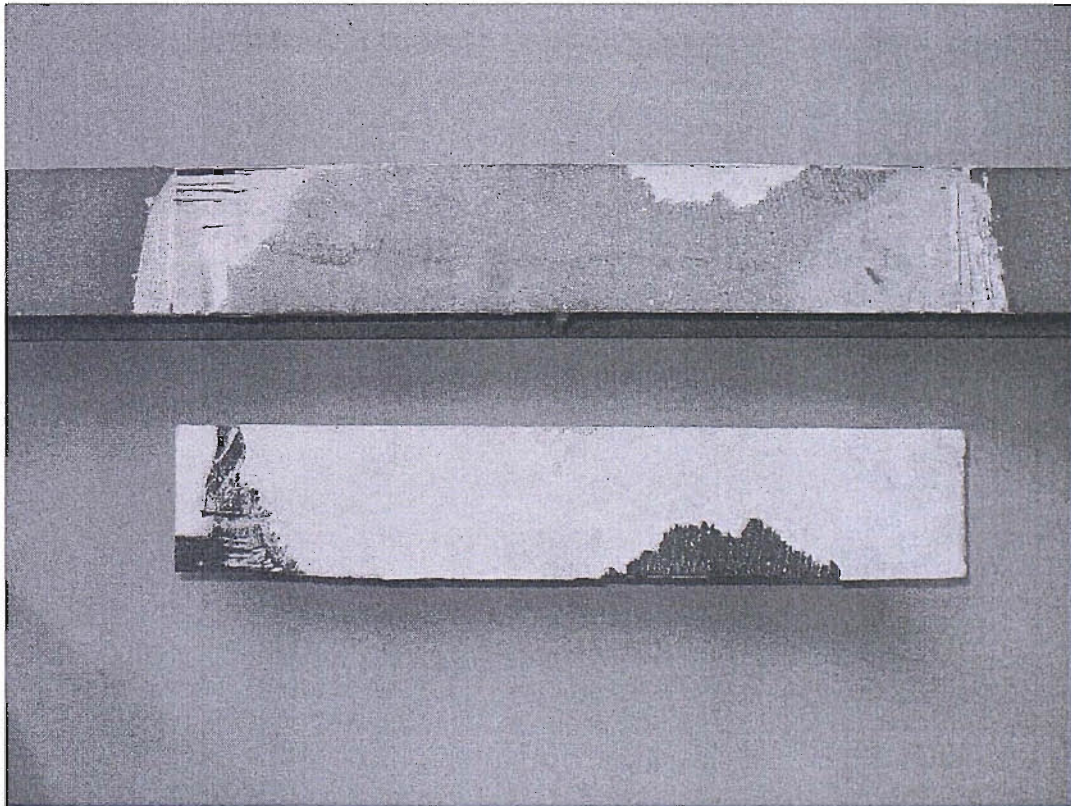


Figure 5.12 The typical debonding failure specimen S304

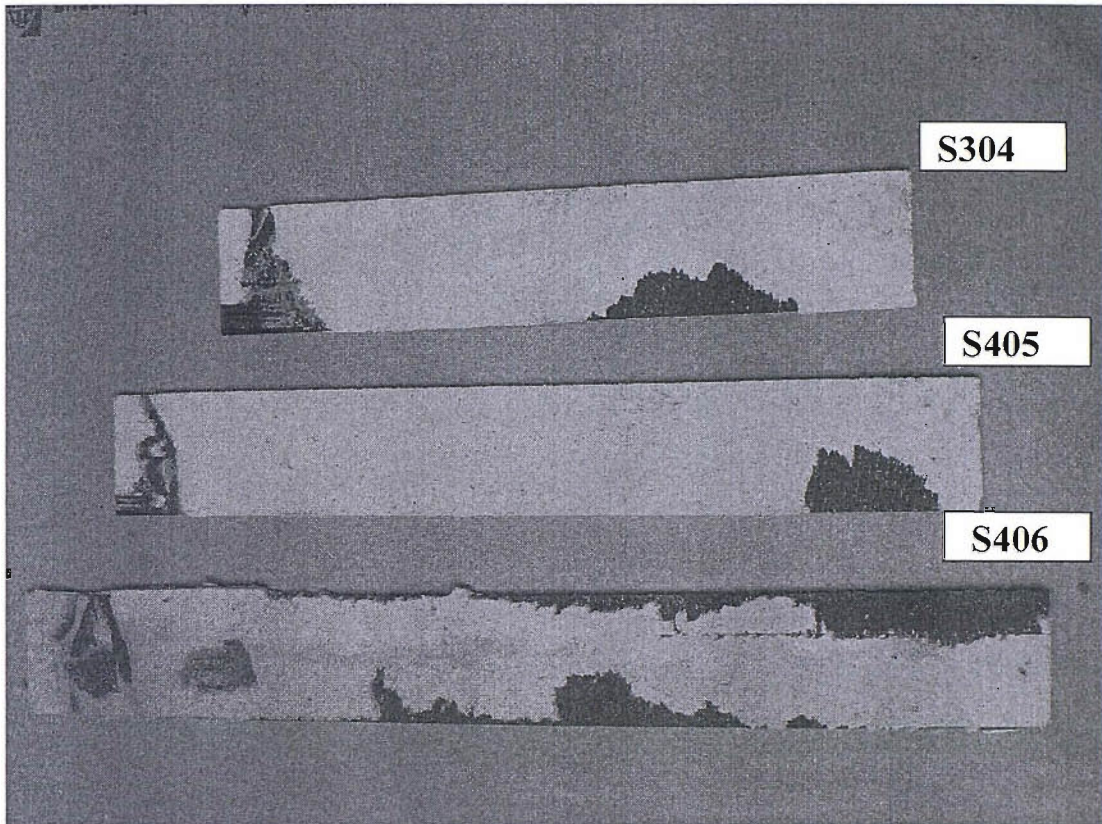


Figure 5.13 The debonded CFRP plates of S304, S405 and S406

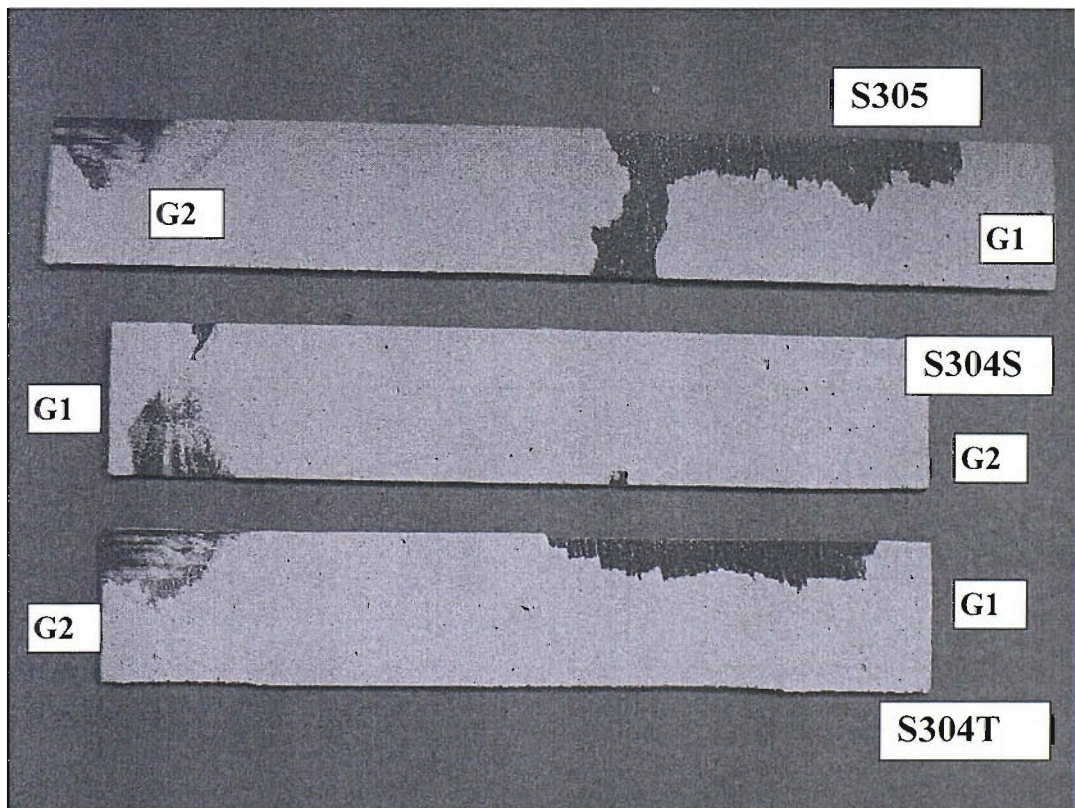


Figure 5.14 The debonded CFRP plate of S305, S304S and S304T

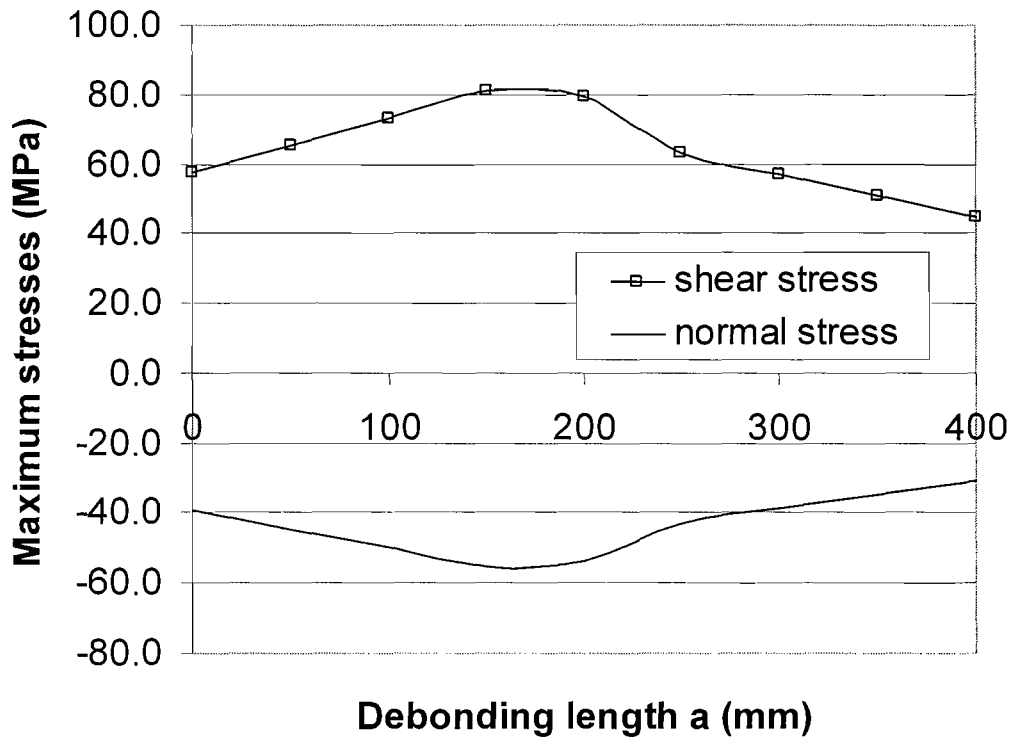


Figure 5.15 Maximum stresses versus crack length a in specimen S304

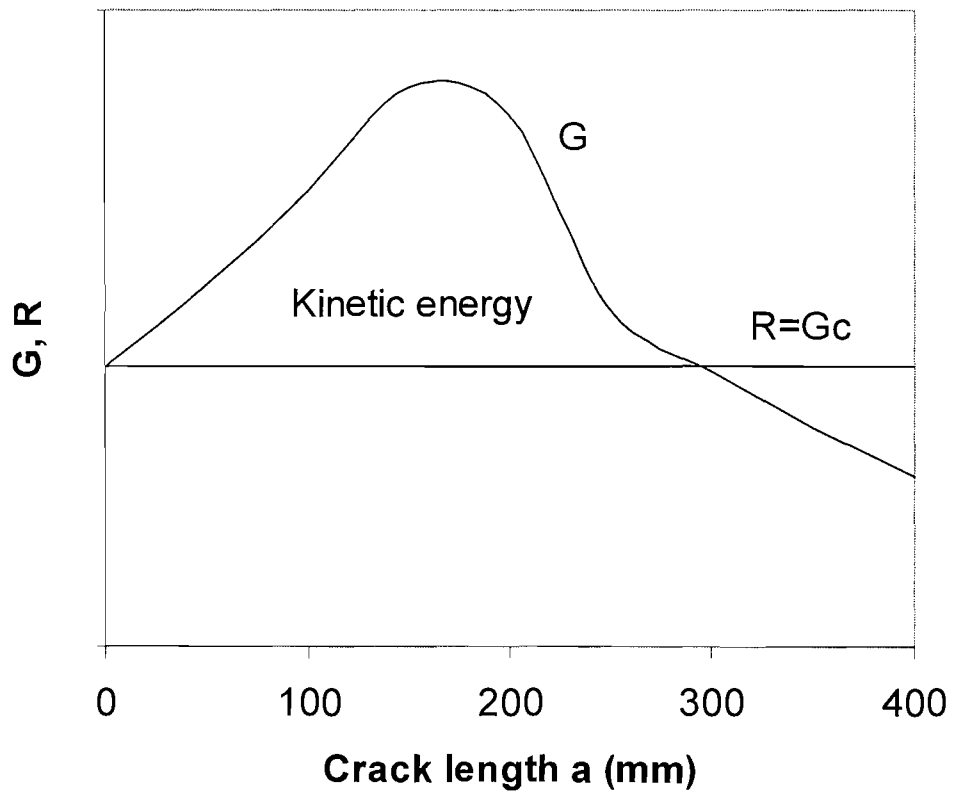


Figure 5.16 Energy release rate G varied with the crack length in specimen S304

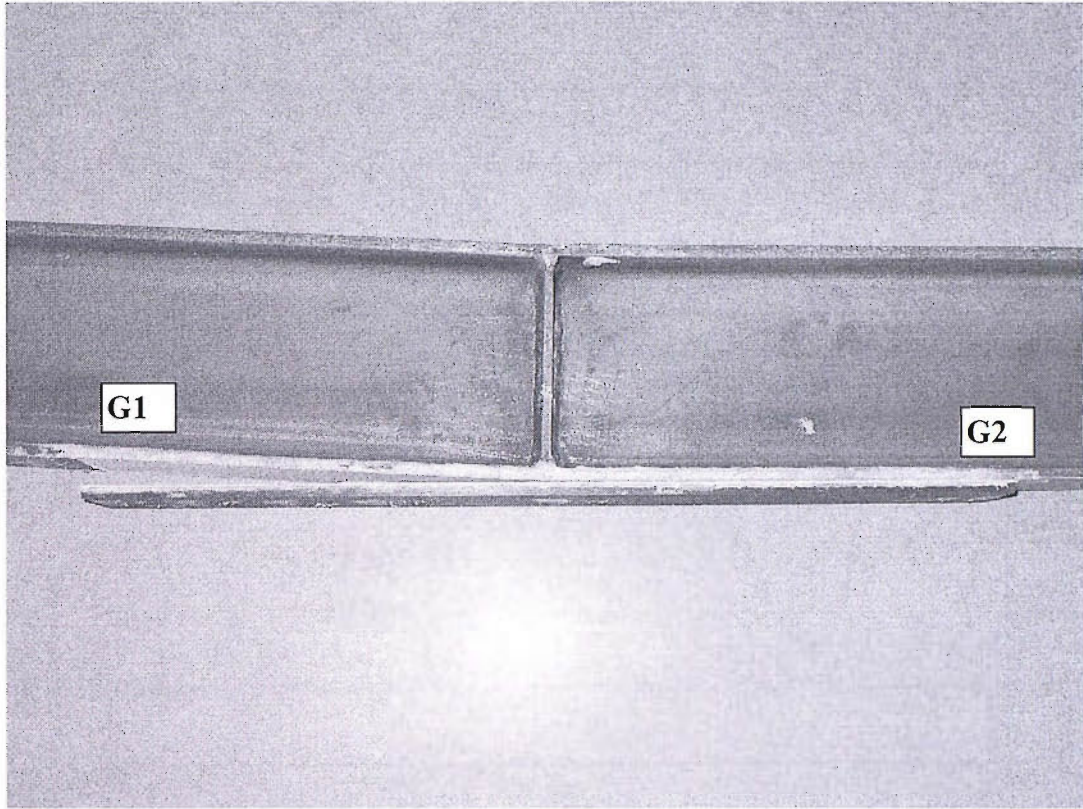


Figure 5.17 Debonding of the CFRP plate in specimen S305D

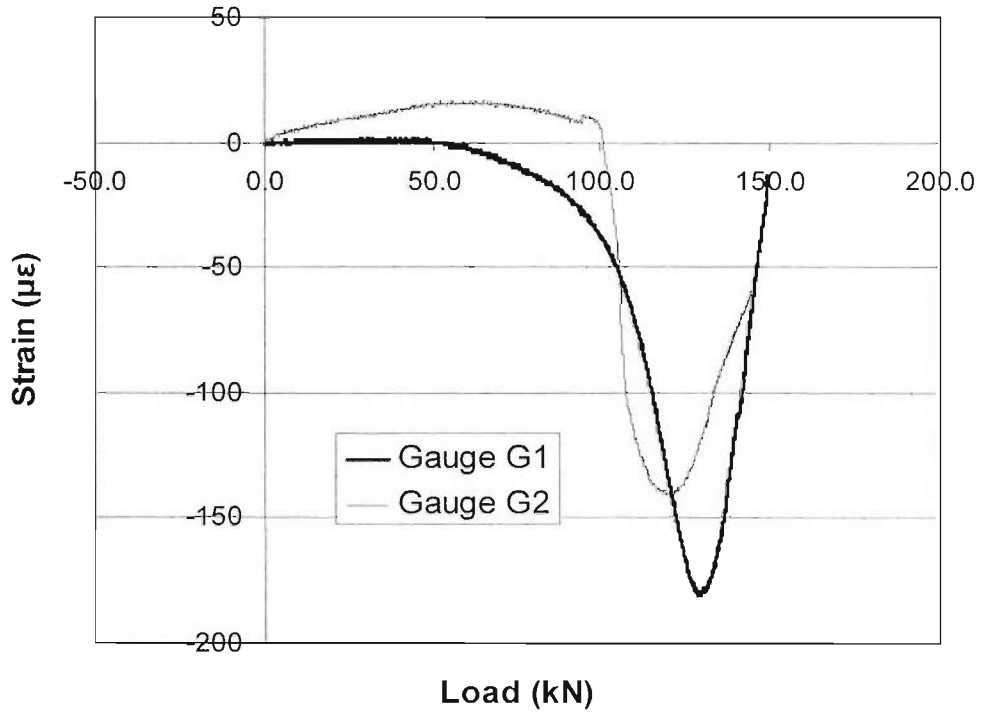


Figure 5.18 Strains at the end of plate of S305 during the test

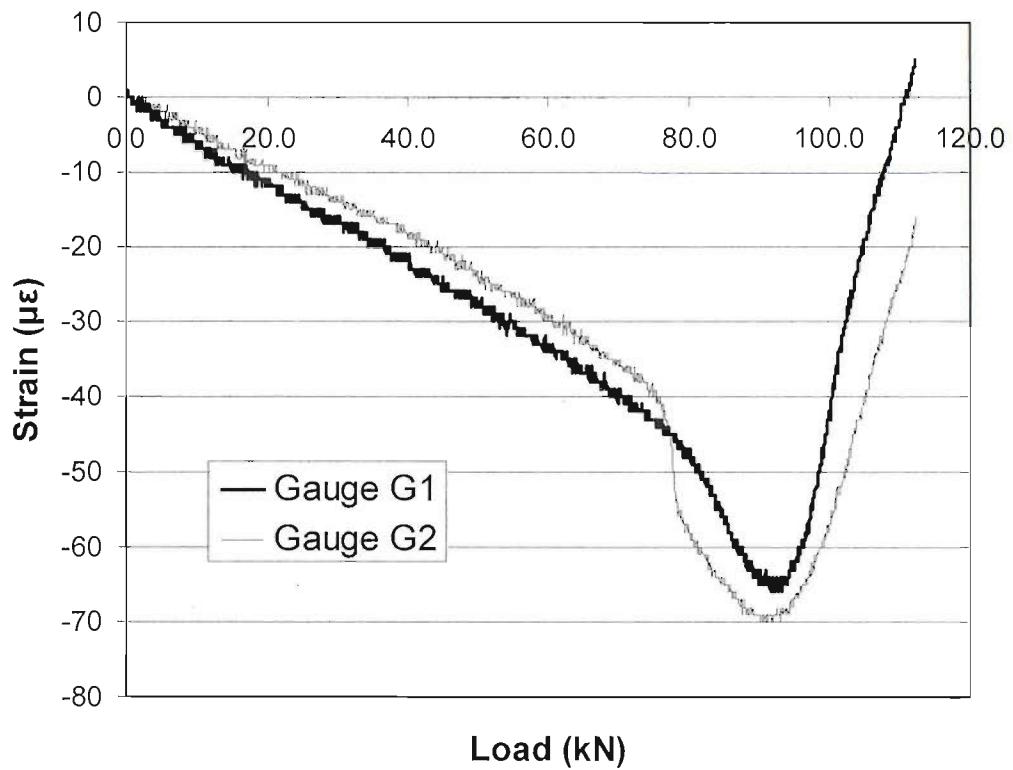


Figure 5.19 Strains at the end of plate of S305D during the test

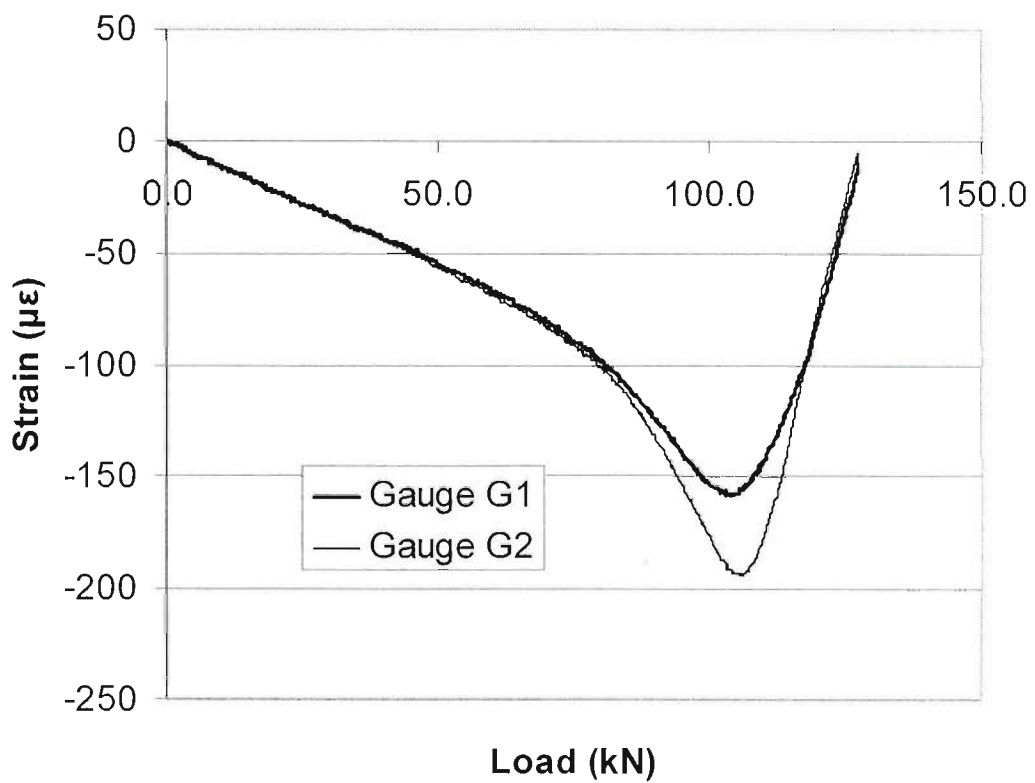


Figure 5.20 Strains at the end of plate of S304S during the test

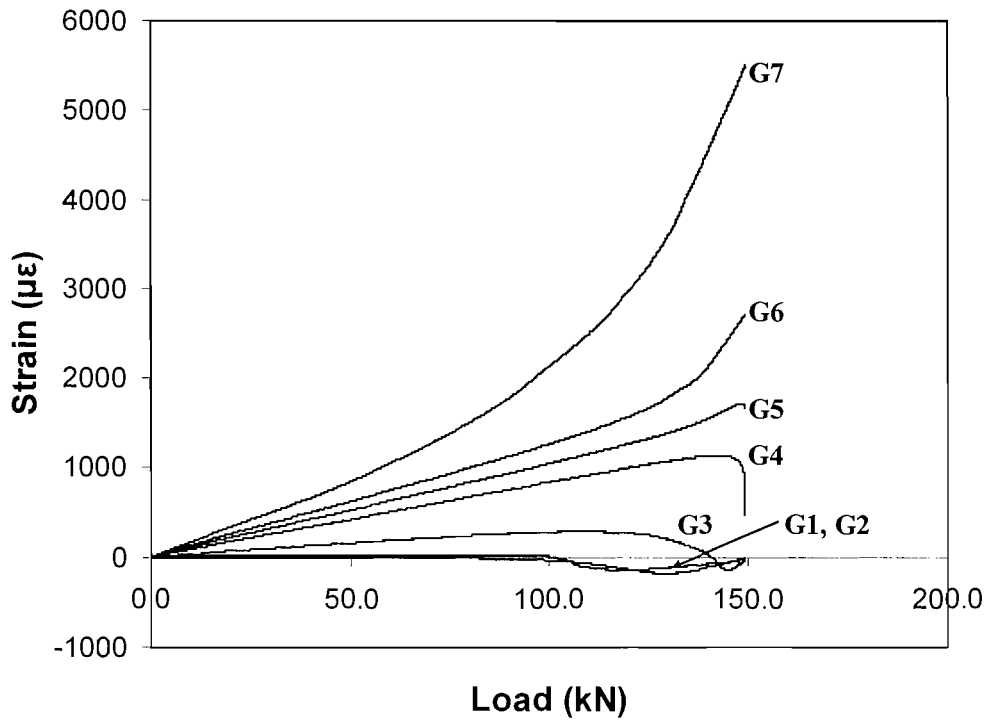


Figure 5.21 Strain in the CFRP plate for specimen S305

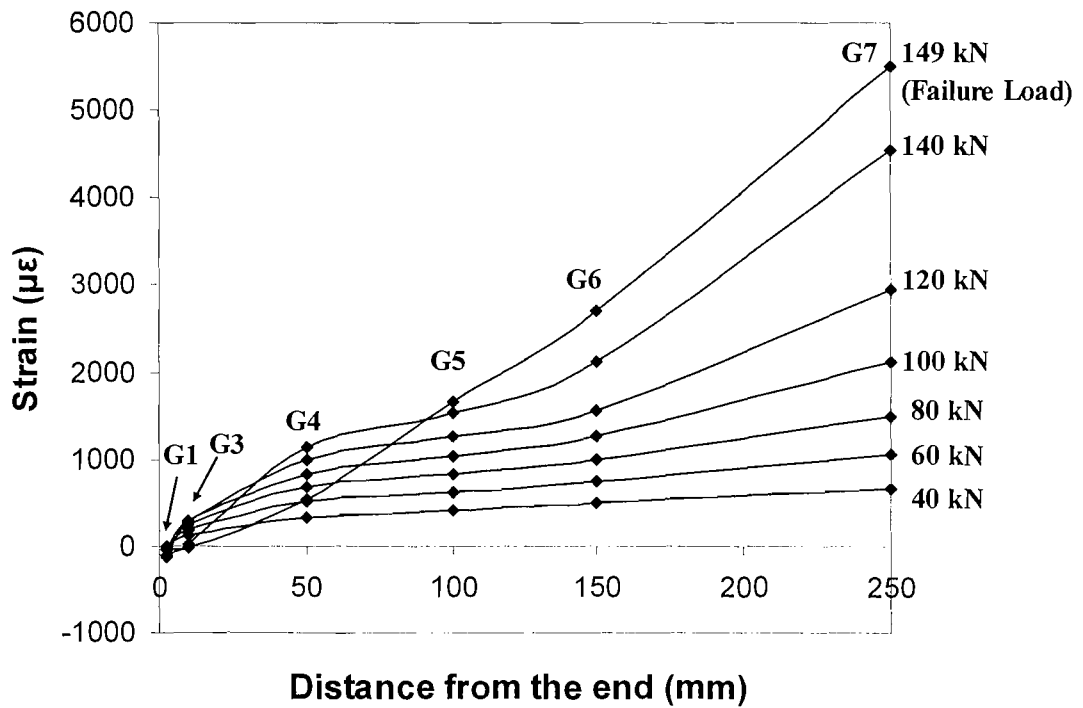


Figure 5.22 Strain distributions in the CFRP plate at different load levels in Beam S305

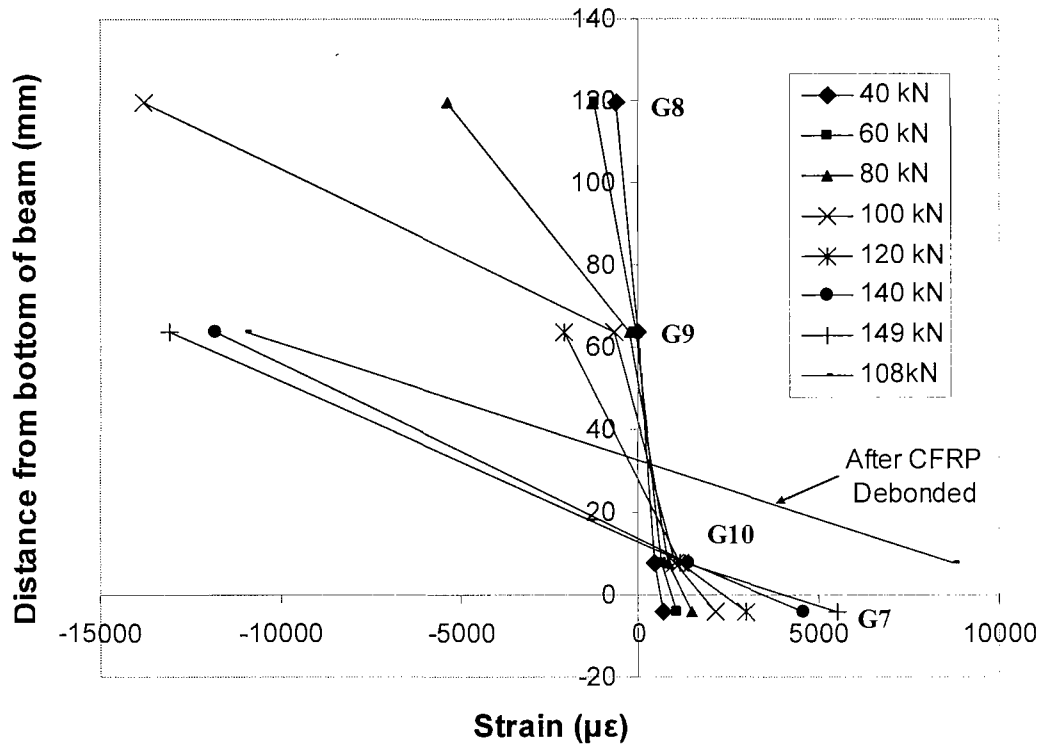


Figure 5.23 Strain in the middle of specimen from G7-10 under different load level in S305

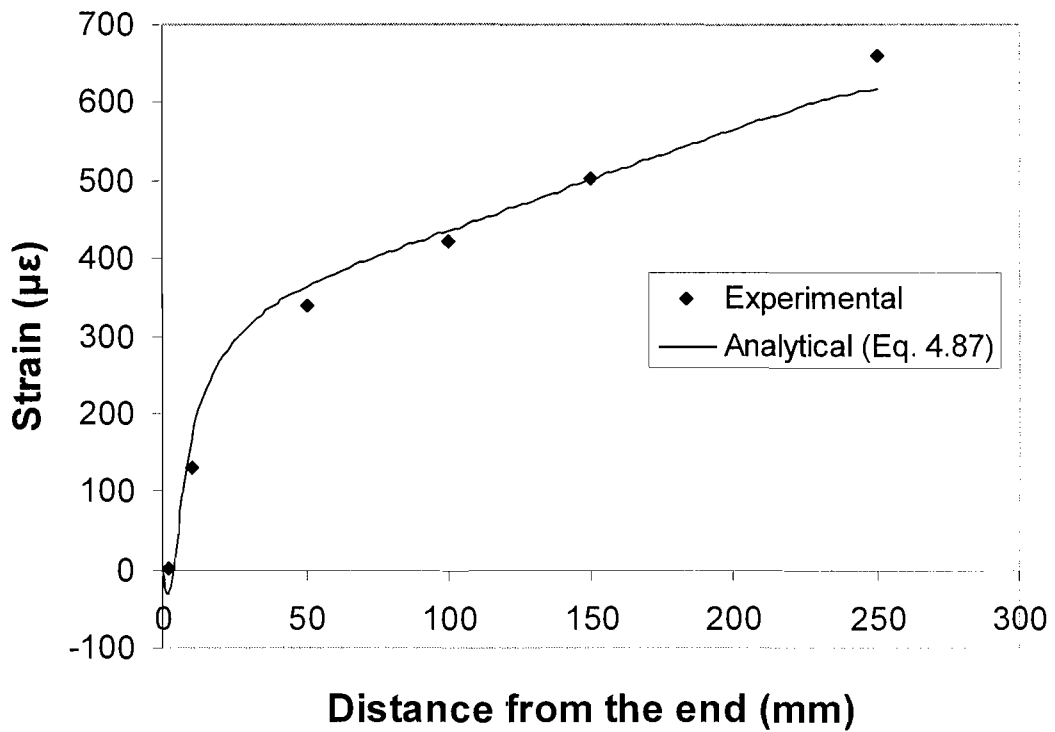


Figure 5.24 Comparison of experimental and analytical results of S305

Chapter 6

Fatigue test of steel beams reinforced with a bonded CFRP plate

6.1 Introduction and objectives

The extremely limited information on the fatigue behaviour of CFRP reinforced metallic structures means that much research is needed if this retrofitting and strengthening technique is to be widely promoted. Although there are some good static test data from literature, these cannot be used to predict the fatigue behaviour of strengthened beams with CFRP plates. Previous research shows the improved fatigue behaviour by bonded CFRP materials or the good fatigue resistance of bond. However, no direct relationship can be shown between the fatigue life, the interfacial stresses and the specimen characteristics. Therefore, the results cannot be extrapolated for practical applications.

In Chapter 4, it has been demonstrated, analytically, the stress concentration in the adhesive layer occurred at the end of the CFRP plate, and this stress concentration may lead to interfacial debonding and eventually fatigue failure of the retrofitted metallic beams. To avoid the fatigue crack initiating in the adhesive at the end of the plate, the maximum interfacial stresses must be limited. Design Guide CIRIA C595 [8] indicated that no S-N curves is currently available to characterise the adhesive joint in an externally-bonded FRP strengthening system. Instead, the use of the S-N curve formulation for FRP from the tests carried out by the National Physical Laboratory on bonded joints was proposed. In this formulation the peak shear stress in a fatigue cycle was suggested not to exceed 20-30% of the ultimate static shear strength.

The principal aim of the work reported in this chapter is to investigate the fatigue performance of the adhesive bonded between the CFRP plate and the steel substrate,

particularly in the regions where the CFRP plates terminate. This was achieved through a fatigue test programme of CFRP plate strengthened steel beams subjected to mechanical cyclic loading.

The experimental work has with the following objectives:

- To observe the crack initiation and development (or debonding) in, and to estimate the mode of cracking of, the adhesive layer.
- To evaluate the change in stiffness of the retrofitted beams with crack development.
- To assess the effect of the spew fillets beyond the plate ends on the fatigue behaviour of the bonded joints.
- To develop an S-N curve from which design fatigue lives can be easily estimated.

6.2 Experimental details

In order to investigate the fatigue behaviour of the adhesive layer in the retrofitted steel beam bonded with CFRP plate, nine small-scale steel beams strengthened with prepreg carbon fibre plates were tested. Due to the stress concentration in the adhesive layer at the ends of CFRP plate, the maximum interfacial stresses at the end of the CFRP plates, calculated by Eq. (4.81), are the fatigue stresses. Different principal stress ranges of 23.8 to 80.4 MPa were considered in the study.

6.2.1 Specimen preparation

The specimen preparation process was the same as that in the static tests detailed in Chapter 5. The steel beams used were 1.2 m long 127x76UB13. The steel had a measured mean yield strength of 357 MPa and a Young's modulus of 206 GPa. The flange surface that received the CFRP plate was sand blasted to SA2½ industry standard and the plate was attached to it within four hours. The CFRP plates used were 3 mm thick and 400 mm long, which were fabricated from 0.3 mm thick unidirectional epoxy prepreg. The adhesive used was a two-part thixotropic epoxy resin epoxy adhesive (Sikadur-31 Normal), with a Young's modulus of 8 GPa and a

shear modulus of 2.6 GPa (data provided by the manufacturer). It was mixed with 1% by weight 1 mm diameter ballotini to ensure a uniform bond thickness. Spew fillets were present at the ends of the plate in each specimen after curing (see Chapter 5).

6.2.2 Experimental setup

The fatigue tests were carried out in a servo-hydraulic Dennison test machine with a maximum capacity of 200 kN, using a three-point bending setup. The clear span was 1.1 m and the loading point was in the middle, as shown in Figure 6.1. The specimens were supported on two rollers, which allowed the specimens to behave in a simply supported manner. Steel bars fixed by clamps were placed on either side of the rollers to prevent any side movements of the system. The loading block had two steel plates with counter seats and a roller in the between to prevent its movement when the test was in progress. A photograph of the test setup is shown in Figure 6.2.

The first of the nine beams (referenced specimen F135) was first tested under static load, by displacement control at a rate of 0.5 mm/second, to determine the failure load, which then governed the maximum load applied to the other eight beams under fatigue loading condition. The test is the same test as that for specimen S304 in Chapter 5. The failure load obtained for this beam was 135 kN. This load was then used to obtain the maximum principal interfacial stress $\sigma_{I_{max}}$ of 80.4 MPa (Table 6.1) at the end of CFRP plate. $\sigma_{I_{max}}$ is calculated by combining the maximum shear stress τ_{max} and the maximum normal stress σ_{max} using Eq. (4.81) proposed in Chapter 4. Both τ_{max} and σ_{max} in this equation can be calculated using the Eqs. (4.79) and (4.80) proposed in Chapter 4 as well. The stress concentrations caused by the discontinuity at the ends of CFRP plate means that $\sigma_{I_{max}}$ is the governing fatigue stresses. The other eight beams were tested under fatigue loading with the maximum centrally applied load P between 40 kN and 125 kN. These loads convert to a range for $\sigma_{I_{max}}$ of 23.8 MPa to 80.4 MPa, as shown in Table 6.1. In this table, N_{i1} , N_{i2} and N_f are the number of cycles up to crack initiation recorded by strain gauges, up to crack initiation observed visually, and up to specimen failure, respectively. End A and End B are two ends in the same specimens.

Referring to Figure 6.3, deflections were measured at three locations using potentiometers, shown as T1, T2 and T3. To investigate the phenomenon of crack initiation and growth, the backface-strain technique was employed on specimen F55. Five 2 mm long strain gauges were mounted on the face of the CFRP plate along the longitudinal centre line, shown as G1 to G5 in Figure 6.3. Furthermore, two 5 mm long strain gauges were mounted on the inner faces of the beam flanges at mid-span to investigate the effect of crack growth on the stress field in the beam (shown as G6 and G7, Figure 6.3). Strain gauges G1 and G2 at the ends of the plate, which were used to detect crack initiating, were mounted on all the specimens. All data, including the load values measured by the sensor in the hydraulic system, were automatically recorded by a data logging system.

6.2.3 Test procedure

A minimum load of 5 kN was applied to all the fatigue tested beams except for specimen F70* (which had a minimum load of 20 kN) so as to ensure firm contact between the beam and the supports. Loading was applied sinusoidally, with a frequency of 1 (for specimens F125, F90 and F70) to 2 Hz (for specimens F55, F50 and F40). This frequency was selected on the basis of Emberson and Mays' research [182], which showed that at frequencies much in excess of 2 Hz the beam was unable to recover fully from one load application before the arrival of the next. Mays and Tilly [119] also indicated that the rates of vehicle loading on highway bridge decks may typically be equivalent to the frequency of 1 Hz.

During the fatigue cyclic loading, the test was stopped at regular intervals, or when cracking was detected, and the specimen was then subjected to three cycles of loading and unloading between 0 kN and the maximum applied load at a rate of 2 kN/second. This was done in order to measure the loads, the strain values at the CFRP plate ends and the deflections during the load cycle, since these data cannot be recorded accurately during the fatigue load cycles.

Apart from monitoring by strain gauges, the initiation and growth of cracks was also monitored visually using a magnifying glass, and the length of the crack with the

associated number of cycles were noted. The test was stopped when crack propagation passed the middle of the specimen or when the crack stopped growing, which means that the CFRP plate had lost its strengthening effect and the specimen failed.

In order to assess the performance of beams which showed no sign of debonding after enduring the fatigue test, specimen F40-2 was tested to failure under static load by displacement control at a rate of 0.5 mm/second after it has endured 4 million cycles of fatigue loading.

6.3 Test results and analysis

6.3.1 Backface-strain technique

As mentioned in the foregoing, strain gauges were mounted on the CFRP plates to investigate crack initiation and growth, which will influence the strains in the plates. In Chapter 5, similar specimens under static loading have been tested under 3 point bending with a centrally bonded 400 mm long CFRP plate. The measured strains at the ends of the CFRP plate, at the same locations as G1 and G2 as the current series of specimens have been shown in Figure 5.20, which indicates that the strain at the end of plate is negative, i.e. compressive. This specimen had adhesive thoroughly cleaned off from the ends of the plate and therefore had no adhesive spew fillet. This finding validates the analytical solutions proposed in Chapter 4, in which Eq. (4.92) for the longitudinal strain ε_{pb} on the CFRP plate at a distance δ ($\delta \ll t_p$, the thickness of the plate) from the end was given as

$$\varepsilon_{pb} = \frac{N_s}{E_p A_p} + \frac{1}{E_p} \frac{3\delta^2}{t_p^2} (-\sigma(0)) - \frac{1}{E_p} \frac{2\delta}{t_p} \tau(0) \quad (6.1)$$

where N_s is the force from the spew fillet, E_p and A_p the Young's modulus and area of the plate, respectively, and $-\sigma(0)$ and $\tau(0)$ the peel stress and shear stress at the plate end, respectively.

The first term on the right of this equation comes from the tensile (positive) force exerted on the plate end by the spew fillet; the second term derives from the peel

stress (again positive); and the third term is dependent on the shear stress. Because $\delta \ll t_p$, the third term is usually much larger than the second term. Without the effect of the spew fillet, the longitudinal strain at the plate end is, according to the Eq. (6.1), negative (compressive). This compressive strain at the plate end is generally small and very much influenced by the size of the spew fillet. When a spew fillet is present, it will exert a positive, or tensile, force at the plate end and the magnitude of the force is proportional to the size of the fillet. A large enough spew fillet will therefore turn the compression at the plate end into tension.

In the current fatigue tests, strains measured at the ends of the CFRP plate by gauges G1 and G2 (denoted as ends A and B, respectively) from the three load and unload cycles, at the rate of 2 kN/second, prior to the start of fatigue tests are shown in Figure 6.4-6.10 for the specimens. The effect of the spew fillet can be used to explain the significant variations between curves for different specimens. Since the specimens were prepared with spew fillets already in place, it was not possible to establish the actual size of the spew fillets with any degree of accuracy. However, the strains measured by gauges G1 and G2 give an indication of the size of the spew fillet. Then the effect of spew fillet on the fatigue behaviour of retrofitted beam can be investigated through these strain measurements. The spew fillets at the two plate ends of each beam are compared, qualitatively, in Table 6.2.

It was observed that the strain-load curves becomes non-linear in Beams F125, F90 and F70 (see Figure 6.4-6.6), indicating that the elastic limit of the adhesive at the ends of the plate has been exceeded and thus displaying non-linear behaviour. The strains in F125A dropped to zero at the third cycle, indicating that a crack had developed. The curves for the ends with compressive strain, i.e. F90B, F70A, F50A, F50B, F40-1A and F40-1B, appear to be more regular and linear than those with tensile strain measured, which suggests that the effect of the spew fillet is not stable.

Figure 6.11-6.16 show the strain range – the range between the minimum strain and the maximum strain in the same cycle – measured by gauge G1 (at one end of the CFRP plate) during the fatigue tests. The strain range, rather than the absolute strain, was used to eliminate the effect from temperature fluctuation. Specimen F125 is not

included in these plots because of its very short fatigue life. All the curves, except those for F40-1A and F40-2A display a trough of maximum compression before finally reduce to almost zero.

From Eq. (6.1), the strain will be more compressive as the effect of the spew fillet reduces and as the peel stress reduces, but will be less compressive as the shear stress reduces. With cracking, or debonding, initiating at the spew fillet, the effect of the spew fillet will lessen and this occurs before any reduction of the peel and shear stresses in the adhesive layer. May and Hutchinson [150] and Pereira and Morais [183] indicates that Mode I is the lowest energy fracture mode for isotropic materials. Cheuk et al. [125] reported that crack initiates in Mode I earlier than in Mode II in composite-metal double-lap joints under fatigue loading. Hence the peel stress will deteriorate earlier than the shear stress in the adhesive layer.

With this background, it is possible to divide each of the curves representing a specimen that fail in fatigue into four distinct phases, shown in Figure 6.12 for specimen F70B. Phase I is from the start to ϵ_s . ϵ_s is the difference in strain measured in a similar specimen without spew fillet under static loads at 70 kN and 5 kN (the maximum and minimum loads for specimen F70), as shown in Figure 5.20 in Chapter 5. In this phase the spew fillet was effective but was losing its strength gradually. Phase II starts from ϵ_s to the maximum compressive strain. During this phase the spew fillet no longer affects the strain, and the peel stress at the plate end reduced gradually. Phase III begins when the strain reaches maximum compression and ends when it is almost zero (N_{II}) as a result of the gradual disappearing of the shear stress at the plate end. Phase IV is the remaining part, when the adhesive close to the plate end has completely lost its strength, and cracking has started.

For the two lightly loaded specimens – F40-1 and F40-2 – the curves in Figure 6.15 and 6.16, respectively, show that the maximum compressive strain, once reached, was maintained until the test stopped. This shows no crack had initiated in these specimens, indicating that 40 kN was the threshold load for the fatigue tests. Comparison between the number of the cycles to when the maximum compressive strain was reached, and to N_{II} , when cracking was initiated, are given in Table 6.2. This comparison shows a larger spew fillet delays crack initiation. The actual numbers

of cycles to N_{ij} are given in Table 6.1. Figure 6.17 clearly shows a delay in crack initiation as the load is reduced, and that below the load of 40 kN, no cracking was detected.

The strain ranges measured in specimen F55 during the fatigue tests are shown in Figure 6.18. It can be observed that:

- The strains from gauges G3 and G4 decreased with the crack growth along the interface, and approached zero at around 80,000 and 90,000 cycles, respectively, when cracking was extended to the location of the strain gauge.
- The strain in gauge G5, in the middle of plate, dropped rapidly from a constant maximum value to zero. The crack grew from G1 to G3, 50 mm apart, in 70,000 cycles, and from G3 to G5, 150 mm apart, also in about 70,000 cycles.
- The strains in G6 and G7 (particularly G7), on the inner flanges of the steel beam, increased as the strain of G5 decrease, indicating that the load was being shed from the plate to the beam.

6.3.2 Stiffness change

Figure 6.19 shows the deflections measured from the three potentiometers during the fatigue test of the beam F70. It can be observed that

- Before crack initiating the stiffness of the beam had remained constant.
- With crack growth, the deflections obtained by the potentiometers increased in the order from T3 to T1, until the crack cross the middle of the retrofitted beam.
- The increase in deflections was small because of the thinness of the plate compared to that of steel beam.

Similar observations were made on the other specimens.

6.3.3 Crack propagation and failure

The crack initiation and propagation in all the specimens were similar except for specimen F125. The load range on this specimen was too high and caused it to debond suddenly from one end after only 30 cycles, similar to the phenomenon observed in

the static tests. The cracking in F125 was shown in Figure 6.20. For all the plates that had debonded, cracking started from the middle of the spew fillet and then propagated to the interface between the steel beam and the adhesive at an angle of 45 degrees. Then the crack grew along the interface and stopped eventually. There was always a short length of adhesive remaining uncracked that bonded the plate to the beam. Figure 6.21 shows the typical crack in the failed specimens except F125.

The cracks initiation, recorded by gauges G1 and G2, has been discussed in section 6.3.1. Furthermore, crack initiation and growth were also observed visually using a magnifying glass. The crack lengths developed on two sides at one plate end were not the same, because the CFRP plates were not bonded onto the steel plate perfectly in the middle, the load was applied may be a little eccentric, and the spew fillets might not be uniform along the edges. The longer ones were chosen as the crack length of the specimen, which were used to plot Figures 6.22 to 6.25. In addition, the numbers to cycles of specimen failure recorded are also shown in Table 6.1. In Figure 6.24, the crack growth curve recorded by strain gauges agrees well with that recorded by sight, while the crack initiating recorded by sight is later than that reported by stain gauges.

Figures 6.22 to 6.25 show the fatigue crack growth curves of some of the specimens, in which all crack growth rates increase rapidly after the initiated and their growth almost stops once one of the two end cracks had advanced pass the middle of the beams. According to the Paris-Erdogan Law (6.2), the crack growth rate increased with the applied stress range and the length of the crack.

$$\frac{da}{dN} = C\Delta K_I^m \quad (6.2)$$

where a is the length of crack, N is the fatigue cycles, C and m are the crack growth material constants, and ΔK , the stress intensity factor range. According to the discussion in Chapter 5, the stress intensity factors are directly proportional to the maximum interfacial stresses, which increase with the crack growth until the crack front goes beyond the middle of the plate. This can explain the crack grew so rapidly in these fatigue tests.

6.3.4 S-N Curve

The applied load versus number of cycles to failure is presented in Figure 6.26. The relationship between the number of cycles to failure (N_f) and the maximum applied load (P) or the normalized maximum applied load (P/P_u) in a load versus log cycle is more or less linear. Linear regression analysis produced the following best-fit curve (with a correlation coefficient $R^2 = 0.97$):

$$P = -6.83Ln(N_f) + 141.57 \quad (6.3)$$

This curve is of no significant practical use as it applies only to the specimens tested.

Since the maximum principal interfacial stress increases with crack growth, the number of cycles to failure cannot be used to develop an S-N curve. However, before crack initiation, theoretical analysis in Chapter 4 shows that the maximum principal interfacial stress is constant. The curves for the maximum principal interfacial stresses ($\sigma_{I_{max}}$) (and the normalized maximum interfacial stresses ($\sigma_{I_{max}}/\sigma_{I_{max,u}}$)) versus the log of the number of cycles to crack initiation (N_{ii}) is presented in Figure 6.27. The relationship is approximately linear and regression analyses produce the following best-fit equation (with a correlation coefficient, $R^2 = 0.96$):

$$\sigma_{\max} = -4.19Ln(N_{ii}) + 78.62 \quad (6.4)$$

It has been established in Chapter 4 that the bonded strength of retrofitted metallic beams is not influenced by the size and material properties of the metallic beams or the CFRP plates. Therefore, this S-N curve can be applied generally as long as the same adhesive is used.

Specimens F40-1 and F40-2 did not fail even after four million cycles. Furthermore, the variation of the strain at the end of plates are very small after 3 million cycles in F40-1 and after 2 million cycles in F40-2 (Fig. 6.15 and 6.16), which indicates that the specimens are not likely to fail in fatigue. Therefore, the fatigue threshold for the tested beams is 40 kN, with a corresponding threshold stress 23.8 MPa for the adhesive. This threshold limit is about 30% of the ultimate failure stress 80.4 MPa under static loading.

6.3.5 Strength of specimen F40-2 after fatigue testing

As detailed in Section 6.2, specimen F40-2 was tested to failure under static loading after the fatigue test. The failure load obtained was 133 kN, which was only marginally lower than 135 kN, the strength of the specimen F135. Figure 6.28 compares the load-deflection curves obtained from these two specimens, which indicate the fatigue test had caused very little, if any, deterioration in the static performance.

The strains measured at the ends of the plates in specimen F40-2 under static load are superimposed onto Figure 5.20, the load-strain curves for a specimen without spew fillet (now labelled as G1 and G2 of S304s), and are shown in Figure 6.29. It is observed that the strains for the current specimen are compressive and the descending segments of the curves are more linear than those for the beam without spew fillets. This indicates that the spew fillets were no longer affecting the strains and that the adhesive at the end of plate was less plastic after the fatigue test.

6.3.6 The effect of the load range

The minimum load on specimen F70* was 20 kN. Therefore, the load range for this beam was 50 kN, which was the same as the load range for specimen F55. The comparisons of the strain range versus cycle curves of F70, F70* and F55 are shown in Figure 6.30. The curve for beam F70* can be seen to be closer to the F70 curve than to the F55 curve. Moreover, the number of cycles up to crack initiation recorded by strain gauges for F70* are 6400 and 7400, which are much closer to those for F70 (3000 and 4000) than those for F55 (17000 and 18000). Therefore, it can be concluded that while the load range affects the fatigue behaviour, it is less significant than the effect of the maximum load.

6.4 Conclusion

In this chapter, the fatigue testing of small-scale steel beams bonded with a 400 mm long CFRP plate is reported. The backface-strain technique was applied to monitor crack initiation and crack growth. The results showed that the strain gauges could detect crack initiation immediately and track the deterioration of the adhesive layer. Therefore, backface-strain technique could be a simple and effective way to monitor retrofitted beams.

The strain recorded by strain gauges showed that a crack initiates and grows in Mode I earlier than in Mode II, which agrees with the conclusion for double-lap joints [125]. The crack growth rates observed both by sight and by backface-strain technique increased rapidly since the applied stress range increased with crack growth. The measured strain showed that the spew fillet was of benefit to the fatigue performance of the bonded joints, but the improvement was not significant. Moreover, the stiffnesses of the retrofitted beams were found to deteriorate with crack growth, but the deterioration was insignificant due to the thin thickness of the plates used in the tests.

An S-N curve was developed from the test results. Since this S-N curve is the relationship between the maximum interfacial stress and the number of cycles, it can be used for different sizes of retrofitted steel beams using the same adhesive. The fatigue limit, i.e. threshold, of the S-N curve is about 30% of the ultimate static failure stress, which validates the fatigue limit suggested by the CIRIA Design Guidance [8].

The static performance of retrofitted beam is not affected in any significant way by fatigue loading under the threshold limit. The fatigue load range will affect the fatigue life, but its significance is much less than the magnitude of the maximum load in the load range.

Table 6.1 Specimen details and test results

Specimen	P (kN)	σ_{1max} (MPa)	P/P _u (%)	N _{i1}		N _{i2}		N _f	
				End A	End B	End A	End B	End A	End B
F135	135	80.4	100	/	/	/	/	/	/
F125	125	74.4	92.6	3	/	30	/	30	/
F90	90	53.6	66.7	700	600	1200	1200	5000	5000
F70	70	41.7	51.2	3000	4000	10000	10000	25000	20000
F55	55	32.8	40.7	17000	18000	47800	60120	130000	130000
F50	50	29.8	37.0	300000	350000	363000	363000	965000	965000
F40-1	40	23.8	29.6	/	/	/	/	/	/
F40-2	40	23.8	29.6	/	/	/	/	/	/
F70*	70	41.7	51.2	6400	7000	7000	9700	28900	28900

Notes:

1. In the specimen reference, the number indicated the maximum load (in kN) on the beam. A and B indicate the two different ends of adhesive joint in same retrofitted beams.
2. F135 was tested under static loading
3. P is the maximum applied load.
4. P_u is the ultimate static load.
5. The minimum applied load was 5 kN except for specimen F70*, which had a minimum load of 20 kN.
6. σ_{1max} is the maximum interfacial stress at the end of the plate under the maximum applied load.
7. N_{i1}, N_{i2} and N_f are the number of cycles up to crack initiation recorded by strain gauges, up to crack initiation observed visually, and up to specimen failure, respectively.

Table 6.2 Comparisons of the spew fillet size and the number of cycles in same retrofitted beams

Beam	Comparison of Spew fillet size*	Comparison of N _m **	Comparison of N _{i1}
F125	A<B	/	A<B
F90	A>B	A>B	A>B
F70	A<B	A<B	A<B
F55	A<B	A<B	A<B
F50	A<B	A<B	A<B

Notes:

* The comparisons of spew fillet sizes according to the strain obtained from gauges G1 and G2 in the third load cycle – higher strain (positive) implies a larger spew fillet.

** N_m indicated the number of cycles up to the maximum compressive strain obtained from either gauge G1 or gauge G2 during the fatigue test.

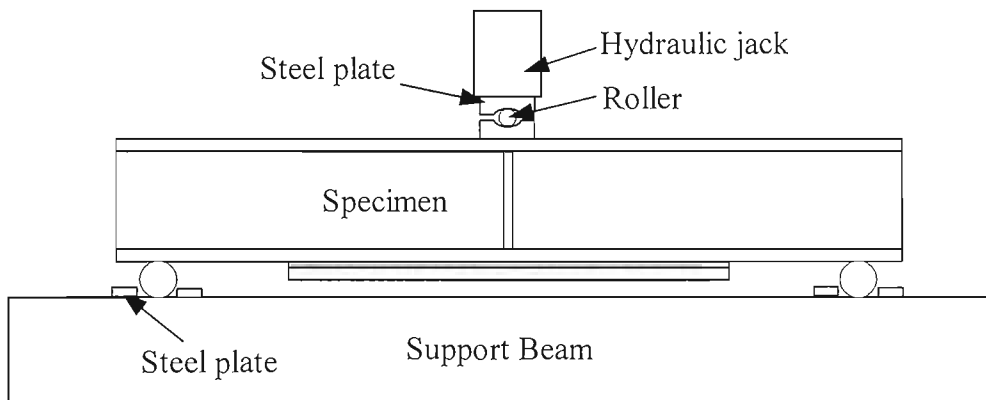


Figure 6.1 Schematic of fatigue test setup

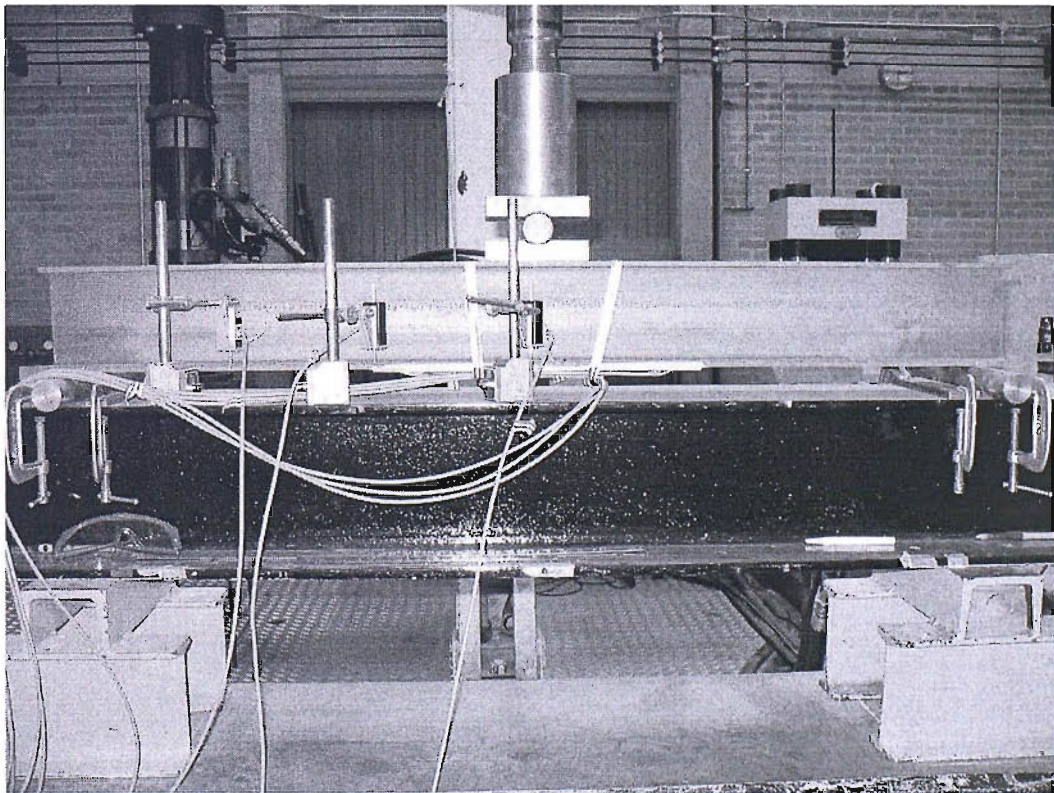


Figure 6.2 Test setup

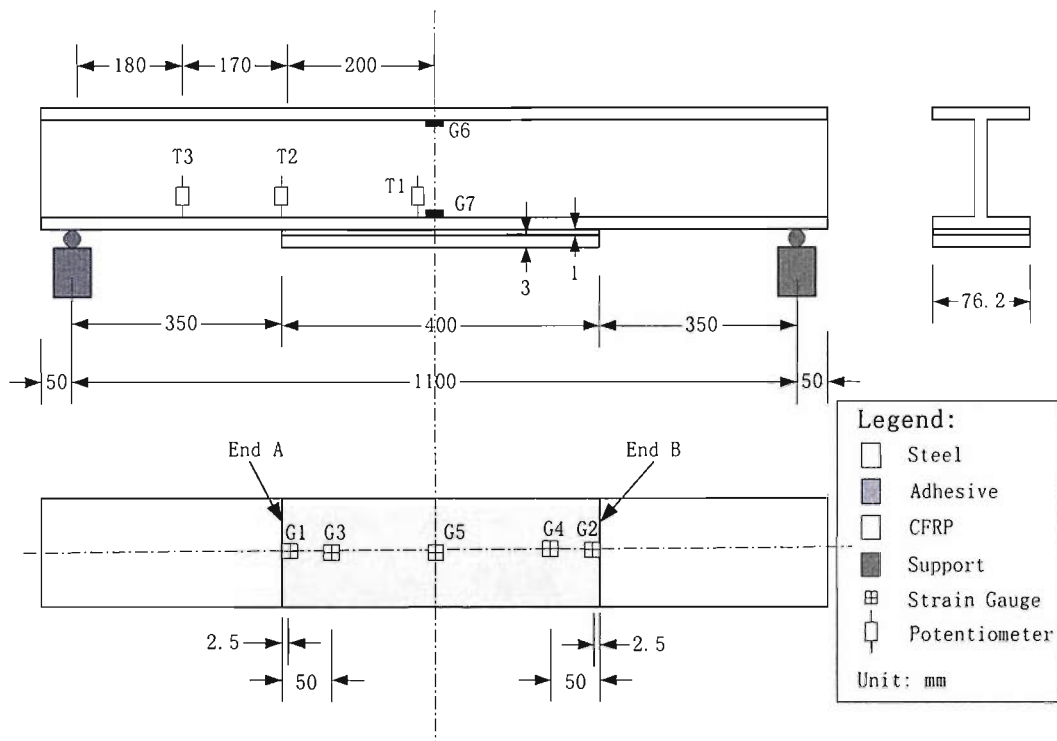


Figure 6.3 Instrumentation on test specimens

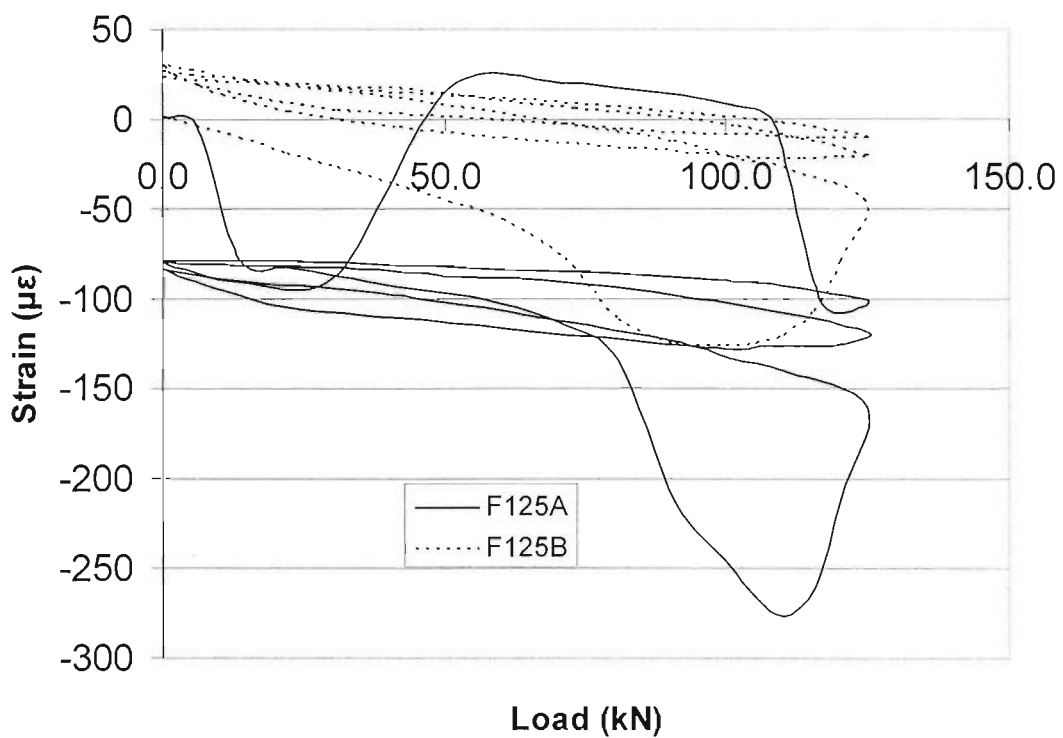


Figure 6.4 Strain measured at the plate ends of specimen F125 from three static load cycles

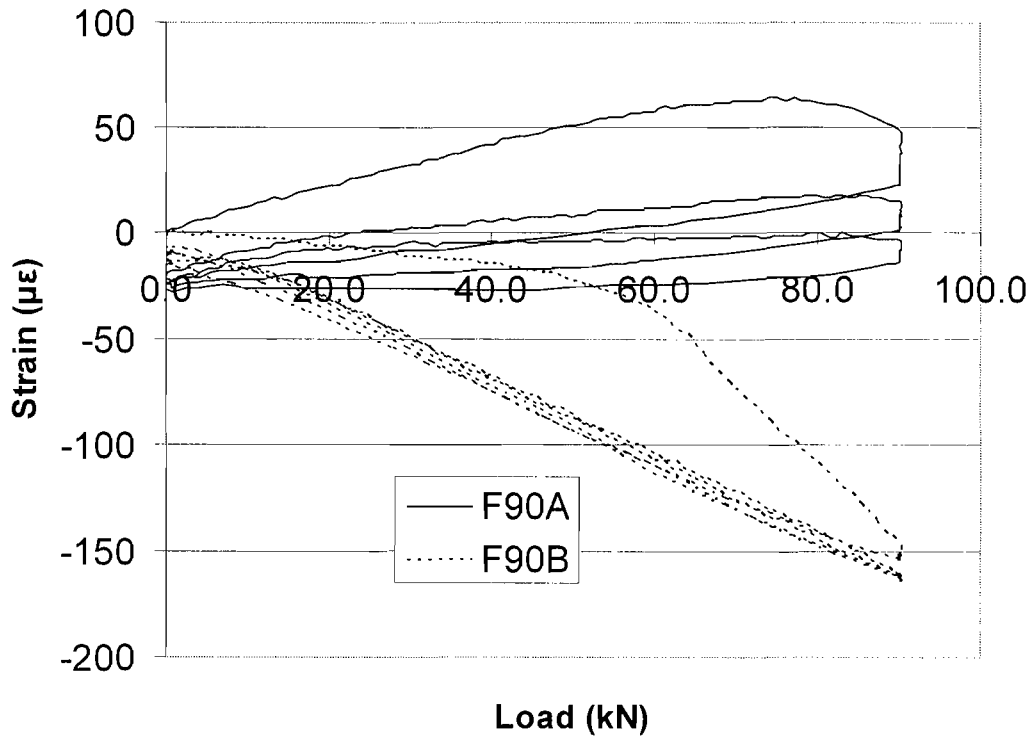


Figure 6.5 Strain measured at the plate ends of specimen F90 from three static load cycles

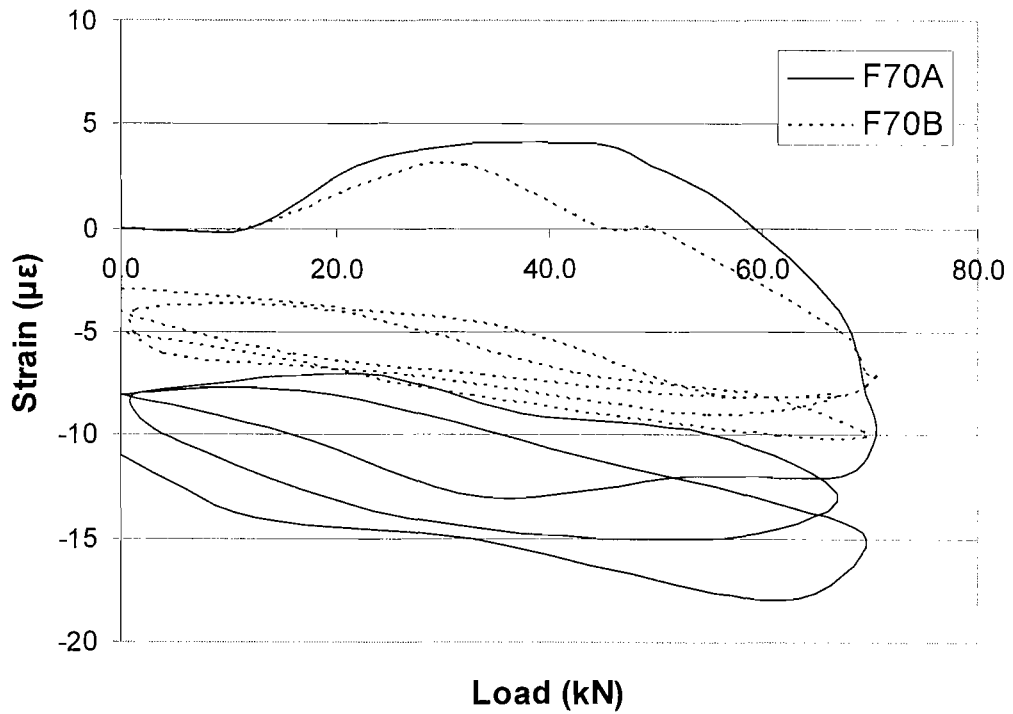


Figure 6.6 Strain measured at the plate ends of specimen F70 from three static load cycles

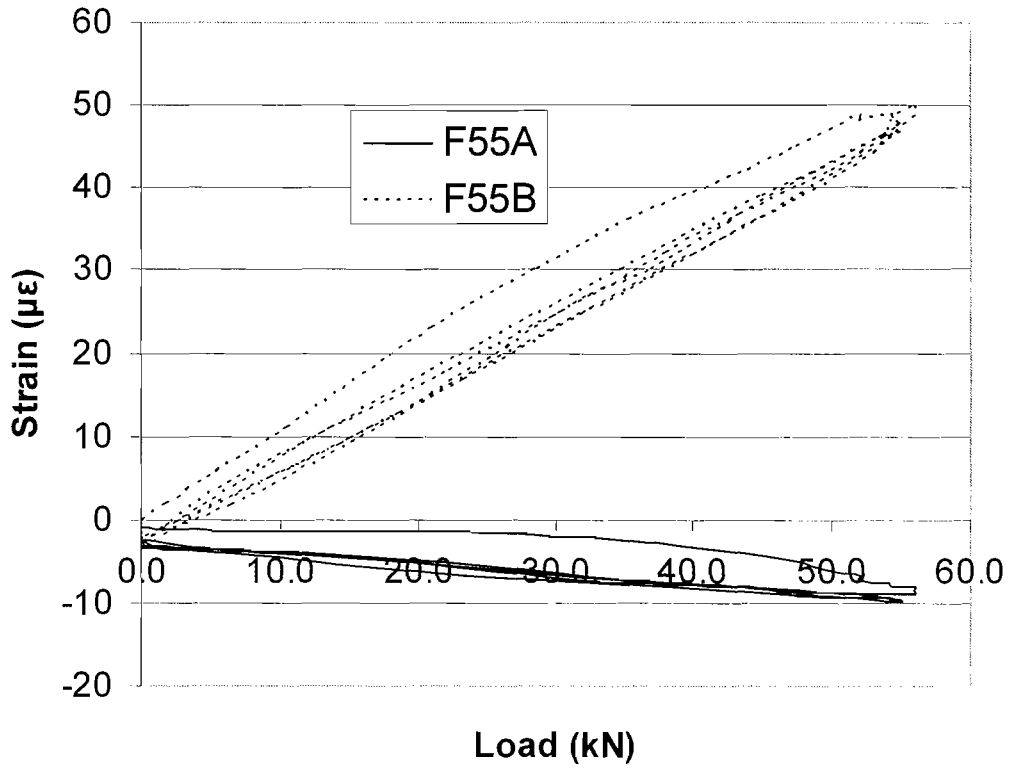


Figure 6.7 Strain measured at the plate ends of specimen F55 from three static load cycles

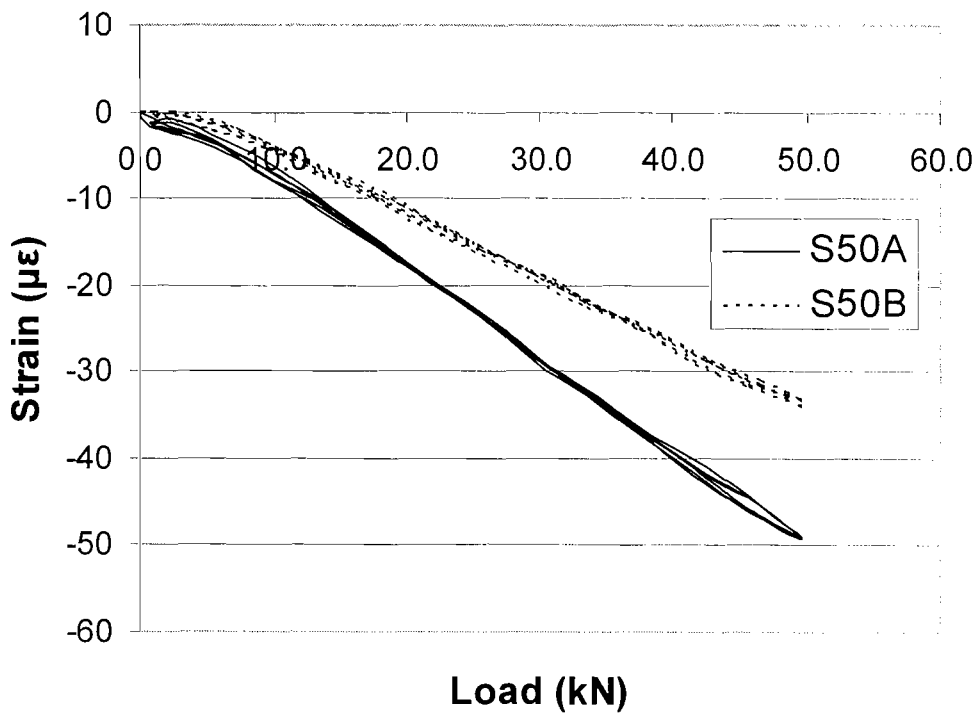


Figure 6.8 Strain measured at the plate ends of specimen F50 from three static load cycles

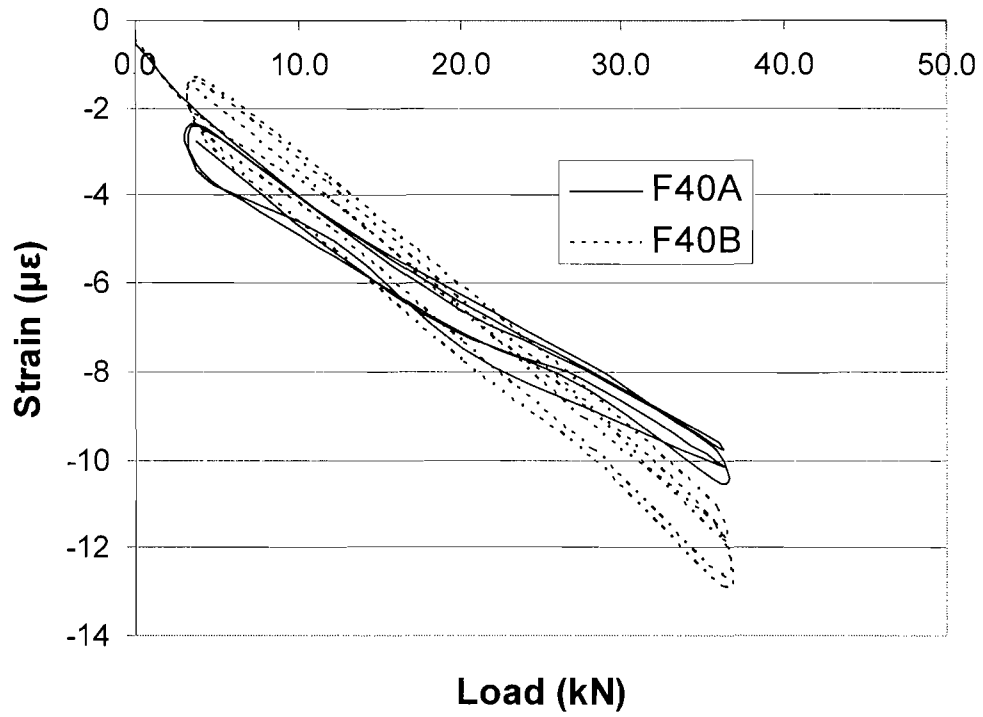


Figure 6.9 Strain measured at the plate ends of specimen F40-1 from three static load cycles

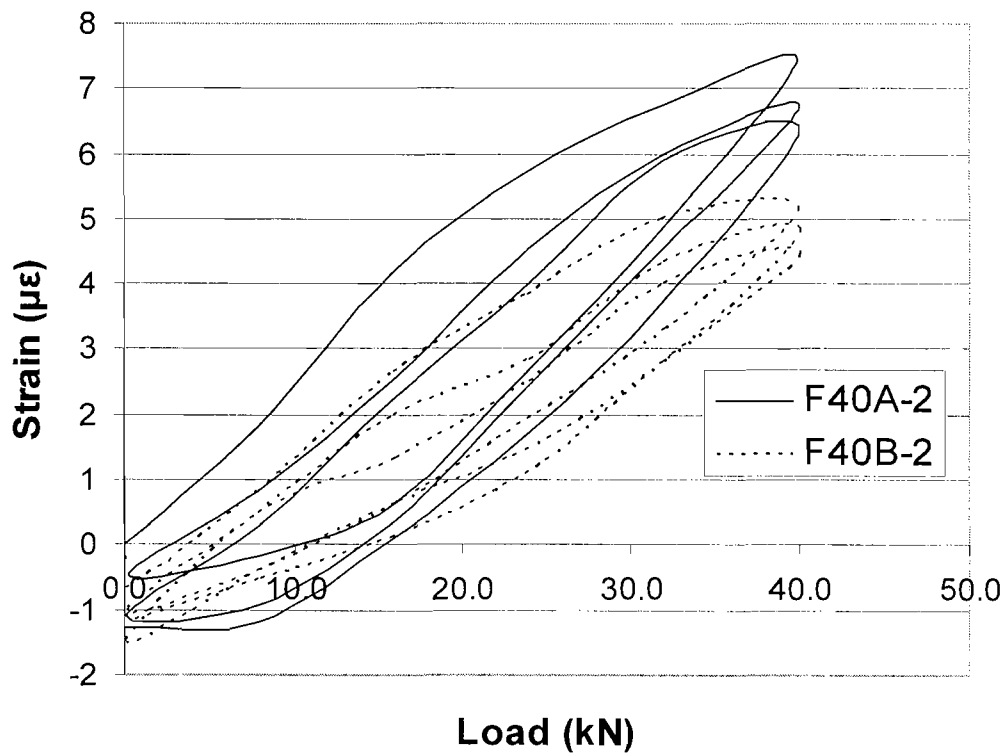


Figure 6.10 Strain measured at the plate ends of specimen F40-2 from three static load cycles

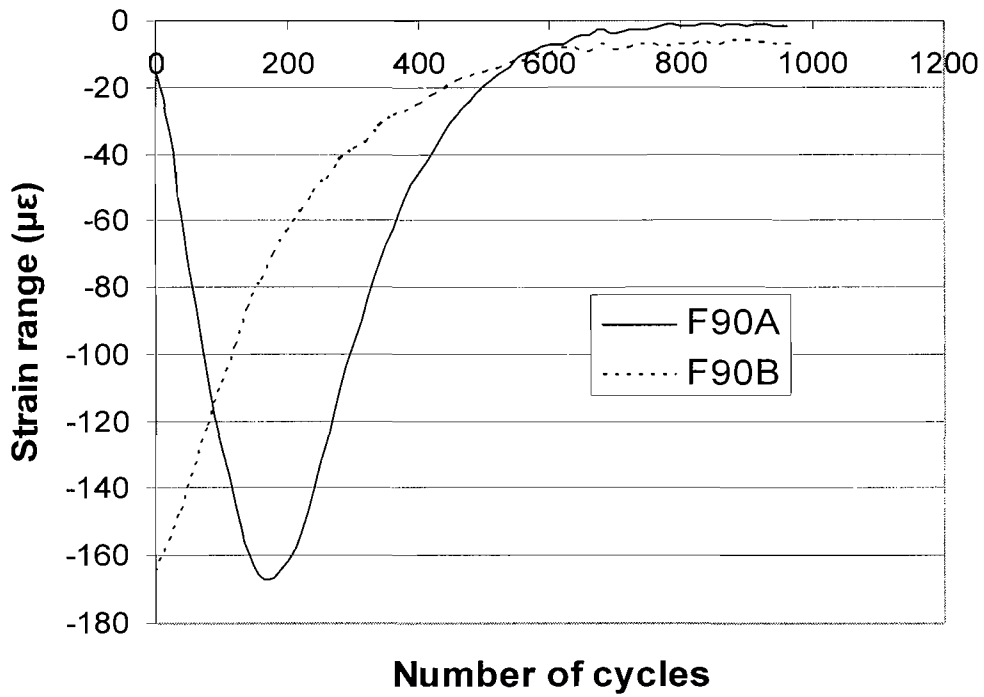


Figure 6.11 Strain ranges measured in F90

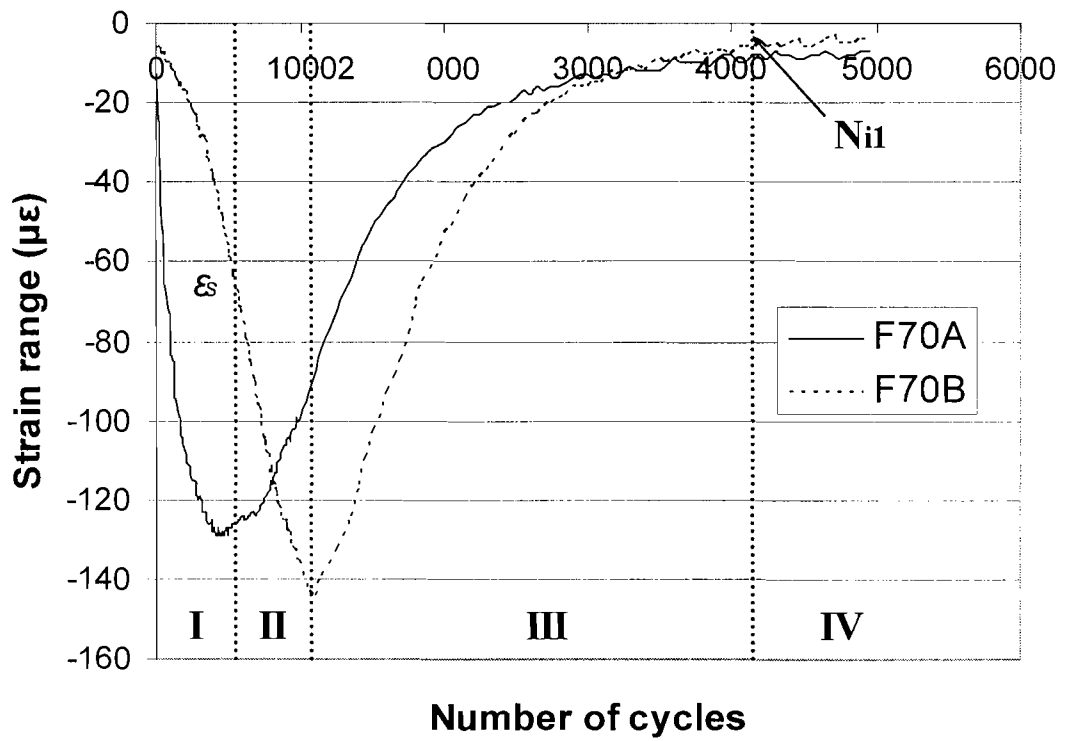


Figure 6.12 Strain ranges measured in F70

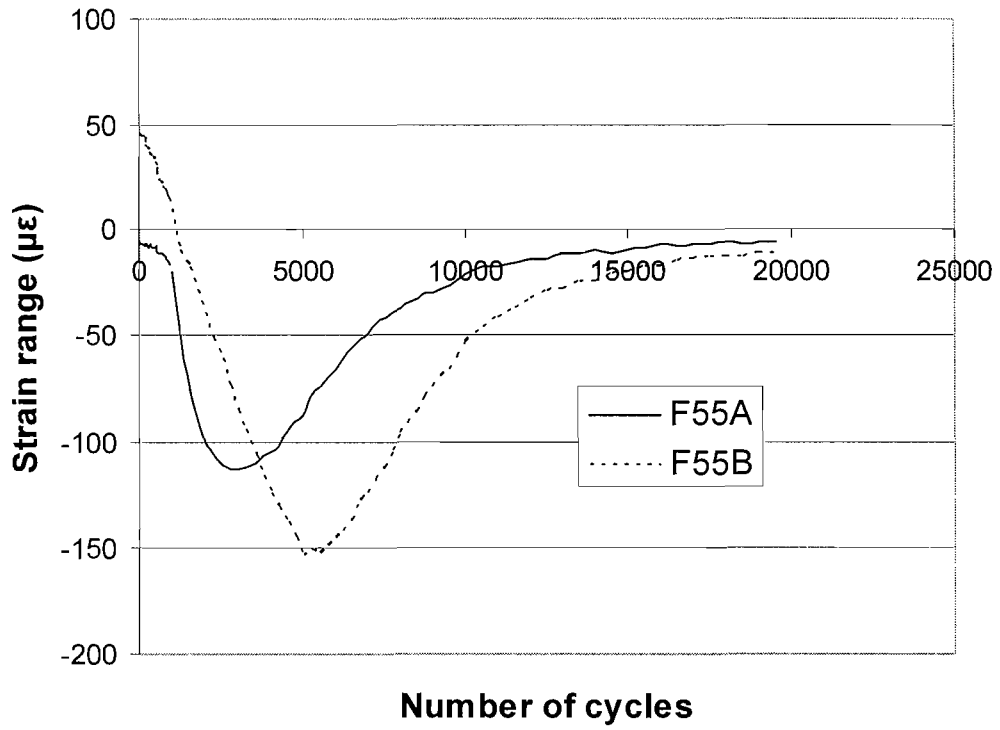


Figure 6.13 Strain ranges measured in F55

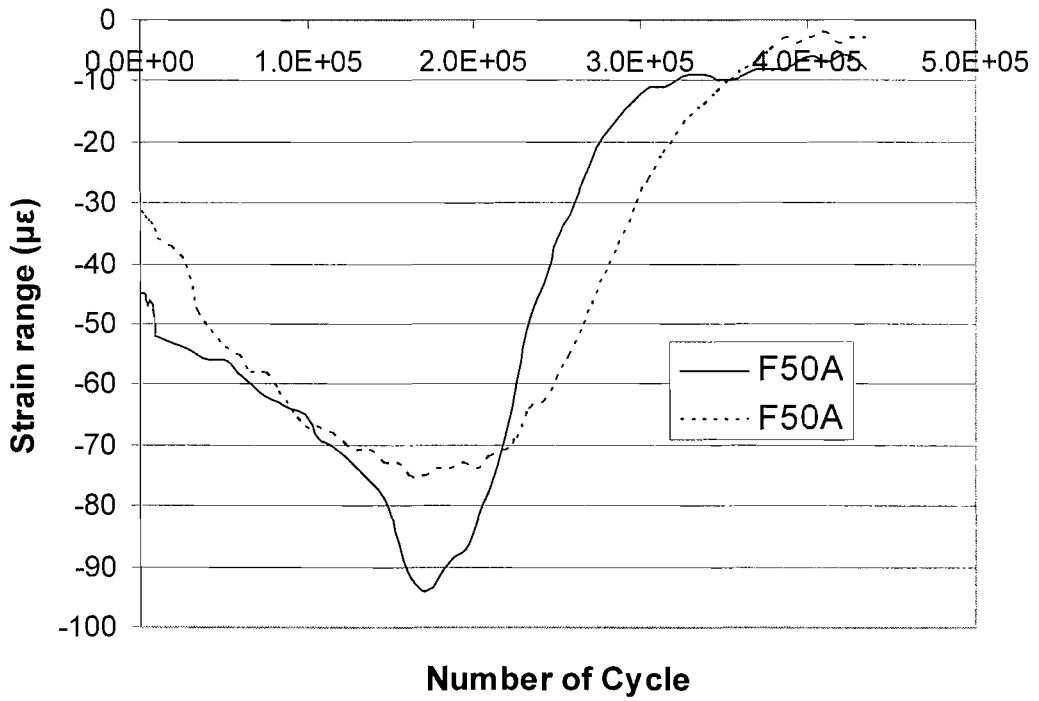


Figure 6.14 Strain ranges measured in F50

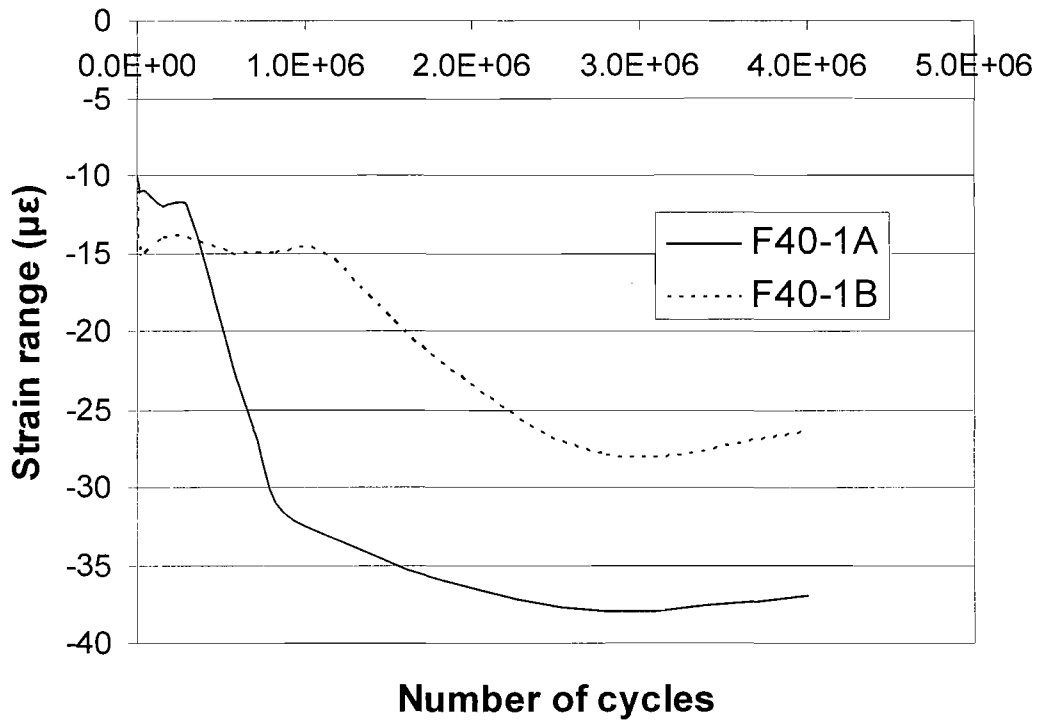


Figure 6.15 Strain ranges measured in F40-1

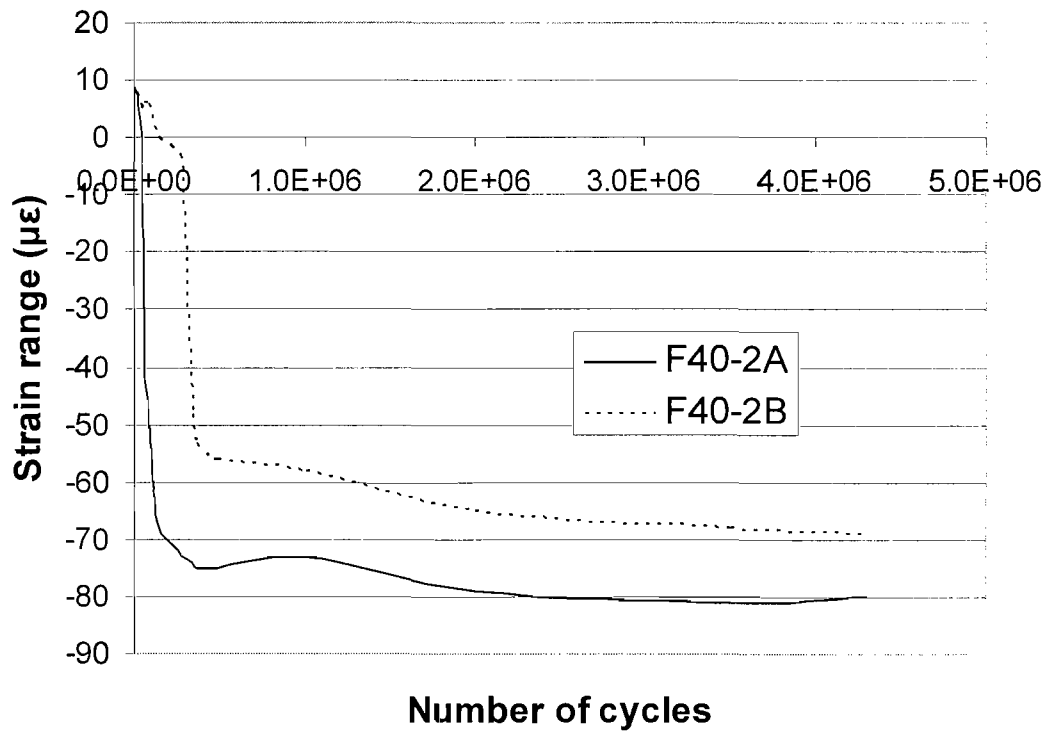


Figure 6.16 Strain ranges measured in F40-2

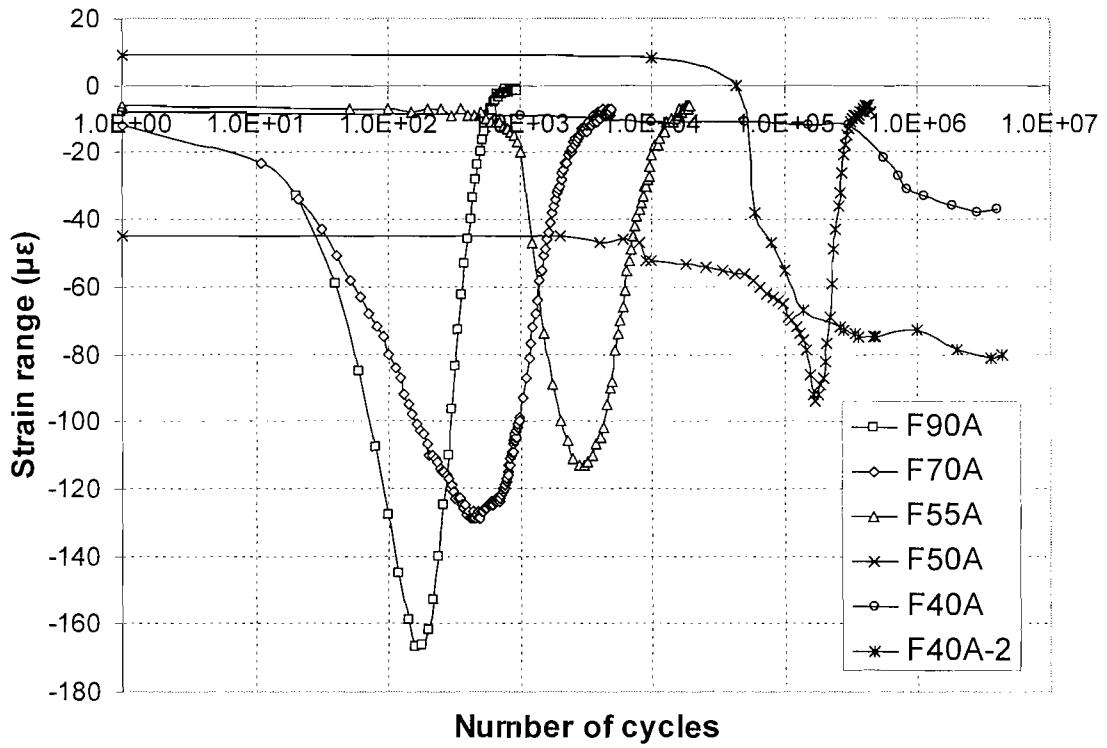


Figure 6.17 Strain range measured in ends A

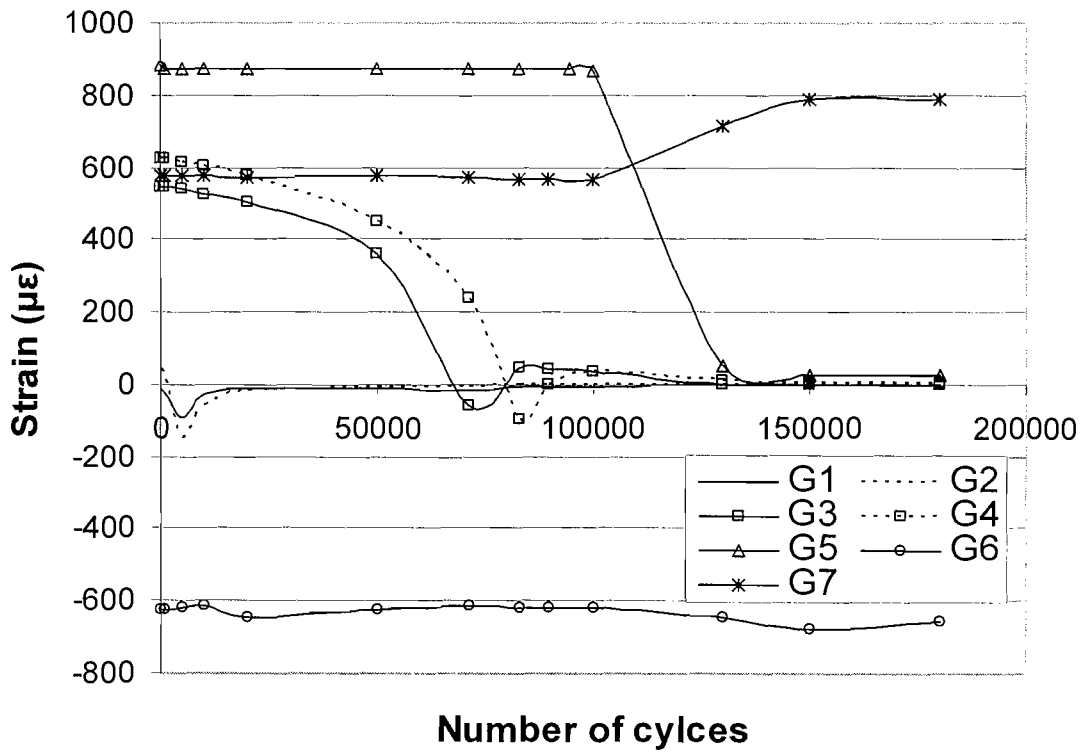


Figure 6.18 The strain ranges measured in specimen F55

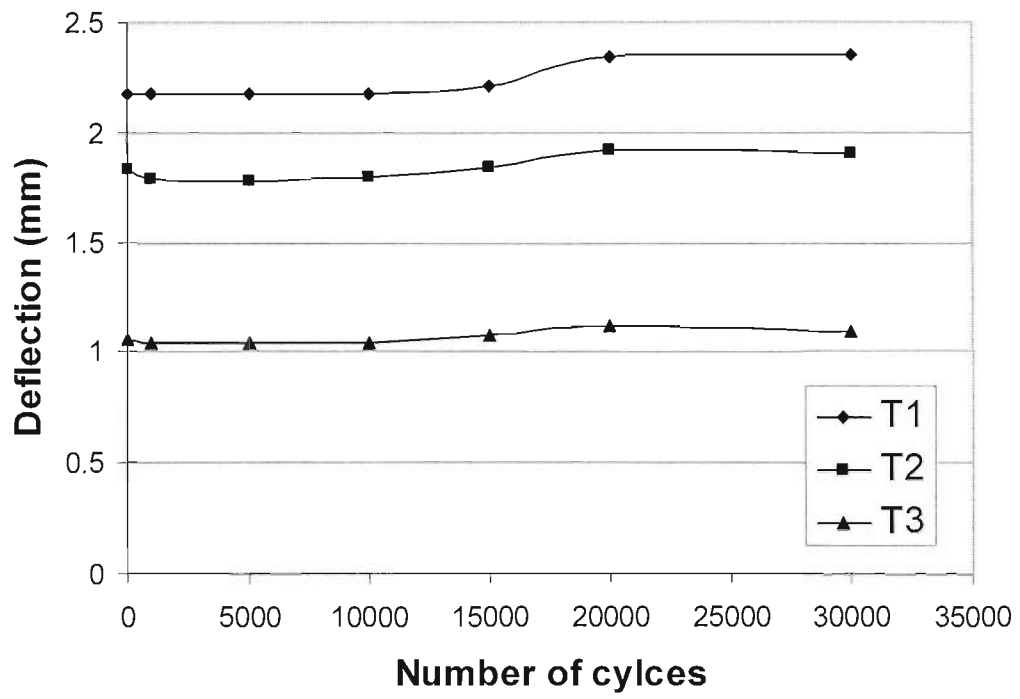


Figure 6.19 Deflections of beam F70 measured during the fatigue test

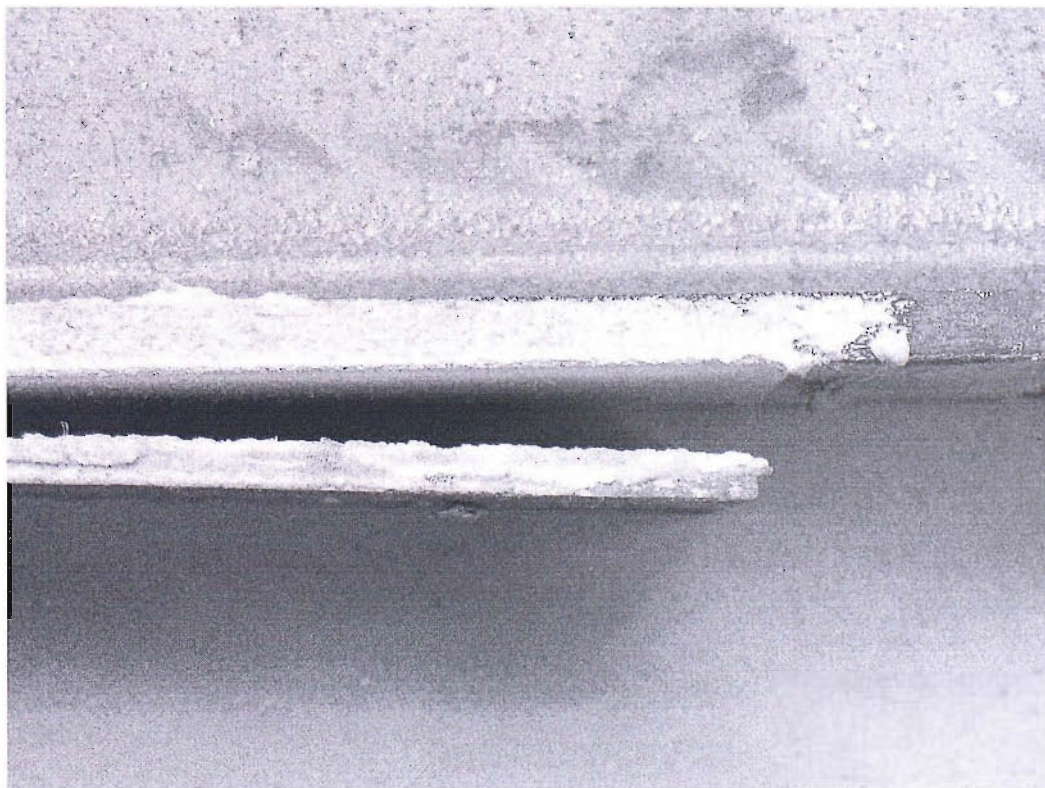


Figure 6.20 Debonding in F125

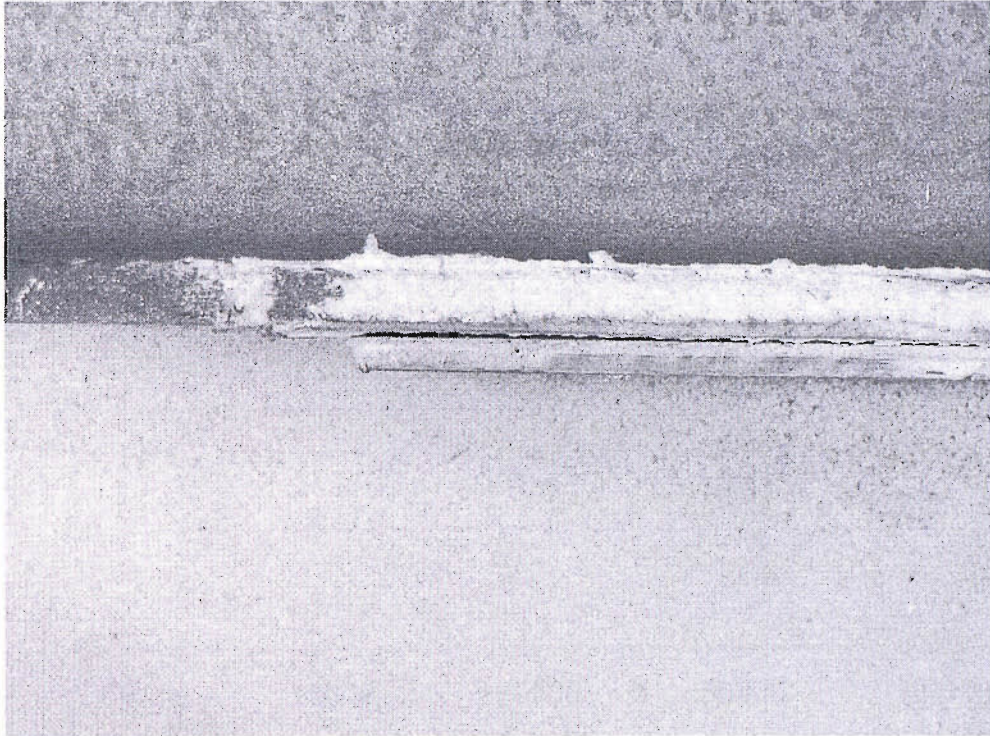


Figure 6.21 The typical debonding

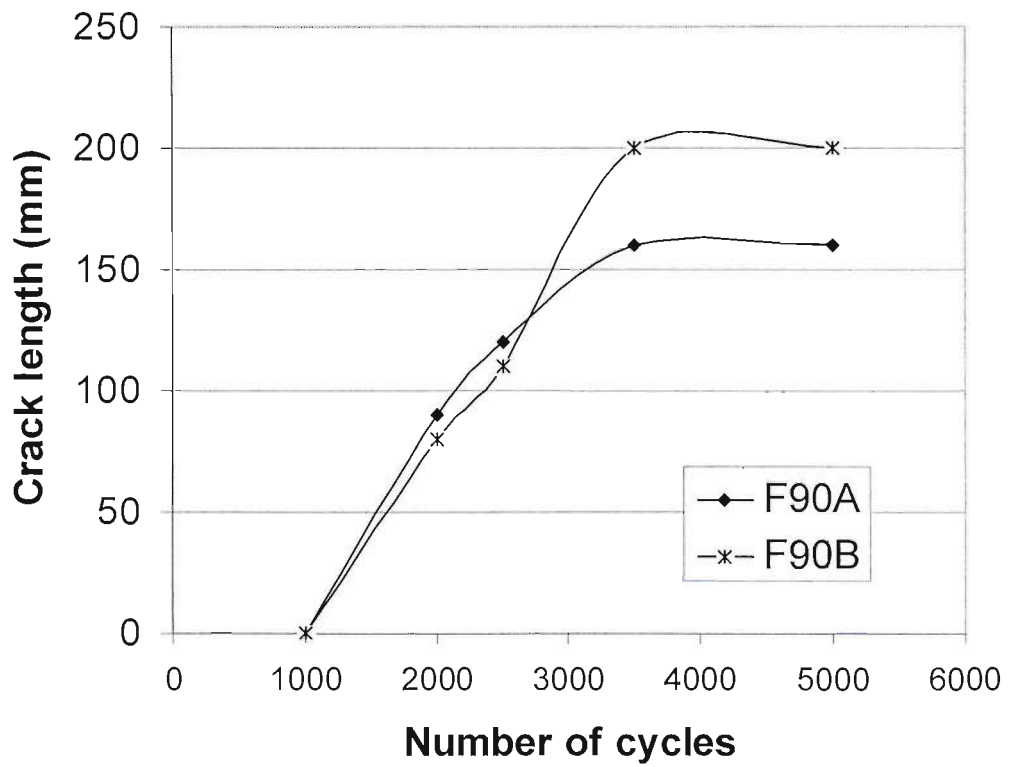


Figure 6.22 Crack growth in specimen F90

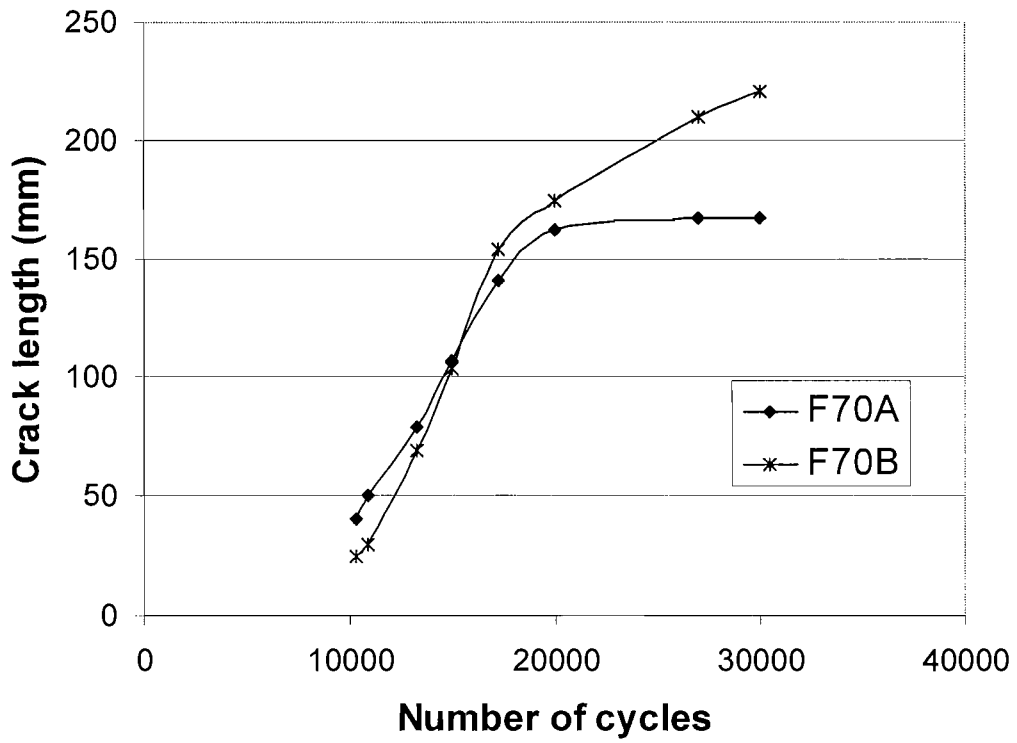


Figure 6.23 Crack growth in specimen F70

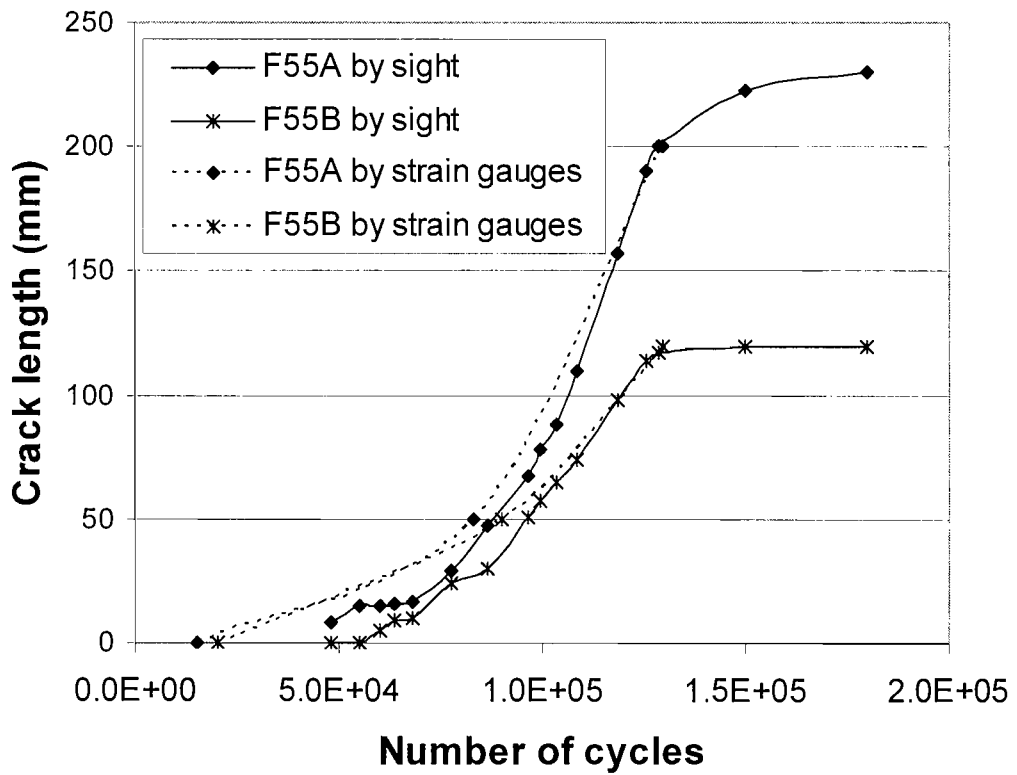


Figure 6.24 Crack growth in specimen F55

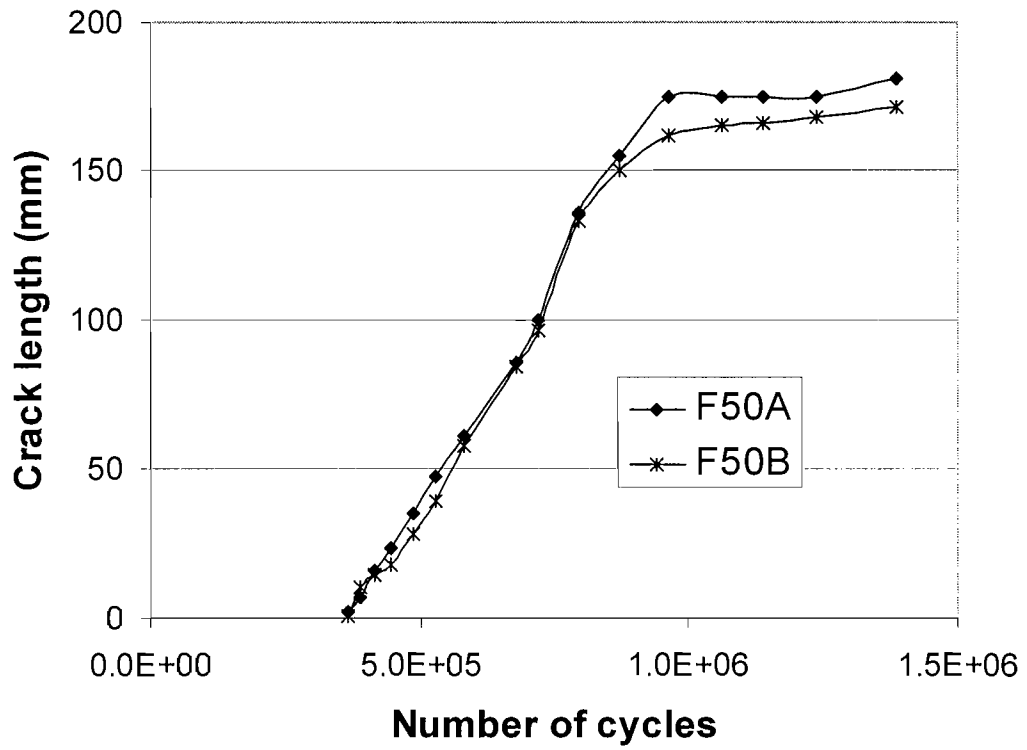


Figure 6.25 Crack growth in specimen F50

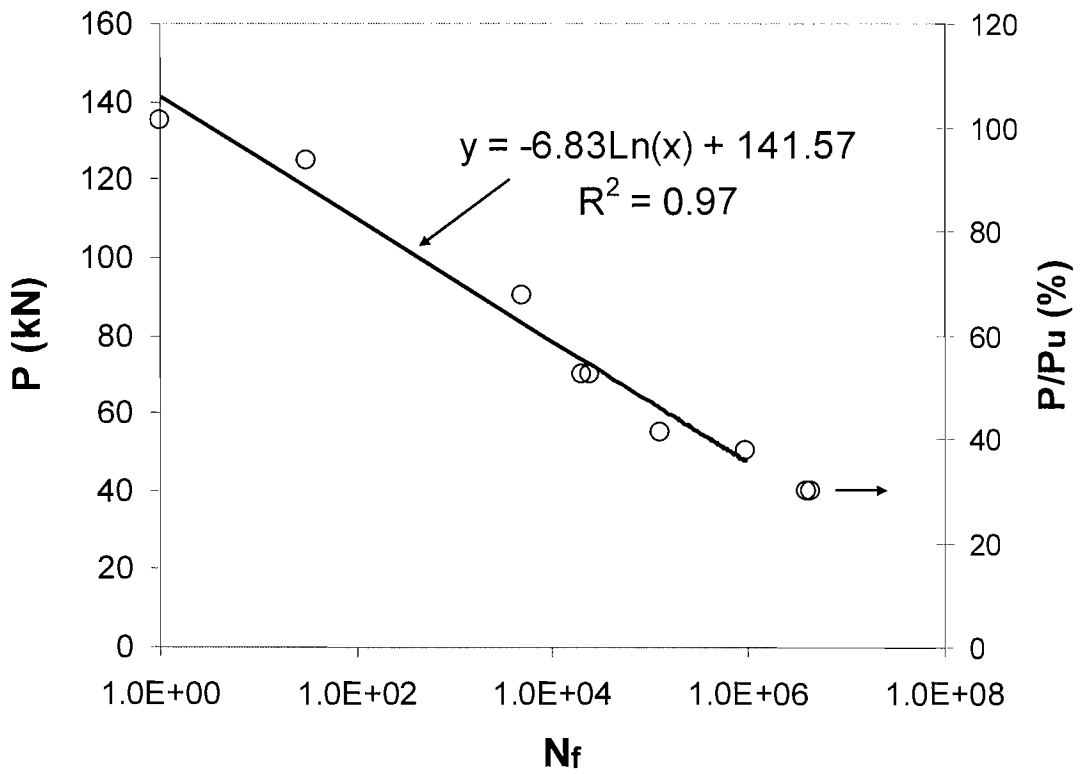


Figure 6.26 P-N curve in logarithmic representation

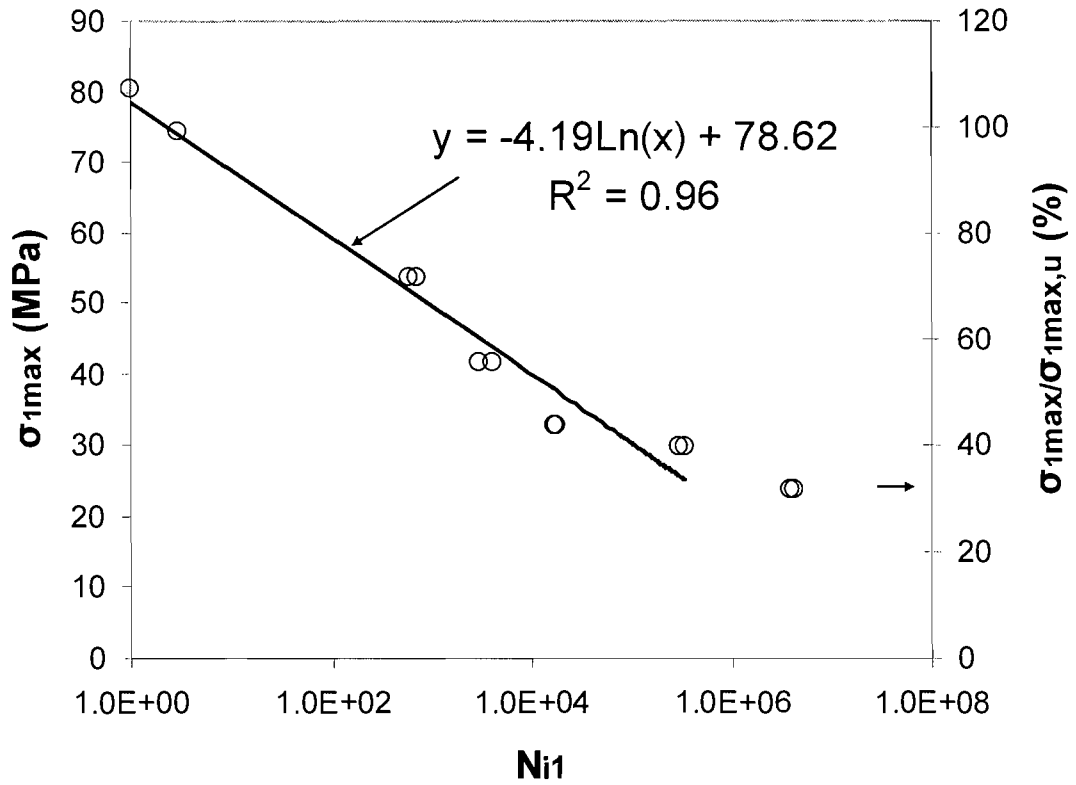


Figure 6.27 S-N curve in logarithmic representation

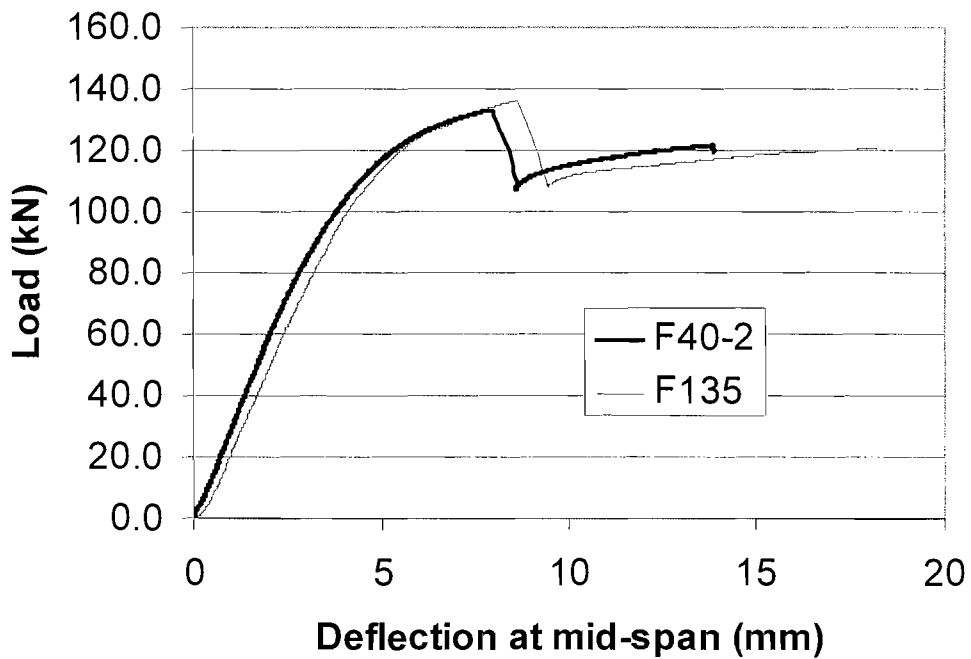


Figure 6.28 Comparisons of Load-deflection curves between specimens with fatigue test and without fatigue test

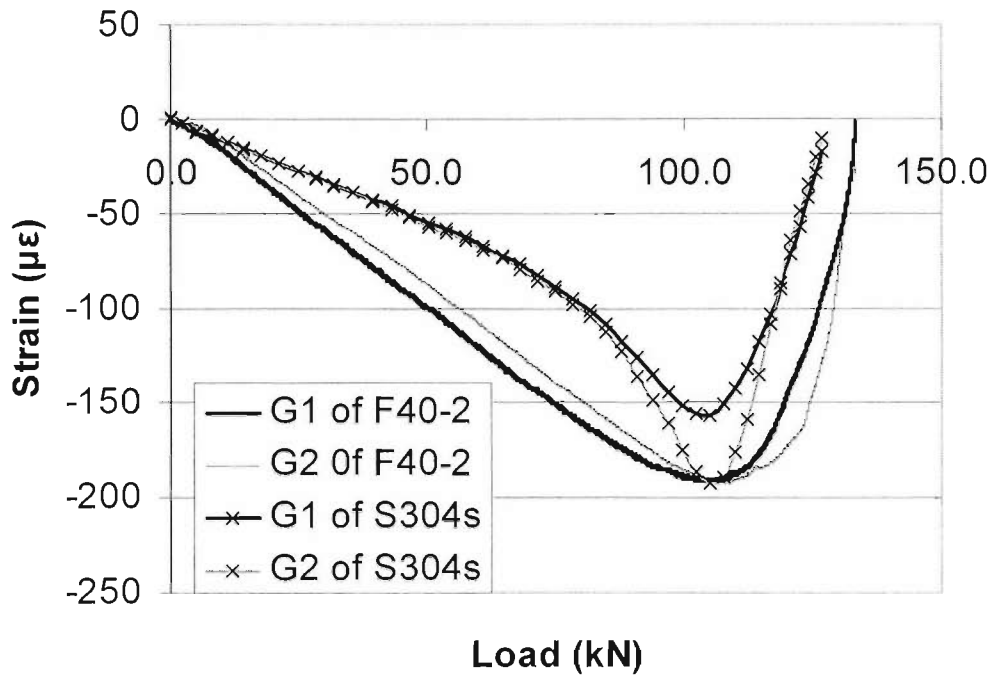


Figure 6.29 Comparisons of stain at the plate ends between beams F40-2 and S304s

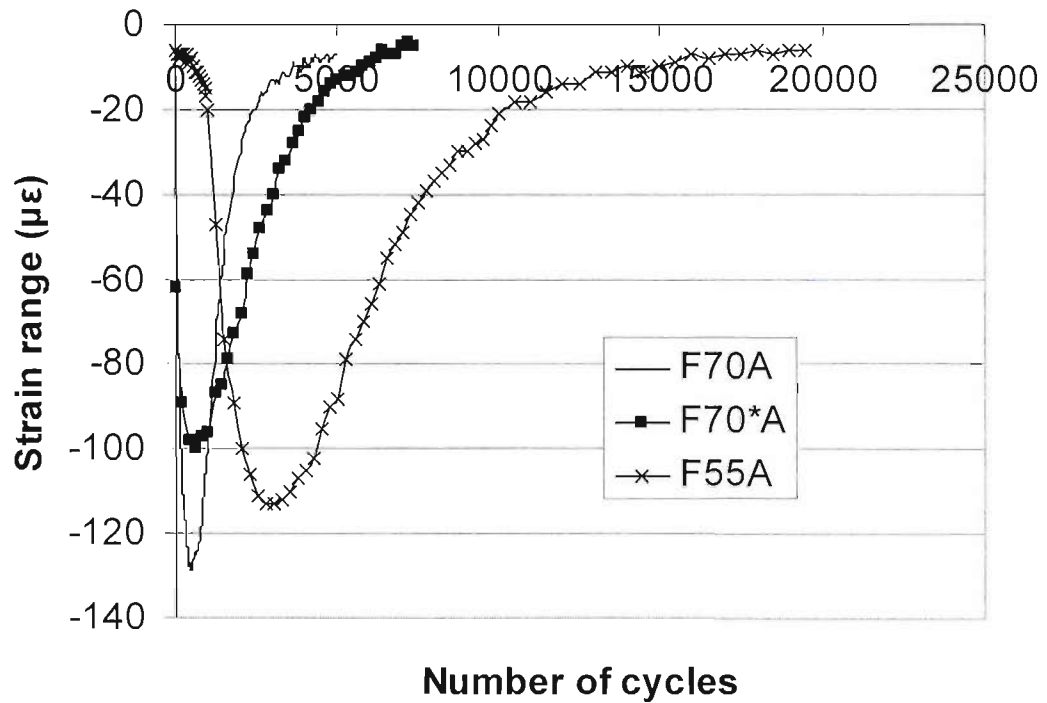


Figure 6.30 Comparisons of the stain ranges obtained for specimens F70A, F70* A and F55A

Chapter 7

Finite element analysis for the end effect

7.1 Introduction and objectives

Interfacial stress concentrations at the plate end of retrofitted metallic beams bonded with CFRP plates is the most detrimental feature of this strengthening technique. The analytical approach to calculate the interfacial stresses of retrofitted metallic beams bonded with a CFRP plate with constant thickness and the numerical approach for the case with tapered CFRP plates have been detailed in Chapter 4. The use of tapered plates has been proposed for reducing the interfacial stress concentration that occurs at the ends of the adhesively bonded plates.

In addition to the tapered plate introduced in Chapter 4 (outside taper), the guidance document CIRIA RP595 [8] proposes a variety of other options for reducing the interfacial stress concentration near the end of the plate. These include a spew fillet covering the plate end, a tapered plate by a matching counter taper in the adhesive thickness (inside taper), the use of lower modulus adhesive near the plate end, and some kinds of mechanical restraint at the plate end. In all of these, the spew fillet and tapers are more practical and reliable. Especially, the surplus adhesive (spew fillet) is always squeezed out at the end of the bonded zone under pressure when the real structural adhesive bonded joints are being manufactured. The square-ended (without spew fillet) adhesive bonded joints are only of theoretical interest. Due to geometrical complexity, however, it is unlikely that a closed-form solution or even a numerical solution can be derived to predict the effects of the spew fillet and the inside taper.

Literature review in Chapter 2 also shows tapers, including inside and outside cases, and spew fillets are beneficial for the reduction of the stress concentration at the end of overlaps. Moreover, inside taper is more beneficial than outside taper and 45°

fillets have been suggested to be used in practice. However, the literatures only consider the effect of spew fillets and inside taper in lap joints. To date, literature on the effect of spew fillets in retrofitted beams is scarce. Rabinovitch and Frostig [184] confirmed the strength improvement in RC beams strengthened with CFRP composites when a spew fillet was introduced.

In the study reported in this chapter, the effects of spew fillets and tapers occurring at plate ends in metallic beams reinforced with a CFRP plate were investigated. A total of eight cases were studied. FE analysis was employed to obtain the stresses in the adhesive layer and the strains in the bottom of the CFRP plate. Using the FE results, the interfacial stresses obtained from different spew fillet cases and different taper cases are compared and discussed. The strains in the bottom of the CFRP plate obtained from the different spew fillet cases are compared to confirm the analytical results in Chapter 4.

7.2 Geometry and material properties

The geometric representation of the retrofitted beam considered in this study is the same as that reported in Chapter 4, and is shown in Figure 4.1, with the following dimensions: $L_p=0.4$ m, $L_0=0.35$ m, $b=76.2$ mm, $t_a=1$ mm, $t_p=3$ mm. The steel beam was a 127 x 76 UB13.

Four different spew fillet configurations were used in this study and are shown in Figure 7.1. The configurations include (a) square end (without fillet), (b) half triangular (45°), (c) full triangular (45°) and (d) full rounded. 45° triangular spew fillets were chosen since triangular spew fillets were used in most of previous research and 45° is the best suited for using in practice [108]. Comparison of the results obtained from the full and the half triangular cases provides the effect of the size of spew fillets. The rounded spew fillet was chosen since it is similar to the naturally obtained structural adhesive fillet, i.e. spew fillets created by squeezing surplus adhesive, which generally have a rounded profile. The outside taper (e) and insider taper (g) have the same plate configurations apart from the facing direction of the

taper. These tapers combined with full triangular fillet (45°) are shown as cases (f) and (h).

The material behaviour of the steel beam was considered isotropic, with the elastic modulus $E_b=205$ GPa and the Poisson's ratio $\nu_b=0.3$. The material behaviour of the adhesive was also isotropic, with the elastic modulus $E_a=8$ GPa, the Poisson's ratio $\nu_a=0.49$, and the shear modulus $G=2.6$ GPa. The material behaviour of the CFRP plate was orthotropic with the elastic moduli $E_{p1}=E_{p2}=7.44$ GPa, and $E_{p3}=212$ GPa (in the direction of the fibres). The Poisson's ratios $\nu_{p12}=0.45$ and $\nu_{p13}=\nu_{p23}=0.015$, and the shear moduli $G_{12}=2.6$ GPa and $G_{13}=G_{23}=4.31$ GPa.

The dimensions and material properties used in this study are the real values obtained in the experimental studies detailed in Chapter 5 and Chapter 6.

7.3 Finite element analysis

FE analysis has been employed in this study to analyse the stress and strain of the retrofitted beam under a concentrated load $P=90$ kN at mid-span. The general purpose software package ABAQUS [185] was used. A linear 3-D FE Model was established, in which one half of the beam only was considered because of symmetry. All nodes at mid-span were restrained to produce the required symmetry, and nodes at the end of the beam were restrained to represent the simple roll-supported condition.

The steel beam was modelled with 4-node doubly curved shell elements (element S4R), which had reduced integration with hourglass control and finite membrane strains. The adhesive and the carbon plate were modelled with 8-node linear brick elements (element C3D8R), which had reduced integration with hourglass control to prevent shear locking.

The interfacial stresses were obtained from the average values of the stresses in the upper (adjacent to steel beam) and the lower (adjacent to CFRP plate) elements of the adhesive layer. The strains in the CFRP plate were obtained from the average values of the strains in the bottom elements of the plate. To examine the convergence

of the FE procedure, the maximum interfacial stresses and the maximum compressive strain in the lower elements in the CFRP plate in the without fillet case (a) were obtained. The stresses with increasing number of elements in the bonded area in the longitudinal direction are shown in Figure 7.2. It indicates that the shear stresses in both the upper and the lower layers, and the normal stresses in the lower layer are insensitive to mesh density. But the normal stresses in upper layer are sensitive to mesh density and are difficult to converge. The same conclusions can be obtained when increasing the number of layers through the thickness of the adhesive. This is because the singularity (point A in Figure 7.1a) exists at the corner between steel beam and adhesive layer. In theory, the point of singularity implies a location of infinite stresses [100]. Since the purpose of this study is to examine the effect of the fillets and the tapers, an identical, or similar, mesh for all cases are beneficial to compare the results. Hence 800 elements in the longitudinal direction in the bonded area and 3 layers in the adhesive were used for all cases. The maximum compressive strain is also insensitive to the number of elements in the longitudinal direction, but is very sensitive to the bottom (lower) element thickness of the plate. The maximum compressive strain is plotted against the reciprocal of the lower element thickness of the plate in Figure 7.3. It indicates that the maximum compressive strain converges when the lower element thickness of the CFRP plate equals 1/96 mm, hence 12 layers with a bias ratio 47 were used through the thickness of the plate. This graded FE mesh for the plate was not used in calculating the interfacial stresses because it is difficult to be achieved in the tapered cases. The stress plots shown in Figure 7.4 and 7.5 indicate the final meshes used in the calculations.

7.4 Results and discussion

7.4.1 Stresses for without fillet case

The basic configuration – square end (without fillet) – has been investigated and reported in Chapter 4. The results show that the agreement is good for the stress distributions between the FE and the analytical solutions. However, the FE results were obtained only from the lower interface, and not from the upper interface.

In this study, FE results obtained from both the upper and the lower interfaces were compared with analytical results calculated using the method detailed in Chapter 4, shown in Figure 7.6. It is observed:

- The stress distributions obtained from upper and lower interfaces in the FE solutions show a difference over a short length of about 4 mm from the plate end. This is because the load transition from the steel beam to the adhesive layer at the singularity (point A in Figure 7.1a) in the upper interfacial corner causes high stress concentration.
- Excluding the short length close to the plate end mentioned above, the stress distributions between the upper and the lower interfaces in the FE solutions are almost the same, and the agreement between the FE and the analytical results is good as well.
- The difference in the maximum normal stresses is much larger than that in the maximum shear stresses. Moreover, the maximum analytical normal stress is close to the maximum FE lower normal stress but both of them are much less than the maximum FE upper normal stress.

Figures 7.7 and 7.9 also clearly show that the maximum shear and normal stresses, respectively, increase from the lower interface (corresponding to the unload adherend – CFRP plate) to the upper interface (corresponding to the loaded adherend – steel beam) at the end. This result agrees with that obtained from lap joints [106,108].

7.4.2 Effect of the spew fillet configuration on stress distribution

Figures 7.7 – 7.10 show the stress contour plots for all the eight cases. The figures show that the presence of spew fillet reduces both the shear and the normal stress concentrations at the corner (point A in Figure 7.1a). But (reduced) stress concentrations still exist at the fillet corner (the entrance corner of the adhesive fillet) in all cases. The reduction of the shear stress concentrations on the lower interface is not significant.

In order to observe the effect of the spew fillet configurations on the stress distribution, the upper interfacial stresses for the without taper cases and the with taper cases are shown in Figures 7.11 and 7.12, respectively. It is observed that:

- The presence of the spew fillet influences the stress distribution only for a short distance from the end of plate (less than 6 mm, twice the thickness of the plate).
- The cases half triangular (b), full triangular (c), and full rounded (d) have similar stress distributions, even in the area close to the end. But for the normal stress distributions, they are very different, especially for the half-rounded case.
- The shear stress distributions close to the end are smoother when a spew fillet is introduced. But the differences in the maximum value are not as significant as in the case of the normal stresses.
- The normal stress concentrations exist at the end of the spew fillet for all the with spew fillet cases except for case (f), outside taper with fillet, where the normal stress concentration is at the end of the plate.

The principal stress patterns are shown in Figures 7.4 and 7.5. It is observed that the without fillet cases (a) (e) and (g), and the full rounded fillet case (d) have the maximum tensile principal stress at the upper adhesive corner. But for the other cases, (b) (c) (f) and (h), this is not so and the tensile principal stresses are almost parallel to the slope of the spew fillets. Mays and Hutchinson [150] indicated that Mode I is the lowest energy fracture mode for isotropic materials and, thus, a crack always propagates along a path normal to the direction of maximum principal stresses. Therefore, crack initiation is at the corners of the spew fillet in cases (a) (d) (e) (g), but develops along face perpendicular to the slope of the spew fillet in cases (b) (c) (f) (h). The crack propagation paths are shown schematically in Figure 7.13. These results are similar to those of Kadioglu et al. [109].

7.4.3 Effect of the taper on stress distribution

In order to observe the effect of the tapers on the stress distribution, the upper and lower interfacial stresses for the without taper case (a) and the with tapers case (e) and (g) are compared in Figures 7.14 and 7.15 respectively. The figures clearly show the

beneficial effect of a taper in reducing stress concentration and that an inside taper is better than an out side taper.

7.4.4 End effect on the maximum interfacial stresses

The maximum interfacial stresses for all the cases are given in Table 7.1. The percentage reductions are indicated in relation to the base case (a). It is noted that:

- For the with fillet cases (b) (c) (d) (f) and (h), the reductions of shear stress are smaller than those of normal stress. Except for the insider taper with fillet case (h), the reductions of shear stress are all less than about 15%. But the reduction of normal stress is all over 30%.
- For the with taper cases (e) and (g), the reductions of shear stress and normal stress are very close. But the percentage reduction of normal stress for the with taper cases is only about 1/3 of the with fillet cases except case (d).
- The inside taper with fillet case (h) performs the best in reducing the maximum interfacial stresses. But the reduction on normal stress is only marginally better than the with fillet cases (b) (c) and (f).
- Spew fillet size does not have a significant influence on the reduction of stresses. The half and the full triangular fillet cases have similar reductions of both the shear and the normal stresses. Although the fillet size of the full rounded fillet case (d) is four times that of the half triangular fillet case (b), the percentage reduction of normal stress for case (d) is only half of that for case (b). Since the entry angle between the fillet edge and the steel beam for case (b) is 45° and that for case (d) is 90° , it is apparent that a small entry angle is more beneficial for reducing the maximum stresses than the absolute size of the spew fillet. This result confirms the findings of Lang and Mallick [106] and Belingardi et al. [108] on lap joints.

In summary, an inside taper in the plate together with a triangular fillet gives the most reduction in the maximum interfacial stresses. However, the configuration of a natural spew fillet is rounded, and it only reduces the shear and the normal stresses by 14% and 31%, respectively. Moreover, most of stress concentration in the without spew fillet case (a) is at the corner (point A in Figure 7.1a). Since the adhesive is not

an ideal elastic brittle material, the peak stress will be reduced in the without spew fillet case. The implication is that the beneficial effect in practice is smaller than what has been calculated.

7.4.5 Effect of the spew fillet size on the strain distribution in the plate bottom

The strains in the bottom surface of the plate for different spew fillet sizes (case (a)-(d)) are shown in Figure 7.16. This figure shows that the spew fillet size has a great effect on the strain close to the plate end. The minimum strain increased with the spew fillet size, which confirms the analytical results given in Chapter 4. The minimum strains for the without fillet case (a) and the half triangular fillet case (b) are negative, i.e. compressive strain and the minimum strains for the full triangular fillet case (c) and the full rounded fillet case (d) are positive, i.e. tensile strain. The influence of the spew fillets in the strain reduces with the distance from the end and the strains for all cases (a)-(d) are almost the same when the distance is larger than 50 mm.

7.5 Conclusion

In this chapter, finite element analysis was employed to determine the effects of the spew fillet and the taper on interfacial adhesive stresses and the strain in the CFRP plate. A total of eight cases with different configurations of spew fillet and different tapers have been considered. The results show:

- (1) The adhesive stresses, especially normal stresses, in the upper and the lower interfaces are different due to the load transfer and the influence of the singularity at the adhesive corner.
- (2) The spew fillet reduces both the shear and the normal stress concentrations at the adhesive entrance corner, and the stress distributions close to the adhesive end are smoother when the spew fillet is introduced. Therefore, in the spew fillet cases fracture may not initiate at the corner as in the without spew fillet cases. But the crack will still progress along the upper surface in all cases.

(3) A small entry angle between the fillet edge and the steel beam is more beneficial for reducing the maximum stresses than the size of spew fillet.

(4) A taper reduces the maximum stresses, but the stress concentration is still quite significant. The beneficial effect of inside taper is about two times than that of outside taper.

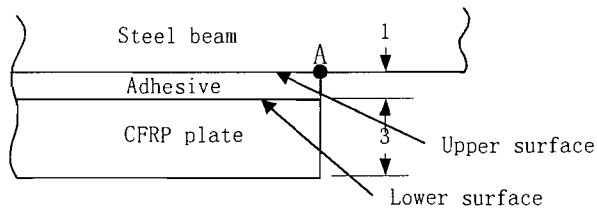
(5) To reduce the normal stress, spew fillets are better than tapers. But the inside taper is more effective in reducing the shear stress than the fillet. Therefore, a combination of inside taper and spew fillet (case (h) investigated) is the best way to reduce the maximum interfacial stresses.

The above conclusions largely agree with the findings on lap joints. But the magnitude of reduction of the maximum shear stress by spew fillets is far less than that for lap joints (only about a quarter of Lang and Mallick's results [106]). Considering that the configuration of real structural adhesive fillet is about rounded, i.e. the entry angle close to 90° , and the stress concentrations on the singularity are reduced by the adhesive plastification, the effect of real spew fillet is limited. This confirmed the results obtained from static tests detailed in Chapter 5, in which the spew fillet only improved the debonding load of the retrofitted beams by about 5%.

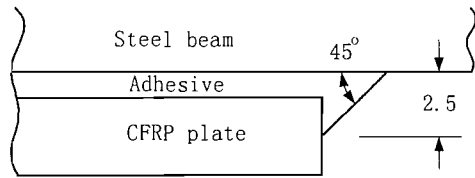
The results of the finite element analysis also show that the spew fillet size has a large effect on the strain close to the plate end. The minimum strain increased with the spew fillet size, which confirms the analytical result given in Chapter 4.

Table 7.1 The maximum interfacial stresses and reduction ratio

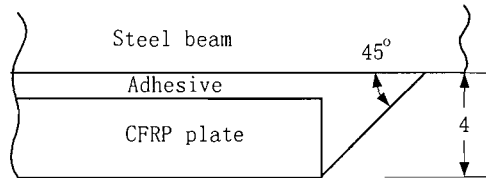
Case	Shear stress		Normal stress	
	Max. value (MPa)	Percentage reduction	Max. value (MPa)	Percentage reduction
(a) Without fillet	33.9	-	-75.7	-
(b) Half triangular fillet	31.0	8.5%	-26.7	64.7%
(c) Full triangular fillet	29.7	12.2%	-21.9	71.1%
(d) Full rounded fillet	29.2	13.8%	-52.1	31.2%
(e) Outside taper	29.9	11.8%	-65.9	13.0%
(f) Outside taper with fillet	28.7	15.2%	-20.2	73.3%
(g) Inside taper	22.3	34.3%	-55.9	26.2%
(h) Inside taper with fillet	19.5	42.3%	-18.2	76.0%



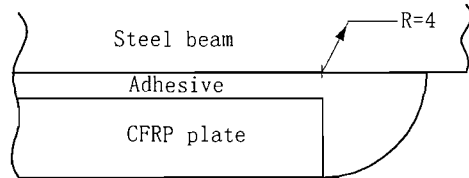
(a) Square end (Without fillet)



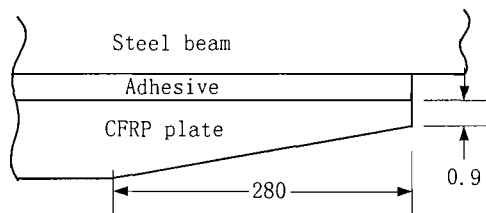
(b) Half triangular fillet



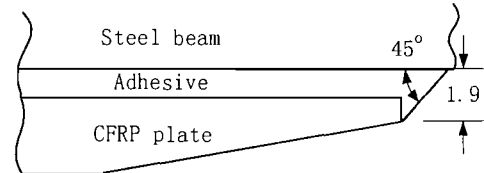
(c) Full triangular fillet



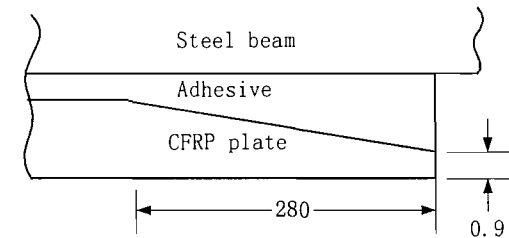
(d) Full rounded fillet



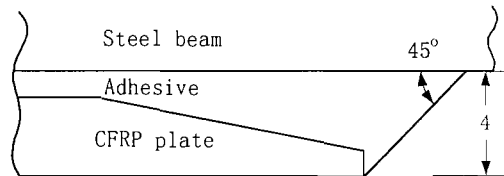
(e) Outside taper



(f) Outside taper with fillet



(g) Inside taper



(h) Inside taper with fillet

Figure 7.1 Schematic representations of spew fillet configurations for all cases

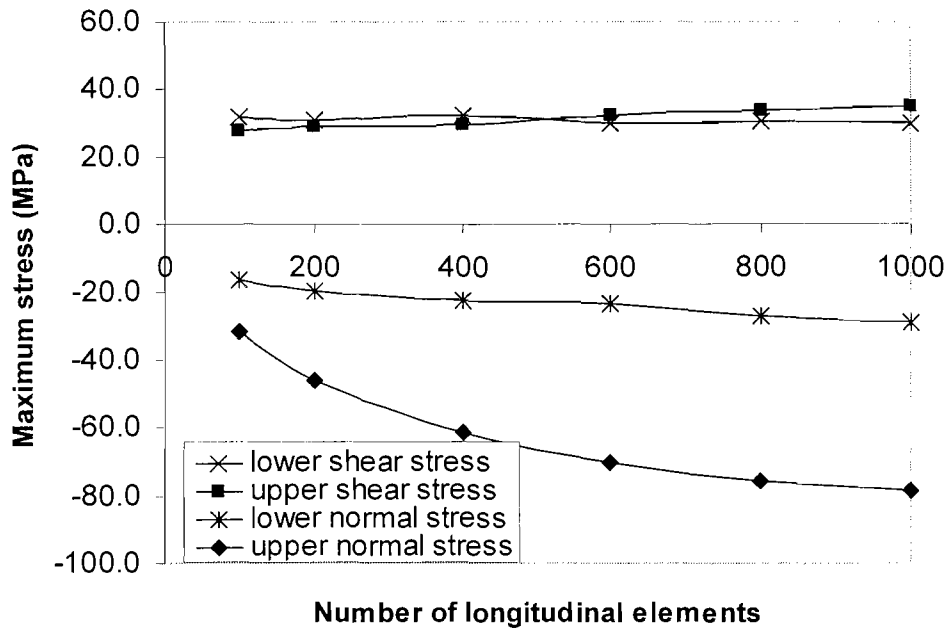


Figure 7.2 Convergence of the finite element results in the longitudinal direction

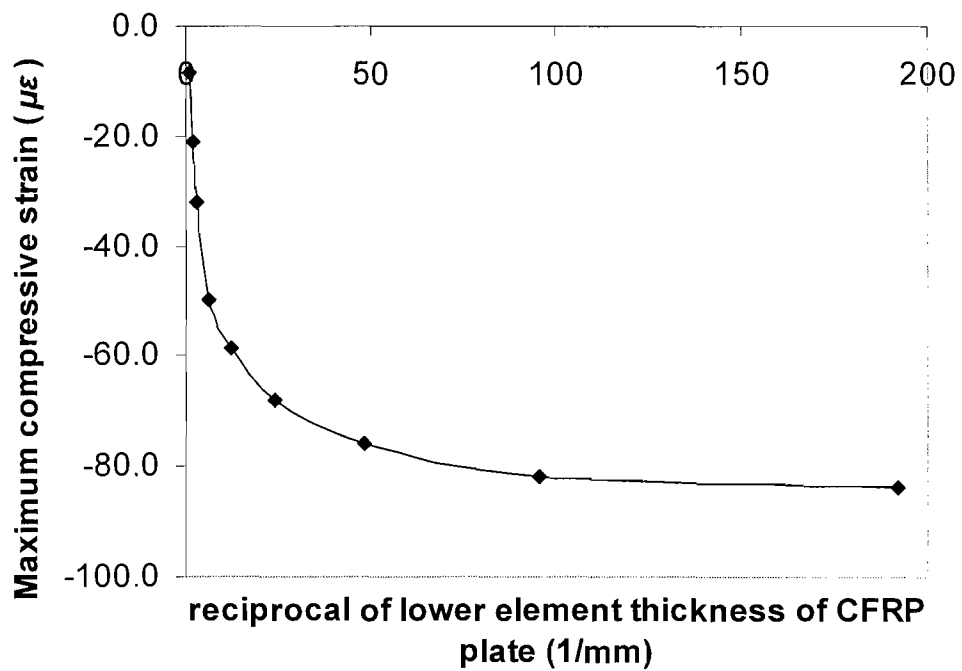
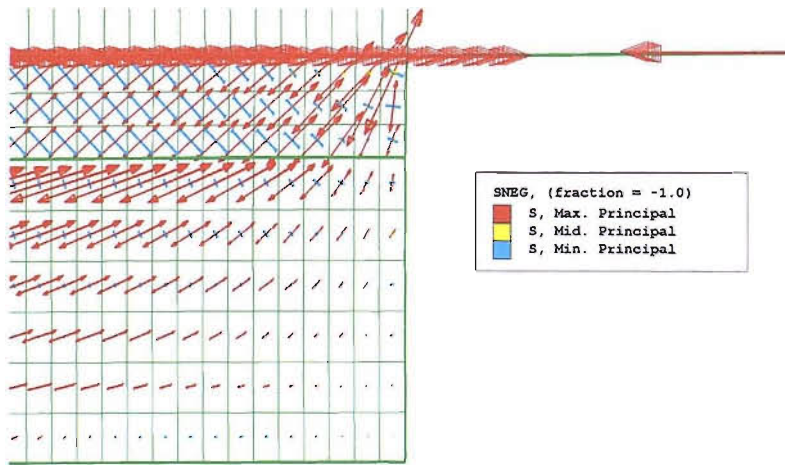
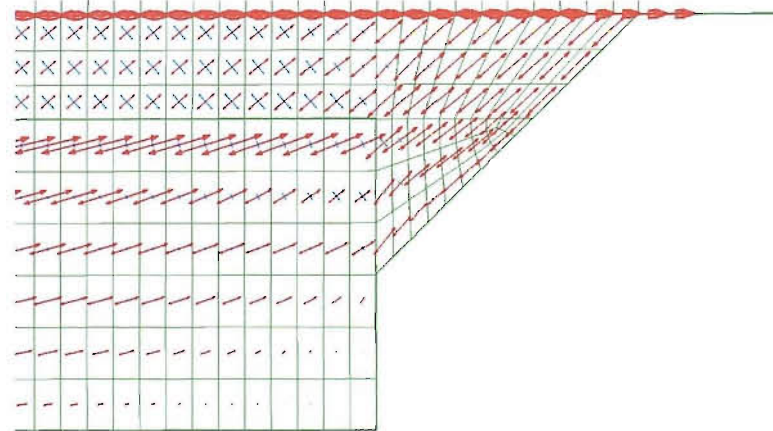


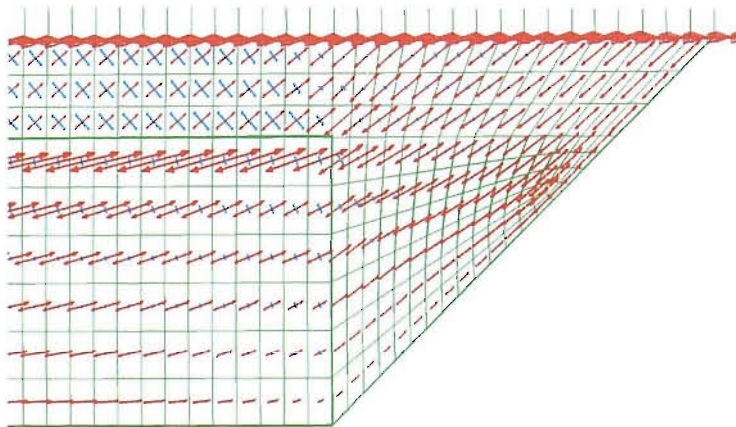
Figure 7.3 Convergence of the finite element results in the vertical direction



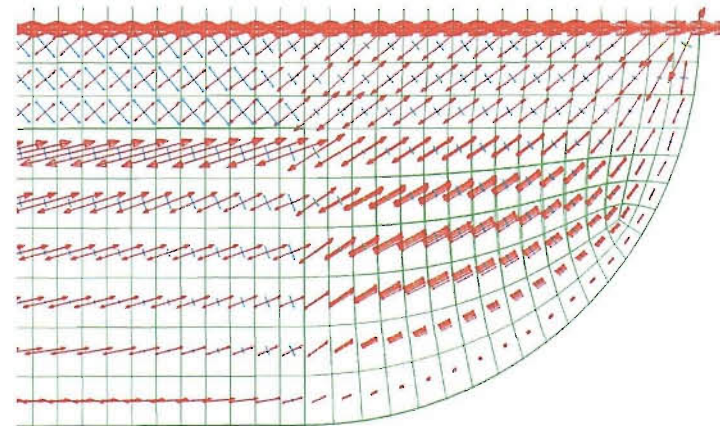
(a) Without Fillet



(b) Half triangular fillet

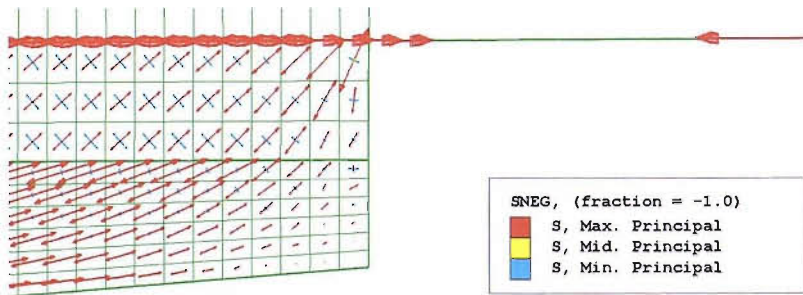


(c) Full triangular fillet

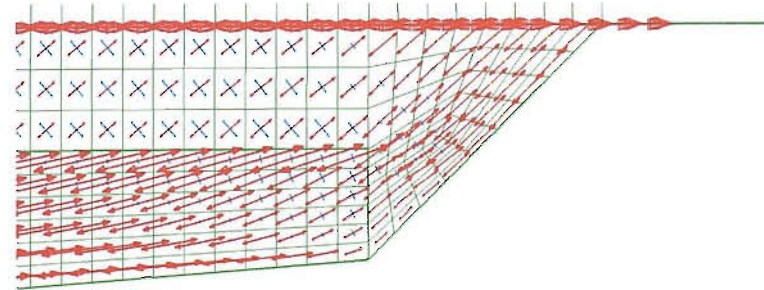


(d) Full rounded fillet

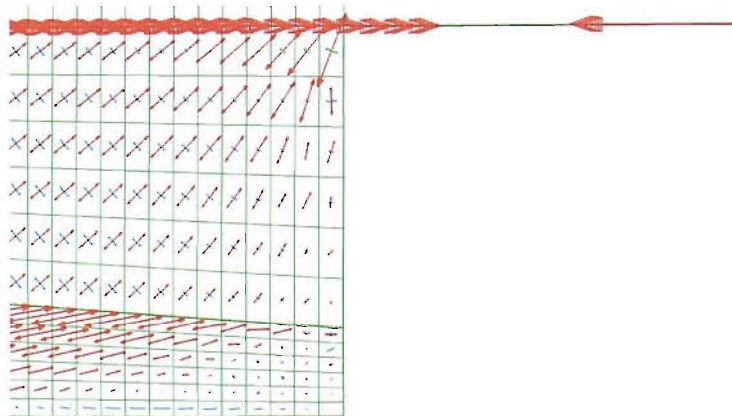
Figure 7.4 Finite element meshes and the principal stress patterns of the without taper cases



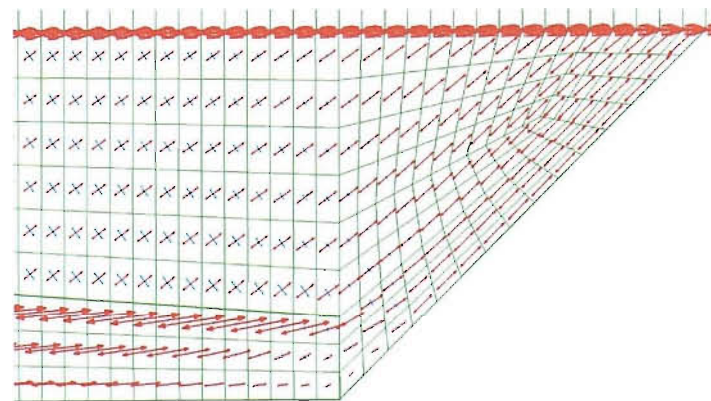
(e) Outside taper



(f) Outside taper with fillet



(g) Inside taper



(h) Inside taper with fillet

Figure 7.5 Finite element meshes and the principal stress patterns of the with taper cases

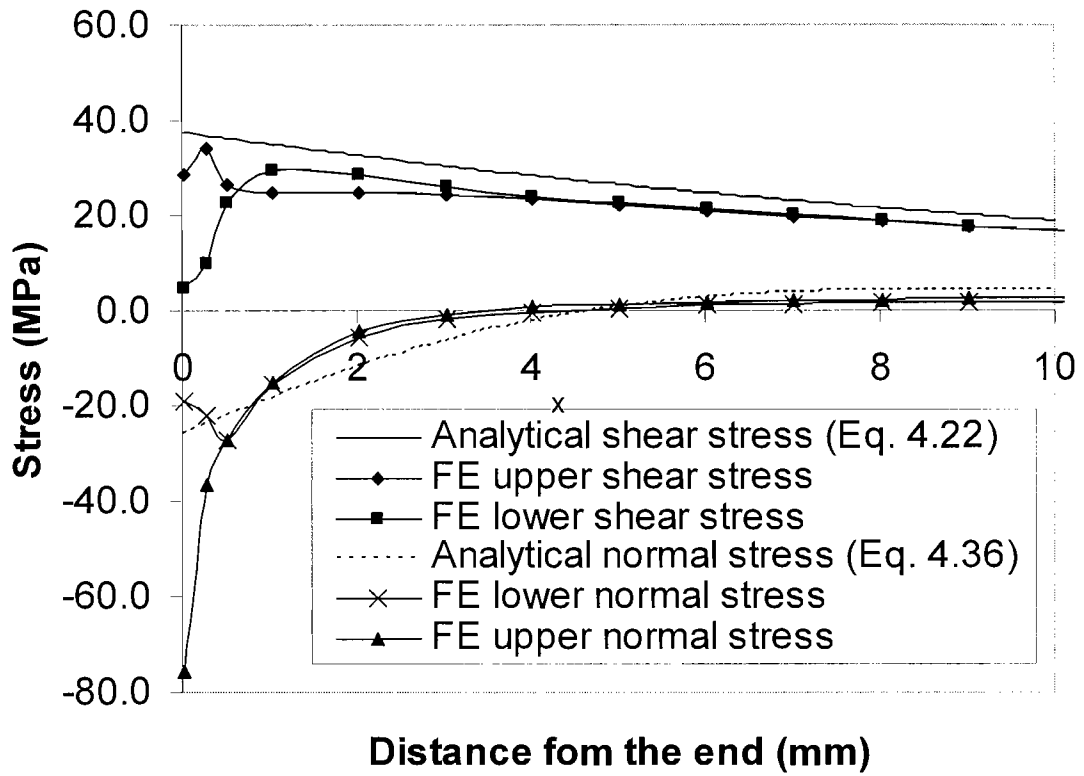
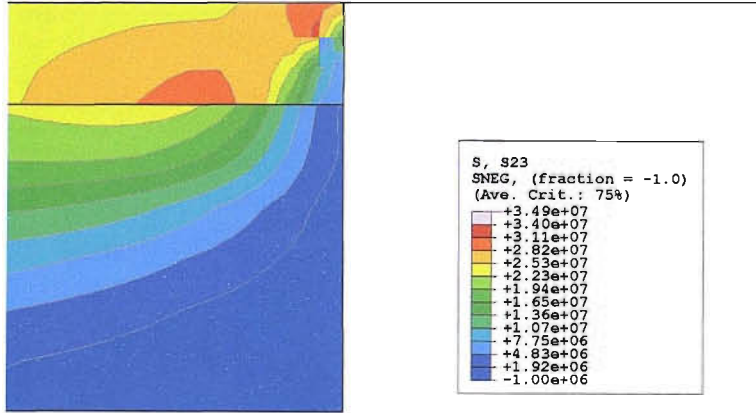
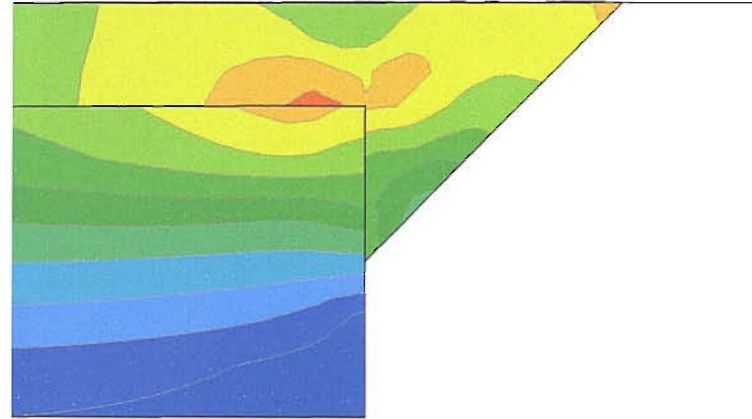


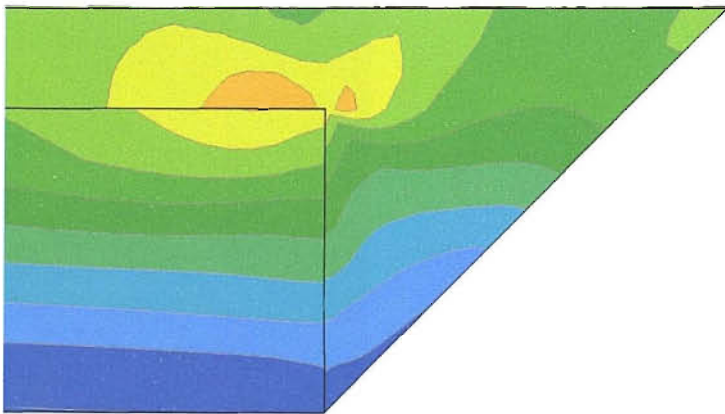
Figure 7.6 Comparisons of the shear and the normal stresses on the upper and the lower surfaces in case (a)



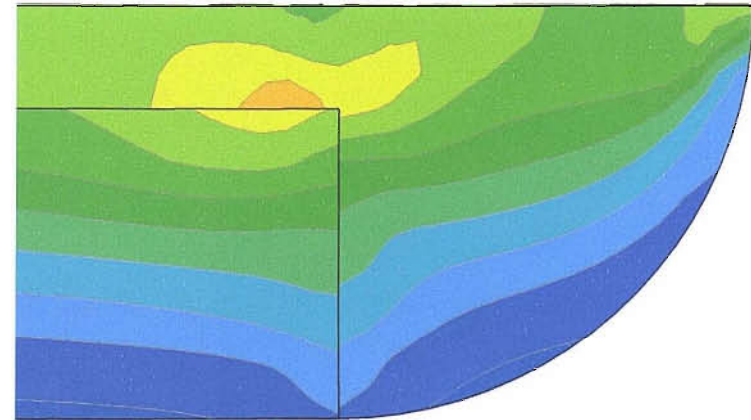
(a) Without fillet



(b) Half triangular fillet

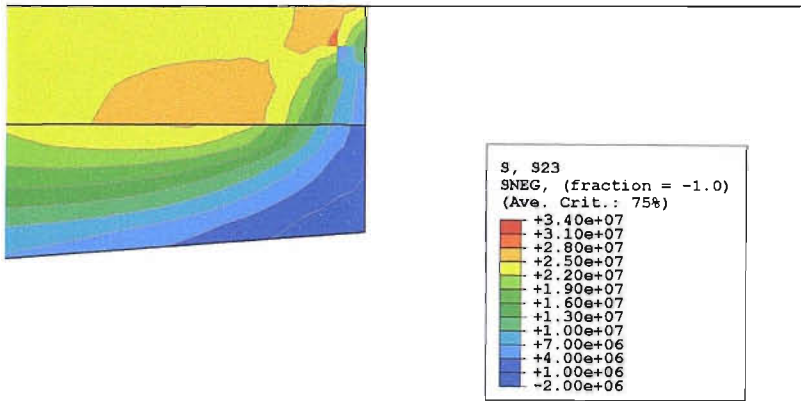


(c) Full triangular fillet

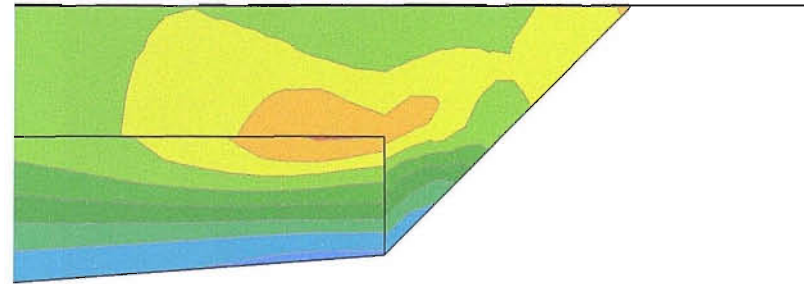


(d) Full rounded fillet

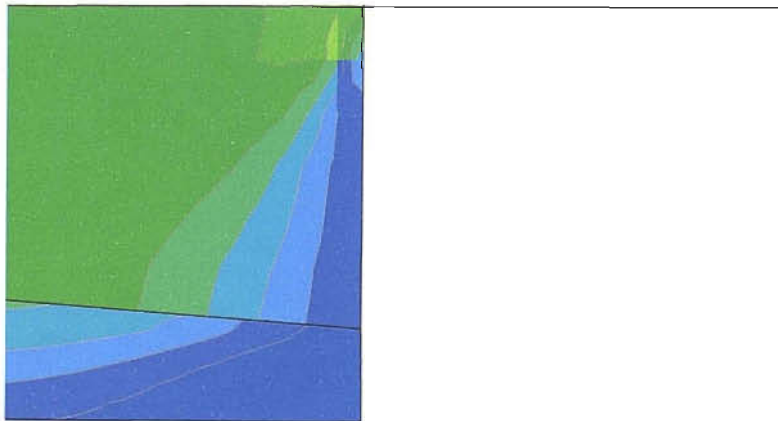
Figure 7.7 Contour plots of the shear stress for the without taper cases



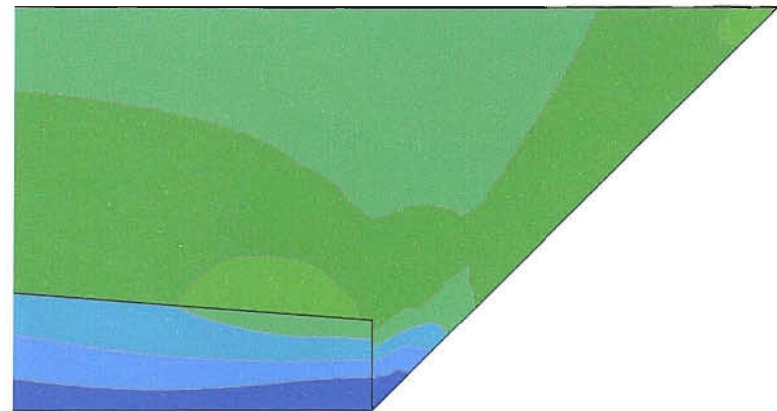
(e) Outside taper



(f) Outside taper with fillet

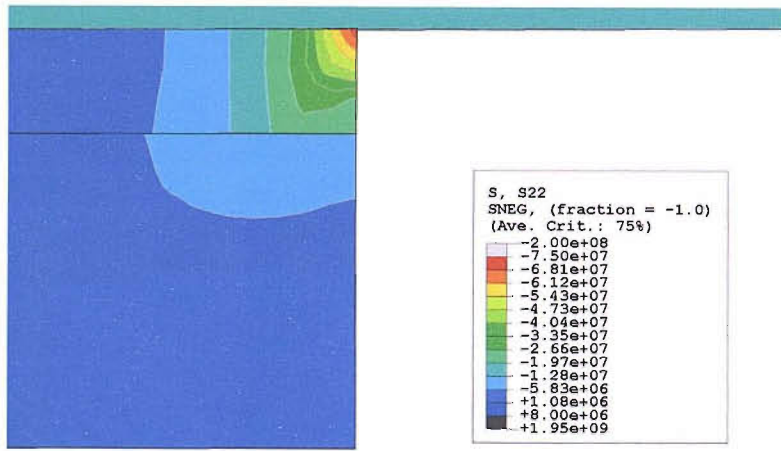


(g) Inside taper

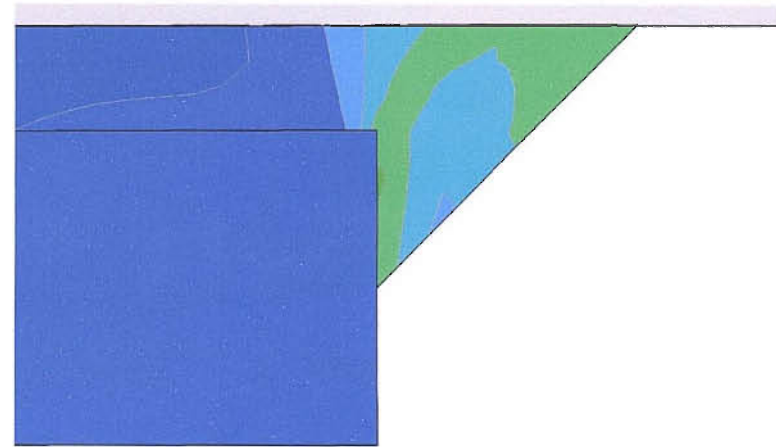


(h) Inside taper with fillet

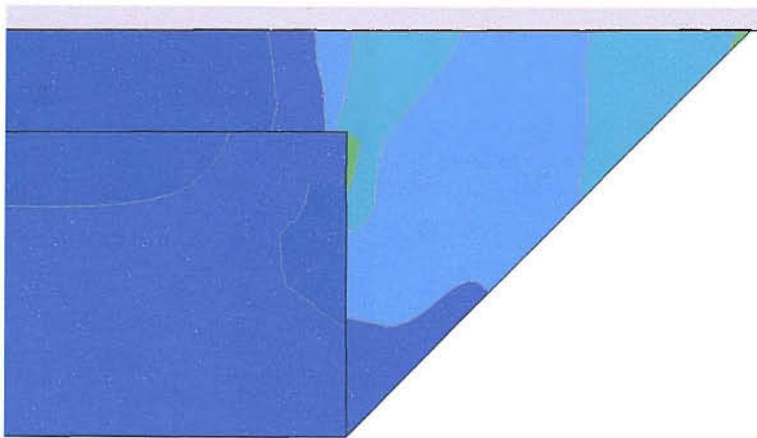
Figure 7.8 Contour plots of the shear stress for the with taper cases



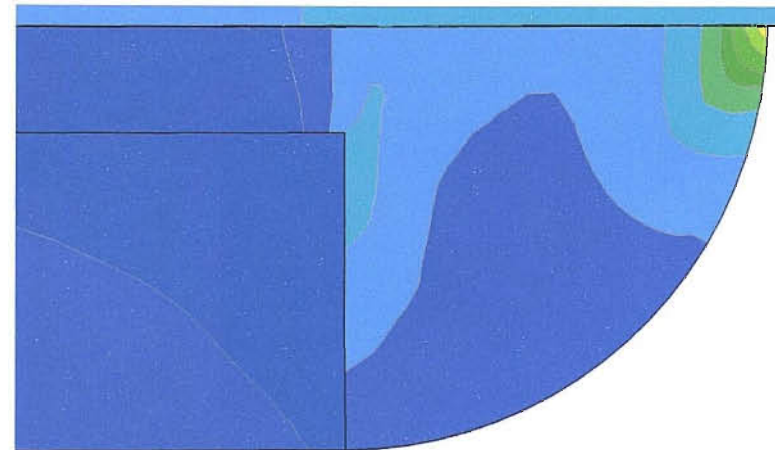
(a) Without fillet



(b) Half triangular fillet

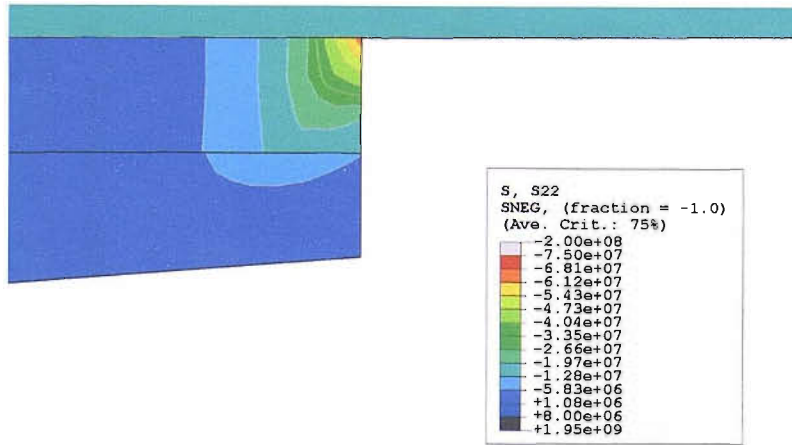


(c) Full triangular fillet

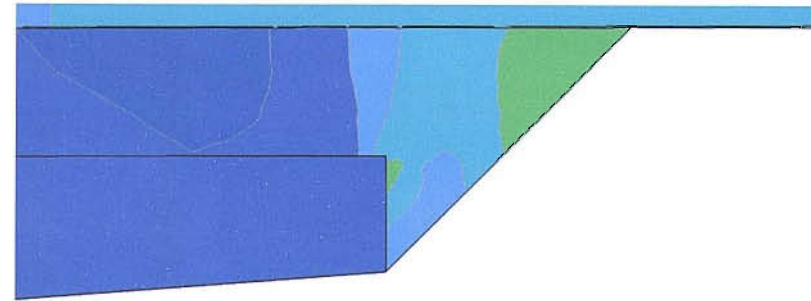


(d) Full rounded fillet

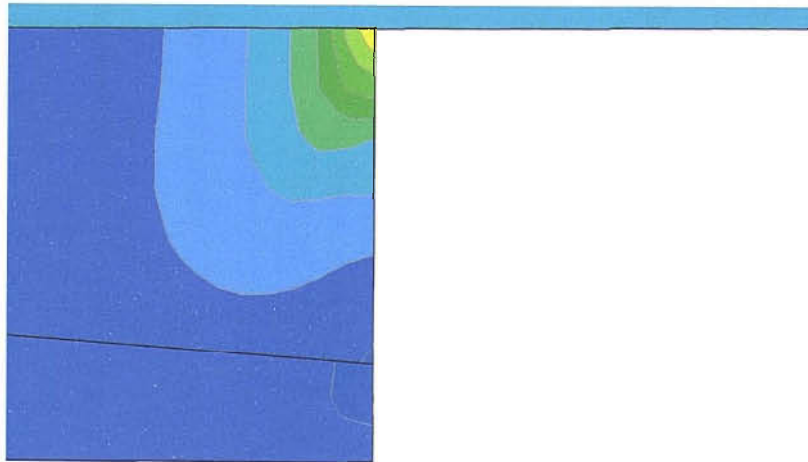
Figure 7.9 Contour plots of the normal stress for the without taper cases



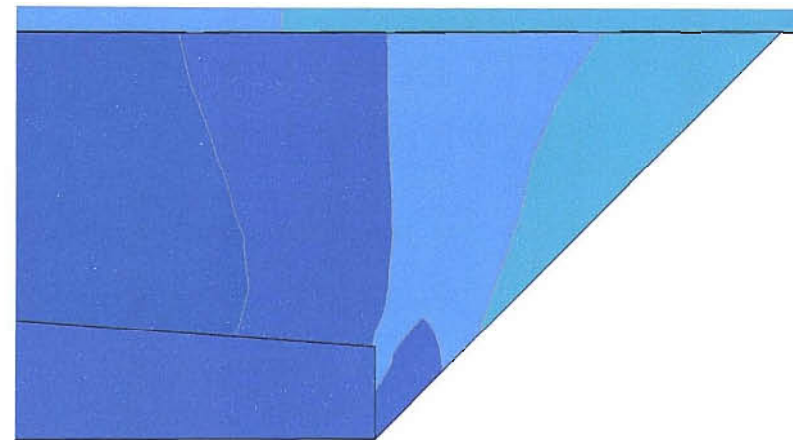
(e) Outside tapert



(f) Outside taper with fillet



(g) Inside taper



(h) Inside taper with fillet

Figure 7.10 Contour plots of the normal stress for the with taper cases

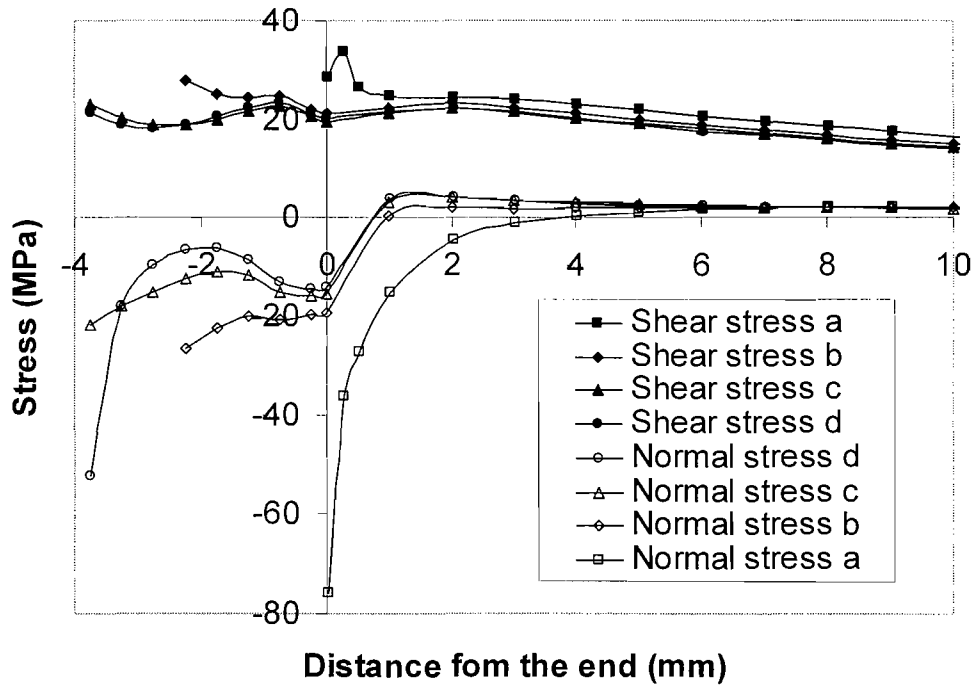


Figure 7.11 Comparisons of the upper interfacial stresses for the without taper cases (a)-(d)

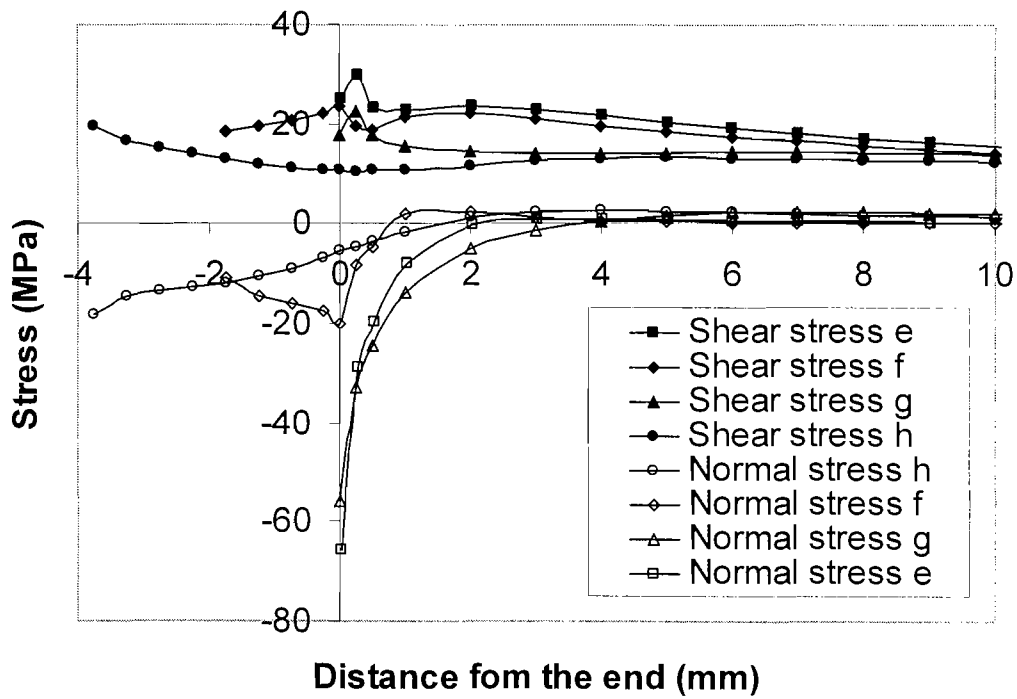


Figure 7.12 Comparisons of the upper interfacial stresses for the with taper cases (e)-(h)

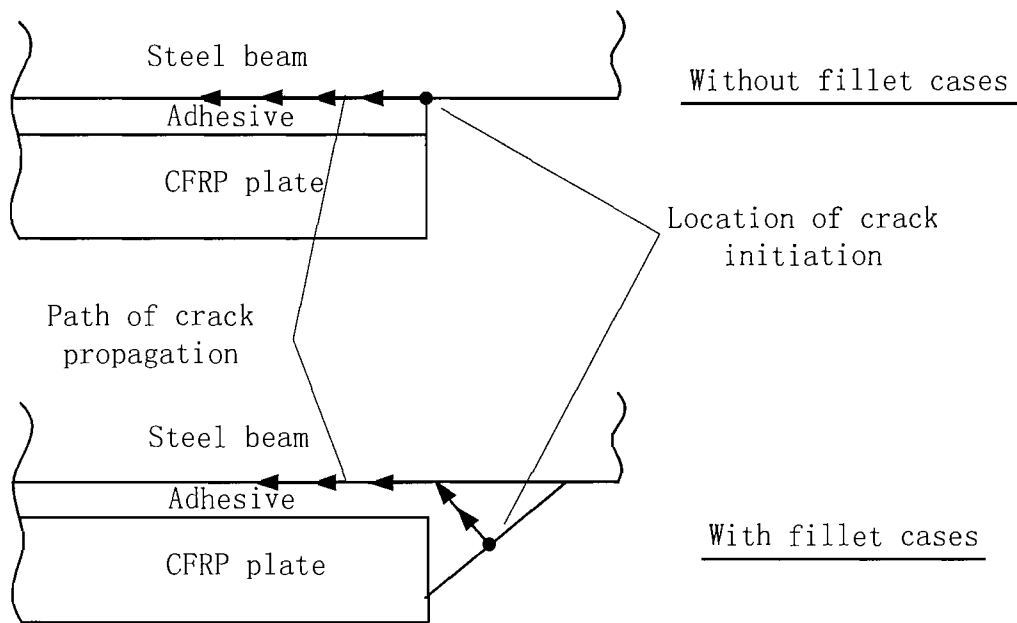


Figure 7.13 Schematic locations of crack initiation and paths of crack propagation

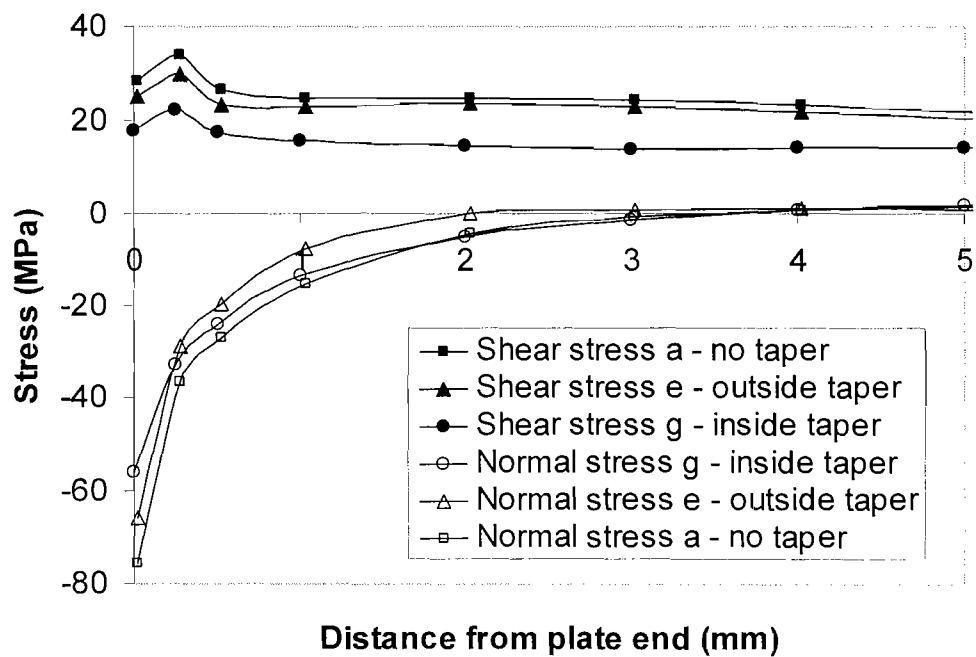


Figure 7.14 Comparisons of the upper interfacial stresses for the without taper case (a), the outside taper case (e) and the inside taper case (g)

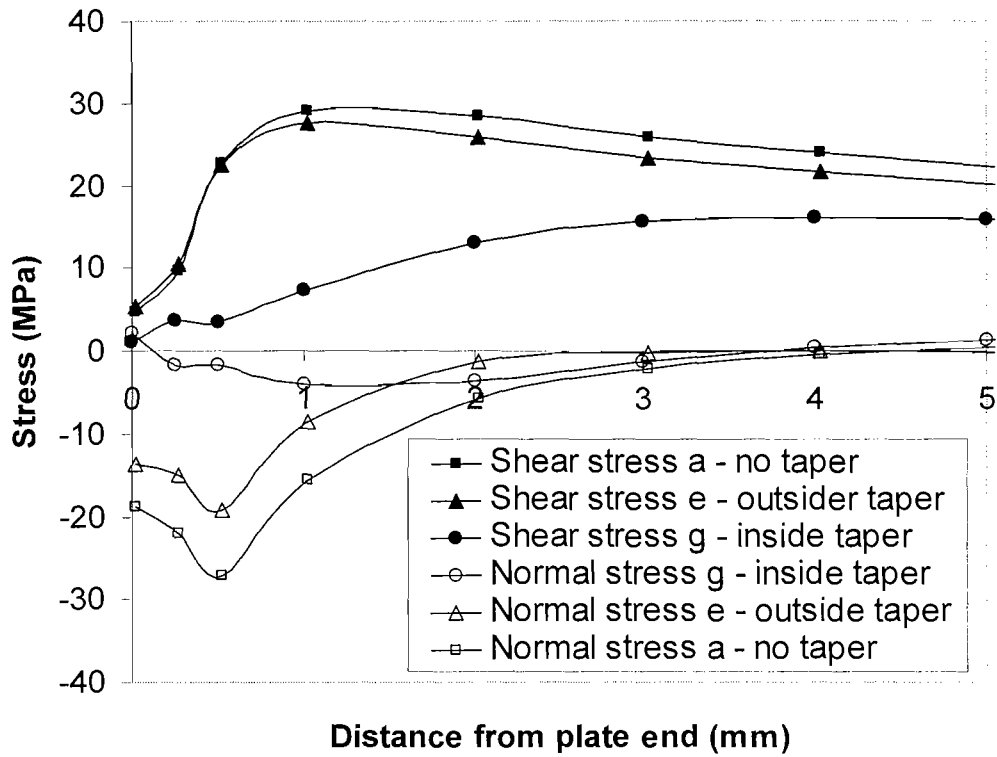


Figure 7.15 Comparisons of the lower interfacial stresses for without taper case (a), outside taper case (e) and inside taper case (g)

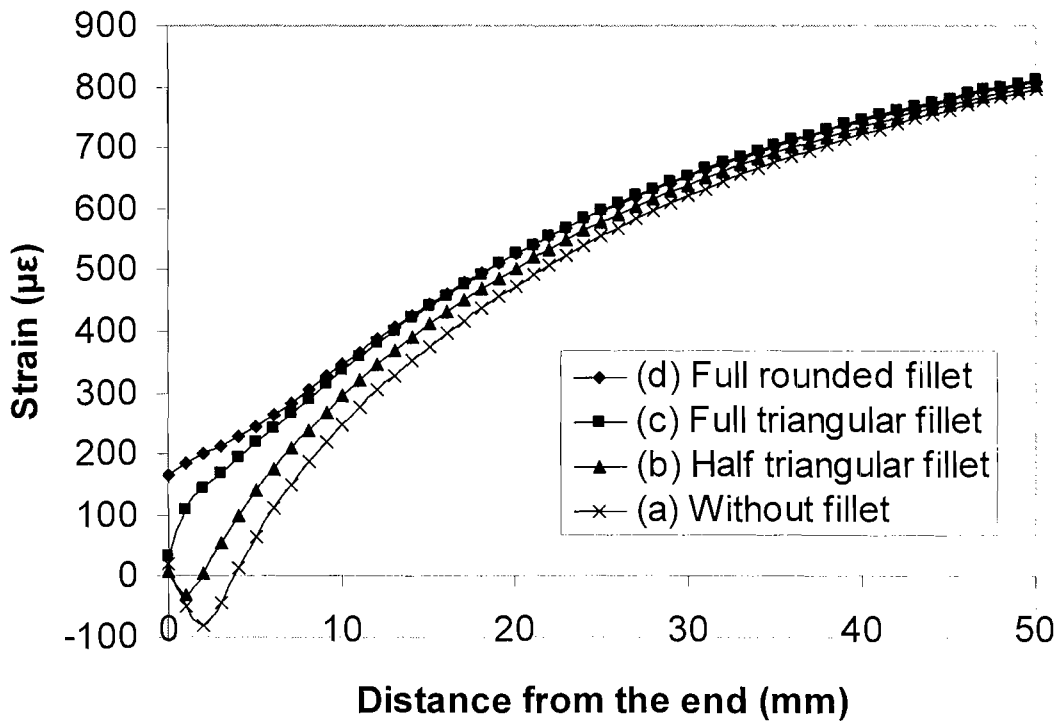


Figure 7.16 Comparisons of the effect of fillet size for the strain on the CFRP plate bottom surface

Chapter 8

Conclusions, design suggestions and future works

8.1 Conclusions

In this thesis, four main aspects have been investigated for reinforced steel beams using CFRP plates. Firstly, a simple closed-form solution to calculate the interfacial stresses of retrofitted metallic beams strengthened with CFRP plates under thermal and mechanical loads was presented, and a simple numerical solution was given for the case when the CFRP plates have tapered ends. FE analysis has been employed to validate the results from the analytical and the numerical solutions, and the agreement between the results obtained from the different solutions is good, which demonstrates that present procedure is simple yet accurate. A parametric study conduct using the methodology developed showed how the maximum stresses have been influenced by the dimensions and the material properties of the adhesive and the adherends. It has been shown that the thickness of the adhesive layer and the geometry of the taper have a significant effect on the magnitude of the stresses in the adhesive.

Secondly, a study on the static behaviour of steel beams bonded with CFRP plates was conducted. A total of 10 specimens were tested for different cases, which include different lengths and thicknesses of CFRP plates, different load cases (3- or 4-point bending), with or without tapers and adhesive spew fillets at the end of plate. The influencing factors on the strength of the steel beams reinforced by different types of CFRP plates, the effects of tapers at the plate ends and of the spew fillets beyond the plate ends, and the validation of the theoretical results of stress analysis were discussed. The study shows that the strength of the retrofitted beams increases with the length of plate but reduces with the thickness of plate. The spew fillets can increase the strength of the retrofitted beams, but the effect of the spew fillet is not as significant as that of the taper, and the test results agree well with the results from the theoretical analysis.

Thirdly, a total of seven 1.2 m length universal beams 127x76UB13 bonded with 400 mm length CFRP plates were tested under cyclic load to examine the fatigue performance. In addition to the fatigue loads and fatigue cycles, the crack initiation and development, and the change of stiffness of the retrofitted beams with the crack development were also recorded. The test results showed that the fatigue performance of the retrofitted beam was significantly weakened by the crack initiated in the adhesive layer at the end of the CFRP plate. Furthermore, the effects of the spew fillets beyond the plate ends on the fatigue behaviour are discussed. In accordance with the test results, design guidance in the form of S-N curves was provided to estimate the fatigue behaviour of adhesive joints in steel beams reinforced with CFRP plates, of which the fatigue limit was about 30% of the ultimate stress in static test.

Finally, the effects of spew fillets and tapers at the plate ends were investigated. A total of eight cases were studied. FE analysis was employed to obtain the stresses in the adhesive layer and the strain in the bottom of the CFRP plate. The results show that the retrofitted beams have similar end effect from tapers and spew fillets as lap joints. But the magnitude of reduction of the maximum shear stress by spew fillets is far less than that for lap joints. Furthermore, the effect of real spew fillet is limited, which confirmed the results obtained from static test. The results also show that the spew fillet size has a large effect on the strain close to the plate end, which confirms the analytical results in this study.

In summary, stress analysis, static behaviour and fatigue behaviour of the bonded joints in steel beams bonded with CFRP plate were studied in this thesis. The design method for the technique of steel beams reinforced with bonded CFRP plates, especially for adhesive bonding, is further developed.

8.2 Design suggestions

The following design suggestions are given in accordance with the findings obtained from this study.

- (1) Calculate the maximum adhesive stresses

- The maximum shear and normal stresses calculated by eqs. (4.79) and (4.80) are the same as those by the equations given in the guidance CIRIA C595 [8], but eqs. (4.79) and (4.80) are more convenient to use.
- Significant stresses are caused by temperature changes, since the difference in the thermal expansion coefficients of the adherends is 10.6×10^{-6} . The thermal effect on the maximum stresses is also included in eqs. (4.79) and (4.80).
- The numerical procedures introduced in Chapter 4 are suggested to solve the maximum stresses in beams bonded with an outside tapered plate, which usually is calculated by finite element analysis.

(2) Use details to reduce the maximum adhesive stresses

- Adhesives with low elastic modulus are suggested to reduce the maximum adhesive stresses. It does not weaken the section strength of the reinforced beams and does not increase the quantity of the adhesive used.
- Taper is suggested to reduce the maximum adhesive stresses as well. Inside taper is more beneficial for the magnitude of the stress reductions than outside taper. However, outside taper is more practical. This is because that the installation of outside tapered plate is easier than insider tapered plate due to bondline thickness and the outside taper case can avoid using finite element analysis.
- The natural spew fillet at the end of plate is suggested to be retained in fabrication, but its effect on the reduction on stress concentration should not be considered in design. It is because both the theoretical and the experimental analyses in this study show that the reduction in the stress concentration caused by the natural spew fillet is limited.

(3) Fatigue limit of the bonded joint in reinforced beams

- To avoid fatigue crack initiation in the adhesive at the end of the plate, the maximum adhesive stresses must be limited. The S-N curve investigated in this study shows the fatigue limit is 30% of the ultimate static failure stress.

- Since only one structural adhesive – Sikadur 31 Normal– was used in this study, similar fatigue tests are suggested to validate this fatigue limit for reinforced beams bonded with other adhesives.

(4) Strength of adhesive

Small scale reinforced beams, like the specimens used in this study, are suggested to estimate the strength of adhesive as an alternative of lap joints. This is because:

- The structural geometries are more similar between reinforced beams than between reinforced beams and lap joints.
- The quality of lap joints is more difficult to control than that of reinforced beams due to the scale. Moreover, the tensile test for lap joints required more precise laboratorial facilities than the bending test for reinforced beams. Ikegami et al. [186] indicate that a large data scatter (up to 40%) in strength of adhesive bonded joints, including butt, single and double lap joints, exists among different testing sites. Contrarily, this study show the fluctuation of adhesive strength obtained from different reinforced beam specimens is very small.

(5) Curtailment of plate length

- The strength and the stiffness of reinforced beams are not influenced by the plate length. Therefore, the plate length is determined by the maximum allowable adhesive stresses.
- Except for the thermal effect, the maximum adhesive stresses are influenced by the applied bending moment and the applied shear force, especially the former. Therefore, to curtail the plate length, the plate ends should be located in an area of low applied bending moment.
- Implementation of any details such as tapers and spew fillets to reduce the stress concentrations is suggested.

(6) Monitor reinforced beam

Backface-strain technique is suggested to be used to monitor the deterioration of the adhesive and crack initiation at the plate end, especially for beams under fatigue load.

8.3 Future works

(1) 3D FE simulation for fatigue progress.

Abdel Wahab et al. [177] develop a generalised numerical procedure using FE analysis to predict of the fatigue lifetime of adhesively bonded structures. In this method, the number of cycles to failure is calculated by integrating a fatigue crack growth law between the initial and the final crack lengths. This method could be applied for the bonded joint in the metallic beams bonded by CFRP plates.

(2) Thermal fatigue behaviour of metallic beams reinforced with CFRP plate.

The difference between the coefficients of thermal expansion of CFRP and metals means that substantial longitudinal shear stresses and normal tensile stresses can be developed in the adhesive layer near to the end of the plate, with the daily variation in temperature giving rise to thermal fatigue problems.

References

- [1] Clayman CB. The human body: an illustrated guide to its structure, function, and disorders. London: Dorling Kindersley Pub., 1995.
- [2] Wainwright SA. Mechanical design in organisms. New York: Wiley, 1976.
- [3] Hartman DK, Sapp G. Historical figures in fiction. Phoenix, Ariz, USA: Oryx Press, 1994.
- [4] Schwartz MM. Composite materials handbook. New York: McGraw-Hill, 1992.
- [5] Middleton DH. Composite materials in aircraft structures. Harlow, Essex, England: Longman Scientific & Technical, 1990.
- [6] Metcalfe G. Interfaces in metal matrix composites. New York: Academic Press, 1974.
- [7] Chawla KK. Composite materials: science and engineering. New York: Springer-Verlag, 1987.
- [8] Cadei JMC, Stratford TJ, Hollaway LC, Duckett WG. Strengthening metallic structures using externally bonded fibre-reinforced polymers - C595. London: CIRIA, 2004.
- [9] Azzi VD, Tsai SW. Anisotropic strength of composites. *Experimental Mechanics* 1965; 5(9):283-8.
- [10] Tsai SW, Wu EM. A general theory of strength for anisotropic materials. *Journal of composite materials* 1971; 5:58-80.
- [11] Jones RM. Mechanics of composite materials. 2nd edn. Philadelphia, PA: Taylor & Francis, 1999.
- [12] Daniel IM, Ishai O. Engineering mechanics of composite materials. New York: Oxford University Press, 1994.
- [13] Hull D, Clyne TW. An introduction to composite materials. Cambridge: Cambridge University Press, 1996.
- [14] Harris B. Engineering composite materials. London: IOM, 1999.
- [15] Hollaway LC. The evolution of and the way forward for advanced polymer composites in the civil infrastructure. *Construction and Building Materials* 2003; 17(6-7):365-78.

- [16] Harvey WJ. A reinforced plastic footbridge, Aberfeldy, UK. *Structural Engineering International* 1993; 3(4):229-32.
- [17] Egan J. Rethinking construction. Report of construction task force to the department of transport, environment and the regions. 1998.
- [18] Head PR. The world's first advanced composite road bridge. *Proceedings, 5th International Conference on Short and Medium Span Bridges*. Calgary: ASCE, 1994.
- [19] Luke S, Canning L, Collins S *et al.* Advanced composite bridge decking system - project ASSET. *Structural Engineering International* 2002; 12(2):76-9.
- [20] Turvey GJ. Bolted connections in PFRP structures. *Progress in Structural Engineering and Materials* 2000; 2(2):146-56.
- [21] Keller T. Recent all-composite and hybrid fibre-reinforced polymer bridges and buildings. *Progress in Structural Engineering and Materials* 2001; 3(2):132-40.
- [22] Mottram JT, Zheng Y. State-of-the-art review on the design of beam-to-column connections for pultruded frames. *Composite Structures* 1996; 35(4):387-401.
- [23] Mottram JT, Turvey GJ. Physical test data for the appraisal of design procedures for bolted joints in pultruded FRP structural shapes and systems. *Progress in Structural Engineering and Materials* 2003; 5(4):195-222.
- [24] Mottram JT. Shear modulus of standard pultruded fiber reinforced plastic material. *Journal of Composites for Construction* 2004; 8(2):141-7.
- [25] Evernden MC, Mottram JT. Structural performance of a modular box beam concept of pultruded fibre reinforced polymer shapes. In: Hamelin P, Bigaud D, Ferrier E, Jacquelin E, eds. *Proceeding of Third International Conference on Composites in Construction (CCC 2005)*. Lyon, France: 2005: 947-55.
- [26] Mottram JT, Brown ND, Anderson D. Buckling characteristics of pultruded glass fibre reinforced plastic columns under moment gradient. *Thin-Walled Structures* 2003; 41(7):619-38.
- [27] Abbaker A, Mottram JT. The influence of shear-flexibility on the elastic critical load for frames of pultruded fibre reinforced plastic section. In: Hollaway LC, Chryssanthopoulos MK, Moy SSJ, eds. *Advanced polymer composites for structural applications in construction: Proceedings of the*

- Second International Conference, held at the University of Surrey, Guildford, UK, on 20-22 April 2004.* Cambridge, England: Woodhead Publishing Ltd., 2004: 437-44.
- [28] Carolin A. Doctoral thesis: carbon fibre reinforced polymers for strengthening of structural elements. 2003. Lulea University of Technology.
- [29] Saadatmanesh H, Ehsani MR. RC beams strengthened with GFRP plates .1. experimental-study. *Journal of Structural Engineering-Asce* 1991; 117(11):3417-33.
- [30] An W, Saadatmanesh H, Ehsani MR. RC beams strengthened with FRP plates .2. analysis and parametric study. *Journal of Structural Engineering-Asce* 1991; 117(11):3434-55.
- [31] Quantrill RJ, Hollaway LC. The flexural rehabilitation of reinforced concrete beams by the use of prestressed advanced composite plates. *Composites Science and Technology* 1998; 58(8):1259-75.
- [32] Hollaway LC, Leeming M. Strengthening of reinforced concrete structures using externally-bonding FRP composites in structural and civil engineering. Cambridge: Woodhead Publishing Ltd., 1999.
- [33] Meier U. Strengthening of structures using carbon fibre epoxy composites. *Construction and Building Materials* 1995; 9(6):341-51.
- [34] Dortzbach J. Carbon fibre reinforcing polymers as negative moment reinforcing in repair of composite steel parking deck. In: Dolan CW, Rizkalla SH, Nanni A, eds. *Fourth International Symposium - Fibre Reinforced Polymer Reinforcement for Reinforced Concrete Structures, SP-188R*. Farmington Hills, Michigan, USA: American Concrete Institute, 1999: 417-28.
- [35] Luke S, Canning L. Strengthening highways and railway bridge structures with FRP composites - case studies. In: Hollaway LC, Chryssanthopoulos MK, Moy SSJ, eds. *Advanced polymer composites for structural applications in construction: Proceedings of the Second International Conference, held at the University of Surrey, Guildford, UK, on 20-22 April 2004.* Cambridge, England: Woodhead Publishing Ltd., 2004: 745-55.
- [36] Meier U. Composite materials in bridge repair. *Applied Composite Materials* 2000; 7(2-3):75-94.

- [37] Kachlakev D, McCurry DD. Behavior of full-scale reinforced concrete beams retrofitted for shear and flexural with FRP laminates. *Composites Part B-Engineering* 2000; 31(6-7):445-52.
- [38] Seible F, Priestley MJN, Hegemier GA, Innamorato D. Seismic retrofit of RC columns with continuous fiber jackets. *Journal of Composites for Construction* 1997; 1:52-62.
- [39] Saadatmanesh H. Extending service life of concrete and masonry structures with fiber composites. *Construction and Building Materials* 1997; 11(5-6):327-35.
- [40] Fukuyama H. Fibre-reinforced polymers in Japan. *Structural Engineering International* 1999; 9(4):263-6.
- [41] Teng JG, Lam L. Understanding and modelling the compressive behaviour of FRP-confined concrete. In: Hollaway LC, Chryssanthopoulos MK, Moy SSJ, eds. *Advanced polymer composites for structural applications in construction: Proceedings of the Second International Conference, held at the University of Surrey, Guildford, UK, on 20-22 April 2004*. Cambridge, England: Woodhead Publishing Ltd., 2004: 73-88.
- [42] Nanni A. Carbon FRP strengthening: new technology becomes mainstream. *Concrete International* 1997; 19(6):19-23.
- [43] Hollaway LC, Head PR. *Advanced polymer composites and polymers in the civil infrastructure*. 1st edn. New York: Elsevier, 2001.
- [44] Jolly CK, Lillistone D. Concrete filled FRP circular columns. *International IABSE Conference Report*. Innsbruck: IABSE, 1997: 1-6.
- [45] De Lorenzis L, Rizzo A, La Tegola A. A modified pull-out test for bond of near-surface mounted FRP rods in concrete. *Composites Part B-Engineering* 2002; 33(8):589-603.
- [46] Triantafillou TC. Composites: A new possibility for the shear strengthening of concrete, masonry and wood. *Composites Science and Technology* 1998; 58(8):1285-95.
- [47] Ojha A. Master thesis: The execution of carbon fibre reinforced polymer strengthening work. 2001. Lulea University of Technology.
- [48] Hollaway LC, Cadei J. Progress in the technique of upgrading metallic structures with advanced polymer composites. *Progress in Structural Engineering and Materials* 2002; 4(2):131-48.

- [49] Mertz D, Gillespie J. Rehabilitation of steel bridge girders through the application of advanced composite material. *NCHRP 93-ID11*. Washington, D.C.: Transportation Research Board, 1996: 1-20.
- [50] Sen R, Liby L, Mullins G. Strengthening steel bridge sections using CFRP laminates. *Composites Part B-Engineering* 2001; 32(4):309-22.
- [51] Moy SSJ, Nikoukar F. Flexural behaviour of steel beams reinforced with carbon fibre reinforced polymer composite. In: Sheno RA, Moy SSJ, Hollaway LC, eds. *Advanced polymer composites for structural applications in construction: Proceedings of the First International Conference on the use of Advanced Composites in Construction, held at Southampton University, UK, on 15-17 April 2002*. London: Thomas Telford, 2002: 195-202.
- [52] Tavakkolizadeh M, Saadatmanesh H. Strengthening of Steel-Concrete Composite Girders Using Carbon Fiber Reinforced Polymers Sheets. *Journal of Structural Engineering* 2003; 129(1):30-40.
- [53] Nikoukar F. Strengthening of metallic structures using carbon fibre composite plates. 2004. University of Southampton.
- [54] Luke S. The use of carbon fibre plates for the strengthening of two metallic bridges of an historic nature in the UK. *Proceedings of the CICE 2001, FRP Composites in Civil Engineering*. Hong Kong: 2001: 975-83.
- [55] Smith I. Maunders road overbridge the behaviour and in-service performance of cast iron bridge girders strengthened with CFRP reinforcement. In: Hollaway LC, Chryssanthopoulos MK, Moy SSJ, eds. *Advanced polymer composites for structural applications in construction: Proceedings of the Second International Conference, held at the University of Surrey, Guildford, UK, on 20-22 April 2004*. Cambridge, England: Woodhead Publishing Ltd., 2004: 711-8.
- [56] Smith ST, Teng JG. Interfacial stresses in plated beams. *Engineering Structures* 2001; 23(7):857-71.
- [57] Denton SN. Analysis of stresses developed in FRP plates beams due to thermal effects. *Proceeding of the Conference on Composites in Civil Engineering*. Hong Kong: 2001: 527-36.
- [58] Mukhopadhyaya P, Swamy N. Interface shear stress: A new design criterion for plate debonding. *Journal of Composites for Construction* 2001; 5(1):35-43.

- [59] Miller TC, Chajes MJ, Mertz DR, Hastings JN. Strengthening of steel bridge girder using CFRP plates. *Journal of Bridge Engineering* 2001; 6(6):514-22.
- [60] El Tawil S, Ogunc C, Okeil A, Shahawy M. Static and fatigue analyses of RC beams strengthened with CFRP laminates. *Journal of Composites for Construction* 2001; 5(4):258-67.
- [61] Garden HN. Use of composites in civil engineering infrastructure. *Reinforced Plastics* 2001; 45(7-8):44-8.
- [62] Moy SSJ, Barnes F, Moriarty J *et al.* Structural upgrading and life extension of struts and beams using carbon fibre reinforced composite. *Proceedings of the Conference on Composites and Plastics in Construction*. Watford, UK: Building Research Establishment, 1999: Paper 15: 1-Paper 15: 9.
- [63] Dodds N. Strengthening a bridge using carbon fibre reinforced plates. *The Structural Engineer* 2003; 81(5):117-9.
- [64] Moy SSJ, Barnes F, Moriarty J *et al.* Structural upgrading and life extension of cast iron struts using carbon fibre reinforced composite. *Proceedings of 8th International Conference on Fibre Reinforced composites*. Newcastle, UK: 2000: 3-10.
- [65] Leonard AR. The design of carbon fibre composite (CFC) strengthening for cast iron struts at Shadwell Station vent shaft. In: Sheno RA, Moy SSJ, Hollaway LC, eds. *Advanced polymer composites for structural applications in construction: Proceedings of the First International Conference on the use of Advanced Composites in Construction, held at Southampton University, UK, on 15-17 April 2002*. London: Thomas Telford, 2002: 219-27.
- [66] Mosallam AS, Chakrabarti PR, Arnold M. Making the connection. *Civil Engineering* 1999; 69(4):56-9.
- [67] Burgoyne CJ. Advanced composites in Civil Engineering in Europe. *Structural Engineering International* 1999; 9(4):267-73.
- [68] Karbhari VM, Zhao L. Use of composites for 21st century civil infrastructure. *Computer Methods in Applied Mechanics and Engineering* 2000; 185(2-4):433-54.
- [69] Bakis CE, Bank LC, Brown VL *et al.* Fiber-reinforced polymer composites for construction-state-of-the-art review. *Journal of Composites for Construction* 2002; 6(2):73-87.

- [70] Van Den Einde L, Zhao L, Seible F. Use of FRP composites in civil structural applications. *Construction and Building Materials* 2003; 17(6-7):389-403.
- [71] Mottram JT. Fibre reinforced polymer composites in structural engineering. *The Structural Engineer* 2005; 82(14):13-4.
- [72] Federal Highway Administration (FHWA). Table of frequently asked NBI information. washington, D.C. www.fhwa.dot.gov/bridge/britab.htm, 2001.
- [73] Buyukozturk O, Gunes O, Karaca E. Progress on understanding debonding problems in reinforced concrete and steel members strengthened using FRP composites. *Construction and Building Materials* 2004; 18(1):9-19.
- [74] Dussek IJ. Strengthening of bridge beams and similar structures by means of epoxy-resin-bonded external reinforcement. *Transport research record* 785. Washington, USA: 1974: 21-4.
- [75] Lerchenthal H. Bonded sheet metal reinforcement for concrete slabs. *Bulletin in RILEM* 1967; 37:263-9.
- [76] Fleming CJ, King GEM. The development of structural adhesives for three original uses in South Africa. *Proceeding of RILEM symposium: synthetic resins in building constructions*. Paris: 1967: 75-92.
- [77] Hugenschmidt F. Epoxy adhesives for concrete and steel. *Proceeding of 1st international congress: polymer concretes, May 1975*. London: The Construction Press, 1975: 195-209.
- [78] Swamy RN, Jones R. Technical notes - behaviour of plated reinforced concrete beams subjected to cyclic loading during glue hardening. *the International Journal of Cement Composites* 1980; 2(4):741-8.
- [79] Raithby KD. External strengthening of bridges with bonded steel plates. Report 612. 1980. Crowthorne, Berkshire, Transport and road research laboratory.
- [80] Klaiber FW, Dunker KF, Wipf TJ, Sanders JR WW. Methods of strengthening existing highway bridges. Washington D.C.: Transportation Research Board, 1987.
- [81] Hutchinson AR. Strengthening of the Quinton bridges with externally bonded steel plate reinforcement. In: Harding JE, Parke GAR, Ryall MJ, eds. *Bridge Management 3*. London: E&FN Spon, 1996: 743-50.
- [82] Xanthakos PP. Bridge strengthening and rehabilitation. Upper Saddle River, N.J.: Prentice Hall PTR, 1996.

- [83] Alexander JGS, Cheng JJR. Field application and studies of using CFRP sheets to strengthen concrete bridge girders. In: El-Badry MM, ed. *Advanced composite materials in bridges and structures : 2nd international conference, Montreal, Quebec, Canada, August 11-14, 1996*. Montreal: Canadian Society for Civil Engineering, 1996: 465-72.
- [84] Rostasy FS, Hankers C, Ranish EH. Strengthening of R/C and P/C structures with bonded FRP plates. *Proceeding of the conference on advanced composite materials in civil engineering structures*. New York, N.Y.: ASCE, 1991: 253-63.
- [85] Shahawy MA, Arockiasamy M, Beitelman T, Sowrirajan R. Reinforced concrete rectangular beams strengthened with CFRP laminates. *Composites Part B-Engineering* 1996; 27(3-4):225-33.
- [86] Smith ST, Teng JG. FRP-strengthened RC beams. I: review of debonding strength models. *Engineering Structures* 2002; 24(4):385-95.
- [87] Saadatmanesh H, Albrecht P, Ayyub BM. Guidelines for Flexural Design of Prestressed Composite Beams - Closure. *Journal of Structural Engineering-Asce* 1991; 117(11):3549.
- [88] Bakht B, Al Bazi G, Banthia N *et al*. Canadian bridge design code provisions for fiber-reinforced structures. *Journal of Composites for Construction* 2000; 4(1):3-15.
- [89] Design guidance for strengthening concrete structures using fibre composite materials: report of a Concrete Society Committee Crowthorne, UK: Concrete Society, 2000.
- [90] Guide for the design and construction of externally bonded FRP systems for strengthening concrete structures Detroit: American Concrete Institute, 2002.
- [91] Goland M, Reissner E. The stresses in cemented joints. *Journal of applied mechanics* 1944; 11:A11-A27.
- [92] Hart-Smith LJ. Adhesive-bonded single-lap joints. NASA Langley Contract Report CR-112236. 1973. Douglas Aircraft Co.
- [93] Hart-Smith LJ. Adhesive-bonded double-lap joints. NASA Langley Contract Report CR-112235. 1973. Douglas Aircraft Co.
- [94] Volkersen O. Nietkraftverteilung in Zugbeanspruchten Nietverbindungen mit konstanten Laschenquerschnitten. *Luftfahrtforschung* 1938; 15:41-7.

- [95] Wu ZJ, Romeijn A, Wardenier J. Stress expressions of single-lap adhesive joints of dissimilar adherends. *Composite Structures* 1997; 38(1-4):273-80.
- [96] Tsai MY, Oplinger DW, Morton J. Improved theoretical solutions for adhesive lap joints. *International Journal of Solids and Structures* 1998; 35(12):1163-85.
- [97] Her SC. Stress analysis of adhesively-bonded lap joints. *Composite Structures* 1999; 47(1-4):673-8.
- [98] Hart-Smith LJ. Advances in the analysis and design of adhesive bonded joints in composite aerospace structures. *SAMPE Process Engineering Series, Vol. 19*. Azusa: SAMPE, 1974: 722-37.
- [99] Vinson JR, Sierakowski RL. The behaviour of structures composed of composite materials. Dordrecht, The Netherlands: Kluwer, 1987.
- [100] Adams RD, Comyn J, Wake WC. Structural adhesive joints in engineering. London: Chapman & Hall, 1997.
- [101] Sancaktar E, Nirantar P. Increasing strength of single lap joints of metal adherends by taper minimization. *Journal of Adhesion Science and Technology* 2003; 17(5):655-75.
- [102] Amijima S, Fujii T. A simple stress-analysis method for adhesive bonded tapered joints. *International Journal of Adhesion and Adhesives* 1989; 9(3):155-60.
- [103] Lee KJ. The nonlinear-analysis of tapered bonded joints. *Computers & Structures* 1995; 56(4):637-43.
- [104] Albat AM, Romilly DP. A direct linear-elastic analysis of double symmetric bonded joints and reinforcements. *Composites Science and Technology* 1999; 59(7):1127-37.
- [105] Tsai MY, Morton J. The effect of a spew fillet on adhesive stress distributions in laminated composite single-lap joints. *Composite Structures* 1995; 32(1-4):123-31.
- [106] Lang TP, Mallick PK. Effect of spew geometry on stresses in single lap adhesive joints. *International Journal of Adhesion and Adhesives* 1998; 18(3):167-77.
- [107] Lang TP, Mallick PK. The effect of recessing on the stresses in adhesively bonded single-lap joints. *International Journal of Adhesion and Adhesives* 1999; 19(4):257-71.

- [108] Belingardi G, Goglio L, Tarditi A. Investigating the effect of spew and chamfer size on the stresses in metal/plastics adhesive joints. *International Journal of Adhesion and Adhesives* 2002; 22(4):273-82.
- [109] Kadioglu F, Vaughn LF, Guild FJ, Adams RD. Use of the thick adherend shear test for shear stress-strain measurements of stiff and flexible adhesives. *Journal of Adhesion* 2002; 78(5):355-81.
- [110] Rispler AR, Tong LY, Steven GP, Wisnom MR. Shape optimisation of adhesive fillets. *International Journal of Adhesion and Adhesives* 2000; 20(3):221-31.
- [111] Roberts TM, Hajikazemi H. Theoretical-study of the behavior of reinforced-concrete beams strengthened by externally bonded steel plates. *Proceedings of the Institution of Civil Engineers Part 2-Research and Theory* 1989; 87:39-55.
- [112] Malek AM, Saadatmanesh H, Ehsani MR. Prediction of failure load of R/C beams strengthened with FRP plate due to stress concentration at the plate end. *Aci Structural Journal* 1998; 95(2):142-52.
- [113] Rabinovich O, Frostig Y. Closed-form high-order analysis of RC beams strengthened with FRP strips. *Journal of Composites for Construction* 2000; 4(2):65-74.
- [114] Yang J, Chen JF, Teng JG. Interfacial stresses in plated RC beams under arbitrary symmetric loads: a higher-order closed form solution. In: Sheno RA, Moy SSJ, Hollaway LC, eds. *Advanced polymer composites for structural applications in construction: Proceedings of the First International Conference on the use of Advanced Composites in Construction, held at Southampton University, UK, on 15-17 April 2002*. London: Thomas Telford, 2002: 153-63.
- [115] Ascione L, Feo L. Modeling of composite/concrete interface of RC beams strengthened with composite laminates. *Composites Part B-Engineering* 2000; 31(6-7):535-40.
- [116] Jones KR, Swamy RN, Charif A. Plate separation and anchorage of reinforced concrete beams strengthened by epoxy-bonded steel plates. *The Structural Engineer* 1988; 66(5/1):85-94.
- [117] Roberts KTM. Approximate analysis of shear and normal stresses concentrations in the adhesive layer of plated RC beams. *The Structural Engineer* 1989; 67(12/20):37-46.

- [118] Barnes RA, Mays GC. Fatigue performance of concrete beams strengthened with CFRP plates. *Journal of Structural Engineering* 1999; 3(2):63-72.
- [119] Mays GC, Tilly GP. Long endurance fatigue performance of bonded structural joints. *International Journal of Adhesion and Adhesives* 1982; 2(2):109-13.
- [120] Moses F, Schilling CG, Raju KS. Fatigue evaluation procedures for steel bridges. NCHRP Rep. No. 299. 1987. Washington, D.C., Transportation Research Board.
- [121] ASTM STP761. Design of fatigue and fracture resistant structures. 1982.
- [122] BS 5400-10. Steel, concrete and composite bridges - code of practice for fatigue. 1980.
- [123] Kinloch AJ. Adhesion and adhesives. London: Chapman and Hall, 1987.
- [124] Krenk S, Jonsson J, Hansen LP. Fatigue analysis and testing of adhesive joints. *Engineering Fracture Mechanics* 1996; 53(6):859-72.
- [125] Cheuk PT, Tong L, Wang CH, Baker A, Chalkley P. Fatigue crack growth in adhesively bonded composite-metal double-lap joints. *Composite Structures* 2002; 57(1-4):109-15.
- [126] Keller T, Tirelli T. Fatigue behaviour of adhesively connected pultruded GFRP profiles. *Composite Structures* 2004; 65(1):55-64.
- [127] de Goeij WC, van Tooren MJL, Beukers A. Composite adhesive joints under cyclic loading. *Materials & Design* 1999; 20(5):213-21.
- [128] Oh BH, Cho JY, Park DG. Static and fatigue behavior of reinforced concrete beams strengthened with steel plates for flexure. *Journal of Structural Engineering-Asce* 2003; 129(4):527-35.
- [129] Meier U, Deuring M, Meier H, Schwegler G. Strengthening of structures with CFRP laminates: research and applications in Switzerland. In: Neale KW, Labossiere P, eds. *Advanced composite materials in bridges and structures*. Montreal: Canadian Society for Civil Engineering, 1992.
- [130] Shahawy M, Beitelman TE. Static and fatigue performance of RC beams strengthened with CFRP laminates. *Journal of Structural Engineering* 1999; 125(6):613-21.
- [131] Heffernan PJ, Erki MA. Fatigue behavior of reinforced concrete beams strengthened with carbon fiber reinforced plastic laminates. *Journal of Composites for Construction* 2004; 8(2):132-40.

- [132] Bizindavyi L, Neale KW, Erki MA. Experimental investigation of bonded fiber reinforced polymer-concrete joints under cyclic loading. *Journal of Composites for Construction* 2003; 7(2):127-34.
- [133] Tavakkolizadeh M, Saadatmanesh H. Fatigue Strength of Steel Girders Strengthened with Carbon Fiber Reinforced Polymer Patch. *Journal of Structural Engineering* 2003; 129(2):186-96.
- [134] Moy SSJ. Early age curing under cyclic loading - an investigation into stiffness development in carbon fibre reinforced steel beams. In: Sheno RA, Moy SSJ, Hollaway LC, eds. *Advanced polymer composites for structural applications in construction: Proceedings of the First International Conference on the use of Advanced Composites in Construction, held at Southampton University, UK, on 15-17 April 2002*. London: Thomas Telford, 2002: 187-94.
- [135] Moy SSJ. FRP composites: life extension and strengthening of metallic structures. London: Thomas Telford, 2001.
- [136] Bussell MN. Appraisal of existing iron and steel structures. Berkshire, UK: Steel Construction Institute, 1997.
- [137] BS EN 10002-1. Tensile testing of metallic materials - part 1: method of test at ambient temperature. 1990.
- [138] Busel JP, Lockwood JD, Walson DK. FRP composite products for bridge application. New York: Harrison, 2000.
- [139] Purslow D, Potter RT. The Effect of Environment on the Compression Strength of Notched Cfrp - A Fractographic Investigation. *Composites* 1984; 15(2):112-20.
- [140] Sanchez-Saez S, Gomez-del Rio T, Barbero E, Zaera R, Navarro C. Static behavior of CFRPs at low temperatures. *Composites Part B-Engineering* 2002; 33(5):383-90.
- [141] Miyano Y, McMurray MK, Kitade N, Nakada M, Mohri M. Loading Rate and Temperature-Dependence of Flexural Behavior of Unidirectional Pitch-Based Cfrp Laminates. *Composites* 1995; 26(10):713-7.
- [142] Hulatt J, Hollaway L, Thorne A. Preliminary investigations on the environmental effects on new heavyweight fabrics for use in civil engineering. *Composites Part B-Engineering* 2002; 33(6):407-14.

- [143] Tavakkolizadeh M, Saadatmanesh H. Galvanic corrosion of carbon and steel in aggressive environments. *Journal of Composites for Construction* 2001; 5(3):200-10.
- [144] Talreja R. Fatigue of composite materials. Lancaster, USA: Technomic Pub. Co., 1987.
- [145] Curtis PT. The fatigue behaviour of fibrous composite materials. *Journal of Strain Analysis* 1989; 24(4):235-44.
- [146] Walton JM, Yeung YCT. Flexible tension member from composite materials. *Proceeding 6th International Arctic Engineering Symposium*. New York: American Society of Mechanical Engineerings, 1987.
- [147] Reifsnider KL. Fatigue of composite materials. Amsterdam: Elsevier, 1991.
- [148] Jones CJ, Dickson RF, Adams T, Reiter H, Harris B. The environmental fatigue behaviour of reinforced plastics. *Proceeding of Royal Society of London* 1984; A396(1811):315-38.
- [149] EN ISO 527-5. Plastics - determination of tensile properties - part 5: test conditions for unidirectional fibre-reinforced plastic composites. 1997.
- [150] Mays GC, Hutchinson AR. Adhesives in civil engineering. Cambridge: University of Cambridge, 1992.
- [151] Shields J. Adhesive bonding. London: Oxford University Press, 1974.
- [152] Anderson GP, Bennett SJ, De Vries KL. Analysis and testing of adhesive bonds. London: Academic Press Inc., 1977.
- [153] Hutchinson AR, Lees DE. A compression test for determining adhesive material properties. *Second International Conference on Structural Adhesives in Engineering, Bristol University*. Butterworth, 1989.
- [154] BS 2782-3. Method of testing plastics - part 3: mechanical properties - methods 320A to 320F: Tensile strength, elongation and elastic modulus. 1976.
- [155] Bredemo R, Gradin PA. Testing of in situ properties of adhesives. *International Journal of Adhesion and Adhesives* 1986; 6(3):153-6.
- [156] Kuenzi EW, Stevens OH. Determination of mechanical properties of adhesives for use in the design of bonded joints. US Forest Products Service Research Note FPL-011. 1963. Madison, Wisconsin, USA, US Dept. of Agriculture.

- [157] Lilleheden L. Mechanical-Properties of Adhesives In-Situ and in Bulk. *International Journal of Adhesion and Adhesives* 1994; 14(1):31-7.
- [158] Jangblad D, Gradin P, Stenstrom T. Determination and verification of elastic parameters for adhesives. In: Johnson WS, ed. *Adhesively bonded joints: testing, analysis, and design*. Philadelphia, PA: ASTM, 1988: 54-68.
- [159] ASTM E229. Standard test method for shear strength and shear modulus of structural adhesives. 1997.
- [160] Weissberg V, Arcan M. A uniform pure shear testing specimen for adhesive characterization. In: Johnson WS, ed. *Adhesively bonded joints: testing, analysis, and design*. Philadelphia, PA: ASTM, 1988: 28-38.
- [161] ASTM D3983. Standard test method for measuring strength and shear modulus of nonrigid adhesives by the thick-adherend tensile-lap specimen. 1998.
- [162] ISO 11003-2. Adhesives - determination of shear behaviour of structural adhesives - part 2: tensile test method using thick adherends. 2001.
- [163] Tsai MY, Morton J, Oplinger DW. In situ determination of adhesive shear moduli using strain gages. *Experimental Mechanics* 1996; 36(4):297-304.
- [164] Kinloch AJ. *Journal of materials science* 1980; 15:2141.
- [165] ASTM D2094. Standard practice for preparation of bar and rod specimens for adhesion tests. 2000.
- [166] ISO 6922. Adhesives - determination of tensile strength of butt joints. 1987.
- [167] ASTM D1002. Standard test method for apparent shear strength of single-lap-joint adhesively bonded metal specimens by tension loading. 2001.
- [168] BS 5350-C5. Methods of test for adhesives - determination of bond strength in longitudinal shear for rigid adherends. 2002.
- [169] Mostovoy S, Ripling EJ, Bersch CF. Fracture toughness of adhesive joints. *Journal of Adhesion* 1971; 3:125-44.
- [170] Kinloch AJ, Shaw SJ. The fracture resistance of a toughened epoxy adhesive. *Journal of Adhesion* 1981; 12:59-77.
- [171] Althof W. Effects on Low Cycle Fatigue on Shear Stressed Adhesive Bondlines. *Adhesive joints: formation, characteristics, and testing*. New York City: Plenum Press, 1984: 659-77.
- [172] Wake WC. Adhesion and the formulation of adhesives. London: Applied Science Publishers, 1982.

- [173] ISO 9664. Adhesives - test methods for fatigue properties of structural adhesives in tensile shear. 1995.
- [174] ASTM D3166. Standard test method for fatigue properties of adhesives in shear by tension loading. 1999.
- [175] Harris JA, Fay PA. Fatigue Life Evaluation of Structural Adhesives for Automotive Applications. *International Journal of Adhesion and Adhesives* 1992; 12(1):9-18.
- [176] Curley AJ, Hadavinia H, Kinloch AJ, Taylor AC. Predicting the service-life of adhesively-bonded joints. *International Journal of Fracture* 2000; 103(1):41-69.
- [177] Abdel Wahab MM, Ashcroft IA, Crocombe AD, Smith PA. Numerical prediction of fatigue crack propagation lifetime in adhesively bonded structures. *International Journal of Fatigue* 2002; 24(6):705-9.
- [178] Abdel Wahab MM, Ashcroft IA, Crocombe AD, Smith PA. Finite element prediction of fatigue crack propagation lifetime in composite bonded joints. *Composites Part A-Applied Science and Manufacturing* 2004; 35(2):213-22.
- [179] Clarke H. Transfer report: reinforcing wrought iron with carbon fibre reinforced polymers. 2005. University of Southampton.
- [180] ABAQUS User's manual, Version 6.3. Hibbit, Kalson and Sorensen, Providence, RI, 2002.
- [181] Colombi P, Panzeri N, Poggi C. Experimental characterization of steel elements reinforced by adhesively bonded CFRP plates. In: Hollaway LC, Chryssanthopoulos MK, Moy SSJ, eds. *Advanced polymer composites for structural applications in construction: Proceedings of the Second International Conference, held at the University of Surrey, Guildford, UK, on 20-22 April 2004*. Cambridge, England: Woodhead Publishing Ltd., 2004: 243-57.
- [182] Enberson NK, Mays GC. Significance of property mismatch in the patch repair of structural concrete: part 3 reinforced concrete members in flexure. *Magazine of Concrete Research* 1996; 48(174):45-57.
- [183] Pereira AB, de Morais AB. Strength of adhesively bonded stainless steel joints. *International Journal of Adhesion and Adhesives* 2003; 23(4):315-22.

- [184] Rabinovitch O, Frostig Y. Experiments and analytical comparison of RC beams strengthened with CFRP composites. *Composites Part B-Engineering* 2003; 34(8):663-77.
- [185] ABAQUS Analysis User's Manual, Version 6.4. Hibbit, Kalson and Sorensen, Providence, RI, 2003.
- [186] Ikegami K, Fujii T, Kawagoe H *et al.* Benchmark tests on adhesive strengths in butt, single and double lap joints and double-cantilever beams. *International Journal of Adhesion and Adhesives* 1996; 16(4):219-26.

Appendix A

Tensile tests on steel to obtain mechanical properties

This test was used to determine the elastic modulus, yield tensile strength, ultimate tensile strength, percentage elongation and percentage reduction of section area of steel. The specimens were cut from the web of a universal steel beam 127x76UB13, which was provided by the same stockist as those beams used in the static test and the fatigue test in this study. The test was conducted according to the recommendations in the standard BS EN 10002-1:1990 [1]. A total of 5 specimens were tested, which are given the serial numbers S1, S2, S3, S4 and S5.

1 Specimen preparation

Cut specimens from the web of the steel beam to specified dimensions. The dimensions are shown in Figure A.1.

2 Test procedures

1) **Dimension measurement:** The section dimensions in the middle were measured by a vernier caliper. The width b , the thickness h and the section area A are shown in Table A.1.

2) **Data collection:** two single element strain gauges (YFLA-10, TML) were mounted in the longitudinal directions on both sides in order to determine the elastic modulus, shown in Figure A.1. During the testing, the load and strains were monitored and recorded using a data logging system.

3) **Test setup:** The tests were done in tensile loading in the displacement control mode using an Instron 1195 universal testing machine with a capacity to 100 kN. The load rate was 2 mm per minute.

3 Results

1) **Tensile strength:** the yield tensile strength σ_y and the ultimate tensile strength σ_u was calculated by:

$$\sigma = \frac{F}{A} \quad (1)$$

where F is the yield tensile load or the ultimate tensile load. The yield tensile load F_y , the yield tensile strength σ_y , the ultimate tensile load F_u and the ultimate tensile strength σ_u are shown in Table A.2.

2) **Elastic modulus:** The elastic modulus was calculated by:

$$E = \frac{\sigma_2 - \sigma_1}{\varepsilon_2 - \varepsilon_1} \quad (2)$$

where σ_1 and σ_2 are the stresses measured at the strain value $\varepsilon_1 = 0.0005$ and $\varepsilon_2 = 0.0015$ respectively. The values are shown in Table A.3.

3) **Percentage elongation at fracture and percentage reduction of area:** The percentage elongation at fracture A_b and the percentage reduction of area Z were calculated by Equation (3) and (4), respectively.

$$A_b = \frac{L_u - L_o}{L_o} \quad (3)$$

$$Z = \frac{A - A_u}{A} \quad (4)$$

where L_u and L_o are the parallel length after fracture and original parallel length, respectively. A_u is the minimum cross-sectional area after fracture. The results are shown in Table A.4.

4) **Failure mode:** The failure mode of specimens is shown in Figure A.2.

4 Conclusion

All of the properties are summarised in the Table A.5.

Reference

- [1] BS EN 10002-1. Tensile testing of metallic materials - part 1: method of test at ambient temperature. 1990.

Table A.1 Dimensions of the specimens

	S1	S2	S3	S4	S5	Mean	CoV (%)
width b (mm)	20.0	20.1	20.1	20.0	20.1	20.1	0.27
Thickness h (mm)	4.1	4.0	4.0	4.0	4.0	4.0	0.62
Area A (mm ²)	81.40	81.00	80.60	80.80	80.60	80.88	0.41

Table A.2 Yield tensile strength and ultimate tensile strength

	S1	S2	S3	S4	S5	Mean	CoV (%)
F_y (kN)	29.3	27.9	29.0	29.3	28.8	28.9	2.00
σ_y (MPa)	360.0	343.9	359.9	362.1	356.9	356.6	2.05
F_u (kN)	38.3	36.3	37.5	37.9	37.5	37.5	2.00
σ_u (MPa)	470.9	452.2	464.9	468.8	465.0	464.4	1.56

Table A.3 Tensile elastic modulus

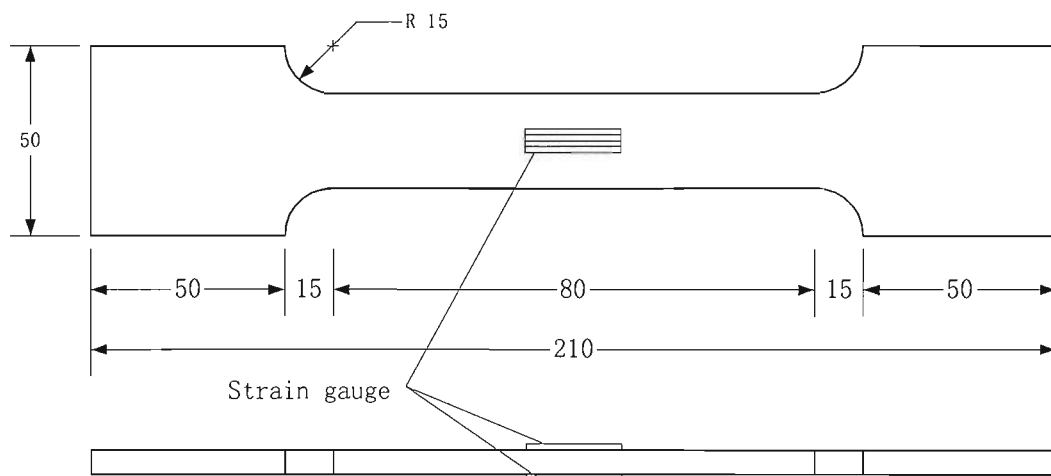
	S1	S2	S3	S4	S5	Mean	CoV (%)
F_1 (KN)	8.5	8.0	8.3	8.2	8.3	8.3	2.0
F_2 (KN)	104.3	99.2	103.0	101.9	102.4	102.1	1.8
σ_1 (MPa)	25.5	24.7	24.6	25.1	24.5	24.9	1.6
σ_2 (MPa)	313.1	305.1	305.1	310.9	304.3	307.7	1.3
E (GPa)	208.9	206.0	202.1	209.0	201.9	205.6	1.7

Table A.4 Percentage elongation and the percentage reduction of area

	S1	S2	S3	S4	S5	Mean	CoV (%)
A_b (%)	21.5	22.8	22.1	21.7	22.2	22.1	2.13
Z (%)	63.7	64.3	63.8	64.5	63.4	64.0	0.68

Table A.5 Mechanical properties reported

Property	Mean	CoV (%)
Yield tensile strength σ_y (MPa)	356.6	2.05
Ultimate tensile strength σ_u (MPa)	464.4	1.56
Elastic Modulus E (GPa)	205.6	1.68
Percentage elongation A_b (%)	22.1	2.13
Percentage reduction of area Z (%)	64.0	0.68



All dimensions in mm

Figure A.1 Specimen dimensions and gauge locations

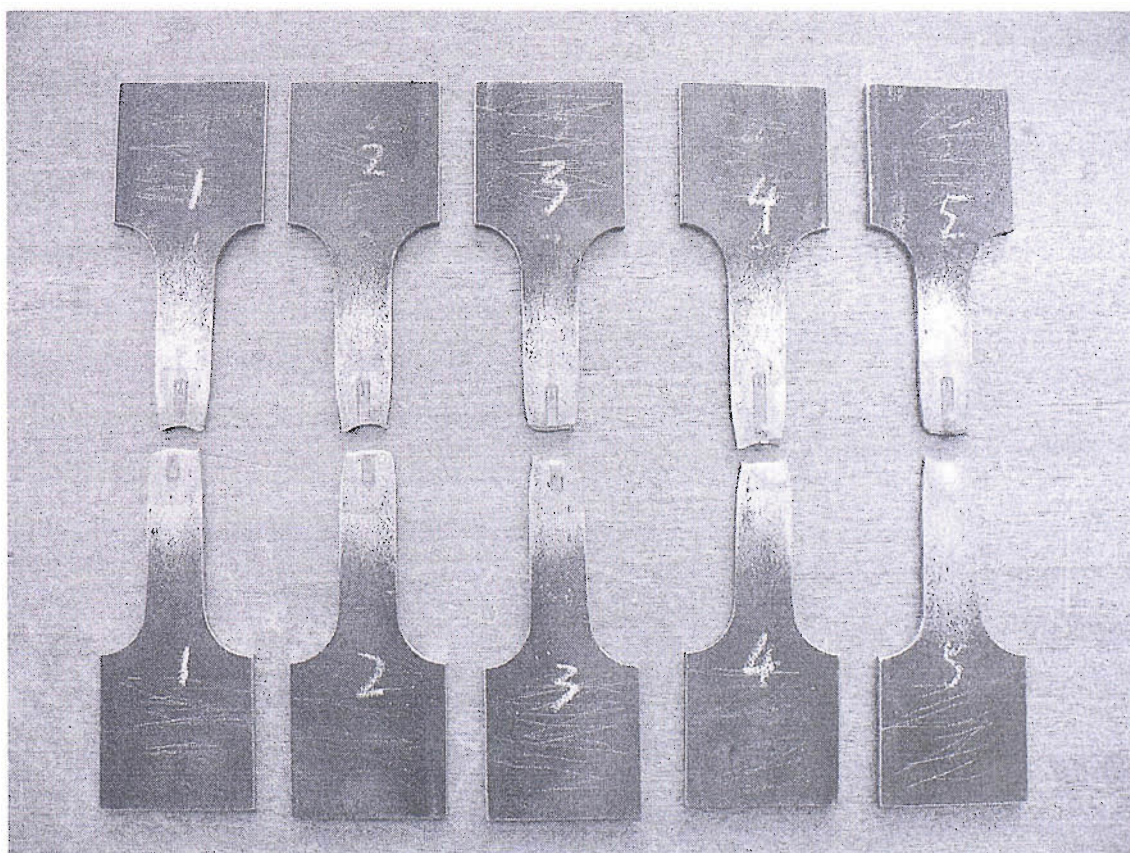


Figure A.2 Failed specimens

Appendix B

Manufacturing of CFRP plates

All CFRP plates used in this study were manufactured by epoxy prepreg SE84LV/HMC/300/400/35%/+/-3%pop, which was supplied by Structural Polymer System Ltd., using the following procedure:

Prepreg lay-up

- 1) Remove rolls of SE84 prepreg from the freezer storage in sufficient time to allow them to warm up to ambient temperature before they were used.
- 2) Cut the prepreg laminate to the required sizes.
- 3) Stack the prepreg laminate layers to the required thickness. Each prepreg laminate layer was 0.3 mm thick.

Debulking and curing

- 4) Bag laminates, as shown in Figure B.1.
- 5) Apply vacuum of no less than 80%.
- 6) Increase temperature at the rate of 1°C/minute from ambient temperature to 75°C.
- 7) Hold temperature at 75°C for 1 hour.
- 8) Increase temperature at the rate of 1°C/minute 75°C to 85°C.
- 9) Hold temperature at 85°C for 7 hour.
- 10) Cool laminate at a rate of 2°C/minute to ambient temperature.
- 11) Release vacuum and remove the vacuum bag.

This procedure is in accordance with the recommendations in the manufacture's technical services report [1].

Reference

- [1] Bannister D, Ness D. Processing notes for SE84 prepreg. Structural Polymer System Ltd. Technical Services Report 0356 Rev:4, 2000.

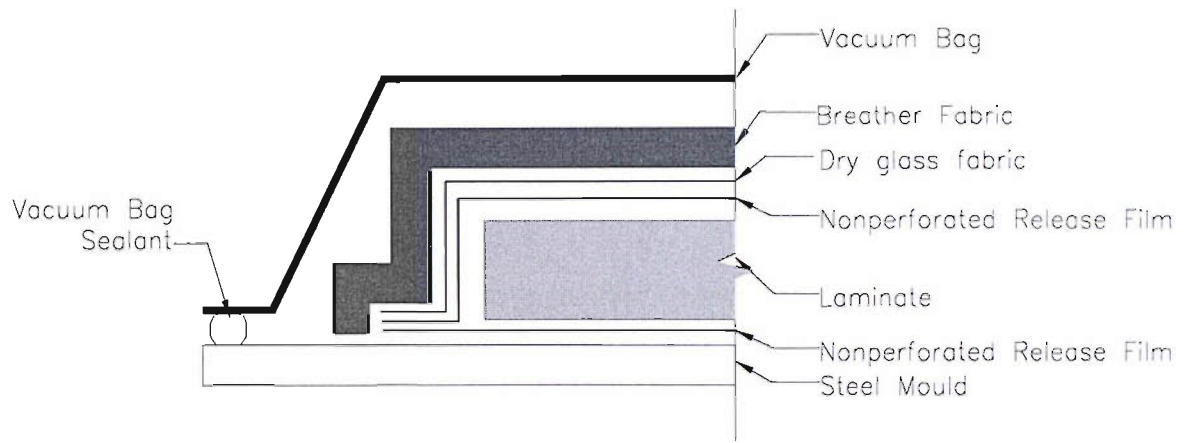


Figure B.1 Laminate bagging

Appendix C

Tensile tests on unidirectional CFRP to obtain mechanical properties

This test was used to determine the elastic modulus, tensile strength and Poisson's ratio of the unidirectional CFRP material in the longitudinal fibre and transverse fibre directions. The test was conducted according to the recommendations in the ISO 527-5 standard [1]. A total of 3 longitudinal direction specimens (Type A) were tested, which were given the serial numbers A1, A2, A3. Also a total of 5 transverse direction specimens (Type B) were tested, which were given the serial numbers B1, B2, B3, B4, B5.

1 Original Material

- Material: Epoxy Prepreg
- Product: SE84LV/HMC/300/400/35%+/-3%pop
- SP Code: PC53-1808
- Manufacturer: Structural Polymer System Ltd.

2 Specimen preparation

- Fabricate 1.2 mm thick (for Type A specimens) and 2.1 mm thick (for Type B specimens) CFRP panels using 0.3 mm thick unidirectional epoxy prepreg. The processing referred Appendix B.
- Cut CFRP panels to specified dimensions with a band saw. The dimensions are shown in Figure C.1.
- Finish the edges of the specimens smoothly using sand papers.

- Bond aluminum end tabs to the ends of the specimens with Araldite 2015 adhesive. The dimensions and locations of the end tabs are shown in Figure C.1.

3 Test procedures

1) **Dimension measurement:** The section dimensions in the middle were measured by a vernier caliper. The width b_1 , the thickness h_1 and the cross sectional area A_1 of the longitudinal direction specimens (Type A) are shown in Table C.1. The width b_2 , the thickness h_2 and the cross sectional area A_2 of the transverse direction specimens (Type B) are shown in Table C.2. The subscripts 1 and 2 denote Type A and Type B, respectively. This notation is used throughout this report.

2) **Data collection:** One 90° 2-element cross strain gauge (FCA-5-11, TML) was mounted with the elements in the longitudinal and the transverse directions in order to determine the elastic modulus and Poisson's ratio, shown in Figure C.1. During the testing, the load and strains were monitored and recorded using a data logging system.

3) **Test setup:** The tests were done in tensile loading in the displacement control mode using an Instron universal testing machine 1195 with a capacity to 100 kN. The loading rate was 1 mm per minute. The test setup is shown in Figure C.2.

4 Results

3) **Tensile strength and failure strain:** the tensile stress σ_u was calculated by:

$$\sigma_u = \frac{F_u}{A} \quad (1)$$

where F_u is the failure load. The failure load F_{u1} , the failure stress σ_{u1} , the failure strain ε_{u1} of Type A specimens were shown in Table C.3. The failure load F_{u2} , the failure stress σ_{u2} , the failure strain ε_{u2} of Type B specimens were shown in Table C.4.

4) **Elastic modulus:** the stress versus strain plot of Type A specimens and Type B specimens during the tests are shown in Figures C.3 and C.4, respectively. the elastic modulus was calculated by:

$$E = \frac{\sigma_2 - \sigma_1}{\varepsilon_2 - \varepsilon_1} \quad (2)$$

where σ_1 and σ_2 are the stresses measured at the strain value $\varepsilon_1 = 0.0005$ and $\varepsilon_2 = 0.0025$, respectively. The values of the elastic modulus obtained for Type A specimens and Type B specimens are shown in Tables C.5 and C.6, respectively.

3) **Poisson's ratio:** the in-plane poisson's ratio was calculated by:

$$\mu = -\frac{\varepsilon_2}{\varepsilon_1} \quad (3)$$

where ε_1 and ε_2 is the strain in the longitudinal direction and the transverse direction respectively. The Poisson's ratios obtained for Type A specimens and Type B specimens are shown in Table C.7 and C.8 respectively.

4) **Failure mode:** The failure mode for Type A specimens is explosive, shown in Figure C.3. It was found in the failed specimens that the fibres were detached from each other and broken. The failure mode for Type B specimens is shown in Figure C.4. The failure plane is almost perpendicular to the loading direction, which indicates that fracture was occurred in the matrix.

5 Conclusion

All of the properties are shown in the Table C.9.

Reference

- [1] EN ISO 527-5. Plastics - determination of tensile properties - part 5: test conditions for unidirectional fibre-reinforced plastic composites. 1997.

Table C.1 Dimensions of Type A specimens

	A1	A2	A3	Mean	CoV (%)
Width b_f (mm)	13.18	13.21	13.32	13.24	0.56
Thickness h_f (mm)	1.05	0.98	1.09	1.04	5.35
Area A_f (mm ²)	13.839	12.946	14.519	13.768	5.73

Table C.2 Dimensions of Type B specimens

	B1	B2	B3	B4	B5	Mean	CoV (%)
Width b_f (mm)	22.70	22.70	22.58	22.48	22.60	22.61	0.41
Thickness h_f (mm)	1.92	1.90	1.91	1.91	1.91	1.91	0.37
Area A_f (mm ²)	43.584	43.130	43.128	42.937	43.166	43.189	0.55

Table C.3 Tensile strengths and failure strains for Type A specimens

	A1	A2	A3	Mean	CoV (%)
F_{u1} (kN)	30.2	30.4	30.3	30.3	0.3
σ_{u1} (MPa)	2182.9	2347.8	2088.6	2206.4	5.9
ε_{u1} (%)	0.9404	0.9235	1.0909	1.0	9.4

Table C.4 Tensile strengths and failure strains for Type B specimens

	B1	B2	B3	B4	B5	Mean	CoV (%)
F_{u2} (kN)	1.076	1.002	0.815	0.869	1.089	0.970	12.69
σ_{u2} (MPa)	24.7	23.2	18.9	20.2	25.2	22.5	12.36
ε_{u2} (%)	0.333	0.322	0.249	0.268	0.333	0.30	13.28

Table C.5 Elastic moduli of Type A specimens

	A1	A2	A3	Mean	CoV (%)
F_{11} (KN)	1.6	1.5	1.7	1.6	7.2
F_{21} (KN)	115.4	119.0	119.2	117.9	1.8
σ_{11} (MPa)	7.9	7.8	8.1	7.9	1.6
σ_{21} (MPa)	569.1	601.9	554.5	575.1	4.2
E_1 (GPa)	226.9	241.4	217.6	228.6	5.3

Table C.6 Elastic moduli of Type B specimens

	B1	B2	B3	B4	B5	Mean	CoV (%)
F_{12} (KN)	0.17	0.18	0.16	0.17	0.18	0.169	4.15
F_{22} (KN)	3.82	4.07	3.75	3.9	4.1	3.923	4.21
σ_{12} (MPa)	0.81	0.79	0.82	0.81	0.83	0.812	1.89
σ_{22} (MPa)	18.70	18.24	18.90	18.96	19.20	18.80	1.92
E_2 (GPa)	7.44	7.09	7.58	7.55	7.54	7.44	2.73

Table C.7 Poisson's ratios for Type A specimens

	A1	A2	A3	Mean	CoV (%)
ε_{11} (10^{-6})	1503	1503	1502	1502.7	0.0
ε_{21} (10^{-6})	-423	-337	-518	-426.0	-21.3
μ_{12}	0.281	0.224	0.345	0.30	21.3

Table C.8 Poisson's ratios for Type B specimens

	B1	B2	B3	B4	B5	Mean	CoV (%)
ε_{12} (10^{-6})	1503	1497	1497	1498	1500	1499	0.17
ε_{22} (10^{-6})	-21	-23	-24	-20	-23	-22	-7.40
μ_{21}	0.0140	0.0154	0.0160	0.0134	0.0153	0.015	7.48

Table C.9 Mechanical properties reported

Property	Mean	CoV (%)
Longitudinal tensile strength σ_{u1} (MPa)	2206.4	5.9
Longitudinal failure strain ε_{u1} (%)	1.00	9.4
Longitudinal elastic Modulus E_1 (GPa)	228.6	5.3
Poisson's ratio ν_{12}	0.30	21.3
Transverse tensile strength σ_{u2} (MPa)	22.5	12.36
Transverse failure strain ε_{u2} (%)	0.30	13.28
Transverse elastic Modulus E_2 (GPa)	7.44	2.73
Poisson's ratio μ_{21}	0.015	7.48

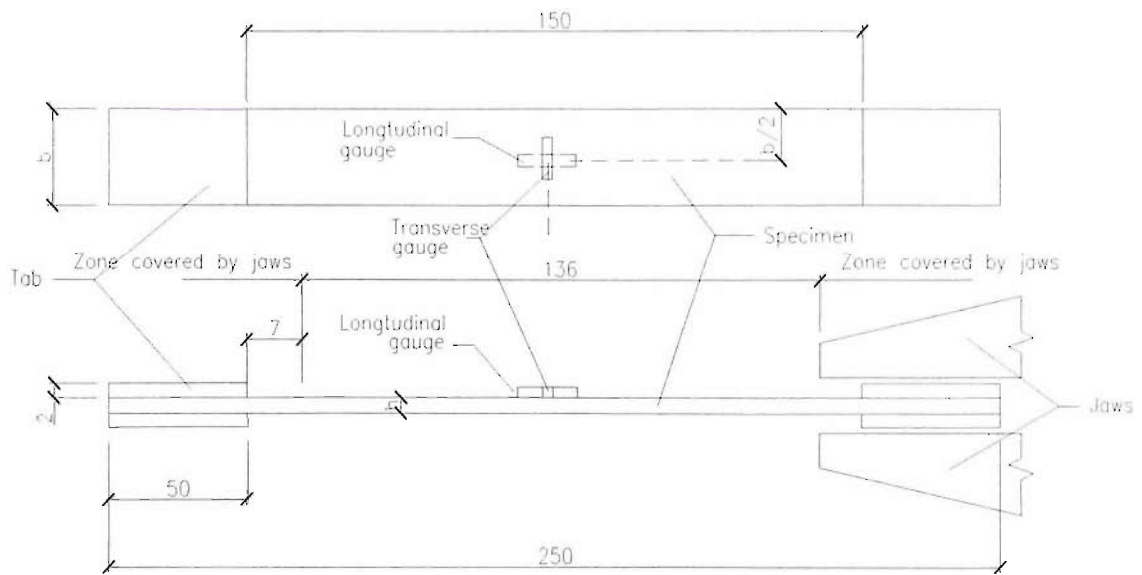


Figure C.1 Specimen dimensions and gauge locations

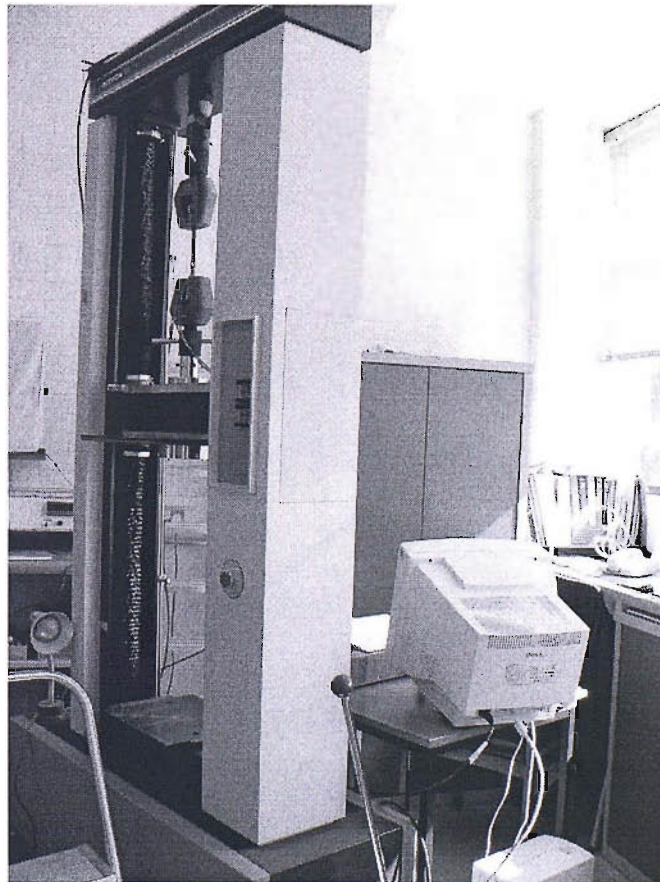


Figure C.2 Test setup

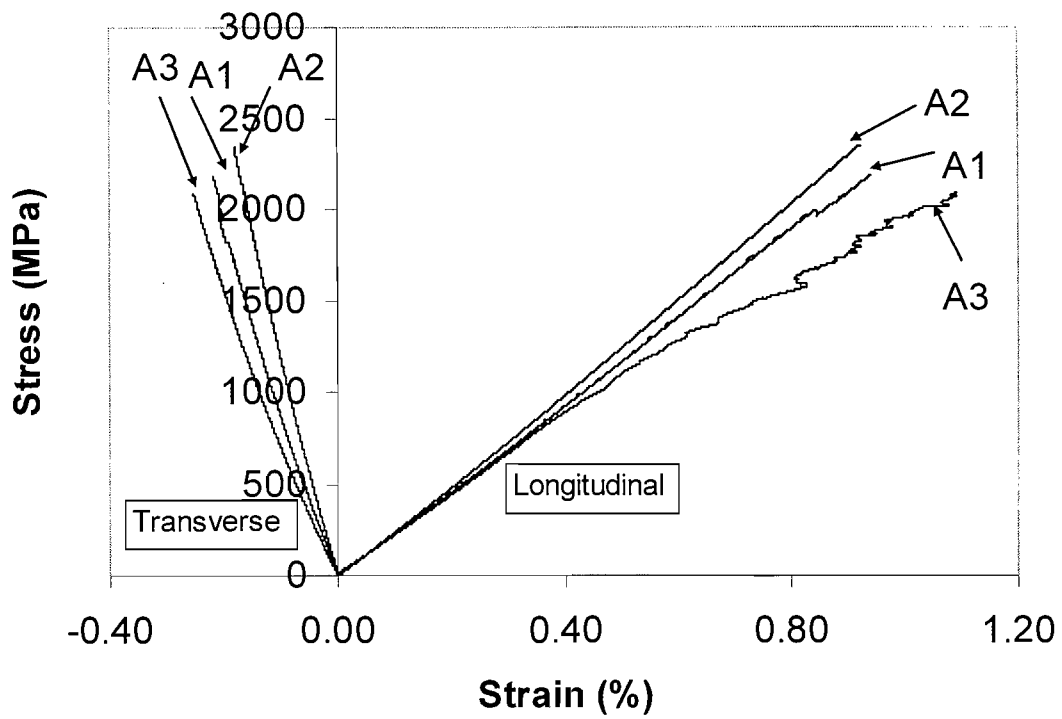


Figure C.3 Stress-strain behaviour of Type A specimens

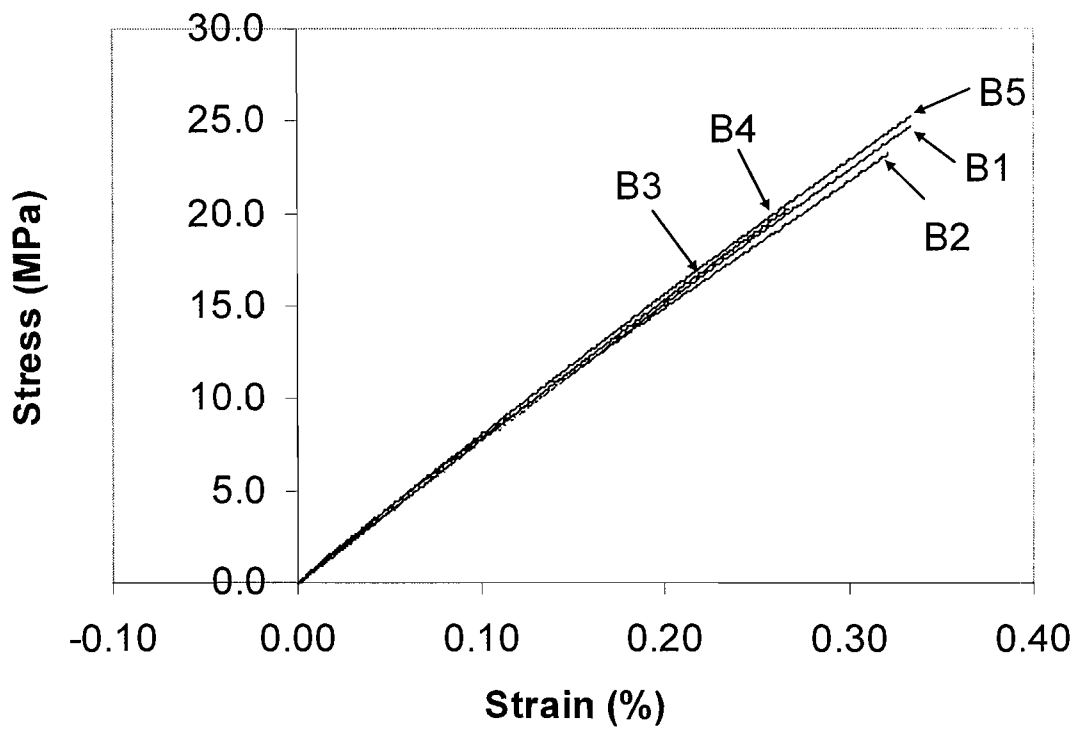


Figure C.4 Stress-strain behaviour of Type B specimens

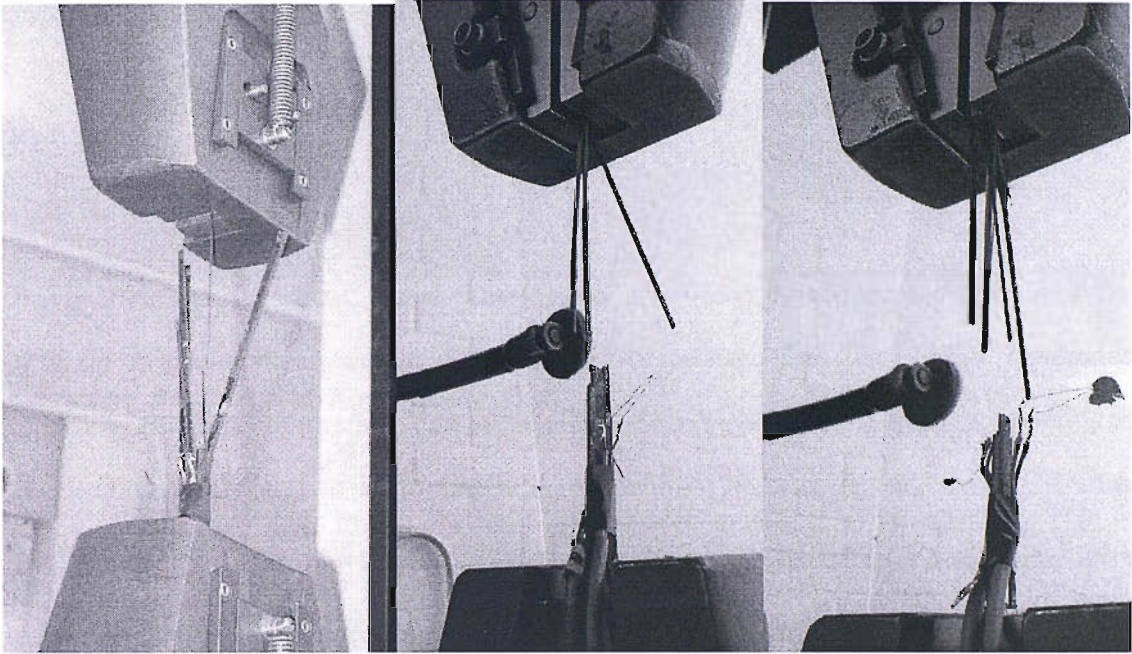


Figure C.5 Failed Type A specimens

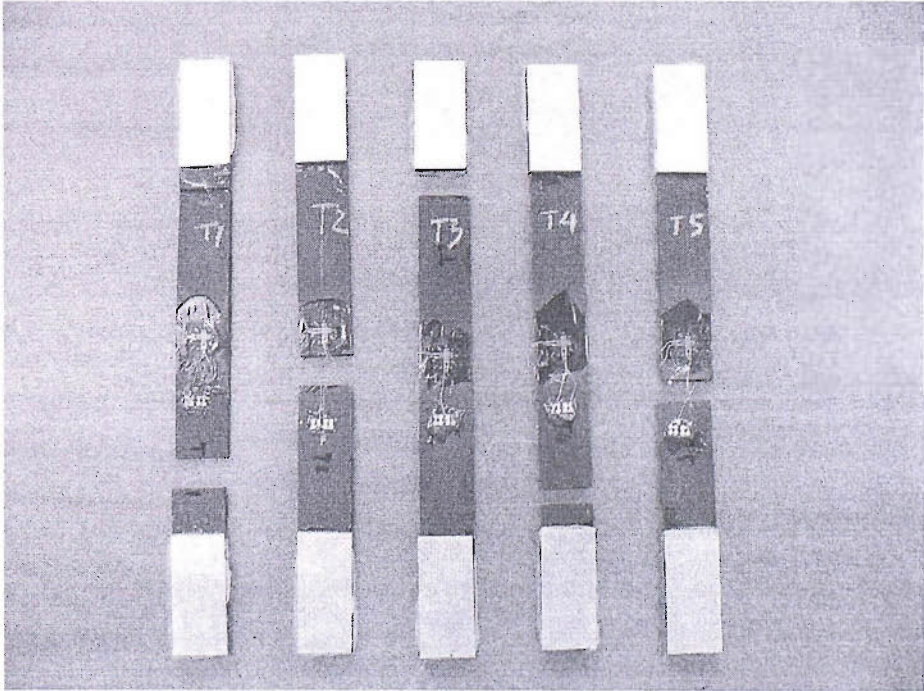


Figure C.6 Failed Type B specimens

Appendix D

Shear tests on thick adherend lap-shear joints

Thick adherend lap-shear joints were tested to obtain the shear modulus and the ultimate average shear stress in the adhesive in situ. The tests were conducted according to the recommendations in the ISO 11003-2 standard [1]. The dimensions of the specimens are shown in Figure D.1, where $L_2=110$ mm, $L_{c2}=80$ mm, $t_2=6$ mm, $b_2=25$ mm, $\eta_2=1$ mm, $\phi_f=12$ mm, $a_2=1.5$ mm, $c_2=5$ mm. A total of 5 specimens were tested, which were given the serial numbers A1, A2, A3, B1 and B2.

1 Original Material

- Material: Sikadur-31 normal, a two-part thixotropic epoxy resin

2 Specimen preparation

Five specimens were prepared with the following procedure:

- **Machining panels:** Two 6 mm thick steel panels were machined to dimensions 250 mm by 110 mm.
- **Surface preparation of panels:** Gluing surfaces were sandblasted to the SA2^{1/2} standard thoroughly within 4 hours before bonding. The bonding surfaces were cleaned with 3M VHB surface cleaner.
- **Mixing adhesive:** Two parts (part A resin and part B hardner in proportion as 3:1) were mixed with 1% weight of ballotini (1 mm diameter), which ensured a uniform thickness of bond line.

- **Bonding panels:** the adhesive was applied on to the panels. The method of applying the adhesive was to lay more adhesive along the centre than the edges. After pressing the panels together and scraping off the spewed adhesive, four clamps were applied to four corners of the bonded panels to ensure the thickness of adhesive layer was uniform at 1 mm.
- **Curing:** The bonded panels were cured at room temperature for more than 72 hours.
- **Cutting panels:** Cut the bonded panels into specimens using a diamond saw.
- **Drilling holes:** The holes were drilled in the specimens as shown in Figure D.1.
- **Milling grooves:** Delineate the overlap zone by milling two grooves as shown in Figure D.1.

3 Test procedures

1) **Dimension measurement:** the section dimensions in the middle were measured by a vernier calliper. The width b_2 , the length of lap c_2 , the thickness of the adhesive layer η_2 and the lap area A_2 of the specimen are shown in table D.1.

$$A_2 = b_2 \times c_2 \quad (1)$$

2) **Data collection:** Two 90° 2-element Cross strain gauges (FCA-2-11, TML) (gauge 1, 2, 3 and 4) were mounted across the adhesive layer in $\pm 45^\circ$ direction on both sides of the specimens B1 and B2, as shown in Figure D.1. During the testing, the load and strains were monitored and recorded using a data logging system.

3) **Test setup:** The tests were done in tensile loading in the displacement control mode using an Instron universal testing machine 1195. The load rate was 0.5 mm per minute. A universal joint, shown as Figure D.2, was used to eliminate the eccentric effect. The test setup is shown in Figure D.3.

4 Results

1) **Shear strength:** ignoring the nonuniform stress distribution in the longitudinal direction in adhesive layer, the average shear stress τ_L was calculated by:

$$\tau_L = \frac{P_L}{A_2} \quad (2)$$

where P_L is the tensile load. The ultimate average shear stress, τ_{Lu} , can be obtained when failure load, P_{Lu} , was applied.

2) **Shear strain:** the shear strain obtained by strain gauge, γ_s , can be calculated by:

$$\gamma_s = |\varepsilon_{+45}| + |\varepsilon_{-45}| \quad (3)$$

where ε_{+45} and ε_{-45} are the strain obtained by strain gauge 1 and 2, respectively. Assuming the shear stress is uniform in region covered by gauges and the adherends and adhesive deform linearly and elastically, and ignoring the shear deformation in adherends, the shear strain in adhesive layer, γ_L , can be calculated by:

$$\gamma_L = \frac{A_s}{A_a} \gamma_s \quad (4)$$

where A_s and A_a are the area of strain gauges and the covered area of strain gauges on the adhesive layer, respectively. A_s equals 0.18 mm^2 ($2 \text{ mm} \times 0.9 \text{ mm}$).

$$A_a = A_s - \frac{1}{2}((2 + 0.9) \cos(45^\circ) - \eta_2)^2 \quad (5)$$

γ_{Lu} is the failure shear strain.

3) **Shear modulus:** The shear modulus G_L was calculated by:

$$G_L = \frac{\tau_{L2} - \tau_{L1}}{\gamma_{L2} - \gamma_{L1}} \quad (6)$$

where τ_{L1} and τ_{L2} are the stresses when the strain γ_{L1} equal 0.05% and γ_{L2} equal 0.5%, respectively. The values are shown in Table D.2.

4) **Failure mode:** the failure mode for the thick adherend lap-shear joint specimens is shown in Figure D.4. All specimens had adhesive failure.

The failure load, P_{Lu} , the ultimate average shear stress, τ_{Lu} , the failure strain, ε_{Lu} , and elastic modulus, G_L are shown in Table D.1. The stress-strain plot is presented in Figure D.5.

References

- [1] ISO 11003-2. Adhesives - determination of shear behaviour of structural adhesives - part 2: tensile test method using thick adherends. 2001.

Table D.1 Dimensions, test results and calculation results of thick adhesive lap-shear joint specimens

Specimen	A1	A2	A3	B1	B2	Mean	CoV (%)
Thickness (η_2) (mm)	1.13	1.13	1.13	1.06	1.08	1.11	3.04
Width (b_2) (mm)	25.45	25.79	24.77	24.96	24.83	25.16	1.76
Length of lap (c_2) (mm)	3.67	4.16	4.56	4.60	4.00	4.20	9.32
Area (A_2) (mm ²)	93.40	107.29	112.95	114.82	99.32	105.56	8.61
Failure shear force (P_{Lu}) (kN)	1.53	2.55	2.05	2.03	1.75	1.98	19.34
Ultimate average shear stress (τ_{Lu}) (MPa)	16.38	23.77	18.15	17.70	17.67	18.73	15.43
Failure shear strain (γ_{Lu}) (%)	/	/	/	1.55	1.85	1.70	12.48
Shear modulus (G_L) (GPa)	/	/	/	2.24	1.89	2.06	11.87

Table D.2 Stresses for calculation shear modulus

Specimen	B1	B2
Shear stress τ_{L1} at 0.05% strain (MPa)	1.35	1.06
Shear stress τ_{L2} at 0.5% strain (MPa)	11.42	9.57

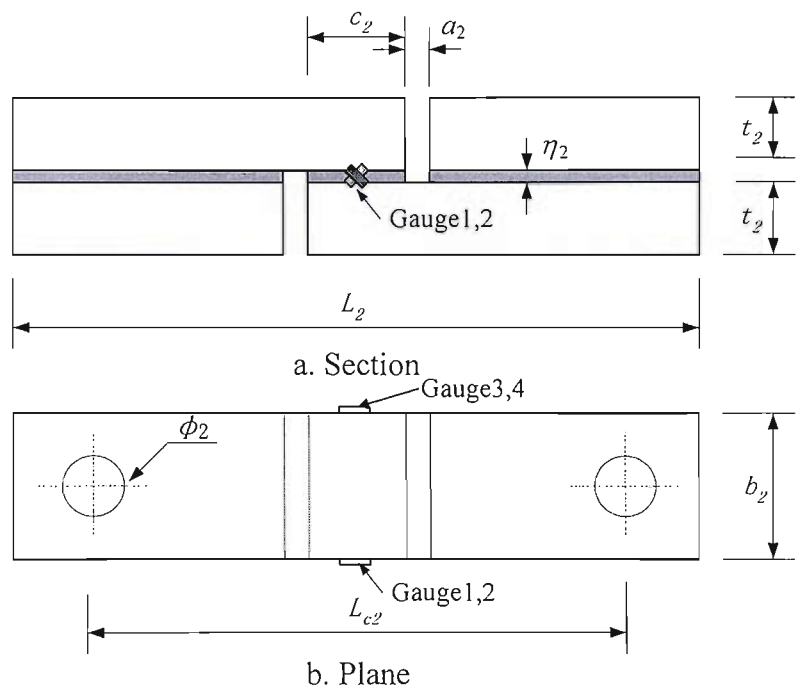


Figure D.1 Dimensions of thick adherend lap-shear joint and the location for strain gauges

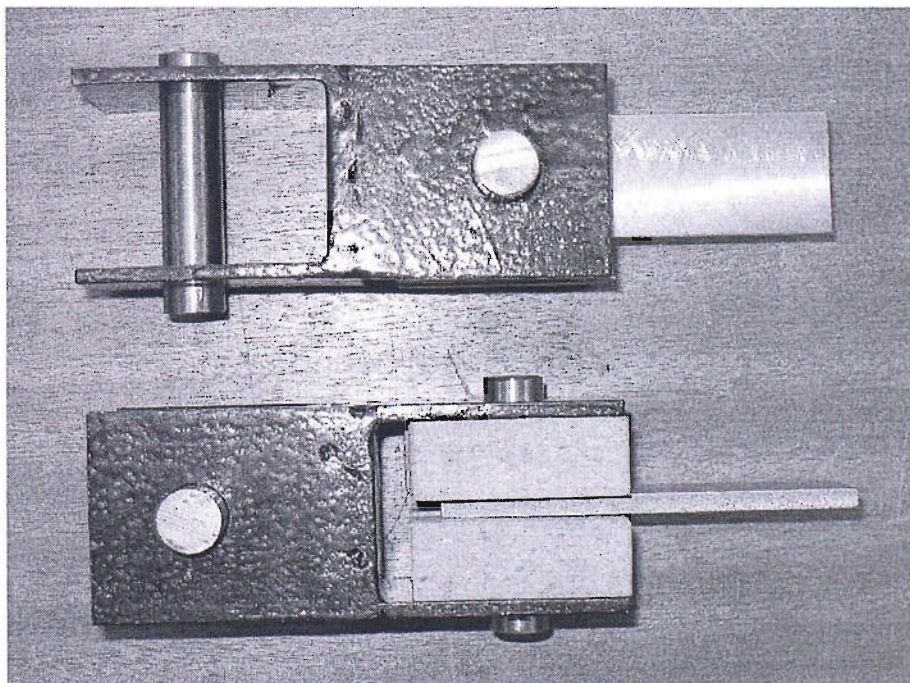


Figure D.2 Universal joints

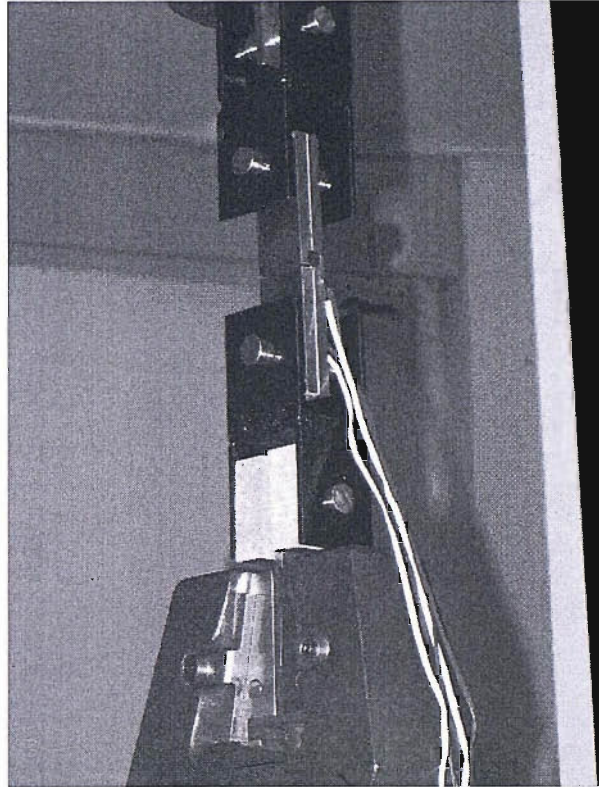


Figure D.3 The test setup

(Note: the strain gauges shown in the figure were only used for specimens B1 and B2)

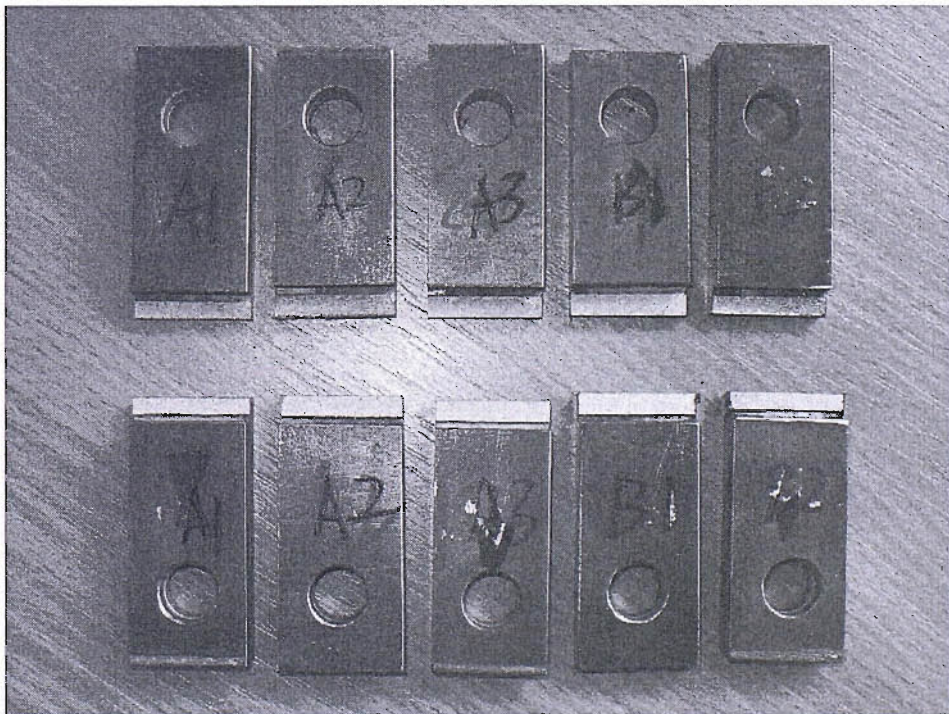


Figure D.4 Adhesive failure of the specimens

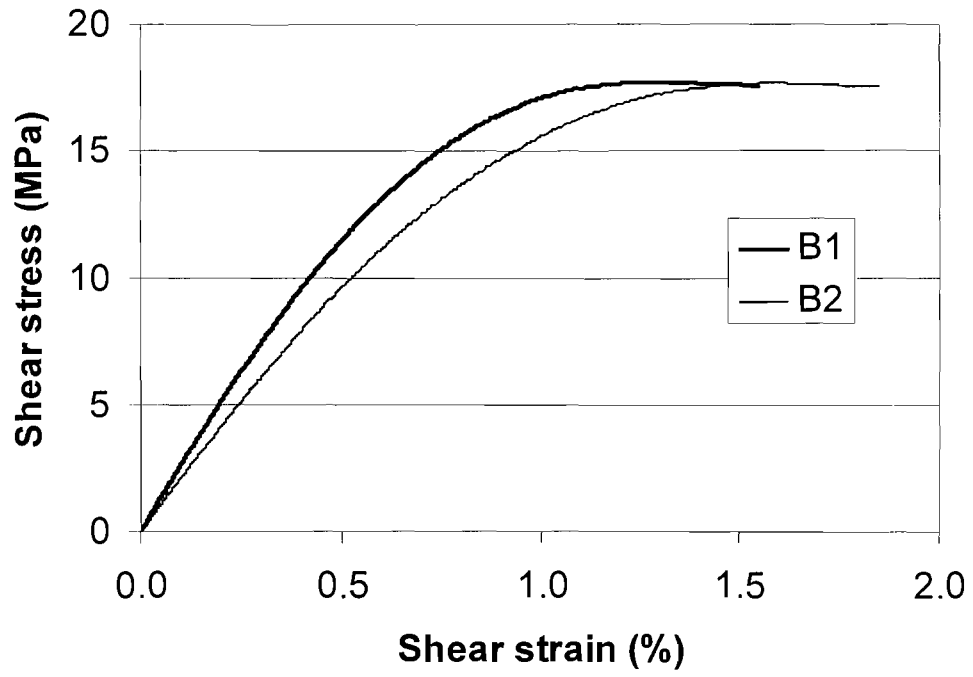


Figure D.5 Stress-strain behaviour of thick adherend lap-shear joints

Appendix E

List of publications

Three journal paper and four conference papers were published in accordance with the work of this thesis.

Journal paper

Deng J, Lee MMK, Moy SSJ. Stress analysis of steel beams reinforced with a bonded CFRP plate. *Composite Structures* 2004; 65(2):205-15.

Deng J, Lee MMK. Behaviour under static loading of metallic beams reinforced with a bonded CFRP plate. *Composite Structures*, In Press, 2005.

Deng J, Lee MMK. Fatigue performance of metallic beam strengthened with a bonded CFRP plate. *Composite Structures*, In Press, 2005.

Conference papers

Moy SSJ, Deng J, Lee MMK. Analysis of the stresses in the adhesive interface of metallic beams reinforced with composite plates. *Proceedings of the Second International Conference on Advanced Polymer Composites for Structural Applications in Construction (ACIC 2004)*. Cambridge, England: Woodhead Publishing Ltd., 2004: 266-73.

Deng J, Lee MMK. Maximum interfacial stresses in beams strengthened with composite plates. *Metropolitan habitats and infrastructure, IABSE symposium report*. Shanghai, China, 2004: 310-1.

Deng J, Lee MMK. Static performance of bonding joints in steel beams reinforced with CFRP plates. *Proceedings of the 26th International SAMPE Europe Conference 2005*. Paris, France, 2005: 117-22.

Deng J, Lee MMK. Fatigue behaviour of steel beams bonded with a carbon fibre composite plate. *Proceeding of Third International Conference on Composites in Construction (CCC 2005)*. Lyon, France, 2005: 329-36.